Production and characterisation of bioresorbable polymers and polymer-glass composites for application in cardiac stents

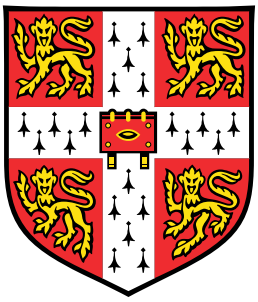

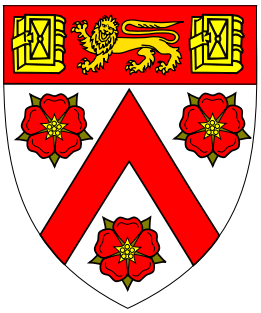

Reece Neil Oosterbeek

Department of Materials Science and Metallurgy

University of Cambridge

This thesis is submitted for the degree of Doctor of Philosophy

Trinity College

July 2020

Declaration

I hereby declare that except where specific reference is made to the work of others, the contents of this dissertation are original and have not been submitted in whole or in part for consideration for any other degree or qualification in this, or any other university. This dissertation is my own work and contains nothing which is the outcome of work done in collaboration with others, except as specified in the text and Acknowledgements. In accordance with University Regulations for the Department of Materials Science and Metallurgy, this dissertation contains fewer than 60,000 words including summary/abstract, tables, footnotes and appendices, but excluding table of contents, photographs, diagrams, figure captions, list of figures/diagrams, list of abbreviations/acronyms, bibliography and acknowledgements.

Reece Neil Oosterbeek

July 2020

Production and characterisation of bioresorbable polymers and polymer-glass composites for application in cardiac stents

Reece Neil Oosterbeek

Bioresorbable polymeric cardiac stents are a promising technology for treating cardiovascular diseases, but current poly-L-lactide (PLLA) stents have been limited by poor mechanical properties and slow degradation. Materials with increased strength and stiffness are needed, to reduce the required stent strut size and elastic recoil, so that the risk of restenosis can be minimised. Long term complications such as strut fracture and late stent thrombosis are also critical concerns, which require increased ductility and accelerated material degradation to be addressed.

This work investigated new materials based on polymer blends and polymer-glass composites, for future application in an effective and safe bioresorbable cardiac stent. PLLA was combined with polyethylene-glycol functionalised poly(L-lactide-co-caprolactone) (PLCL-PEG) to form a semi-miscible set of polymer blends with increased ductility and degradation rate. To provide mechanical reinforcement to these polymers, water soluble phosphate glass (P_2O_5-CaO-Na_2O) particles were incorporated to produce polymer-glass composites. These phosphate glasses were also studied to understand their structure and dissolution behaviour, to inform the subsequent design of composite materials. Material samples were degraded *in vitro* in phosphate-buffered saline (PBS) at 37℃ to determine their relative rates of degradation. Mechanical testing was carried out immersed in 37℃ water to simulate body conditions, and after various stages of degradation, to assess the evolution of mechanical properties. Thermal analysis (differential scanning calorimetry, ashing) and structural analysis (X-ray diffraction, scanning electron microscopy) techniques were used to study the microstructural changes and their effects on mechanical properties.

To assess the long-term degradation behaviour of PLLA:PLCL-PEG blends, and the evolution of their mechanical properties during degradation, blends of PLLA with varying amounts of PLCL(80:20)-PEG or PLCL(70:30)-PEG were created by solvent casting. Tests undertaken in PBS at 37℃ revealed that the addition of the faster degrading PLCL-PEG component catalysed and accelerated PLLA degradation. The onset of degradation was reduced controllably from 16 months for pure PLLA, to between 2 and 12 months for PLLA:PLCL-PEG blends. The miscibility of blend components had a strong impact on the ductility in ambient conditions and blends with low PLCL-PEG content underwent brittle failure, while samples with a higher PLCL-PEG content exhibited ductile failure, due to the formation of a PLCL-PEG-rich phase via phase separation or bulk changes. Under simulated body conditions all blend compositions exhibited significant ductility (>400%) due to the elevated temperature and hydration state. After 30 days of degradation several structural changes were observed. Moderate PLCL-PEG addition (10-30%) stabilised the structure and retained approximately 200% ductility, while other compositions displayed severe embrittlement resulting from enthalpy relaxation, or degradation-induced crystallisation.

Phosphate glasses are attractive as a reinforcing phase in polymer-glass composites to improve the mechanical properties, however uncertainty remains over their dissolution mechanisms, specifically the multi-stage behaviour sometimes observed. This work aimed to understand the factors affecting the multi-stage dissolution mechanisms, and the cause of the transition between them, as well as measuring the relative dissolution

rates of the glasses tested. The dissolution behaviour of $(P_2O_5)_{90-x}(CaO)_x(Na_2O)_{10}$ glasses (where x = 40, 45, 50) was assessed in water, PBS, and PBS pH-adjusted with lactic acid (to simulate polymer degradation) using mass loss and pH measurements, as well as structural analysis methods mentioned above. Dissolution was accelerated by lower CaO concentration in the glass, and lower solution pH. Two-stage dissolution was observed, and a new mechanism was proposed to explain this, where diffusion-limited conversion layer formation is followed by reaction-limited layer dissolution. The transition between these stages is a result of stabilisation of the conversion layer, which is dependent on layer composition and solution conditions. This mechanism is important for understanding and predicting glass behaviour, particularly in complex solutions such as body fluids and acidic polymer degradation products within polymer composites.

Phosphate glass microparticles with $d_{0.5}$ = 1.4 ±0.3 µm were incorporated into polymer-glass composites by precipitation of the polymer onto glass particles within a slurry, followed by injection moulding. This method was confirmed by electron microscopy and X-ray microtomography to give good dispersion. The polymer matrix composition (PLLA, 90PLLA:10PLCL(70:30)-PEG), glass composition (45, 50% CaO), and glass filler loading (0, 15, 30wt.%) were all varied to optimise and study their effects on mechanical and degradation behaviour. Glass particles provided significant mechanical reinforcement, increasing the modulus from 3.3 ±0.04 GPa to 5.1 ±0.2 GPa for PLLA with 30wt.% glass. Up to 15wt.% glass could be incorporated into the composites without ductility reduction, while interfacial adhesion resulted in comparable composite yield strength (41 ±2 MPa, 42 ±1 MPa) to the unfilled polymer (43 ±2 MPa), demonstrating that the composites are non-inferior to existing polymers in terms of yield strength and the resulting stent strut size required. Degradation testing revealed two-stage behaviour for composites, dominated initially by water absorption, followed by glass dissolution. The presence of glass suppressed polymer structural changes that lead to embrittlement, while also accelerating water absorption into the composite. Composite materials displayed a gradual reduction in mechanical properties during degradation. There was a decrease in elastic modulus (2.8 ±0.2 GPa to 1.4 ±0.2 GPa) and strain to failure (290 ±20% to 70 ±30%) after 4 months for the PLLA:PLCL-PEG composite with 15wt.% glass, which might allow slow transfer of loading to newly healed tissue. These results provide understanding of the evolution of composite mechanical properties during degradation, which is crucial in the design of effective bioresorbable cardiac stent devices.

This work has shown the important influence that polymer matrix composition and glass filler loading have on the evolution of polymer blend and polymer-glass composite mechanical properties during degradation, and the degradation rate itself. These findings have significant implications for the design of materials for bioresorbable polymer-based cardiac stents. Although this work investigated a selected set of material compositions, the mechanisms revealed provide a broader understanding that can be applied to a range of other polymer blend and composite systems. This work has made significant advances towards improved bioresorbable polymer-based materials for cardiac stents, and has developed a theoretical framework that allows design of composite mechanical properties, and their evolution during degradation.

Table of contents

Acknowledgements

As the culmination of my formal education, completing my PhD has been a challenging but extremely rewarding experience, and one I could not have accomplished without the support of many others along the way.

Firstly I would like to thank my supervisors, Professor Ruth Cameron and Professor Serena Best, for providing their constant and invaluable guidance and support, while also allowing me the independence to develop my own ideas. I would also like to thank the CCMM group for their knowledge and friendship, and in particular Dr Kyung-Ah (Joanne) Kwon for her technical and moral support in many aspects of this work. I would also like to express my deepest appreciation to my mentor and previous supervisor Professor Cather Simpson, who was instrumental in my development as a researcher.

None of this work would have been possible without the generous financial support I have received during my studies. I am immensely grateful to the Woolf Fisher Trust and the Cambridge Trust for the provision of a PhD scholarship, which has given me this incredible opportunity, and to Woolf Fisher Trust Secretary Dr Nigel Evans for his care and support. I would also like to thank Lucideon Ltd., and my industrial supervisor Professor Xiang Zhang, for their support of this project. During my studies I have been honoured to present my work at several conferences, and am indebted to various organisations for their support to fund these trips, including Trinity College Cambridge, the Armourers and Brasiers Company, the Cambridge Trust, the Cambridge Philosophical Society, the Institute of Physics, and the Institute of Materials, Minerals and Mining.

I have also benefited greatly from the technical expertise and assistance from various staff members at the Department of Materials Science and Metallurgy. Firstly I would like to thank Mr Wayne Skelton-Hough for his continual technical support and problem-solving ability. I would also like to express my gratitude for their assistance to Mr Andrew Rayment (mechanical testing), Mr Robert Cornell (polymer characterisation), Mr Andrew Moss and Ms Mary Vickers (XRD), Mr Simon Griggs (SEM), Sue Gymer (heat treatment), and Mr Paul Nicholls (workshop).

Some of the work reported on in this thesis has been carried out in collaboration with others, and I would like to express my appreciation to these collaborators. The assistance of Mr Ian Campbell (Lucideon Ltd.) was essential in preparation of phosphate glass materials, and I am also thankful for his insightful comments and advice. I would like to thank Mr Craig Donald (Lucideon Ltd.) for his assistance in providing ICP-OES services. I am also very grateful to Dr Christopher Lovell (Lucideon Ltd.) for providing materials and for his hospitality during my research trips to Lucideon. Dr Seán McMahon and Dr Patrick Duffy (Ashland Specialties Ireland Ltd.) provided crucial GPC data as well as helpful discussions regarding polymer degradation, and I am very grateful for their assistance. I would also like to thank Dr Abil Aliev (University College London) for his assistance with solid-state NMR spectroscopy measurements. Some of the work on phosphate glasses presented here was carried out in collaboration with Ms Kalliope Margaronis as part of a final year undergraduate research project in the Department of Materials Science and Metallurgy at the University of Cambridge, and I am very grateful for her contribution.

Throughout my years of education my parents Raymond and Geraldine have provided continual encouragement, and I would like to thank them for their support, hard work, and sacrifices that have enabled me to pursue my academic aspirations. Finally, I want to thank my wife Laura, for her constant love, support, and understanding, for always standing by me and helping make this possible.

Publications and presentations

Publications

Some of the work presented in Chapters 3 and 4, on PLLA/PLCL-PEG blends, has been published in a peer-reviewed journal article as detailed below:

- R. N. Oosterbeek, K-A. Kwon, P. Duffy, S. McMahon, X. C. Zhang, S. M. Best, R. E. Cameron, *Tuning structural relaxations, mechanical properties, and degradation timescale of PLLA during hydrolytic degradation by blending with PLCL-PEG*, Polymer Degradation and Stability, 170(109015) **2019**

Presentations

Some of the work presented in this thesis has also been presented in various formats, at national and international conferences as detailed below:

- R. N. Oosterbeek, P. Duffy, S. McMahon, X. C. Zhang, S. M. Best, R. E. Cameron, *Controlling structural relaxations, mechanical properties, and degradation timescale of PLLA during hydrolytic degradation*, Oral and poster presentations at: ESB 2019 (European Society for Biomaterials), Dresden, Germany, **September 2019**

- R. N. Oosterbeek, P. Duffy, S. McMahon, X. C. Zhang, S. M. Best, R. E. Cameron, *Structural and mechanical changes in PLLA-based polymer blends during hydrolytic degradation*, Poster presentation at: TCES-UKSB 2019 (Tissue and Cell Engineering Society & UK Society for Biomaterials), Nottingham, UK, **June 2019**

- R. N. Oosterbeek, P. Duffy, S. McMahon, X. C. Zhang, S. M. Best, R. E. Cameron, *Bioresorbable polyester blends: controlling degradation rate and physical properties*, Poster presentation at: Cambridge University Bioengineering Conference, Cambridge, UK, **March 2019**

- R. N. Oosterbeek, X. C. Zhang, S. M. Best, R. E. Cameron, *Investigation of phosphate glasses and PLLA/PLCL-PEG blends for the development of novel bioresorbable composite cardiac stents*, Oral presentation at: Bioceramics30, Nagoya, Japan, **October 2018**

- R. N. Oosterbeek, X. C. Zhang, S. M. Best, R. E. Cameron, *Development of a new generation of bioresorbable cardiac stents - Investigation of phosphate glass and toughened PLLA/PLCL-PEG blends*, Oral and poster presentations at: ESB 2018 (European Society for Biomaterials), Maastricht, Netherlands, **September 2018**

- R. N. Oosterbeek, X. C. Zhang, S. M. Best, R. E. Cameron, *Exploration of phosphate glass and PLLA/PLCL-PEG blends for novel bioresorbable composite cardiac stents*, Oral presentation at: UKSB 2018 (UK Society for Biomaterials), Bath, UK, **June 2018**

- R. N. Oosterbeek, X. C. Zhang, S. M. Best, R. E. Cameron, *Non-linear dissolution behaviour of ternary P_2O_5-CaO-Na_2O glasses for bioresorbable implants*, Poster presentation at: Cambridge University Bioengineering Conference, Cambridge, UK, **March 2018**

- R. N. Oosterbeek, X. C. Zhang, S. M. Best, R. E. Cameron, *Non-linear dissolution behaviour of ternary P_2O_5-CaO-Na_2O glasses for bioresorbable implants*, Poster presentation at: STEM for Britain, Houses of Parliament, London, UK, **March 2018**

Abbreviations and symbols

Abbreviation /symbol	**Definition**
α	Glass mass fraction dissolved (w/w or wt.%)
ΔG_m	Gibbs energy of mixing (J mol^{-1})
δ	Hildebrand solubility parameter ($MPa^{0.5}$)
δ_U, δ_L	Upper and lower solubility limits ($MPa^{0.5}$)
ε, ε_B	Strain, strain at break (m/m or %)
2θ	Bragg diffraction angle (°)
µCT	X-ray micro-computed tomography
σ, σ_y	Stress, yield stress (MPa)
ϕ	Volume fraction (v/v)
ϕ_f	Volume fraction of filler particles in composite (v/v)
χ	Flory-Huggins interaction parameter
BMS	Bare metal stent
BVS	Bioresorbable vascular scaffold
CAD	Coronary artery disease, a.k.a. CHD, IHD
CHD	Coronary heart disease, a.k.a. CAD, IHD
CL	Caprolactone (component in copolymer)
CVD	Cardiovascular disease
d_{max}	Maximum particle diameter (µm)

d_x	Particle diameter, where x fraction (v/v or vol.%) are smaller than this value (µm)
DALY	Disability-adjusted life year
DCM	Dichloromethane
DES	Drug eluting stent
DI	Deionised (water)
DSC	Differential scanning calorimetry
E	Young's modulus (GPa)
EDS	Energy Dispersive X-ray Spectroscopy, a.k.a. EDX
FTIR	Fourier-transform infrared spectroscopy
GPC	Gel permeation chromatography
ICP-OES	Inductively coupled plasma optical emission spectrometry
IHD	Ischaemic heart disease, a.k.a. CAD, CHD
k_{CVM}	Dissolution rate parameter for contracting volume model (µm day^{-1})
k_{DM}	Dissolution rate parameter for diffusion model (µm day$^{-0.5}$)
LA	Lactide/lactic acid (component in copolymer)
M_w	Weight average molecular weight (kg mol^{-1})
M_n	Number average molecular weight (kg mol^{-1})
NMR	Nuclear magnetic resonance
PBS	Phosphate-buffered saline
PCL	Polycaprolactone, a.k.a. poly-ε-caprolactone
PDLLA	Poly-D,L-lactic acid (Poly-D,L-lactide)
PEG	Polyethylene glycol
PGA	Polyglycolic acid (Polyglycolide)
PLA	Polylactic acid (Polylactide)
PLLA	Poly-L-lactic acid (Poly-L-lactide)
PLCL	Poly(lactide-co-caprolactone)
PLCL-PEG	PEG functionalised PLCL

PLGA	Poly(lactide-co-glycolide)
R	Ideal gas constant (J mol^{-1} K^{-1})
SA/V	Surface area/volume ratio (m^{-1})
SDT	Simultaneous DSC and TGA
SEM	Scanning electron microscopy
T	Temperature (°C)
T_g	Glass transition temperature (°C)
$T_c,\ T_d,\ T_m$	Crystallisation, degradation, and melting temperatures (°C)
TGA	Thermogravimetric analysis
t_{trans}	Transition time between dissolution regimes (days)
V_m	Molar volume (cm^3 mol^{-1})
w	Weight fraction (w/w or wt.%)
X	Degree of polymerisation
X_c	Crystallinity (%)
XRD	X-ray diffraction

Chapter 1

Introduction

1.1 Medical and health background

Cardiovascular diseases (CVDs) are one of the leading causes of death worldwide, resulting in 28% of all deaths in the UK, and 31% worldwide [1–3]. The World Health Organisation has identified two specific CVDs - coronary artery disease (CAD) and stroke - as "the world's biggest killers", accounting for a total of 15 million deaths worldwide in 2015 [4]. CAD has been the world's leading cause of total deaths since at least 1990, and since then has also overtaken communicable diseases such as lower respiratory infections and diarrhoeal diseases, as well as neonatal preterm birth complications, as the number one cause of DALYs[1] [5]. This trend is a result of an ageing population with lowering child mortality - surviving until age 5 decreases a person's likelihood of dying from communicable diseases, and those that survive to adulthood then tend to be affected by cardiovascular diseases [5].

In addition to this cost of human life and health, there is a substantial economic burden associated with CVDs. In 2015 alone, all CVDs combined are estimated to have cost the UK healthcare system €12 billion, 5% of total healthcare expenditure. If

[1]DALY (disability-adjusted life year) is a metric that measures the total health loss a person experiences, incorporating years of life lost from premature death, and the years lived with a disability.

informal care and productivity costs are included, the total cost to the UK economy can be estimated at €26 billion. CAD, the most significant and prevalent CVD, alone accounts for €2.2 billion in healthcare expenditure and a cost to the UK economy of €9 billion in 2015 [1, 6].

From these statistics it is clear that CVDs, and in particular CAD, have an immense cost to society. Therefore, any new technology that can reduce the incidence of this disease, or treat it more effectively, will have a significant benefit to societal health and to the economy.

1.1.1 Coronary artery disease

Coronary artery disease (CAD), also known as coronary heart disease (CHD) or ischaemic heart disease (IHD), occurs as a result of atherosclerosis of the coronary arteries, where fatty plaque is deposited on the inner wall of the artery, restricting blood flow to the heart [7]. This can lead to inadequate oxygen supply to the heart, causing chest pain, heart attack, and death [7]. Atherosclerosis is depicted in Fig. 1.1, where fatty deposits (plaque) can be seen on the inner arterial wall, narrowing the artery and restricting blood flow.

CAD is usually treated using a procedure known as balloon angioplasty, which is illustrated in Fig. 1.2. The obstructed blood vessel is mechanically dilated by inserting a collapsed balloon into the affected area using a guide wire and catheter. The balloon is then inflated, forcing the artery open and compressing the plaque that blocks the vessel. This same process can also be used to deploy a stent, with the stent being crimped onto the balloon and inserted in a compressed state, and then expanded by the balloon. The catheter and guide wire are then retracted to leave the expanded stent in place and restore normal blood flow [7].

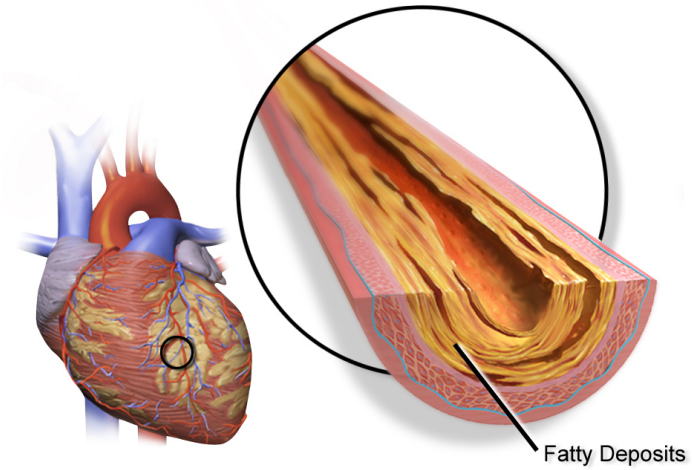

Fig. 1.1: Illustration of atherosclerosis in a coronary artery, showing the fatty plaque buildup. Reproduced with permission under CC BY 3.0 [8] from [9].

1.1.2 Current stent solutions

Selecting the material of construction for a stent is perhaps the most crucial aspect of stent design, and is where materials science can contribute to combating CAD. To date, three main types of stents have been used to treat CAD: bare metal stents (BMS), drug eluting stents (DES), and bioresorbable vascular scaffolds (BVS) [12]. Examples of these types of stents are shown in Fig. 1.3

Bare metal and drug eluting stents are typically constructed using 316L stainless steel, cobalt-chromium alloys, or nitinol shape memory alloys [17]. In addition, DESs have a polymer coating that elutes antiproliferative or anti-inflammatory drugs [12]. BMSs were the first type of coronary stent implemented, and although this represented a significant advance, drawbacks included a 30 - 40% rate of clinically relevant restenosis [17] (re-narrowing of the blood vessel after angioplasty [7]). This led to the development of DESs, which release drugs that reduce neointimal growth (growth of muscle cells on the vessel wall, which thickens walls and decreases lumen space) [17]. Use of DESs reduced the problem of restenosis, however it also introduced a new issue - late stent thrombosis (where a stented artery is suddenly blocked by thrombus formation) [12]. Second-generation DESs have altered strut design, polymer coatings,

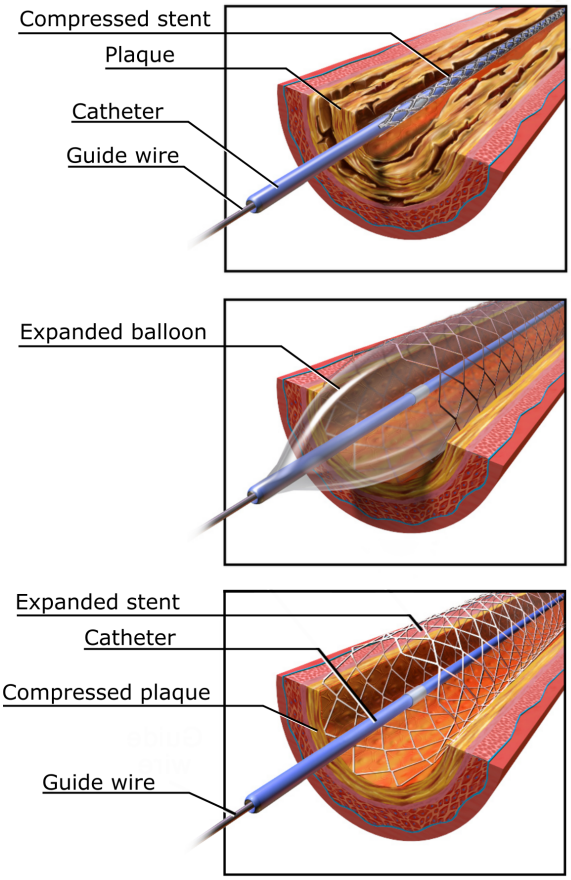

Fig. 1.2: Illustration of balloon angioplasty, showing how the inflation of the balloon compresses the plaque and expands the stent. Reproduced and adapted with permission under CC BY-SA 4.0 [10] from [9, 11].

and drugs, thus reducing the risk of late stent thrombosis and other problems [12, 18]. In spite of these advances, there are concerns that permanent DESs are still linked to chronic inflammation, neoatherosclerosis, restenosis and late stent thrombosis (including thrombosis resulting from stent fracture) [17, 19–21]. For these reasons, a fully bioresorbable stent is an attractive proposition to alleviate these issues.

Fully bioresorbable stents are an emerging technology, with only a handful of devices being manufactured commercially, most of which are based on polylactic acid (PLLA) [17]. It was only in 2016 that the first absorbable stent was approved by the U.S. FDA to treat CAD - the Abbott Absorb GT1 BVS [22, 23]. Early clinical data showed promising results, with bioresorption allowing return to normal vessel

Fig. 1.3: From left to right: examples of (a) bare metal stent (BMS), (b) drug eluting stent (DES), and (c) bioresorbable vascular stent (BVS). (a) reproduced and adapted with permission under CC BY-NC-SA 4.0 [13] from [14], (b, c) reproduced and adapted with permission from Elsevier and AME Publishing Company [15, 16].

physiology and vasomotion, and no evidence of a greater incidence of adverse effects [12, 17, 24–28]. In contrast, later results from large scale randomised clinical trials concluded that the Absorb bioresorbable vascular scaffold was associated with increased rates of target lesion failure and device thrombosis [29, 30]. The Absorb stent was subsequently permanently withdrawn from sale by Abbott, citing low commercial sales [31].

The limitations of the current generation of BVSs have also been revealed by these studies, including the thick struts required (due to the lower mechanical strength of the polymeric materials), making the device bulky with the potential for fracture, with some studies also suggesting that thicker struts increase late luminal loss. In addition, the larger device size compared with metallic stents makes BVSs less deliverable and reduces the procedural success rate [12, 32, 33]. The limited range of dilation possible with polymeric BVSs compared with DESs is also a key issue, as is the need for slow dilation and lack of visibility in X-ray images [26]. The slow resorption of PLLA has also been identified as an important drawback. Although there is no clear consensus on the optimal stent resorption time, it is generally thought that resorption on a timescale that mimics the natural healing time of the human body (6 - 12 months) would be beneficial, which is significantly faster than typical PLLA resorption times [34–36]. From the clinical literature, there is a clear mandate for development of stent materials with faster resorption times, and greater strength, stiffness, and ductility [36, 37].

1.1.3 Stent requirements

From a materials science perspective, a cardiac stent has a number of material property requirements that must be carefully considered when designing new materials for this application. A summary of some properties of relevant candidate materials is shown in Table 1.1.

Table 1.1: Summary of properties of some stent materials [38–45].

Material	σ_y (MPa)	ε_B (%)	E (GPa)	Recoil (%)	Degradation (months)
PLLA[1]	65	4	3.8	-26 - 24	∼24
316L Stainless Steel	170	40	200	2 - 20	-
Co-Cr alloy	450	8	220	2 - 17	-
Nitinol[2]	105	8.5	35	-3 - 33	-

[1] σ_y, ε_B, and E for PLLA measured under standard conditions (dry at room temperature). [2] Strain shown for Nitinol is the maximum shape memory strain rather than fracture strain.

Yield strength: Once inserted, cardiac stents are under constant radial pressure as they hold the blood vessel open. Stents are designed so as to be able to withstand this force, which means that stents made from weaker materials tend to have larger struts to support this force (strut thickness for PLLA stents tends to be about double that for metallic implants [46]), which can increase blood flow turbulence, thereby increasing the incidence of restenosis [12, 32, 47, 48]. PLLA stents tend to be bulky, while those made of 316L stainless steel and Co-Cr alloys allow thinner struts to be used, improving clinical outcomes [47]. Unlike metals, the mechanical properties of polymers such as PLLA can vary significantly between ambient conditions and the elevated temperature, hydrated state experienced *in vivo*, therefore changes in mechanical properties resulting from implantation and degradation must also be taken into account. [49, 50].

Elongation: Ductility is another essential property of a stent material, as it must be able to be deformed significantly during crimping and deployment as part of the balloon angioplasty procedure, all without fracturing. The brittle nature of PLLA leads to a limited range of dilation [26], while the increased ductility of metallic stents allows a greater range of expansion. Embrittlement during degradation is also a concern, and can lead to catastrophic failure of the device [51, 52].

Elastic recoil: Once a stent is expanded in vivo, significant contraction is undesirable as this presents a risk of restenosis [47]. The elastic modulus of the material plays a large role here, with stiffer materials displaying reduced recoil. The effect of material properties is compounded however, by other factors such as stent design, as well as patient variability, both of which can have a significant effect on the measured recoil [39, 40]. Although manufacturers typically claim elastic recoil of $< 3\%$, 7 - 10% is more common, with the discrepancy arising from testing being done in air with no external force [53].

Flexibility: In order to be deployed in vivo, a stent must be able to bend to follow the contours of the blood vessels. Although material stiffness plays a small part here, it is the stent design that is the major contributor to stent flexibility [47].

Radiopacity: Visibility of the stent in X-ray imaging is another important property to consider. Metallic stents are often visible, however polymer based stents require modification to enhance visibility. Methods used include Pt, Au, or Ta markers, or incorporation of iodine into the polymer [46].

Degradation: Using bioresorbable stents offers the advantage of reducing some of the long term risks associated with permanent stents, including fracture, neoatherosclerosis, restenosis and late stent thrombosis [12, 17]. Early tests with PGA (polyglycolic acid) stents failed due to the polymers quick degradation within 2 - 4 weeks [54], while

PLLA stents are seen to take $\sim$ 24 months to degrade [46]. Currently the optimal timescale of degradation is unclear, however it is generally accepted that pure PLLA is resorbed too slowly, and that a stent resorption time of around (6 - 12 months) would be advantageous [17, 34–36]. Biodegradable metallic stents consisting of Fe-based, Zn-based, and in particular Mg-based alloys have also been investigated due to their high strength compared with polymeric materials, however their low ductility, fast and uneven corrosion behaviour, and the release of hydrogen gas are significant limitations. Efforts to achieve slower and more consistent degradation have included surface treatments or alloying elements, however these must be considered carefully due to the potentially harmful effects of release of elements such as Al, Zr, or Ce into the body [55, 56].

Biocompatability: Bioactive implant materials such as these must be designed to elicit a desired response from the body, promoting endothelialisation and not causing inflammation. BMSs, DESs and BVSs have all been seen to cause inflammation [57, 58], and in addition the poor wettability of PLLA can lead to thrombosis.

1.2 Thesis aims

This thesis aims to develop new bioresorbable stent materials with improved properties compared with current PLLA stent technology. Although achieving comparable mechanical robustness to metallic stents ($\sigma_y \geq 100$ MPa, $E \geq 200$ GPa) is unrealistic, improvements in these properties that close the gap between polymer-based and metallic stents will allow the disadvantages of bioresorbable stents over the short term to be reduced. Current PLLA stents also display inferior ductility compared with metallic stents, leading to a reduced range of radial expansion and potential fracture if over-dilated *in vivo* [28, 35, 59], however this is an area where material development has the potential to match and even exceed the performance of metallic stents, in terms of crimping and deployment performance.

The main advantages of bioresorbable polymer stents over metallic stents lie in their long-term performance, where degradation can restore normal physiological behaviour. The current long-term performance is not optimal however, so this project aims to accelerate the material degradation time to around 6 - 12 months, and reduce the tendency of PLLA to become embrittled during degradation to prevent catastrophic device fracture or fragmentation.

To achieve these aims, novel polymer blends and polymer-glass composites will be fabricated and tested, specifically investigating the microstructure, mechanical properties, and degradation behaviour. The interactions between these factors will also be examined, in order to gain a mechanistic understanding of the materials' behaviour in dry, wet, and degraded conditions. Polymer components will be based on commercial PLLA and novel PEG functionalised PLCL copolymers (PLCL-PEG), while phosphate glass microparticles will be used as a filler material within a polymer composite, in order to provide mechanical reinforcement and influence composite degradation. Chapter 2 will describe the current state of the art for these bioresorbable polymers and blends, bioactive glass, and composite materials.

Chapter 2

Literature review

2.1 Resorbable polymers

Since development of synthetic biodegradable polymers began in the 1960s, a huge range of polymers have become available, from polyesters such as polylactide and polycaprolactone, to polyurethanes, polyanhydrides, and many more [60, 61]. Despite this wide range, there are a limited number of polymers that have suitable mechanical and degradation properties for use as a cardiac stent. Here I will focus on polylactide (PLA) and polycaprolactone (PCL), their copolymers, and polyethylene glycol (PEG).

2.1.1 Homopolymers and copolymers

2.1.1.1 Polylactide

Polylactide (also known as polylactic acid, PLA) is one of the most commonly used resorbable polymers. Its structure is shown in Fig. 2.1, showing it is a chiral molecule, giving rise to two isomers - poly-L-lactide and poly-D-lactide - which have significantly different properties. PDLA is amorphous (compared with the semi-crystalline nature of PLLA), mechanically weaker, and degrades faster [60, 62]. Hence most applications use the L- isomer of PLA.

The mechanical properties of PLLA compare favourably with most other resorbable polymers, with a yield strength of around 60 MPa, and elastic modulus of around 4 GPa in dry, ambient conditions [38, 63]. This has lead to its application in multiple orthopaedic fixation devices, particularly interference screws [60, 64–66], but also scaffolds for ligament replacement [67, 68] and resorbable stents [12, 17, 26, 46, 69]. PLLA also displays relatively low toughness, with ε_B around 4%, limiting its use in applications where significant plastic deformation is necessary [38, 63].

PLLA is a relatively hydrophobic polymer [60], leading to a very slow degradation rate. It is reported that PLLA can take between 2 and 5.6 years to be completely resorbed in vivo [66, 70], but begins to lose strength after 6 months [62]. It degrades via bulk hydrolysis into lactic acid, which is a normal product of the human metabolism [60].

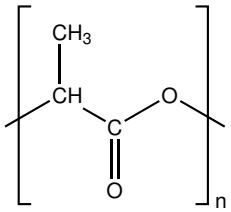

Fig. 2.1: Structure of PLA (polylactide).

2.1.1.2 Polycaprolactone

Polycaprolactone (PCL) is a semicrystalline polymer with crystallinity ranging between 30 - 50%, depending on molecular weight [71]. Its structure is shown in Fig. 2.2. [60]. PCL has reduced strength compared with PLA, with a tensile strength of approximately 23 MPa, however it is extremely ductile with $\varepsilon_B > 700\%$ [60]. Similarly to PLA, PCL undergoes bulk hydrolytic degradation, with a slower rate of degradation (2 - 3 years).

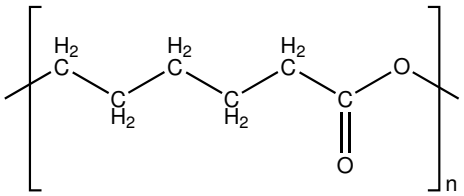

Fig. 2.2: Structure of PCL (polycaprolactone).

2.1.1.3 Poly-lactide-co-caprolactone

Early work on copolymers of PLA and PCL for biodegradable implants was carried out by Schindler et al. in the late 1970s and early 1980s [72, 73]. They found that the stability of the copolymers under ambient conditions decreases with increasing lactide content, until T_g exceeds ambient temperature, which was attributed to lack of crystallinity in the copolymers with lower lactide content. Copolymers with lactide content from 10 - 90 mol.% displayed rapid degradation in terms of molecular weight, but weight loss took longer and was significantly dependent on lactide content, with copolymers with higher lactide content losing weight faster [72, 73]. Dependence of degradation on initial molecular weight is also seen, with onset of weight loss occurring later for higher starting M_n [73].

In 1996 Seppälä et al. published a series of studies describing a set of PLCL copolymers (poly(lactide-co-caprolactone)), where they comprehensively investigated the effects of L- and D,L- lactide content on the mechanical, thermal and degradation behaviour of PCL copolymers [74–76]. The mechanical and thermal properties of these polymers is shown in Fig. 2.3, with intermediate compositions displaying reduced mechanical strength and stiffness, which was attributed to low crystallinity at these compositions. The reduced crystallinity for intermediate copolymer compositions also explains the faster degradation of these compositions seen by Schindler et al. [72, 73], Ye et al. [77], and Seppälä et al. [75], emphasising that crystallinity is a key factor in degradation behaviour.

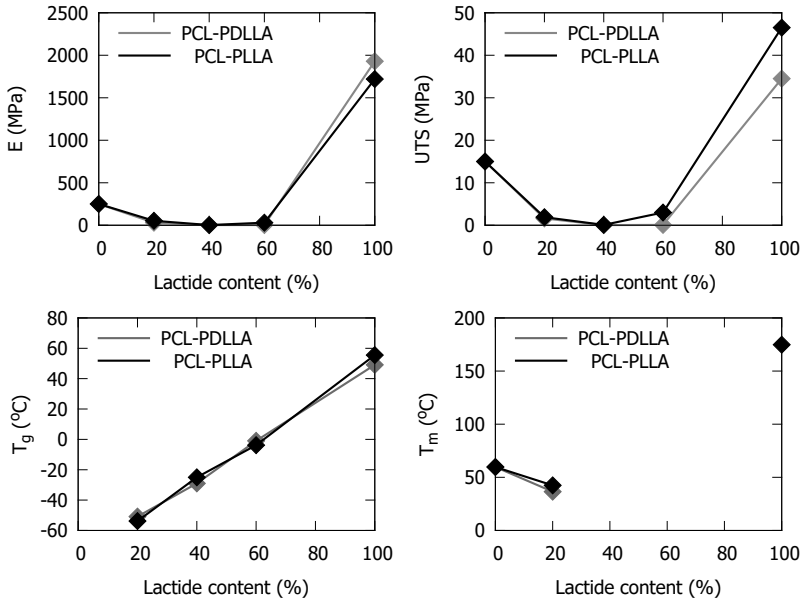

Fig. 2.3: Mechanical and thermal properties of PLCL copolymers. Figures created from data from Seppälä et al. [74].

In their third work of the series, Seppälä et al. investigated the effect of hydrolytic degradation on the mechanical properties of PLCL copolymers [76]. Surprising results were seen for some of the copolymers, which showed increased stiffness and yield strength after degradation (up to a 9× increase in σ_y for PLCL(40:60) (40% lactide)) - see Fig. 2.4. This increase in mechanical strength during the degradation process was subsequently studied by other groups, particularly Saha and Tsuji, who found that this increase is the result of crystallisation of the amorphous copolymer, which is accelerated by the presence of water due to enhanced chain mobility [78, 79].

From 2012 to 2014 Fernández and Sarasua et al. carried out comprehensive surveys of the thermal and mechanical properties of multiple PLCL copolymers, investigating the effect of and susceptibility to ageing [80–82]. Similarly to Seppälä et al. and Saha and Tsuji, they found that ageing of PLCL copolymers, even under dry, ambient conditions, causes crystallisation and subsequent increases in elastic modulus.

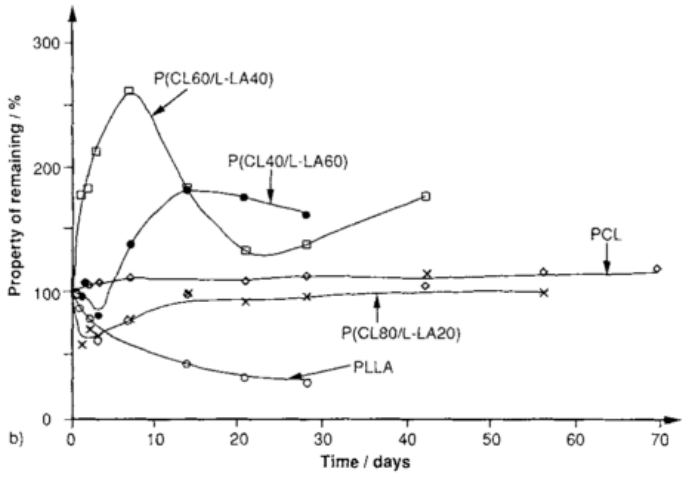

Fig. 2.4: Changes in the tensile modulus of PLCL copolymers and PLLA and PCL homopolymers during hydrolysis at 37°C. Figure reproduced with permission from John Wiley and Sons [76].

Fernández and Sarasua et al. also investigated which copolymer compositions are prone to this effect, finding that in copolymers with high lactide content, chain mobility is hindered, and ageing does not occur [80]. They studied the effect of the degree of randomness in the copolymer chains on the ageing behaviour, finding that copolymers with a high degree of randomness are less prone to ageing, in contrast to copolymers with a structure more similar to block copolymers, which exhibit significant crystallisation upon ageing [81, 82]. They also determined the effect that different chain microstructures have on the thermal properties of PLCL copolymers, finding that more random microstructures have a shorter average sequence length, which reduces the degree of crystallinity and T_m [83, 84].

PLCL copolymers with lactide content in the range 60 - 90% have also been seen to display a shape memory effect, with the crystalline PLLA domains acting as the crosslinker, and the amorphous phase acting as the reversible phase [85, 86]. This effect may be useful for stent applications, similar to how shape memory alloys such as nitinol are used.

2.1.1.4 PEG copolymers

Polyethylene glycol (PEG) is a water soluble polymer, whose structure is shown in Fig. 2.5. Early studies on block copolymers of PEG with PLLA, PDLLA, and PCL indicated that addition of PEG reduces crystallinity and T_g/T_m, increases hydrophilicity, and significantly increases the water absorption [87–91]. These copolymers have also been used as drug release "pastes" [92], or eye injections [93].

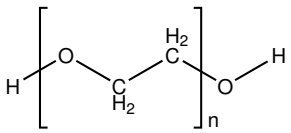

Fig. 2.5: Structure of PEG (polyethylene glycol).

A significant application of PEG is for injectable temperature sensitive hydrogels initially developed by Kim et al. in 1997 [94–96]. They developed diblock and triblock copolymers of PEG-PLLA with varying molecular weights, and observed temperature sensitive sol-gel behaviour at concentrations between 10 - 60 wt.% in aqueous solutions. The sol-gel transition is tunable using the molecular weights of the PLGA and PEG components.

PEG copolymerised with PLA/PCL has been heavily studied for applications in injectable hydrogels for drug delivery [91, 97], but the compounds studied here are not suitable for load bearing devices such as stents due to their mechanical properties. In 2007 Bramfeldt et al. investigated (PDLLA-co-PCL)-(PEG)-(PDLLA-co-PCL) block copolymers with high molecular weights, intended to have greater mechanical strength suitable for 3D scaffold applications [98]. Although Bramfeldt's polymers contained large amounts of PEG, with (CL+LA):EG ratios around 3:1 - 4:1, the high molecular weight resulted in polymers with mechanical strength comparable to pure PCL. Bramfeldt et al. found that inclusion of the PEG block increases hydrophilicity, increasing water absorption and hydrolysis, as well as stabilising mechanical strength during degradation [98].

Other authors have also investigated PLLA-PEG copolymers for applications where increased mechanical strength is required. Hu et al. in 1994 studied PLLA-PEG copolymers with PEG content of up to 18 wt.%, concluding that PEG addition increases both hydrophilicity and degradation rate. The increased degradation rate was attributed to a greater rate of ester cleavage at the link between PEG and PLLA blocks [99]. In 2005 Lee et al. examined similar PLLA-PEG copolymers, with PLLA/PEG mole ratios from 6:1 to 0.9:1, and found that addition of PEG increased the water absorption, flexibility and hydrophilicity of the material [100].

2.1.1.5 PEG short chain functionalisation

Recent work by Cameron et al. in the author's research group at the University of Cambridge, in collaboration with the group of Wang et al. at University College Dublin, has investigated functionalising PLLA, PCL and PLCL copolymers with very short PEG end groups [101–104]. In contrast to earlier work discussed in section 2.1.1.4, these polymers typically contain around 1 mol.% PEG, a much smaller proportion than previously tested in these copolymers.

PLLA functionalised with PEG groups of length 550 - 5000 Da was tested, with the addition of PEG groups decreasing T_g by 10 - 15°C, and increasing water absorption and mass loss during degradation. PEG groups also appear to enhance chain mobility, encouraging crystallisation during degradation [101]. Similar results were seen when fuctionalising PLCL copolymers with 550 Da PEG groups - reduced T_g (in most cases), increased degradation rate, and a greater tendency to crystallise. This work included mechanical tests, and found that PEG addition increases ductility for all copolymer compositions except 100% PLLA [102, 103].

2.1.2 Resorbable polymer blends

As discussed above, polymer properties can be effectively tuned by synthesising new polymers using copolymerisation or functionalisation. Despite this, polymer blending is a common alternative technique used to combine two different polymers to achieve a desired set of properties. This method is made more attractive by its ease of use and cost-effectiveness, allowing material properties to be customised quickly and relatively cheaply. In addition, regulatory frameworks that require approval of any new materials, especially for medical applications, can make blending of already-approved materials a favourable option.

When considering polymer blends for any application, the miscibility of the components is of critical importance. The miscibility of a polymer blend can be determined using the Gibbs energy of mixing (ΔG_m) which is given by Eq. 2.1 [105, 106]:

$$\frac{\Delta G_m}{RT} = \frac{\phi_1}{X_1}\ln(\phi_1) + \frac{(1-\phi_1)}{X_2}\ln(1-\phi_1) + \phi_1(1-\phi_1)\chi \tag{2.1}$$

where R is the ideal gas constant, T is temperature, ϕ_1 is the volume fraction of component 1 in the mixture, X_1 and X_2 are the degrees of polymerisation of components 1 and 2, and χ is the Flory-Huggins interaction parameter which accounts for enthalpy change upon mixing. In this way the miscibility is sensitive to both entropic effects, where smaller polymer chains are more miscible, and enthalpic effects, where small changes in the structure of the polymer macromolecule can shift the balance in either direction [107].

The result of these effects is that many polymer blends form immiscible, two-phase mixtures. This is often clearly observed using DSC (Differential Scanning Calorimetry), where distinct glass transitions are seen for each of the separate phases [108–112]. In many cases compatibilisation of immiscible blends is desirable, to provide improved interfacial adhesion and finer dispersion. Compatibilisation strategies include addition

of a component miscible with both phases, addition of a copolymer where different parts of the copolymer are miscible with each phase, and modification of one polymer component to develop locally miscible regions [107].

Depending on the composition, two-phase polymer blends can develop a range of morphologies including dispersed spheres and cylinders, as well as co-continuous structures including double-diamond and gyroidal structures [113]. A critical phenomenon known as phase inversion occurs around the centre of the composition range, where a change in composition results in the continuous and dispersed phases switching, which can have significant effects on various properties [107, 113].

For medical applications, and in particular for cardiac stents, blends based on PLA are of primary interest, due to the strength and bioresorbability provided by PLLA. Its brittle nature at room temperature is a significant drawback however, leading to efforts to develop tougher bioresorbable polymers via blending. In addition, the slow degradation rate of PLLA can be undesirable for medical applications, where the implanted device should be replaced by native tissue or resorbed within a certain healing timeframe [114].

2.1.2.1 PLA/PCL blends

Initial works by Seppälä et al. on blends of PLLA with PCL found that this system formed an immiscible blend, and that addition of the weaker, more ductile PCL to PLLA reduced the elastic modulus and yield strength, and increased the ductility [115]. Similar results were observed by Tsuji and Ikada, and Sarasua et al. from investigations of blends of PCL with PLLA and PDLLA [112, 116]. In general, PLA/PCL blends are observed to form a dispersed droplet morphology, and assessment of polymer crystallisation behaviour has shown that addition of PCL reduces the ability of PLA to crystallise [112, 117, 118].

Recent work by Navarro-Baena et al. has demonstrated that during hydrolytic degradation, PCL loses mass more quickly than PLLA due to chain scission of end groups into soluble fragments, leading to slow reduction of molecular weight and constant mass loss. By contrast PLLA undergoes scission of the main polymer chain, leading to faster reduction of molecular weight but without mass loss [119]. Due to the immiscible nature of PLA/PCL blends, it has been shown that individual components in the blend follow the same mechanism as they do in their pure state, indicating that no interaction takes place between the degrading components. As a result, addition of PCL to PLLA is generally seen to reduce the rate of molecular weight reduction by hydrolysis [115, 119].

Slouf et al. found that the properties of these PLA/PCL blends are very sensitive to the processing and subsequent microstructure of the two-phase mixture. They developed processing techniques involving melt-mixing and selection of melt viscosity to control the phase microstructure of these immiscible blends. This resulted in PLA/PCL blends (80/20 composition) with submicron PCL droplets dispersed within a PLA matrix, resulting in greatly increased toughness (>16× greater than pure PLA) without significant reduction in stiffness [120–122].

2.1.2.2 PLA/PLCL blends

Despite the advances made in developing PLA/PCL blends to achieve suitable properties for biomedical applications, these materials have not found widespread use as cardiac stent materials. Although the addition of PCL improves the toughness and ductility of PLA, useful for crimping and expansion with decreased likelihood of fracture, it also leads to reduced strength and increased degradation time, both of which are unsuitable for stent materials [35]. In order to improve miscibility with PLA, and thereby achieve superior properties, blending with a PLCL copolymer has been utilised by a handful of authors.

Early work was again carried out in 1996 by Seppälä et al., blending PLLA with a PLCL copolymer (49/51 LA/CL mass ratio). These blends showed good miscibility due to the presence of the LA component in the copolymer, and the addition of PLCL had a similar effect on mechanical properties as PCL, reducing the yield strength and elastic modulus, while increasing the toughness and ductility [115]. Contrary to blends with PCL, addition of PLCL to PLLA accelerated the hydrolytic degradation process. Later Park et al. studied the structure and degradation of PLA/PCL blend systems compatibilised with PLCL, finding that PLCL enhances the compatibility of this usually immiscible blend [123, 124]. The addition of PLCL also increased the rate of hydrolytic degradation of PLA/PCL blends, with a random copolymer compatibiliser having a larger effect than a block copolymer.

More recently, in 2015 Wang et al. utilised PLLA/PLCL blends for production of nanofibrous scaffolds for engineering blood vessels [125]. Here the reduced modulus and increased ductility observed when PLCL is blended with PLLA was advantageous for mimicking the mechanical properties of native blood vessels, and heparinised PLLA/PLCL blends exhibited good haemocompatability and anticoagulant activity. Further work in 2018 by Sarasua et al. focused on blends of PLLA with PLCL (70/30 LA/CL molar ratio) [109]. Here PLLA and PLCL were found to be partially miscible (miscible for $\leq$ 30 wt.% PLCL) after melt processing but immiscible after athermal processing such as precipitation and solvent casting. The authors suggested an explanation for this miscibility behaviour involving the formation of a third, compatibilising component, formed by a transesterification reaction of PLLA and PLCL in the high temperature molten state. The findings here on the mechanical properties of PLLA/PLCL blends were also consistent with previous works, observing a reduced yield strength and elastic modulus upon addition of PLCL to PLLA, along with increased ductility.

To date these blends of PLLA and PLCL have not been frequently studied, however their properties show significant promise for biomedical applications, specifically for

bioresorbable cardiac stents. The improved toughness and ductility compared with pure PLLA is important for reducing the likelihood of fracture during crimping and expansion, and the miscibility and accelerated degradation compared with both pure PLLA and PLLA/PCL blends can facilitate degradation within a more appropriate physiological timescale [35, 36].

2.1.2.3 Blends with PEG copolymers

As described previously in sections 2.1.1.4 and 2.1.1.5, incorporating a PEG component into a bioresorbable polymer is a popular and useful technique for tuning its properties, especially those relevant for biomedical applications. These can then be blended with other more conventional biopolymers to achieve easily tunable properties.

In 2002 Na et al. investigated blends of PLLA and PDLLA with a PCL-PEG block copolymer, finding that the PEG component of the copolymer is miscible with PLA, while the PCL component is not miscible [126]. This allowed PCL-PEG to be used as a compatibilising agent in blends of PLA and PCL to improve increase the toughness and ductility while reducing negative effects on the yield strength and modulus.

Kim et al. studied the effects of blending PLLA-PEG copolymers with PLLA in 2011 [127]. The copolymers contained $\sim$ 20 mol.% PEG, and were blended with PLLA with a copolymer:PLLA weight ratio of 90:10. Addition of PEG in this way decreased the tensile strength and modulus slightly, reducing the glassy character of the PLLA. The copolymer addition also increased the swelling of the blended polymer films due to the increased hydrophilicity of PEG.

The PEG-functionalised PLCL copolymers investigated by Cameron et al. and Wang et al. (section 2.1.1.5) have also undergone limited testing in blends with commercial PLLA, with selected results shown in Fig. 2.6 [103]. The mechanical properties

of these blended polymers are more appropriate for load bearing applications such as cardiac stents, with blends in the middle of the composition range displaying relatively high strength as well as good ductility. Although the copolymer used for blending contains 70% lactide, they are seen to be immiscible with pure PLLA [103]. This is most likely due to the high molecular weight of the polymers used. This immiscibility is theorised to provide an optimal combination of properties under body conditions, with the different phases each in their glassy and rubbery states (below and above T_g) at 37°C.

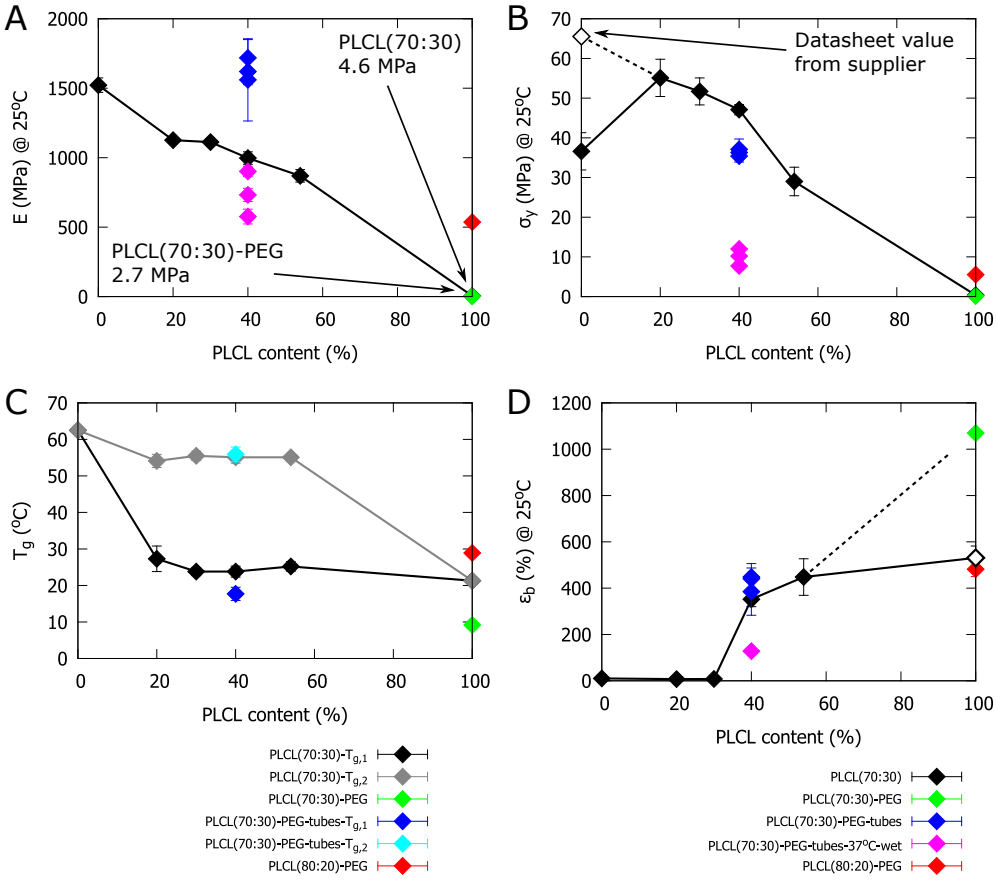

Fig. 2.6: Mechanical and thermal data for PLLA:PLCL and PLLA:PLCL-PEG blends. (A) elastic modulus, (B) yield stress, (C) glass transition temperature(s), and (D) elongation at fracture - open black marker represents sample that slipped rather than fractured. Dotted line represents possible ε_f for true fracture. Figure created from data from Cameron et al. [103]

2.1.3 Polymer structure and properties

Bioresorbable polymers such as PLLA undergo hydrolytic degradation in an aqueous environment, allowing them to be resorbed into the body. Understanding the mechanisms of this degradation is important to controlling the degradation process, and designing materials with a desired lifetime. The microstructure of these polymers is also of critical importance, as this determines many of the relevant mechanical properties for medical applications. Polymer degradation and microstructure are also closely linked, with changes in microstructure affecting degradation behaviour. Conversely, microstructural changes can be induced by hydrolytic degradation, as well as by simple ageing and other changes that occur over time. This section will explore factors affecting PLLA degradation, the polymer microstructure, and the relationship between these.

2.1.3.1 Degradation rate and mechanisms

When immersed in an aqueous solution, aliphatic polyesters including PLA undergo hydrolytic degradation. Initially water uptake occurs with water diffusing into the polymer, with Fickian diffusion kinetics [128]. Although this occurs from the outside in, any heterogeneity in water concentration across the material is usually evened out after several days [129]. This is relatively fast compared with the overall degradation rate, therefore the hydrolysis of ester bonds is typically considered to begin homogeneously across the material from the start of immersion. As degradation proceeds, oligomers with carboxylic end groups are produced, which autocatalyse the hydrolysis reaction [72]. Mass transport of soluble oligomers then becomes important, with those close to the surface able to leach out easily. Those inside the matrix cannot easily diffuse out so remain in place, increasing the concentration of these acidic groups in the centre and accelerating the autocatalytic hydrolysis reaction. This results in the formation of a "skin" on the outside of the polymer, the thickness of which depends on various factors including the diffusion and hydrolysis rates [129]. This phenomenon is summarised in Fig. 2.7.

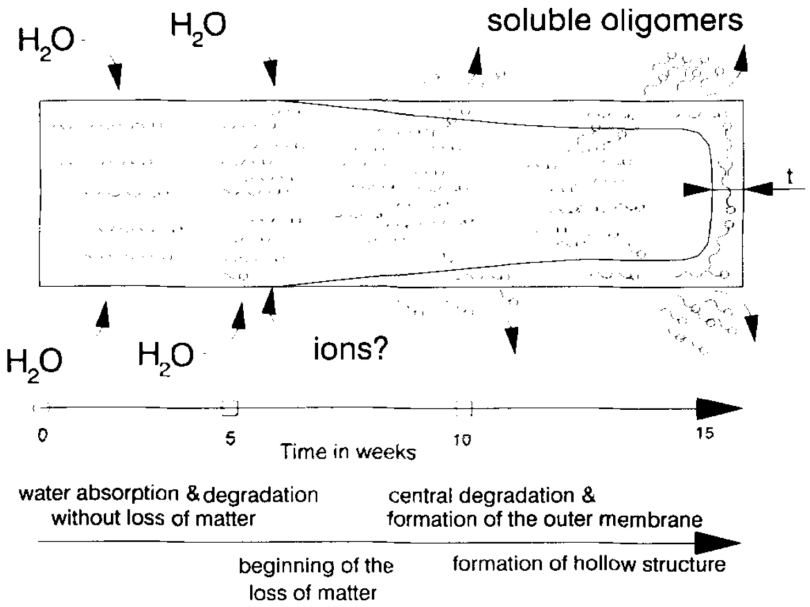

Fig. 2.7: Schematic diagram of the water uptake, reaction, and diffusion effects occurring during hydrolytic degradation of bulk polymers. Figure reproduced with permission from Elsevier [129].

Molecular weight reduction via this autocatalytic mechanism can be described by Eq. 2.2, where $M_n(t_1)$ and $M_n(t_2)$ are the (number average, g mol^{-1}) molecular weights of the polymer after hydrolysis times of t_1 and t_2 respectively, and k is the hydrolysis rate constant [130, 131].

$$ln\ M_n(t_2) = ln\ M_n(t_1) - kt \tag{2.2}$$

Values of the hydrolysis rate constant k for PLLA degradation in conditions commonly used to simulate *in vivo* degradation (immersed in PBS at 37°C) typically range from 3 - 7 $\times 10^{-3}$ day^{-1} [131]. The work of Tsuji and Ikarashi in 2004 further explored the effects of different factors on this hydrolysis rate. Significant dependence on hydrolysis temperature was seen, with increased temperature accelerating hydrolysis, consistent with Arrhenius-type behaviour up to 97°C [132]. The solution pH also has an effect on the hydrolysis rate, with hydrolysis being slowest at pH 7, and then increasing when the pH is modified away from this value [133]. Hydroxide and hydronium ions were found to have a catalytic effect on PLLA hydrolysis, with the effect of hydroxide ions being two orders of magnitude greater than the effect of hydronium ions.

Since 2008 a more sophisticated model has been developed and refined by J. Pan et al., describing the reduction in molecular weight and mass loss by accounting for various types of hydrolysis and mass transport phenomena. These include noncatalytic and autocatalytic end scission, and noncatalytic and autocatalytic random scission, as well as oligomer production and diffusion, and surface and interior erosion [134–136]. These models have also been modified to incorporate the crystallisation of PLLA which has been observed to occur during degradation as a result of scission providing additional mobility for polymer chains to crystallise [137]. The work of J. Pan et al. in developing and validating this model has uncovered several interesting aspects of the interaction between crystallinity and degradation. Crystallisation typically occurs much faster than hydrolysis, resulting in a crystalline phase that is much more resistant to hydrolysis than the original amorphous phase. Despite this, it has been shown that in the semi-crystallised polymer the amorphous chains between crystalline lamallae (trapped within the spherulite) degrade significantly faster, and in a more autocatalytic fashion than those outside the spherulite within an extended amorphous phase [137–139].

2.1.3.2 Structure and structural changes

The crystallisation of PLLA can result in several different structures, with α, α', β, and γ crystalline phases, as well as a stereocomplex between PLLA and PDLLA all having been reported [140–148]. The α form is the most stable and commonly observed during degradation, and can be described by an orthorhombic unit cell with lattice parameters (a, b, c) of 10.683, 6.170, and 28.860 Å.

Other structural changes can occur in polymers such as PLLA over time; one such process is enthalpy relaxation, sometimes referred to as ageing (although this term is also sometimes used to describe any structural changes that occur over time, including crystallisation). After thermal processing and cooling to below its T_g, polymer chain mobility is slowed and the material is characterised as an amorphous glassy

polymer - unless cooling is slow enough for crystallisation to occur. The glassy state is thermodynamically unstable and will slowly rearrange to reach equilibrium even at temperatures below T_g, reducing the free volume between polymer chains [149]. This rearrangement can be observed in DSC as an increase in the endothermic peak just after the glass transition, which represents additional energy that must be supplied during the glass transition, due to the fact that polymer chains have lost energy to their surroundings during relaxation to a lower energy state. This process also results in a higher T_g due to the reduced free volume and increased intermolecular interactions [150–153]. Both of these effects can be observed during extended ageing in Fig. 2.8. These rearrangements can also have a significant effect on the polymer properties, in particular the mechanical behaviour. In 2007, P. Pan et al. conducted a comprehensive study on the effect of enthalpy relaxation on quenched PLLA [51]. The ductility was seen to significantly decrease, while the yield strength and elastic modulus increased after ageing as shown in Fig. 2.8. This was correlated to conformational changes and closer packing in the aged polymer, decreasing chain mobility.

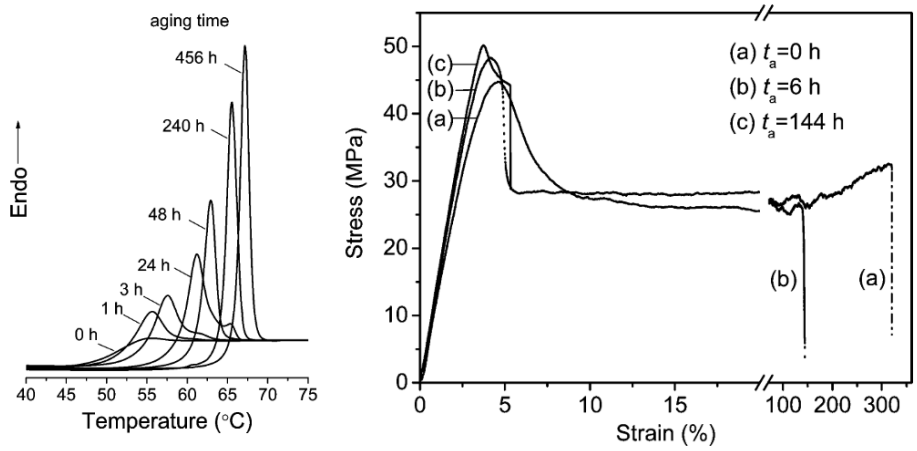

Fig. 2.8: Left: DSC curve showing the glass transition region for PLLA samples aged at 40°C for the time indicated. Right: Tensile stress-strain curves for unaged PLLA and PLLA aged at 25°C for the time indicated. Figures reproduced with permission from [51], copyright © 2007, American Chemical Society.

2.1.3.3 Hydration and mechanical properties

Although medical applications such as cardiac stents require material service conditions of elevated temperature (37°C), and hydration with body fluid, there is a dearth of evidence on the effect of these conditions on the mechanical properties of PLLA. It is sometimes assumed that provided the service temperature does not exceed the T_g, then properties measured in ambient conditions can be easily translated to *in vivo* conditions, however this has proven not to be the case. Tensile testing of PLLA in the dry state at various temperatures demonstrated large changes in mechanical behaviour at temperatures close to but lower than the glass transition temperature, with the material exhibiting drawing without yielding [108]. Significant changes in mechanical behaviour were also seen below the T_g as well, with the yield strength continually decreasing as the temperature increased from 10°C, while the strain at break increased.

Vyavahare et al. examined the hydration behaviour of PLLA and the effect this has on the polymer structure using FTIR and DSC, observing that even though the water uptake is low (0.5 - 1 wt.%), the formation of water clusters within the polymer disrupts dipole-dipole interactions between PLLA chains, increasing the free volume and chain mobility [50]. It was also seen that this hydration considerably accelerates the enthalpy relaxation process due to this enhanced mobility, leading to faster ageing and densification than in the dry state. Cameron et al. investigated the mechanical behaviour of PLLA in dry and hydrated conditions, and also found that water has a plasticising effect on PLLA, resulting in changes in the micro-scale mechanism of deformation (formation of new crazes dominates in wet conditions, rather than development of existing crazes why the material is dry) [154]. A reduction in yield stress was observed after hydration from 62.2±1.5 MPa to 53.2±1.7 MPa, however large changes in the bulk mechanical behaviour were not observed, possibly because the testing temperature remained constant throughout. Bobel et al. also conducted tests under a range of temperatures and hydration conditions using solvent cast PLLA films, finding that more plastic behaviour is associated with a higher temperature and a reduced strain rate [49].

2.1.4 Outlook for resorbable polymers

Due to its bioresorbability and relatively high strength compared with other similar polymers, PLLA is likely to remain a major component of any bioresorbable cardiac stent device. In spite of this, it still displays numerous disadvantages that hinder its application in this area and where progress in materials development can be made, namely its brittle nature and slow degradation. Blending with other polymers is a promising technique for tuning polymer properties; and blends of PLLA with PCL have been shown to provide improved toughness and ductility, although these are immiscible and actually increase the degradation lifetime. Blends of PLCL with PLLA have not been investigated as thoroughly but are perhaps more encouraging for this application, as they enable similar toughness and ductility increases, while improving the miscibility behaviour and accelerating the degradation rate as desired.

There is also evidence that incorporating PEG functional groups into the polymer blends, for instance by blending PLLA with PLCL-PEG, can have certain advantages. The good miscibility of PEG with PLLA allows PEG groups to compatibilise blends with PLLA, improving the blend miscibility, and its plasticising effect also increases toughness and ductility without a large reduction in yield strength or elastic modulus. The greater hydrophilicity afforded by PEG also increases water absorption and therefore the hydrolytic degradation rate, essential for allowing resorption of cardiac stents within a desired functional lifetime.

Improvement of material properties by blending is anticipated to improve the degradation behaviour of PLLA, as well as increasing the material toughness and ductility. No improvement in yield strength or elastic modulus is expected, in fact blending PLLA with PCL or PLCL typically reduces these parameters compared with pure PLLA, and careful control of composition and processing is important to minimise this reduction. For successful implementation as cardiac stent materials, the yield strength and elastic modulus require improvement over the properties seen for pure

PLLA, in order to reduce stent recoil and decrease the stent strut size, both of which are associated with an increased restenosis risk. Incorporating an inorganic component such as phosphate glass to produce a polymer-glass composite is one technique for providing the mechanical reinforcement required, where the hard and brittle inorganic phase provides reinforcement to the softer and more ductile polymer matrix. Section 2.2 will provide an overview of relevant literature relating to these bioactive glasses, while section 2.3 will discuss the state-of-the-art for polymer composites.

2.2 Bioactive glasses

2.2.1 Bioglass®

The original bioactive glass (Bioglass®) was developed by Hench et al. in 1969 [155–157]. This was a SiO_2-Na_2O-CaO-P_2O_5 system (Fig. 2.9) which displayed very strong bonding with bone - such that the adhesion strength was stronger than the cohesive strength of bone [156]. Since its invention, Bioglass® has been approved for and used in prosthetic devices such as ossicular reconstruction prostheses (ear bone replacement), dental implants, particulate bone grafting (NovaBone®) and others [157]. A key advantage of this material is its ability to form strong bonds with both hard and soft tissue.

The mechanism of this bonding was a subject of controversy for some time, however it has been revealed that the release of soluble silica and calcia ions, and the subsequent formation of a high surface area hydrated silica/hydroxy carbonate apatite (HCA) on the glass surface is important. This influences adsorption of growth factors and the attachment and differentiation of osteoblasts. The matrix then mineralises and cells are encased in a collagen-HCA matrix within 6-12 days [157].

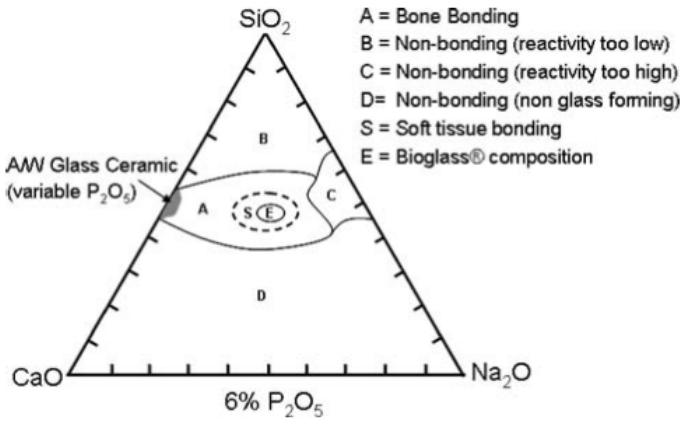

Fig. 2.9: Compositional diagram for bone-bonding biactive glasses. Region S is a region of Class A bioactivity where bioactive glasses bond to both bone and soft tissues and are gene activating. Region C is a region where glasses do not bond and are resorbable. Figure reproduced with permission from Springer Nature [157].

Although some compositions in this system are bioresorbable (region C, Fig. 2.9), these are typically resorbed too quickly (within 10 - 30 days of implantation [158]) to be of use for resorbable load bearing implants.

2.2.2 Phosphate glasses

In order to overcome the limitations of silica-based glasses, much work in recent years has focused on phosphate-based glasses, in particular the P_2O_5-CaO-Na_2O system. This has been led by the research groups of Abou Neel, Ahmed and Knowles at University College London, and Rudd, Scotchford and Walker, and later Ahmed, at the University of Nottingham.

2.2.2.1 Phosphate vs. silicate glasses

Phosphorus and silicate glasses both use a tetrahedral unit as the main building block, however the PO_4^{3-} unit has some crucial differences to the SiO_4^{4-} unit. In comparison to silicon (4^+), phosphorus has a 5^+ charge, meaning that when forming a tetrahedral network one of the P-O bonds is a double bond (i.e. a terminal rather than a bridging

oxygen atom). This limits sharing of oxygen atoms and decreases connectivity and therefore rigidity [159].

These phosphate tetrahedra are classified according to the number of oxygen atoms shared with neighbouring phosphorus atoms, known as bridging oxygens. These are labelled using Q^i, where i is the number of bridging oxygens, and can vary from 0 to 3, as shown in Fig. 2.10 [159, 160]. Pure vitreous P_2O_5 contains only Q^3 tetrahedra, while the addition of modifying oxides reduces the number of bridging oxygens and therefore changes the dominant Q^i species according to $Q^3 \rightarrow Q^2 \rightarrow Q^1 \rightarrow Q^0$ [159–161].

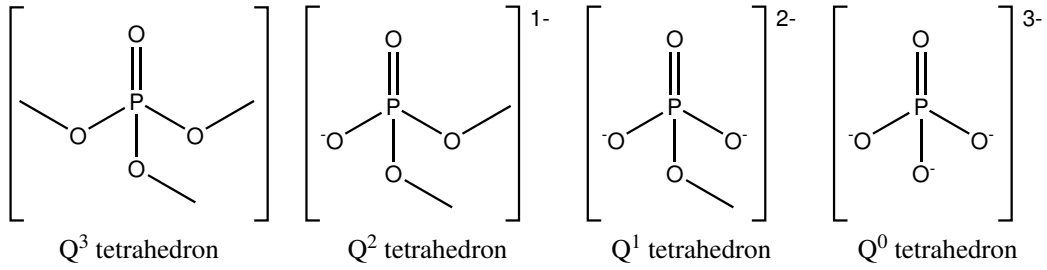

Fig. 2.10: Nomenclature and representation of phosphate tetrahedra with different polymerisations [159].

Pure vitreous SiO_2 glass is chemically stable, but pure P_2O_5 glass by contrast is not - it is vulnerable to hydrolysis of the P-O-P bond by atmospheric moisture, giving it a hygroscopic nature [159, 160, 162]. In order to reduce its tendency to hydrolyse, metal oxides are often added to phosphate glasses to improve chemical stability, as the P-O-M^+ bonds (where M is a metal cation) are more stable than P-O-P bonds with regards to hydrolysis [159]. Although the solubility of the phosphate species makes it less chemically stable than silicate glass, this solubility is responsible for the formation of the apatite layer when Bioglass® bonds to bone, leading to strong bone bonding [159, 163].

2.2.2.2 Composition effects on dissolution

The ternary P_2O_5-CaO-Na_2O system was first developed by Uo et al. in 1998 [164] - these have P_2O_5 content around 50 mol.% or higher. They characterised the dissolution rate of these phosphate glasses, and the dependence on composition [164], finding that CaO content has a large effect on the dissolution rate. This is illustrated in Figure 2.11, and was verified in further studies by Knowles et al. [165].

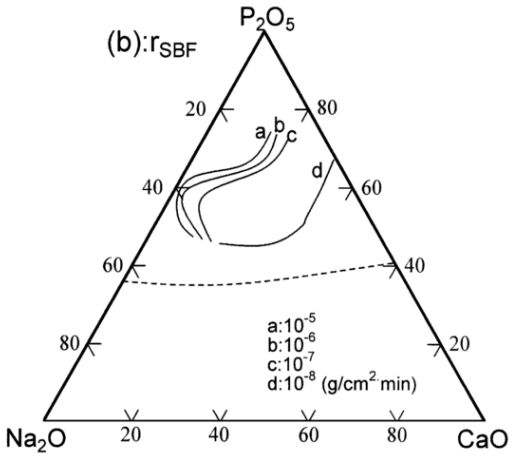

Fig. 2.11: Dissolution rate of ternary phosphate glasses in SBF at 37°C. Figure reproduced with permission from Elsevier [164].

Nazhat and Knowles et al. investigated the effect of Fe addition to phosphate glass in the $(P_2O_5)_{50}(CaO)_{30}(Na_2O)_{20-x}(Fe_2O_3)_x$ system, where $x = 0 - 5$ [166]. Addition of Fe_2O_3 increased the hydrophobicity, and reduced the degradation rate from $\sim 2.7 \times 10^{-6}$ to $\sim 4.5 \times 10^{-8}$ g/cm^2.h. In 2006 Walker and Rudd et al. also examined the effect of Fe_2O_3 addition, along with MgO and CaO [167]. It was found that addition of these metals reduces the dissolution rate, and that the effect increases according to Fe > Mg > Ca, as shown in Fig. 2.12.

Multiple quaternary systems based on the P_2O_5-CaO-Na_2O ternary system have been studied. Knowles et al. investigated addition of K_2O, and replacement of Na_2O with K_2O. This greatly increased the dissolution rate, in some cases so much that biocompatability studies were not possible [159, 168].

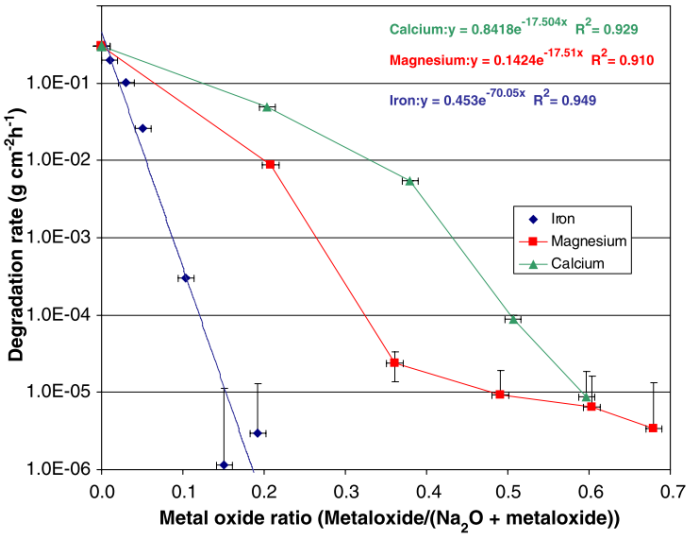

Fig. 2.12: Variation in degradation rate of phosphate glasses with respect to increasing metal oxide content. Figure reproduced with permission from Elsevier [167].

Quaternary $(P_2O_5)_{45}(CaO)_{32-x}(Na_2O)_{23}(MgO)_x$ systems were studied by Knowles et al., substituting MgO in place of CaO. This decreased the degradation rate as expected from the results of Walker and Rudd et al. [167, 169]. Further studies by Walker and Rudd et al. on the addition of MgO in these quaternary systems indicates that high MgO content (30%) makes the glass more prone to devitrification, but even low amounts of MgO (10%) can reduce the dissolution rate by about 10 × [170].

Knowles et al. examined the effect of ZnO in the $(P_2O_5)_{50}(CaO)_{40-x}(Na_2O)_{10}(ZnO)_x$ system, finding that it increases the degradation rate and surface hydrophilicity [171, 172]. The effect of addition of TiO_2 has also been studied by Knowles et al., in the composition range $(P_2O_5)_{50}(CaO)_{30}(Na_2O)_{20-x}(TiO_2)_x$, where $x = 1, 3, 5$. TiO_2 addition has a stabilising effect on the glass structure, forming chain terminating rather than chain extending groups, resulting in slower dissolution [171, 173–176].

In 2013 Walker and Rudd et al. characterised the dissolution behaviour of the phosphate glass system commonly used in their polymer composites (see section 2.3) - $(P_2O_5)_{45}(MgO)_{24}(CaO)_{16}(Na_2O)_{11}(Fe_2O_3)_4$. The dissolution rate was found to be

between 2.9×10^{-6} and 4.8×10^{-8} g/cm^2.h, depending on the dissolution time (dissolution slowed after around 2 days) [177].

2.2.2.3 Biological effects

Much of the research into the biological effects of phosphate glasses has focused on their potential application as hard tissue (i.e. bone) implants, as their mechanical properties make them a natural choice for this application. Phosphate glasses are only considered for use in stents when part of a composite with a polymer, therefore their biological effects in this context will be discussed in section 2.3. Here I will briefly discuss the biological effects of phosphate glasses when used as an implant in isolation.

The dissolution rate of phosphate glasses has been seen multiple times to be closely linked to the biocompatibility of the material. In order to support cell adhesion and survival, the glass surface must have an appropriate dissolution rate - if it dissolves too fast, the surface is too unstable for physical bonding [178–181]. The addition of different metal oxides can also be used to control the biological effects of the glass, with MgO and TiO_2 having a beneficial effect on cell attachment, proliferation, and viability [169, 172], while addition of ZnO does not promote cell adhesion [171].

Due to their solubility, phosphate glasses have been heavily investigated for use as controlled release glasses, where the dissolution of the glass is used to release a certain ion or ions, to elicit a desired effect from the host system. Some key examples of this are the use of phosphate glasses doped with Cu, Co and Se to treat trace element deficiencies in animals [182, 183], and those doped with Cu, Ag or Ga for their antibacterial effect, to prevent infection [184–189].

In the use of phosphate glasses, the dissolution products are of crucial importance. The release of ionic dissolution products such as calcium, silica, phosphate, and sodium

ions from bioactive glasses can have a significant impact on the biological response, increasing production of certain growth factors and osteoblast activity, however dosage is important, as too high an ionic concentration can be toxic [155, 173]. In addition to calcium and phosphate ions, other components can be included in phosphate glasses that play a role in bone formation, including zinc, magnesium, strontium, titanium and boron [173, 190, 191]. As mentioned above, copper has been incorporated into phosphate glasses for its antibacterial effect, however it is also known to play a role in angiogenic processes [173, 192–195]. It is therefore conceivable that copper delivery from phosphate glasses could be used to promote vascularisation, although as yet this has not been tested [173, 193].

There is also evidence that the presence of extracellular pyrophosphate ions ($P_2O_7^{4-}$) plays a major role in preventing vascular calcification. The work of Villa-Bellosta et al. has demonstrated that synthesis of calcification inhibitors is the main mechanism by which cells can prevent vascular calcification (i.e. formation of hydroxyapatite). Pyrophosphate ions are one of the main inhibitors of calcification, and act by binding directly to nascent hydroxyapatite crystals, preventing further crystal growth [196–199]. Although they are not the final product of the complete phosphate glass hydrolysis reaction (Eq. 2.4), release of these ions during dissolution prior to complete hydrolysis has been observed [176, 200]. These are promising results, and suggest that phosphate glass composites could be used to provide a slow release of pyrophosphate ions from a cardiac stent, suppressing vascular calcification and improving the long-term outcomes of cardiac stent implantation.

2.2.2.4 Dissolution mechanics

The dissolution of phosphate glasses in aqueous media is known to depend on a variety of factors, including the glass composition, solution pH, temperature, and solution concentration [201–203]. The work of Bunker et al. in 1984 was one of the first to investigate

the dissolution mechanisms of these glasses, utilising the $(P_2O_5)_{50}(CaO)_x(M_2O)_{50-x}$ system (where M is Li or Na) [201]. They proposed that phosphate glass dissolution in water occurs by two interdependent steps, hydration and hydrolysis, as shown in Eqs. 2.3 and 2.4 respectively.

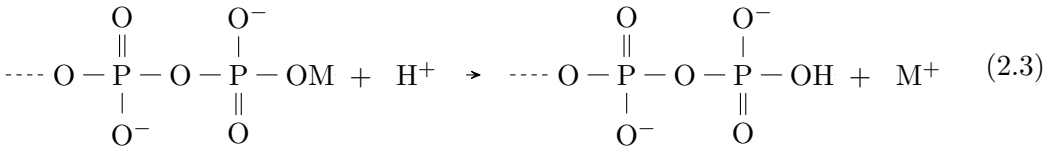

(2.3)

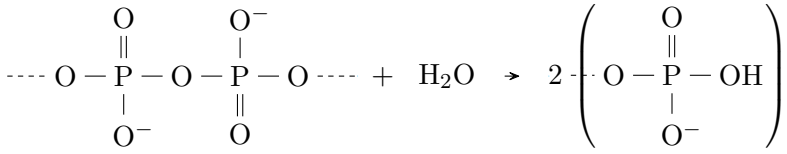

(2.4)

The hydration reaction involves ion exchange where the glass exchanges metal cations (often Na or Ca) with the hydrogen ions in water, forming a hydrated layer on the surface [201, 204]. The hydrolysis reaction by contrast is a network breakage reaction, where the P-O-P bonds in the hydrated layer undergo cleavage by hydrogen ions and water molecules, breaking down the phosphate glass network into chains of differing lengths [202]. When all bridging oxygen bonds (P-O-P) have been hydrolysed, orthophosphate ions can dissolve directly, however polyphosphate ions can also be released into solution before undergoing complete hydrolysis [176, 200].

Bunker et al. also identified two distinct regimes of dissolution kinetics, with an initial period where weight loss is a function of $t^{1/2}$, and a second stage where weight losses are linear with time [201]. This phenomenon was also corroborated by other authors [200, 205], however Delahaye et al. did not observe this and suggested that the $t^{1/2}$ dependence seen was a result of increasing ionic strength in the solution during the early stages of dissolution [163]. The effect of the ion exchange reaction that is theorised to occur during this kinetic regime has also been debated, with Gao et al. proposing that diffusion of water molecules into the bulk glass is the rate limiting step in formation of the hydrated layer, rather than ion exchange [203].

The formation of this hydrated layer is generally accepted, however its nature is also subject to uncertain evidence. Delahaye et al. reported that the composition and structure of the hydrated layer was the same as in the pristine glass [163], while Massera et al. demonstrated that the hydrated layer consists of various crystalline metal salts, depending on the glass and solution composition [204]. In the original work of Bunker et al. the nature of the hydration layer was not described, although an alteration layer composed of hydroxyapatite crystals was observed [201]. It is clear that the existing literature on the mechanisms of phosphate glass dissolution still leaves some questions remaining.

Observations of the effects of different parameters on the glass dissolution rate are also valuable for assessing dissolution behaviour. The effect of solution pH has been described in a number of studies, finding that modification of the pH away from a neutral value of 7 accelerates the dissolution process [163, 201, 204], while increases in temperature are seen to increase the dissolution rate consistently, according to an Arrhenius relationship [200, 203, 205]. The solution concentration can also play a significant role, with increased ionic concentration reducing the dissolution rate [163, 203].

2.2.2.5 Dissolution rate models

When characterising phosphate glasses for resorbable implants, accurate measurement of the dissolution behaviour is key. Much of the research carried out on phosphate glasses in recent (since the early 2000s) years reports dissolution rates in $g.cm^{-2}.h^{-1}$, assuming a linear weight loss with time (i.e. zero-order release), in spite of the fact that weight loss is often non-linear [177, 206]. Indeed, it was shown by Bunker et al. as early as 1984 that phosphate glasses (in the $(P_2O_5)_{50}(CaO)_x(M_2O)_{50-x}$ system, where M is Li or Na) show non-linear dissolution, with a first stage where weight loss is a function of $t^{1/2}$, and a second stage where weight losses are linear with time [201].

In 2017 Ma et al. built on the work of Bunker et al. and used a two-stage model to describe the dissolution of phosphate glasses [205]. Here the first stage is controlled by 3D diffusion, involving penetration of H_2O into the glass and diffusion of ions through the hydrated layer back into solution. This can be modelled by Eq. 2.5, where α is the mass fraction dissolved after time t, and k_{DM} is the reaction rate parameter for the diffusion model, assuming spherical particles. This is equivalent to the Jander equation [207–209].

$$1 - (1 - \alpha)^{1/3} = k_{DM} t^{1/2} \tag{2.5}$$

The second stage of the dissolution process is controlled by linear reaction rate kinetics. Here the hydrolysis reaction on the surface is the rate limiting step, so the reduction in surface area as volume decreases determines the mass loss. This can be modelled by Eq. 2.6, where k_{CVM} is the reaction rate parameter for the contracting volume model [208–210].

$$1 - (1 - \alpha)^{1/3} = k_{CVM} t \tag{2.6}$$

An example of this two-stage diffusion and contracting volume model is shown in Fig. 2.13, and it is clear that this more accurately describes the dissolution kinetics than either model alone, or a simple linear (zero-order) weight loss. A physical explanation for the cause of the transition between these two stages of dissolution is not currently known, however Ma et al. have speculated that it may be related to the nature of the alteration layer that forms on the glass surface [205].

2.2.3 Outlook for phosphate glasses

Phosphate glasses are a powerful and versatile technology for biological applications. Their dissolution rate can be tuned over many orders of magnitude by varying the composition, and in addition to their bioactivity, the biological response to these

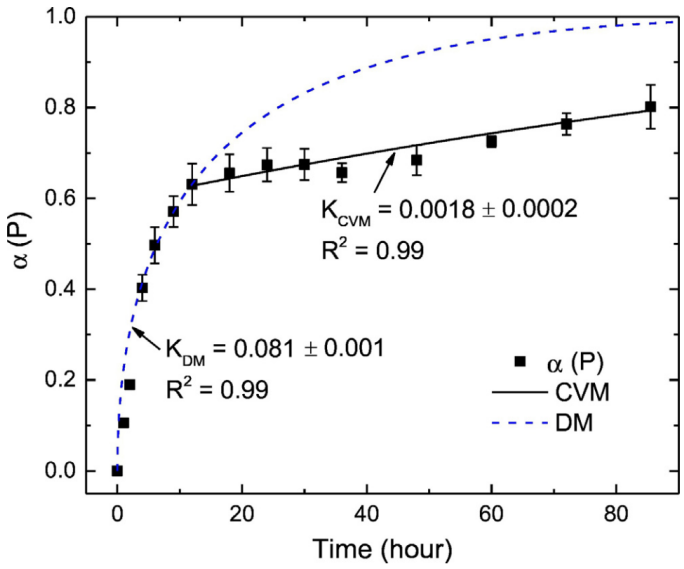

Fig. 2.13: Mass fraction (α) of phosphate glass dissolved during static dissolution test at 60°C, fitted with 3D diffusion model (DM, dashed line) and contracting volume model (CVM, solid line). Figure reproduced with permission from Elsevier [205].

materials can also be controlled by adapting the glass composition. Despite previous work in this area however, there still remain several fundamental questions about the dissolution behaviour of these glasses. Multi-stage dissolution is often observed, however the cause of this transition and the factors affecting it remain unclear. It has been suggested that the hydration or alteration layer may play a role in this transition, but this hypothesis has not been thoroughly investigated. The nature of this layer itself is also subject to conflicting evidence in terms of its structure and composition.

In medical applications, knowledge of phosphate glass dissolution under *in vivo* conditions is crucial to designing effective and safe implant materials. Although simplified environments are preferable for investigations of the multi-stage mechanisms of dissolution, it is important to understand how these mechanisms will behave in their eventual application. Unfortunately, relatively few studies to date have investigated these multi-stage mechanisms under simulated body conditions. For applications of phosphate glass as a reinforcing phase in polymer-glass composites for cardiac stents, knowledge of the dissolution behaviour in more complex environments is also critical.

As well as contributions from body fluid, the degradation of polymers (in this case typically into lactic acid) provides additional complexity to the dissolution environment. In order to apply these materials to polymer-glass composite stents, knowledge of the effect of these more complex environments on the dissolution rate and mechanisms is required.

The influence of pyrophosphate ions, a phosphate glass dissolution product, on vascular calcification, is another promising finding with particular relevance to applications in cardiac stents. This suggests that incorporating phosphate glass into polymer composite stents could provide the additional advantage of suppressing vascular calcification, however this effect has not yet been tested for pyrophosphate supplied by an implanted device.

2.3 Polymer glass composites

2.3.1 Composite processing

2.3.1.1 Solvent methods

Solvent methods are one of the more common methods of fabricating polymer composites with a filler such as phosphate glass. This method typically works by dissolving the polymer in a solvent such as acetone, chloroform, dichloromethane or similar, adding the filler in particulate form and stirring (sometimes with sonication), and then casting films. The films are often vacuum dried at slightly elevated temperature to remove any residual solvent. [211–215].

In order to use this method for composites with nanoparticles of filler, rather than microparticles, Best and Cameron et al. developed a method using attritor milling to obtain an evenly dispersed nanocomposite [216–218]. This involves attritor milling of the filler material in acetone to reduce particle size to the nanoparticle range, gradual

dissolution of the polymer into this slurry, and then similar drying steps to the procedure described above.

Solvent based methods offer a versatile and simple method of producing polymer glass composites, however their drawbacks include use of large quantities of solvent, which can be hazardous and expensive, especially when scaling up production to larger quantities. In addition, it can be difficult to remove all traces of residual solvent from the composite, which can be harmful to cells or tissue, as well having a plasticising effect on the mechanical properties [219]. Although the filler component can be well dispersed into the slurry, particle agglomeration can occur during solvent removal, depending on the drying speed and conditions, leading to inferior properties [220].

2.3.1.2 Melt blending

Melt blending is another popular technique for incorporating a particulate filler material into a polymer composite. This requires the use of an extruder/compounder, which heats the polymer above its melting temperature, and uses the rotation of the screw(s) inside the extruder to mix the filler and polymer together [218, 221–223]. This has the advantage of being a very scalable method that is already widely used industrially, and does not require large amounts of hazardous solvent. The method is not without drawbacks however, requiring expensive, specialised equipment, and involving extended thermal cycling at high temperature combined with shear forces which can degrade the molecular weight of the polymer [224], leading to loss of mechanical properties and degradation resistance [103, 220].

A similar but even more severe effect has been observed during thermal processing of Bioglass®-PDLLA composites, where a reaction takes place at the polymer-glass interface, forming carboxylate salts and leading to significant molecular weight reduction. This in turn leads to a reduction in the mechanical properties of the composite. [225].

This reaction effect has not been observed for composites with phosphate glass, however it is clear that thermal processing of these composites must be carried out carefully.

2.3.1.3 Fibre mat stacking

The fibre mat stacking process has been used extensively by Rudd and Ahmed et al. for making composites using phosphate glass fibres, and is similar to the process used for lay-up of conventional fibreglass that is ubiquitous in many areas of construction (examples include aircraft, boats, swimming pools, water tanks, roofing etc.). Glass fibres are arranged in random or unidirectional mats, which are then stacked alternatively with films of the desired polymer component. The completed stack can then be heated and pressed to form the final composite [226–230].

This process is readily scalable, and the ability to selectively orient the glass fibres is attractive from an engineering standpoint - mechanical properties can be enhanced to withstand stress in a certain direction. This does mean however, that glass fibres do not provide comparable reinforcement in the stacking direction. The process also results in a structure that is somewhat ordered, rather than a well mixed distribution of glass filler within the polymer matrix. One technical difficulty is that the process first requires that the glass used is drawn into fibres, which is non-trivial.

2.3.1.4 In situ polymerisation

Preparation of composites by in situ polymerisation has been developed for fibre composites with a matrix of polycaprolactone. In this method, a reaction mixture containing the monomer and catalyst is added to a mold that contains glass fibres, which is then heated to initiate polymerisation [231–235]. This typically results in very good bonding between the glass and polymer matrix, however good mixing may be difficult if glass fibres are not used. In addition, the process is specific to the exact

polymer matrix used, and would need to be modified for each different polymer, making it inflexible compared with the other techniques discussed. In situ polymerisation methods can also be prone to incomplete reaction, leading to encapsulation of residual unreacted monomer within the composite. This in turn can have an adverse effect on the desired properties, catalysing polymer degradation or weakening the structure [220].

2.3.2 Mechanical properties

Addition of a filler material (such as phosphate glass or other glass/ceramic particle) usually has consistent effects on the mechanical properties of the composite. Typically the elastic modulus is increased [211, 213, 215, 236, 237], which is expected from the comparably higher stiffness of the filler material, and known composite mixing rules [44]. Similarly, a reduction in strain at break (ε_B) is also often seen upon the addition of stiffer particles to the composite [211, 213]. The behaviour of the yield strength is more varied. It could be expected that the addition of particles with higher yield strength would increase the yield strength of the composite [213, 215, 237]. However, the degree of adhesion between the matrix polymer and the particles plays a large role in the yield strength, and therefore it is sometimes that case that if this is insufficient, the yield strength can be decreased by addition of filler [211]. A key parameter to control when the mechanical properties of the composite are important is the dispersion of particles within the composite. Enhancement of strength and stiffness is seen to be directly related to achieving good dispersion within the polymer matrix, and agglomeration generally leads to inferior outcomes. This is also the case for the ductility, where agglomeration of inorganic particles creates larger defects, resulting in reduced strain at break when compared with a well dispersed composite [220].

Significant work has been done by Rudd, Walker and Ahmed et al. on the use of various coupling agents to increase the bonding strength between the polymer matrix and phosphate glass fibres [233]. Coupling agents including HEMA (2-hydroxyethyl

methacrylate), APS (3-aminopropyltriethoxysilane), EA (etidronic acid), HDI (hexamethylene diisocyanate), Mg metal, and sorbitol-ended PLA oligomers are seen to improve the interfacial shear stress between phosphate glass fibres and the polymer matrix, and therefore improve bulk properties such as the elastic modulus and yield strength [234, 238–240]. This improved adhesion between the polymer matrix and glass fibres is also seen to reduce the rate of degradation, possibly by reducing the wicking effect up the fibres, or the effect of the coupling agent making the polymer more hydrophobic. The retention of mechanical properties during degradation is also seen to be improved by the increased adhesion caused by these coupling agents [230, 234, 235, 240, 241].

2.3.3 Degradation behaviour

In addition to the adhesion discussed above, there are a number of factors relating to the composite that affect the degradation behaviour, including the size and morphology of the glass filler, the amount, and the composition of the glass.

2.3.3.1 Size and morphology

Early in the development of composites with bioactive glass, Seppälä et al. used a silica based glass ($(SiO_2)_{53}(Na_2O)_{23}(CaO)_{20}(P_2O_5)_4$) in composites with a PLCL matrix, finding that a smaller particle size increases the rate of degradation, as seen in Fig. 2.14. This was attributed to high water absorption in the composites (possibly due to increased interfacial area), leading to increased polymer hydrolysis [242]. In the work of Rudd, Walker and Ahmed et al., wicking of fluid up the glass fibres along the interface is seen to increase the degradation rate, especially for continuous fibres [230]. It is clear that the size and shape of the glass component in a composite has a significant impact on the degradation properties, via its effect on the interfacial area, which can act as a conduit and reservoir for dissolution media.

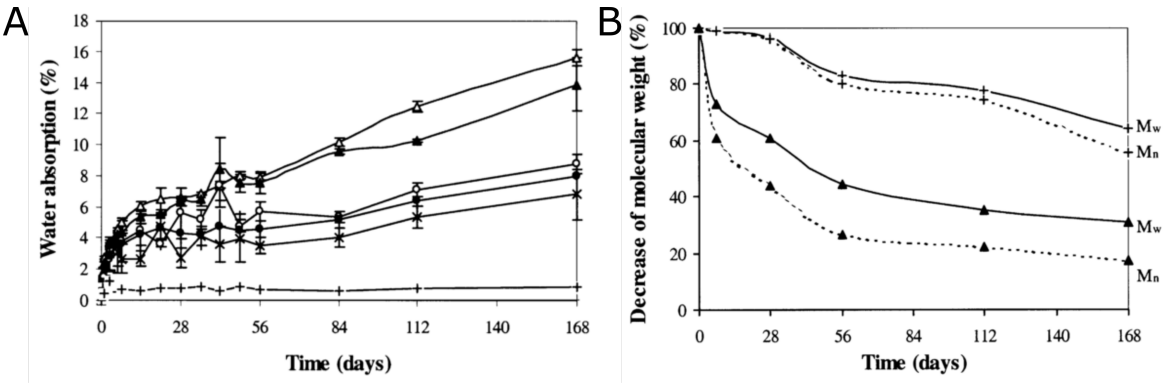

Fig. 2.14: (A) Water absorption in P(CL/DL-LA) (+), and composites BG40S (△), BG60S (▲), BG40L (○), BG60L (●) and BG70L (×). S and L denote small and large particles, and 40, 60, 70 are the wt. % glass content. (B) Changes in average (by number and weight) molecular weights of P(CL/DL-LA) polymer (+) and BG60S composite (▲). Figures reproduced with permission from Elsevier [242].

There is an opposing effect at work as well however, relating to the buffering effect that arises from dissolved filler particles. The work of Best and Cameron et al. on PLGA-αTCP (tricalcium phosphate) composites has shown that smaller particles are more effective at slowing degradation, as they are more soluble and thus display a more effective buffering action [217]. This buffering effect is heavily dependent on the composition of the filler, and will be discussed further in section 2.3.3.3.

2.3.3.2 Particle loading

The amount of filler present in the composite (also known as the loading) is another important factor that determines the degradation properties. The effect of particle loading is dependent on the relative solubility of the polymer and glass components - in many cases the glasses used are more soluble than the PLA/PCL matrix, therefore a greater amount of more soluble glass leads to greater mass loss [230, 242–244]. In cases where the polymer matrix is more soluble, such as with PLGA filled with Si-based glass, a greater amount of less soluble glass leads to lower mass loss [245].

Of more interest is the effect on the molecular weight of the polymer component, but unfortunately on this matter there is little consistent evidence. There is some indication that increased loading of glass reduces molecular weight loss in PLA based copolymers [245–247], but conflicting evidence shows increased loading accelerating molecular weight degradation in PCL based copolymers [242]. In addition, the studies cited here use silicate-based glass rather than phosphate glasses, so it remains to be seen how loading of phosphate glasses affects molecular weight reduction during degradation.

2.3.3.3 Glass composition

The glass composition is one of the most crucial factors in determining the degradation of polymer glass composites. As previously discussed, the composition of the glass directly affects the dissolution rate of the glass, which in turn can affect the weight loss of the composite. However there are also more complex interactions at play, involving the buffering effect that arises from dissolution of bioceramics and bioglasses [246, 248–252]. This is proposed to occur by exchange of protons in water for alkali ions in the glass, resulting in a pH buffering effect at the surface of the polymer [252].

Knowles et al. investigated PCL composites with phosphate glass filler, in the $(P_2O_5)_{45}(CaO)_x(Na_2O)_{55-x}$ system, and found that increased CaO content in the glass leads to a reduced degradation rate [253, 254]. Increased CaO content in phosphate glass is known to reduce the dissolution rate (see section 2.2.2.2), however this is not simply an effect arising from a more slowly dissolving glass, as increased CaO content was also seen to reduce the rate of molecular weight degradation. This does not appear to be the result of increased buffer capacity from the CaO-rich glass however, as the higher CaO glass dissolved slower and thus resulted in a lower concentration of Ca ions in solution. The mechanism of this reduced hydrolysis rate is currently unclear, but may be related to the smaller pH drop that occurs upon from dissolution of high CaO glasses.

A similar study was carried out by Ahmed, Rudd and Nazhat et al., where PCL or PLA polymer matrices were filled with phosphate glass fibres with composition $(P_2O_5)_{50}(CaO)_{40}(Si_2O)_{10-x}Fe_2O_3)_x$ [214, 228, 255]. Phosphate glasses with higher Fe content dissolved more slowly and and reduced solution pH much less (when dissolving in isolation without the polymer matrix) compared with glasses with Si_2O substituted for Fe_2O_3. When incorporated into composites, the higher Fe_2O_3 glass significantly reduced the degradation rate, however in this case no reduction in polymer molecular weight was seen after 56 days degradation.

2.3.4 Biological effects

2.3.4.1 Silicate-based glasses

The biological effects of polymer-glass composites are critical to their eventual application as implant materials, and these effects have been investigated in multiple ways. Boccaccini and Hench et al., as well as Erdemli et al., used osteosarcoma cells to assess the biocompatability of PDLLA and PCL composites filled with silicate-based bioactive glasses [256, 257]. They found that addition of glass to the polymer improved the adhesion and proliferation of these cells. Kim et al. conducted a similar series of studies, investigating the effect of PDLA and PCL composites with silica-based bioactive glass, using preosteoblastic cells to assess the material's suitability for orthopaedic applications [236, 258, 259]. They also observed improved cell growth and proliferation on the composite samples, which also displayed good cell viability, adhesion, and improved differentiation and mineralisation behaviour of the cells.

Boccaccini et al. used bone marrow cells to investigate the biocompatability of PDLLA composites with silicate-based bioactive glass, and also found that addition of glass improved cell differentiation, adhesion, spreading and proliferation [260]. This improvement was greater for composites with 5 wt.% glass than for 40 wt.%, suggesting

that increased ion release from a larger glass content could be cytotoxic. Seppälä et al. and Boccaccini and Hench et al. used fibroblasts to study the biocompatability of PCL and PGA composites with silicate-based bioactive glasses, finding that addition of glass increased fibroblast adhesion [261], and increased vascularisation and secretion of VEGF (vascular endothelial growth factor), a promising result for cardiac stent applications [262]. Examples of increased VEGF secretion from fibroblasts, and vascularisation of tissue around the implant can be seen in Fig. 2.15.

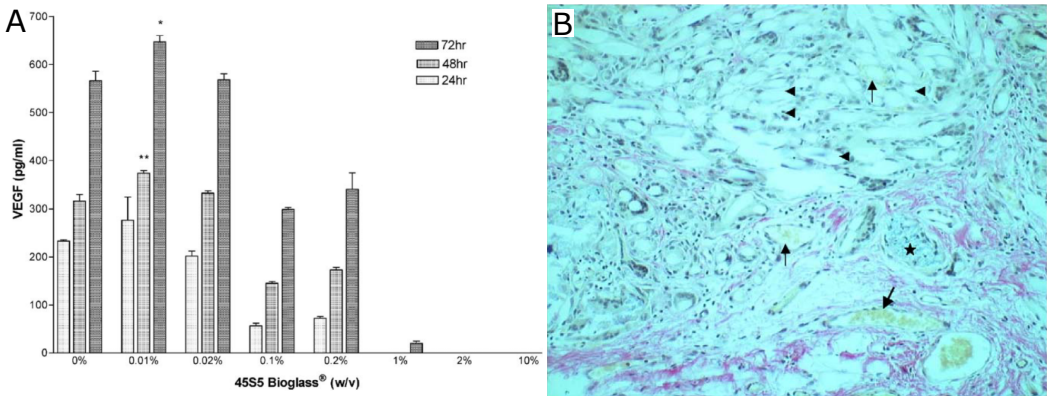

Fig. 2.15: (A) VEGF secretion by fibroblasts grown on cell plates coated with bioactive glass (*p<0.05, **p<0.01). (B) Blood vessels (arrows) with red blood cells present in the lumen are shown throughout the glass ($\star$) -composite mesh (◀) and surrounding tissue after 42 days in vivo. Stained with haematoxylin and van Gieson's stain. Figures reproduced with permission from Elsevier [262].

These results indicate that composites with polyesters and silicate based bioactive glasses are compatible with a wide range of cell types, and can elicit favourable biological responses compared with the unfilled polymer.

2.3.4.2 Phosphate-based glasses

The biocompatability of polymer composites with phosphate glasses has also been investigated by Rudd, Ahmed and Nazhat et al., Kim and Knowles et al., and Navarro et al., using osteoblastic cells [253, 255, 263]. They looked at PCL and PLA composites with phosphate glasses, finding that these composites are cytocompatible and display no adverse effects, and that the addition of glass improves cell viability and proliferation.

This is at odds with other work by Knowles and Nazhat et al., where addition of phosphate glass to PLA was seen to reduce osteoblast proliferation and attachment, however this was attributed to the rapid dissolution of the glass used here [244]. Other results by Rudd and Ahmed support this, indicating that reducing the dissolution rate of the glass in the composite improves the biocompatability by providing a more stable surface for cell attachment [227, 264]. This is similar to the behaviour of phospate glasses when used alone, as described in section 2.2.2.3.

Knowles et al. and Rudd, Ahmed and Nazhat et al. also investigated the effect of altering the glass composition within the composite on biocompatability. Addition of TiO_2 to the glass appeared to improve cell proliferation [265], while addition of SiO_2 did not affect the cytocompatability [228]. Rudd, Walker and Ahmed et al. also assessed the biocompatability of selected coupling agents used to improve interfacial properties of the composite (discussed in section 2.3.2) using osteosarcoma cells, osteoblasts, and macrophages. It was found that interfacial treatments with silane, APS, HDI, Mg metal and sorbitol-ended PLA oligomers were all cytocompatible, and made no difference to the cell activity, attachment, and proliferation [233, 239, 241].

2.3.4.3 In vivo effects

A limited number of in vivo studies have been performed on polymer-glass composites to date. In 1997 Lowry et al. used phosphate glass-PCL composites to repair humerus fractures in rabbits, finding that although the composite caused minimal inflammation, it was not mechanically strong enough for fracture fixation [266]. Erdemli et al. and Kim et al. both tested PCL composites filled with silicate-based bioactive glass as bone implants, finding that these composites displayed good bone ingrowth, which was enhanced for the composite compared with unfilled PCL [236, 257]. The enhanced *in vivo* bone growth for the composite compared with PCL is shown in Fig. 2.16.

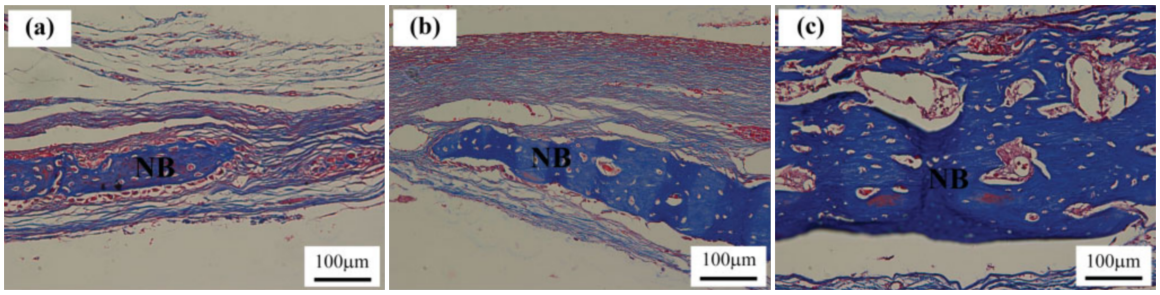

Fig. 2.16: Optical images of newly formed bone near the defect centre showing the empty defect (a), pure PCL membrane (b), and PCL-bioactive glass composite membrane (c). NB denotes new bone. Figures reproduced with permission from John Wiley and Sons [236].

2.3.5 Outlook for polymer-glass composites

Polymer-glass composites have been the subject of considerable research, in particular due to their suitability for orthopaedic applications. A variety of effective composite fabrication methods have been reported, but it remains a challenge to achieve good dispersion of glass particles within the polymer matrix, without encountering other drawbacks such as molecular weight degradation or residual monomer content.

The factors affecting composite mechanical properties are reasonably well understood, with even dispersion being critical, as well as good interfacial bonding between the polymer and glass components. This latter property can be improved through the use of different interfacial layers or treatments, however the effectiveness of this technique has only been demonstrated for glass fibre composites, rather than the dispersed microparticle composites applicable to cardiac stent applications.

The degradation of these composites, and evolution of their properties during degradation must also be considered, and here it is consistently observed that absorption of water by the composite is a critical step leading to loss of mechanical strength. There is significant evidence on the effects of parameters such as glass particle size, particle loading, and composition, however studies are carried out with a large variation in the components used, making it difficult to compare and draw conclusions across the published literature. The effect of glass dissolution on polymer degradation is a

particular issue, where there is little clear evidence, and different polymers and glass compositions appear to have contrasting effects. Further to this, a comprehensive theory of composite degradation, integrating the structure and properties of individual components and how these evolve during degradation, has not been developed. This would be highly advantageous and allow for more informed design of composite materials for medical applications.

Understandably, much of the work assessing the biological performance of polymer-glass composites focuses on their suitability for orthopaedic applications, where the favourable properties of bioactive glasses generally improve their performance (provided the glass does not dissolve too fast). There is some evidence that bioactive glass within a composite improves vascularisation, which could be beneficial for cardiac stent applications, however more testing is needed on the biological performance of polymer-glass composites for cardiac stents.

2.4 Thesis context

From the clinical literature, there is a clear mandate for development of bioresorbable stent materials with improved material properties, to advance bioresorbable stent technology and close the gap with respect to the currently preferred option, drug eluting metallic stents. Increased mechanical properties (stiffness and strength) would decrease the stent recoil experienced, and also allow use of thinner stent strut sizes, reducing the incidence of restenosis. Greater ductility would also improve the materials' performance during crimping and deployment, an important drawback of current PLLA stents. The slow degradation of PLLA is another key limitation for cardiac stent applications that material development can address. Accelerating degradation from the current time of 2 years to around 6 - 12 months would provide a much closer approximation of the body's natural healing time. The evolution of mechanical properties during degradation also

needs careful consideration, to avoid embrittlement as well as rapid loss of strength and stiffness. This thesis aims to address these issues and develop materials with improved mechanical and degradation performance, by utilising several different materials.

A range of polymer blending techniques have been investigated in the literature to adjust the mechanical and degradation properties of PLLA for medical applications. Those incorporating PLCL with PLLA have not been studied thoroughly, but do show particular suitability for stent applications where improvements in toughness and degradation rate are necessary. Incorporating PEG into these blends by functionalisation of PLCL is another emerging technique that shows promise for improving blend miscibility by compatibilising PLLA with PLCL, as well as providing additional toughness and enhancement of the degradation rate. This thesis will investigate blends of PLLA with novel PEG functionalised PLCL copolymers (PLCL-PEG), with the aim of achieving a balance of strength and stiffness with ductility. This method is also hypothesised to allow control of the time-dependent properties of the material, tuning the degradation rate, and evolution of mechanical properties during degradation.

Composites of bioresorbable polymers with bioresorbable glass/ceramic materials have also proven to be an effective technique for improving the mechanical properties of polymeric materials. Much of this work however, has focused on composites designed for orthopaedic applications, which do have somewhat different constraints and requirements to cardiac stents. This thesis therefore, will build upon work carried out on polymer blends, and investigate polymer composites intended for cardiac stent applications. Dispersion of filler particles within the composite has been shown to play a key role in composite performance, so a suitable composite processing method that achieves good dispersion will be developed. Ca-Na-P glasses show favourable dissolution behaviour and provide a good baseline for comparison to other works, as well as exceptional tunability of properties by varying the Ca/P ratio, so these will be incorporated into polymer-glass composites. In this way this work aims to provide

improved mechanical properties compared with pure polymers or polymer blends. By comprehensively investigating the effects of composite composition, this thesis also aims to elucidate the effect of glass dissolution on polymer degradation, as well as pursuing an overall mechanistic theory of the factors affecting composite degradation and its interaction with material properties.

For both polymer blends and polymer-glass composites, a key approach used in this thesis will be to carry out mechanical testing under conditions relevant to the eventual application of the material in bioresorbable stents. This includes testing in dry, ambient conditions, representative of the crimping procedure used to compress the stent onto the catheter before implantation. The subsequent deployment of the stent *in vivo* can also be reproduced by mechanical testing of materials while immersed in body temperature water. The evolution of stent mechanical properties during material degradation is crucial to engineering the transfer of stress to the newly healed tissue, so the mechanical properties will also be assessed at various stages of degradation, in physiological conditions.

In order to properly understand the degradation of these polymer-glass composites and design effective cardiac stent materials accordingly, a good understanding of the phosphate glass dissolution is required. However from a review of the literature it is clear that there is still uncertainty over the different stages of dissolution for these phosphate glasses. This is particularly true for dissolution in more complex environments such as within the body, or within a polymer composite. This thesis therefore, will aim to not only characterise the dissolution behaviour of the glasses produced for incorporation into polymer-glass composites, but also to develop a more complete understanding of the multi-stage dissolution mechanisms of these glasses. This includes analysis of the various factors affecting glass dissolution, as well as investigation of dissolution in a range of different environments.

2.5 Thesis structure

The structure of this thesis is shown in Fig. 2.17, and is as follows:

Background

- Chapter 1 introduces the medical problem of cardiovascular disease, how stents are used to treat this, and the limitations of current stent technology.
- Chapter 2 reviews the current state of the art for materials relevant for bioresorbable cardiac stents, namely bioresorbable polymers, bioactive glasses, and polymer-glass composites.

Bioresorbable polymers

- Chapter 3 describes the production of PLLA:PLCL-PEG blends, and characterises their structure and mechanical properties.
- Chapter 4 presents the results of an *in vitro* degradation experiment of these polymer blends, demonstrating how their structure evolves during degradation, and the effect this has on the mechanical properties.

Phosphate glasses

- Chapter 5 describes the production of a set of P_2O_5-CaO-Na_2O glasses, and characterises their physical and chemical structure and properties.
- Chapter 6 presents the results of an *in vitro* dissolution experiment of these P_2O_5-CaO-Na_2O glasses, and introduces a new dissolution mechanism to understand these results.

Polymer-glass composites

- Chapter 7 describes the development of a composite processing method, and characterises the structural and mechanical properties of the produced composites.

- Chapter 8 presents the results of an *in vitro* degradation experiment of these polymer-glass composites, demonstrating how the composite structure evolves during degradation, and the effect this has on the mechanical properties.

Summary and future work

- Chapter 9 summarises the overall conclusions and findings of this thesis.
- Chapter 10 outlines suggestions for future work that have arisen as a result of these findings.

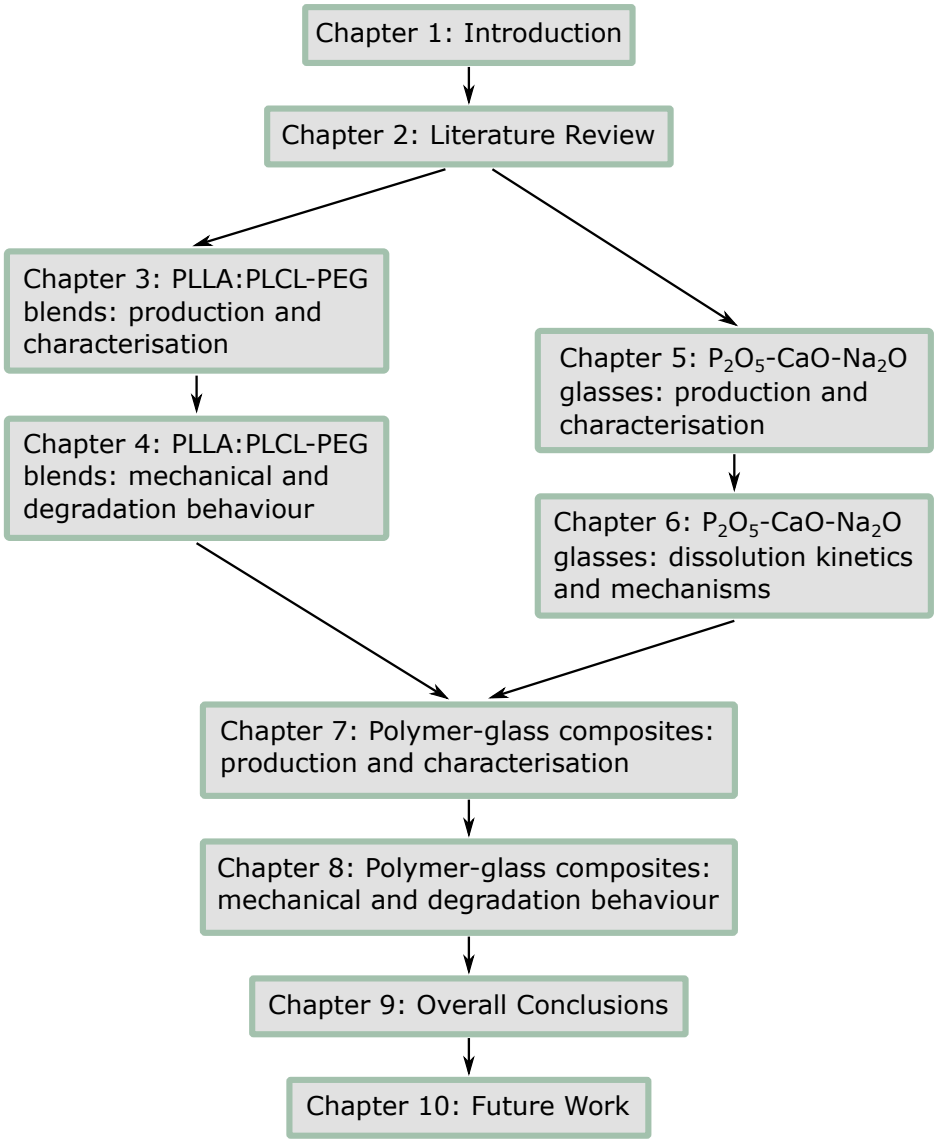

Fig. 2.17: Outline of the structure of this thesis.

Chapter 3

PLLA:PLCL-PEG blends: production and characterisation

3.1 Background and aims

The choice of polymer in a resorbable glass-containing composite must be considered carefully. In order to understand the influence on the mechanical performance of the glass-reinforced phase, the intrinsic properties of the polymer first need to be characterised and understood.

Polymer blending provides a convenient solution to tune the material properties of PLLA to address some of its inherent drawbacks for cardiac stent applications, however many of these blend systems (particularly those including PCL, a popular addition to improve ductility) are incompatible and form a phase separated, immiscible structure [112, 118]. To achieve better compatibility while also allowing tuning of polymer properties, blends of PLLA with PLCL have been developed and show improved miscibility [109, 115, 267], however this promising blend system has not yet been extensively studied. Functionalisation of bioresorbable polymers with PEG is another developing technology that can be used in conjunction with blending to improve polymer ductility and accelerate the degradation rate, as well as potentially compatibilising blends of PLLA and PLCL [101, 103, 104, 126].

Design of polymer blends to elicit desired properties is complex, and must take into account not only the properties of the individual component polymers, but also their mutal solubility. Differences in properties between miscible and immiscible blends can be significant, so it is necessary to understand the factors affecting miscibility of the blend components, as well as the effect of miscibility on eventual properties. The evolution of the polymer blend structure and mechanical properties during degradation are also of crucial importance for any bioresorbable implant application. In order to understand this evolution during degradation, the polymer blend structure, and its relationship to the mechanical properties must be accurately and thoroughly determined in the initial state.

In this chapter a recently-developed range of PLCL copolymers, with short chain PEG functionalisation, were used [101, 103, 104], along with a commercial PLLA polymer for comparison. Blends of PLCL-PEG with PLLA were investigated to achieve an optimal combination of degradation rate, strength, stiffness, and ductility for cardiac stent applications. The aims addressed in this chapter are to:

- Characterise the thermal properties and miscibility behaviour of the individual polymer components
- Determine the initial mechanical properties of the polymer blends, and explain these in terms of their composition and structure
- Determine the effect of different testing conditions on the mechanical properties of polymer blends

3.2 Materials and Methods

3.2.1 Materials

Commercial PLLA (Ingeo 2500 HP) was supplied by Natureworks LLC, USA. PEG-functionalised polymers were synthesised and supplied by Ashland Specialties Ireland

Ltd. (Dublin, Ireland), including PLLA-PEG, PCL-PEG, PLCL(80:20)-PEG, and PLCL(70:30)-PEG. The copolymer molar ratio (LA:CL) for PLCL copolymers is specified in brackets. These polymers contained a singular PEG end-group of length 550 g mol^{-1}. The presence of PEG was confirmed by the supplier by utilising ^{1}H-NMR to determine the chemical composition of the copolymers. DCM was supplied by Merck KGaA, Germany, and chloroform was purchased from Sigma Aldrich.

3.2.2 Processing

Polymer blends were prepared by blending PLLA with 10, 20, 30, 40, 50, and 60 wt% PLCL(80:20)-PEG or PLCL(70:30)-PEG. Solvent cast films of pure and blended polymers were produced by dissolution in DCM (0.1 g mL^{-1}) and casting into petri dishes. Once the films were dry enough to be removed from petri dishes (approximately 12 hours) they were dried under vacuum at 50°C for 10 days until constant mass. Polymer films were then processed into dumbbell (19 mm length, 5 mm gauge length, 0.6 mm thick) or disc shaped (5 mm diameter, 0.6 mm thick) samples using micro-injection moulding (IM 5.5, Xplore Instruments BV, The Netherlands) and custom-made moulds in ambient conditions. Micro-injection moulding was carried out at the minimum melt temperature required for complete mould filling and uniform sample appearance, which ranged from 173 - 236°C depending on blend composition, with the mould held at ambient temperature. A pressure of 7.5 bar was applied and held for 60 s to fill the mould and minimise shrinkage during cooling.

3.2.3 Characterisation

3.2.3.1 DSC

DSC (Differential scanning calorimetry) was carried out using a DSC Q2000 (TA Instruments, USA), in Al hermetic pans at a heating rate of 20°C min^{-1}, from -80

to 250℃ (-20 to 230℃ was used for PLLA:PLCL-PEG blends) under 50 mL min^{-1} N_2 gas flow. When measuring the inherent properties of the as-received polymers, samples were then cooled at the same rate back to the starting temperature and a second heating run carried out, with the second heating used for analysis. In all other cases, a single heating run was used to measure the properties of the polymers and blends after processing. To measure the effect of hydration, polymer samples for DSC (approximately 3 mg) were immersed in 2 mL deionised water at 37℃ for 20 minutes, in Eppendorf tubes. Samples were dabbed dry to remove surface water, and then sealed in hermetic pans as described above, to prevent removal of absorbed water. TA Universal Analysis software was used for data analysis, and the glass transition temperature T_g was taken at the inflection point. Crystallinities (X_c) were calculated using reference values for ΔH_m° of 107 J g^{-1} for PLLA [268] and 139 J g^{-1} for PCL [269, 270].

3.2.3.2 TGA

TGA (Thermogravimetric analysis) was carried out using a TA Instruments TGA Q500. Polymer samples were placed in a platinum pan, and heated from room temperature to 600℃ at 20℃ min^{-1}. N_2 was used as the balance and sample gas, with flow rates of 40 and 60 mL min^{-1} respectively. Thermal properties were analysed using the TA Universal Analysis software, degradation temperatures were taken as the onset point.

3.2.3.3 XRD

XRD (X-ray diffraction) was carried out using a Bruker D8 Advance diffractometer with Cu Kα radiation in a 2θ range of 5-50°, with a 0.05° step size and dwell time of 1.0 s $step^{-1}$. Analysis was carried out using HighScore Plus (Malvern Panalytical).

3.2.3.4 SEM

SEM (Scanning electron microscopy) was undertaken using an FEI Nova NanoSEM, using an accelerating voltage of 5 kV. Samples were prepared by cryo-fracturing in liquid nitrogen to view the cross-section, and then sputter coating with approximately 10 nm of gold using an Emitech K550 sputter coater (40 mA deposition current for 1 minute, under an argon atmosphere).

3.2.3.5 GPC

GPC (Gel permeation chromatography) samples were prepared by dissolving 3 - 7 mg of polymer in 2 mL of chloroform followed by filtration using a Millipore filter (0.20 µm pore size, Dia 13 mm, Millipore SLFG013NL, Fluropore PTFE (F) membrane). GPC measurements were performed using an Agilent triple detector system with an Agilent Technologies column (PLgel 5 µm MIXED-C 300×7.5 mm). The columns were calibrated with polystyrene standards supplied by Agilent Technologies at a concentration of 10 mg mL^{-1}. Chloroform (Sigma Aldrich) was used as the mobile phase with a flow rate of 1.0 mL min^{-1}, and molecular weight data was collected using the refractive index peak. GPC data was collected by Dr Seán McMahon and Dr Patrick Duffy at Ashland Specialties Ireland Ltd., and analysed by the author.

3.2.4 Turbidimetric titration

Turbidimetric titration was used to measure the Hildebrand solubility parameters of the polymers used [271]. Polymers were dissolved in DCM (8 mg mL^{-1}), and then ethanol (a non-solvent) was added while stirring until the cloud point was observed visually. The solubility parameter of the mixed solvent is then equal to the upper limit of solubility δ_U. The lower limit of solubility δ_L was determined in a similar fashion by adding n-heptane instead of ethanol. The upper and lower limits of solubility can be

calculated using Eq. 3.1, where δ_1 and δ_2 are the solubility parameters of the solvent and non-solvent, and ϕ_1 and ϕ_2 are their respective volume fractions.

$$\delta_{U/L} = \phi_1\delta_1 + \phi_2\delta_2 \tag{3.1}$$

The solubility parameter of the polymer can then be calculated using Eq. 3.2.

$$\delta = \frac{\delta_U + \delta_L}{2} \tag{3.2}$$

3.2.5 Mechanical testing

Tensile testing was carried out using an H5KS Benchtop Tester (Tinius Olsen Ltd, UK) with a 250 N load cell, using filament grips (121-013, Tinius Olsen Ltd, UK), under a constant elongation rate of 2 mm min^{-1}. Dumbbell samples (5 mm gauge length, 600 µm thick) were tested in ambient (dry at 25℃) and simulated body conditions (immersed in deionised water at 37℃) using a Saline Test Tank with Heater (Tinius Olsen Ltd, UK). After loading samples into the grips and immersing them in water, they were left for approximately 10 minutes for the temperature to equilibrate. Strain was measured using a video extensometer and custom-built LabVIEW software, and dry transfer letters (black, approximately 1 mm squares, Chartpak Inc., USA) were used as strain markers. Yield strength (σ_y) for polymers was taken as the 0.2% offset yield point, and the elastic modulus (E) was calculated from the linear region of the stress-strain curve before yield.

3.3 Results

3.3.1 As-received polymers

The molecular weights of the as-received polymers are summarised in Table 3.1. Most of the polymers had comparable masses, with M_w around 200 kg mol^{-1}, while those with greater CL content had slightly lower mass.

Table 3.1: Molecular weights of the as-received polymers, measured by GPC.

Polymer	Copolymer ratio (LA:CL)	M_w (kg mol^{-1})	M_n (kg mol^{-1})
PLLA	100:0	209	88
PLLA-PEG*	100:0	222	119
PLCL(80:20)-PEG	80:20	212	116
PLCL(70:30)-PEG	70:30	177	89
PCL-PEG	0:100	125	47

* PLLA-PEG supplied as a mixture of two batches, these values are averages of the individual batches.

Example DSC and TGA curves for the as-received polymers are shown in Fig. 3.1 and Fig. 3.2 respectively, and their thermal properties are summarised in Table 3.2 and Fig. 3.3. PLLA and PLLA-PEG showed behaviour typical of semi-crystalline polymers, with a glass transition, followed by a cold crystallisation exotherm and then a melting endotherm. The PLCL-PEG copolymers appeared completely amorphous on the second heating curve, with only a glass transition visible. PLCL(80:20)-PEG was observed to have a small amount of crystallinity in its as-received state ($X_{c,1}$, due to a long storage time), which was lost upon melting, while PLCL(70:30)-PEG displayed no crystallinity in either case. PLLA and PLLA-PEG also showed the presence of some initial crystallinity, which was reduced upon remelting. PCL-PEG displayed a high tendency for crystallisation, with a very small amorphous T_g and very large melting endotherm. The crystallinity of PCL-PEG was only slightly reduced after remelting. The T_g of PLLA was observed to decrease by functionalisation with PEG, as well as by addition of CL through copolymerisation.

During thermal degradation tests, complete mass loss was seen to occur between about 200-400℃ which is expected for polymers. By looking at the onset temperature of degradation (T_d), it is clear that the addition of CL to LA in a copolymer increased the degradation temperature, while functionalisation with PEG reduced the thermal

stability. The derivative weight loss is also shown, where the polymers tended to display a single sharp peak (PLLA and PCL-PEG), or two broad peaks (PLLA-PEG, PLCL(80:20)-PEG, PLCL(70:30)-PEG).

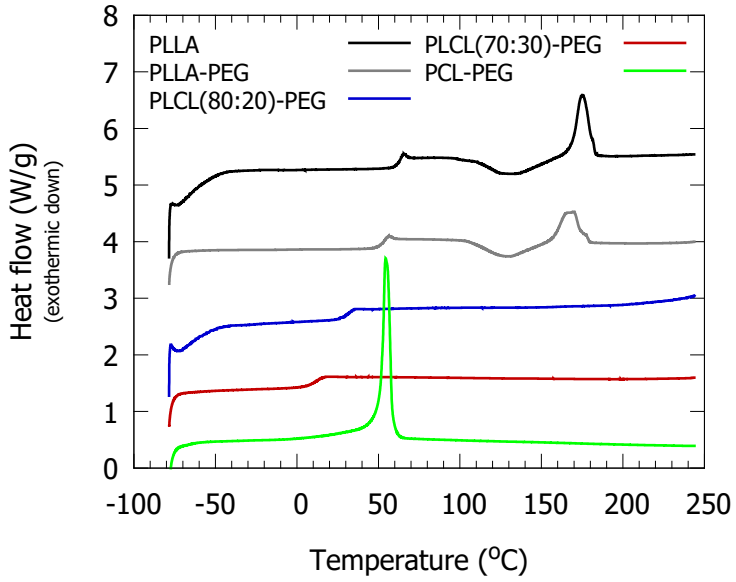

Fig. 3.1: Example DSC curves for the polymers used (on second heating). Curves offset vertically for clarity.

Table 3.2: Measured thermal properties for the polymers used, with standard deviations. T_d is measured for as-received polymers, while T_g and T_m relate to the second DSC heating run, and $X_{c,1}$ and $X_{c,2}$ denote the polymer crystallinities measured on the first and second heating runs respectively.

Polymer	T_g (°C)	T_m (°C)	$X_{c,1}$ (%)	$X_{c,2}$ (%)	T_d (°C)
PLLA	63.5 ±0.3	175.3 ±0.3	40.7 ±0.9	1.4 ±3	358 ±2
PLLA-PEG	55 ±2	167 ±3	13.0 ±0.5	10 ±4	283 ±2
PLCL(80:20)-PEG	31.4 ±0.8		3.1 ±2		283 ±5
PLCL(70:30)-PEG	11.5 ±0.5				292 ±3
PCL-PEG	-65 ±1	54.8 ±0.3	62.0 ±0.6	49.4 ±0.6	319 ±1

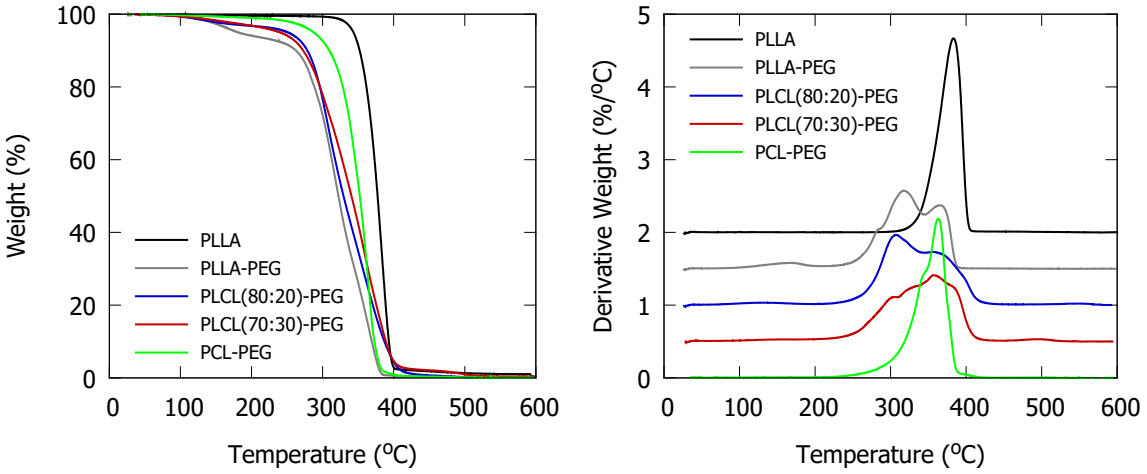

Fig. 3.2: TGA curves for the as-received polymers. Left: weight loss, right: derivative weight loss, offset vertically for clarity.

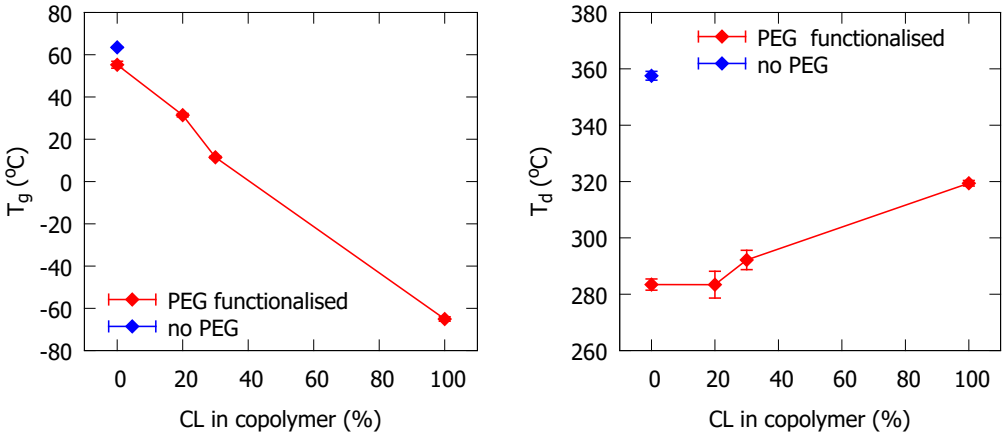

Fig. 3.3: T_g (left) and T_d (right) for PEG functionalised polymers, and commercial PLLA without PEG. Error bars denote standard deviation (n = 3).

3.3.2 Polymer miscibility

The solubility parameters of PLLA, PLCL(80:20)-PEG, PLCL(70:30)-PEG were measured using turbidimetric titration, and are shown in Fig. 3.4. The value for PLLA was consistent with results previously reported on [272], however no data were available for PLCL or PLCL-PEG. Here it can be seen that copolymerisation of PLLA with CL units increased the solubility parameter δ, with greater CL content resulting in an even higher solubility parameter.

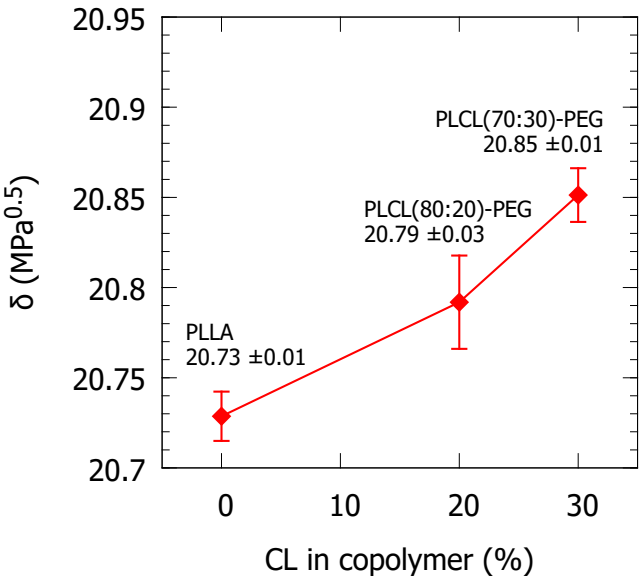

Fig. 3.4: Hildebrand solubility parameter δ for PLLA, PLCL(80:20)-PEG and PLCL(70:30)-PEG, measured using turbidimetric titration. Error bars denote standard deviation (n = 3).

3.3.3 PLLA:PLCL-PEG structural characterisation

Measured glass transitions of injection-moulded polymer blends are shown in Fig. 3.5, and it is clear that blends of PLLA with PLCL(80:20)-PEG were completely miscible across the composition range studied, showing a single T_g for each composition. Blends of PLLA with PLCL(70:30)-PEG were partially miscible, with blends containing $\leq$ 20 wt% of the copolymer showing single phase behaviour, and blends with $\geq$ 30 wt% were phase separated. The effect of hydration (for 20 minutes in deionised water) can also be seen - there was a general decrease in the T_g of approximately 5°C.

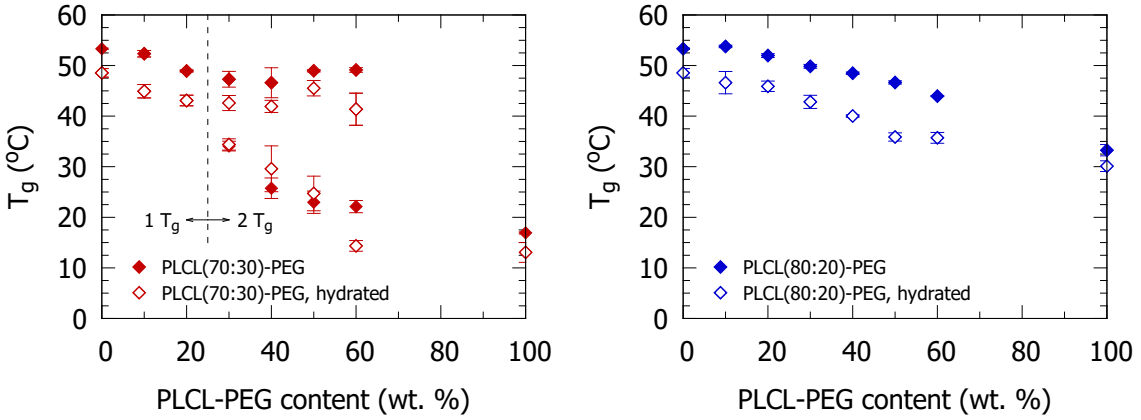

Fig. 3.5: Glass transition temperature(s) measured by DSC for different PLLA:PLCL-PEG blend compositions, in dry and hydrated (for 20 minutes in deionised water) states. Blends of PLLA with PLCL(70:30)-PEG (left) and PLCL(80:20)-PEG (right) are shown. Error bars denote standard deviation, n = 3. Reproduced from Oosterbeek et al. [273].

After injection moulding, polymers were examined by XRD to determine whether crystallisation had taken place during processing. All samples were determined to be amorphous after injection moulding, with no crystalline peaks observed in XRD patterns (Fig. 3.6). This can be attributed to the fast cooling provided by the room temperature mould, quenching the polymer quickly into an amorphous state.

From the molecular weight distributions (Table 3.3, Fig. 3.7), it can be seen that all the pure polymers had comparable molecular weights, with 184 (± 8) kg mol^{-1} for PLLA, 188 (± 4) kg mol^{-1} for PLCL(80:20)-PEG, and PLCL(70:30)-PEG slightly lower at 129 (± 4) kg mol^{-1}. These were slightly lower than the equivalent weights measured before processing (film casting, injection moulding) shown in Table 3.1, indicating that some molecular weight degradation occurred during processing. The molecular weight distributions measured by GPC show the broad, polydisperse nature of the polymers used, which made resolving differences between the two polymer components in the blends challenging. To overcome this issue, theoretical distributions for the polymer blends were calculated based on a linear combination of the two component polymer distributions as shown in Eq. 3.3

$$D_{a:b} = w_a D_a + w_b D_b \tag{3.3}$$

where a and b denote blend components, D is the molecular weight distribution for the blend (a:b) or components (a or b), and w is the weight fraction of components in the blend. The calculated distributions matched the measured distributions well, and the associated p-value indicated no evidence of a difference between the distributions (chi-squared test $p > 0.05$, H_0 = no difference between distributions).

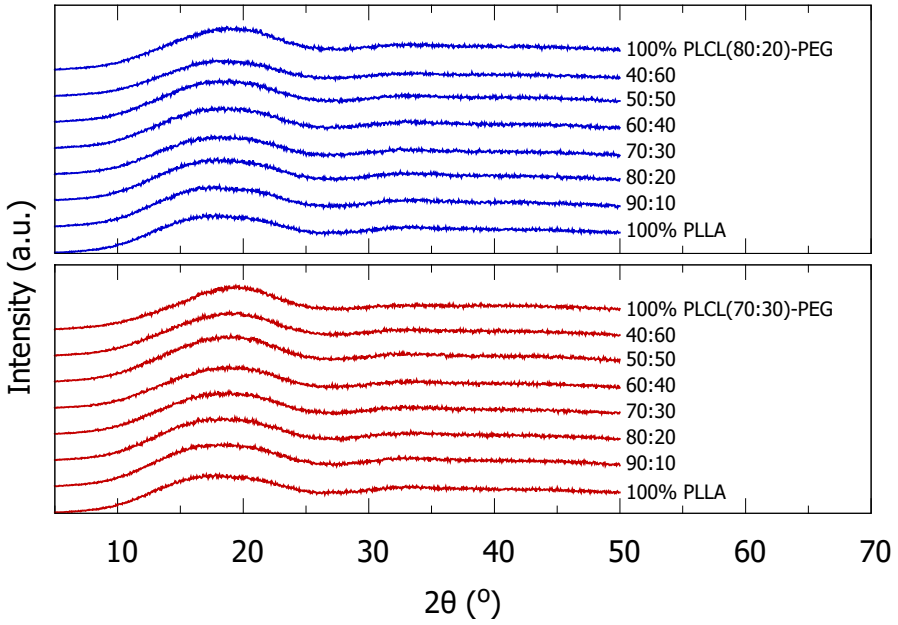

Fig. 3.6: Representative X-ray diffraction patterns for PLLA:PLCL-PEG blends after moulding, labels denote PLLA:PLCL-PEG blend ratio, and datasets are offset for clarity. Reproduced from Oosterbeek et al. [273].

Table 3.3: Molecular weights of PLLA:PLCL-PEG blends measured by GPC after processing. Error shown is the standard deviation from three measurements.

	M_w (kg mol^{-1})		M_n (kg mol^{-1})	
wt% PLCL-PEG	PLCL(80:20)-PEG	PLCL(70:30)-PEG	PLCL(80:20)-PEG	PLCL(70:30)-PEG
0	184 (±8)		99 (±6)	
20	190 (±5)	173 (±6)	98 (±7)	87 (±4)
50	181 (±2)	159 (±2)	96 (±2)	76 (±2)
100	188 (±4)	129 (±4)	94 (±2)	63 (±1)

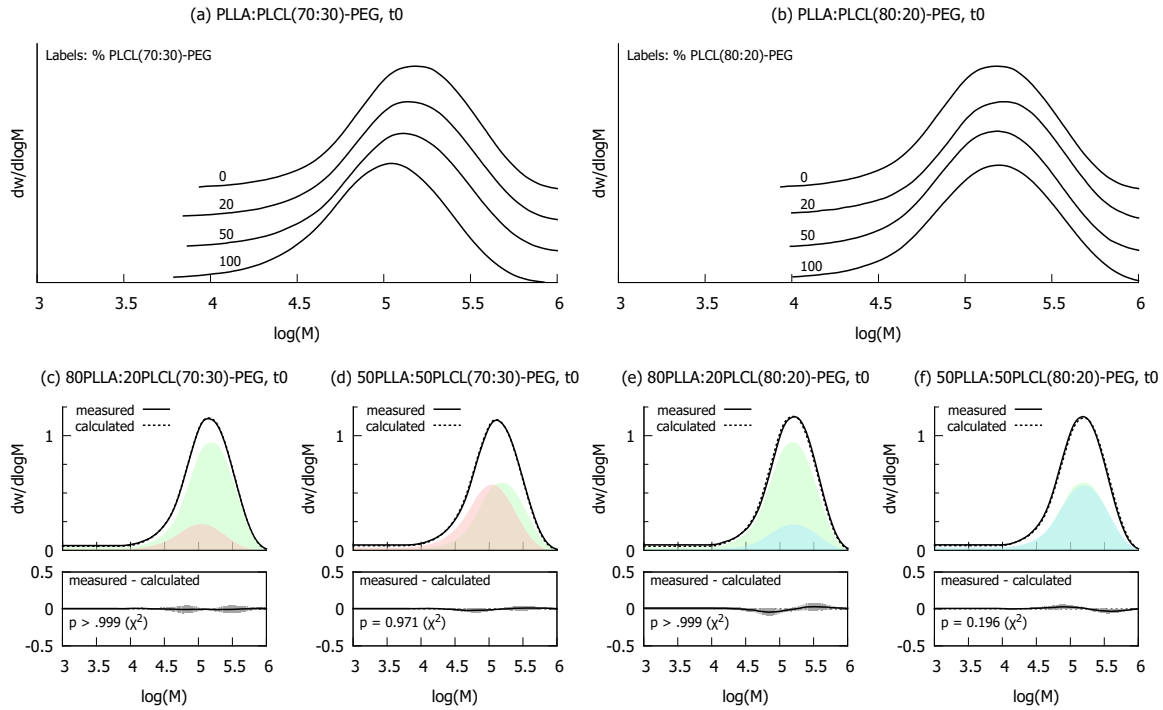

Fig. 3.7: GPC molecular weight distributions for as-fabricated PLLA:PLCL(70:30)-PEG blends (a) and PLLA:PLCL(80:20)-PEG blends (b); curves are offset for clarity. Bottom row (c-f) shows measured and calculated distributions, based on a linear combination of the individual components (green = PLLA, red = PLCL(70:30)-PEG, blue = PLCL(80:20)-PEG). Shaded region in difference plot denotes standard deviation, n = 3. Reproduced from Oosterbeek et al. [273].

3.3.4 PLLA:PLCL-PEG mechanical properties

Representative stress-strain curves, and a summary of mechanical properties are given in Figs. 3.8 and 3.9. These blends displayed either brittle or ductile behaviour (discussed further below). Brittle polymer blends showed an initial linear stress-strain response, followed by yield and failure shortly afterwards at relatively low strain. Ductile polymer blends displayed a similar initial linear stress-strain response, but after yield the stress decreased to a plateau. The stress continued to plateau up to relatively high strain (several 100%) before beginning to gradually increase, reaching another peak and then failure.

Under ambient conditions (dry at 25°C), the addition of the softer PLCL-PEG to PLLA reduced its strength and stiffness (Fig. 3.9) as has been reported previously

for PLLA:PLCL blends [109, 115], with the PLCL(70:30)-PEG copolymer having a larger effect than PLCL(80:20)-PEG. Pure PLLA was brittle as expected ($\varepsilon_B \sim 2.4\%$), as were blends with small amounts of PLCL-PEG. However, once a certain amount of copolymer was added ($\geq$ 30 wt% PLCL(70:30)-PEG, or $\geq$ 50 wt% PLCL(80:20)-PEG), a step change was seen and large scale ductility was observed ($\varepsilon_B \sim$ 200 - 400%). This step change occurred at the same composition as the formation of a PLCL-PEG-rich phase in the polymer blend, either by phase separation in the case of PLLA:PLCL(70:30)-PEG blends (Fig. 3.5), or by simply altering the bulk composition in the case of miscible PLLA:PLCL(80:20)-PEG blends.

Under simulated body conditions (immersed in deionised water at 37°C), the combined effect of hydration and elevated temperature had a dramatic effect, reducing the strength and stiffness while increasing the ductility such that all polymers tested, including pure PLLA, exhibited ductile failure. Pure PLCL(70:30)-PEG, which showed the greatest elongation at break of 560% in ambient conditions, was deformed to 1600% and reached the maximum travel of the water bath without fracture (denoted by dotted line in Fig. 3.9e).

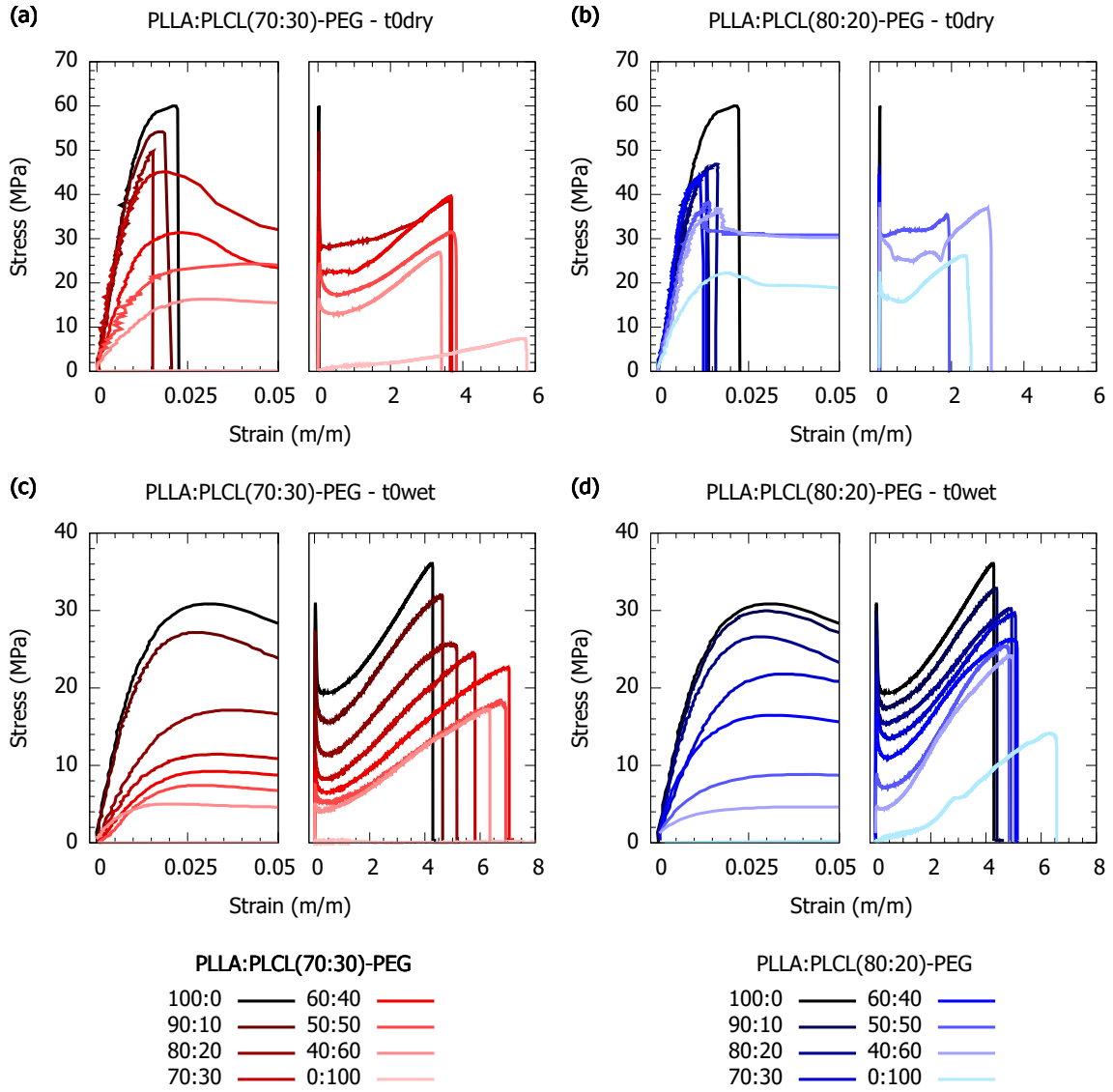

Fig. 3.8: Representative stress-strain curves for tensile testing of PLLA:PLCL-PEG blends under various conditions. As-fabricated PLLA:PLCL(70:30)-PEG blends (a) and PLLA:PLCL(80:20)-PEG blends (b) tested dry at room temperature, and as-fabricated PLLA:PLCL(70:30)-PEG blends (c) and PLLA:PLCL(80:20)-PEG blends (d) tested immersed in 37°C water.

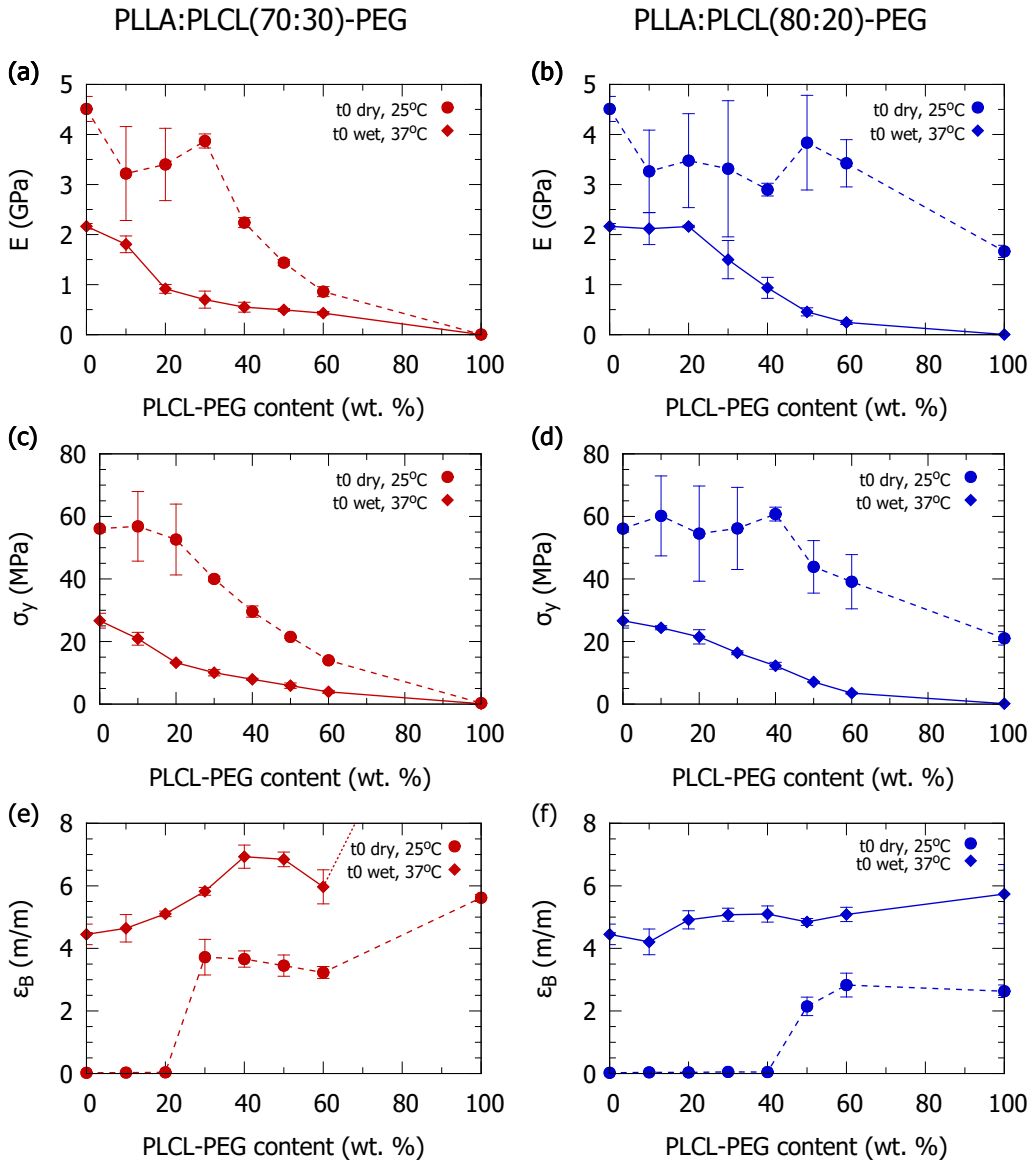

Fig. 3.9: Mechanical properties measured by tensile testing for PLLA:PLCL-PEG blends under various conditions. **t0 dry, 25°C** denotes as-fabricated samples tested dry at room temperature, and **t0 wet, 37°C** denotes as-fabricated samples tested immersed in 37°C water. Top row: elastic modulus (a, b), middle row: yield strength (c, d), bottom row: elongation at break (e, f). Left column: PLLA:PLCL(70:30)-PEG blends (a, c, e), right column: PLLA:PLCL(80:20)-PEG blends (b, d, f). Error bars denote standard deviation, n = 3.

3.4 Discussion

3.4.1 As-received polymers

Characterisation of the as-received polymers indicated clear differences in their tendency to crystallise. Homopolymers (PLLA, PLLA-PEG and PCL-PEG) showed significant crystallinity before - and sometimes after remelting. PLCL(80:20)-PEG showed a small amount of crystallinity in its as-received state due to long storage time, which was lost after melting, while PLCL(70:30)-PEG displayed no crystallinity in either case. This indicates the reduced tendency of copolymers to crystallise, due to the different monomer groups present, hindering chain packing [74–76].

The decrease in T_g upon addition of CL to the copolymer might be expected from literature due to the lower T_g of PCL [274]. This effect was also seen for functionalisation with PEG, where PEG addition to PLLA resulted in a noticeable decrease in T_g, again consistent with previous results [87, 101]. PEG also had a detrimental effect on the T_d, reducing the thermal stability. Derivative weight-loss measurements showed decomposition of the two copolymer components, resulting in two broad peaks for PLCL-PEG copolymers, compared with a single peak for homopolymers. PLLA-PEG appeared to not follow this trend, however this material was supplied as a mixture of two batches so this may be a result of slight differences between the two batches (see Table 3.1).

3.4.2 Polymer miscibility

According to Flory-Huggins solution theory [105, 106] the Gibbs energy of mixing (ΔG_m) for a polymer blend is given by:

$$\frac{\Delta G_m}{RT} = \frac{\phi_1}{X_1}\ln(\phi_1) + \frac{(1-\phi_1)}{X_2}\ln(1-\phi_1) + \phi_1(1-\phi_1)\chi \tag{3.4}$$

where R is the ideal gas constant, T is temperature, ϕ_1 is the volume fraction of component 1 in the mixture, X_1 and X_2 are the degrees of polymerisation of components 1 and 2, and χ is the Flory-Huggins interaction parameter. Values of the interaction parameter are only available for certain polymer-solvent systems, but can be calculated using the Hildebrand approach, which calculates the interaction parameter on the basis of solubility parameters, as shown in Eq. 3.5 [275–277]

$$\chi = \frac{V_m(\delta_1 - \delta_2)^2}{RT} \tag{3.5}$$

where V_m is the molar volume, and δ_1 and δ_2 are the solubility parameters of components 1 and 2. Considering the form of Eq. 3.4, an increased interaction parameter χ will increase the tendency for the blend to separate into two different phases. Therefore considering Eq. 3.5, if the polymers have more similar solubility parameters (δ) the interaction parameter will decrease and the blend will be more likely to be miscible. Conversely if the solubility parameters are very different the interaction parameter will increase and the blend will be more likely to be immiscible.

Results of turbidimetric titrations indicate that the solubility parameter increased from 20.73 $MPa^{0.5}$ for PLLA, up to 20.79 $MPa^{0.5}$ for PLCL(80:20)-PEG and 20.85 $MPa^{0.5}$ for PLCL(70:30)-PEG. This was a direct result of the copolymer composition; for random copolymers the effective solubility parameter can be varied continuously with composition [276]. From these results it can be expected that PLLA is more likely to form a miscible blend with PLCL(80:20)-PEG than PLCL(70:30)-PEG.

3.4.3 PLLA:PLCL-PEG structure and mechanical properties

DSC measurements of the glass transition temperature T_g revealed the miscibility behaviour of the PLLA:PLCL-PEG blends studied (Fig. 3.5). Blends of PLLA with PLCL(80:20)-PEG were completely miscible, due to their similar solubility parame-

ters, however blends of PLLA with PLCL(70:30)-PEG showed only partial miscibility. Phase separation occurred for PLCL(70:30)-PEG content $\geq$ 30 wt%, due to the greater difference between the solubility parameters of these components. The miscibility behaviour of PLLA:PLCL(70:30)-PEG blends observed here is comparable with that reported by Ugartemendia *et al.* [109], who observed phase separation at $\geq$ 40 wt% PLCL(67:33) (for melt-blending with PLLA) - the small difference observed could be attributed to the different thermal history, or an effect of PEG functionalisation.

The subsequent reduction in T_g upon hydration can be attributed to water absorption and plasticisation, as water molecules diffuse between polymer chains, increasing free volume and reducing inter-chain bonding [50, 154, 278, 279]. This has a profound impact on the mechanical properties, resulting in the increased ductility observed (Fig. 3.9) when blends are tested in 37℃ water instead of in ambient conditions. This is consistent with recent works illustrating the plasticising effect of water on the bulk mechanical properties of PLLA [280, 281].

GPC measurements indicated that molecular weight reduction occurred during processing (film casting and injection moulding). This can be attributed to the shear forces and high temperature experienced by the polymer during the injection moulding process [224]. Although the different polymer blend components could not be resolved in GPC curves due to their polydispersity, the contribution of the different blend components was observed by calculating an expected distribution based on the ratio of the different components. The close match between the experimentally measured and calculated distributions provides validation for the use of this method.

A difference was also observed in the T_g of pure PLLA between the as-received polymer, and after processing, where the T_g was reduced from 63.5℃ to 53.3°C. This could be an effect of molecular weight reduction during processing, but can also be explained as the result of the different cooling process from the melted state. The T_g

of the as-received PLLA was measured from the second heating run after cooling from the melt at 20℃ min^{-1}, which is significantly slower than would be expected during the injection moulding procedure used, where molten polymer is injected into a thin cavity in a mould held at room temperature. This faster cooling would be expected to result in the formation of a glassy polymer with greater free volume and therefore lower T_g [51]. The amorphous nature of the polymer blends measured by XRD also supports this, with amorphous polymers more likely to form when the cooling rate is higher.

3.5 Conclusions

The properties of the as-received polymers were characterised to form a baseline for comparison with PLLA:PLCL-PEG blends. Addition of CL to LA in a copolymer, and functionalisation with PEG both reduce the T_g of PLLA. Copolymerisation with CL also increases the solubility parameter of PLLA relative to the copolymer content, leading to PLLA:PLCL(80:20)-PEG blends being completely miscible, while PLLA:PLCL(70:30)-PEG blends are partially miscible.

Addition of the softer PLCL-PEG component to PLLA reduces the strength and stiffness of the fabricated polymer blends, both in ambient and simulated body conditions. The phase behaviour of PLLA:PLCL-PEG blends has a strong impact on the ductility in ambient conditions. Low PLCL-PEG blends ($\leq$ 20 wt% PLCL(70:30)-PEG, or $\leq$ 40 wt% PLCL(80:20)-PEG) were brittle, however once a PLCL-PEG-rich phase was formed (either by phase separation or bulk changes), blends became ductile.

Water also has a significant effect on the properties of PLLA:PLCL-PEG blends, with hydrated polymers displaying a lower T_g, as well as signficantly reduced strength and stiffness, and high ductility regardless of blend composition.

Chapter 4

PLLA:PLCL-PEG blends: mechanical and degradation behaviour

4.1 Background and aims

Poly-L-lactide (PLLA) is a popular bioresorbable implant material, and has been a favoured choice for load bearing applications due to its high strength and stiffness compared with other biodegradable synthetic polymers. Significant research has been directed towards development of PLLA based stents, including the ABSORB BVS® (Abbott Vascular) and DESolve® (Elixir Medical), however their use has been limited to date, in large part due to the mechanical and degradation properties of the material [34, 35].

Although PLLA can be resorbed by the body, its slow degradation is a key issue that has been identified by medical experts, requiring further materials development to meet clinical needs. As a wound healing event, arterial patency is typically recovered within the first six months [282, 283], however typical PLLA resorption can take several years [35, 36, 62, 284, 285]. PLLA experiences brittle failure in ambient conditions, and can

also become embrittled over time, which can lead to catastrophic failure of implanted devices [51, 52, 285]. This embrittlement can be caused by either enthalpy relaxation or crystallisation. Enthalpy relaxation (also known as physical ageing), is a result of the thermodynamically unstable nature of the fast-cooled glassy polymer - the material tends to equilibrium through slow rearrangements, resulting in densification without long-range order, greater intermolecular interactions, and loss of ductility [51, 149]. Enthalpy relaxation of PLLA can occur after several days at temperatures below T_g [51]. Crystallisation is also driven by the non-equilibrium nature of the frozen glassy state, and requires higher chain mobility to form ordered structures. It is therefore typically seen when PLLA is heated above its T_g, however it also occurs during degradation when hydration and hydrolysis-induced chain scission provide additional chain mobility [138, 139, 286].

This chapter aims to:

- Develop a set of PLLA:PLCL-PEG blend compositions that allow tuning of the mechanical properties and degradation profile
- Assess the long-term degradation behaviour of PLLA:PLCL-PEG blends in simulated body conditions
- Reveal the mechanisms involved in PLLA:PLCL-PEG blend structural changes, and how these influence the evolution of mechanical properties during degradation

4.2 Materials and methods

4.2.1 Materials and processing

Materials were supplied and processed according to the methods described in sections 3.2.1 and 3.2.2.

4.2.2 Characterisation

4.2.2.1 DSC

DSC (Differential scanning calorimetry) was carried out using a DSC Q2000 (TA Instruments, USA), in Al hermetic pans at a heating rate of 20℃ min^{-1}, from -20 to 230℃ under 50 mL min^{-1} N_2 gas flow. A single heating run was used to measure the properties of the polymers and blends after and degradation. Polymer properties were measured after 30 days degradation (according to the method in section 4.2.3) in their hydrated state, by removing them from the degradation solution and dabbing them dry to remove surface water, before sealing in hermetic pans to prevent removal of absorbed water and testing immediately. Measurements were also carried out after degradation in the dry state, after drying at room temperature in a vacuum oven until constant mass was reached. TA Universal Analysis software was used for data analysis, and the glass transition temperature T_g was taken at the inflection point.

4.2.2.2 XRD

XRD (X-ray diffraction) was carried out using a Bruker D8 Advance diffractometer with Cu Kα radiation in a 2θ range of 5-50°, with a 0.05° step size and dwell time of 1.0 s $step^{-1}$. The crystallinity was estimated using HighScore Plus (Malvern Panalytical), by fitting crystalline and broad amorphous peaks above the instrument background.

4.2.2.3 SEM

SEM (Scanning electron microscopy) was undertaken using an FEI Nova NanoSEM, using an accelerating voltage of 5 kV. Samples were prepared by cryo-fracturing in liquid nitrogen to view the cross-section, and then sputter coating with approximately 10 nm of gold using an Emitech K550 sputter coater (40 mA deposition current for 1 minute, under an argon atmosphere).

4.2.2.4 GPC

GPC (Gel permeation chromatography) samples were prepared by dissolving 3 - 7 mg of polymer in 2 mL of chloroform followed by filtration using a Millipore filter (0.20 µm pore size, Dia 13 mm, Millipore SLFG013NL, Fluropore PTFE (F) membrane). GPC measurements were performed using an Agilent triple detector system with an Agilent Technologies column (PLgel 5 µm MIXED-C 300×7.5 mm). The columns were calibrated with polystyrene standards supplied by Agilent Technologies at a concentration of 10 mg mL^{-1}. Chloroform (Sigma Aldrich) was used as the mobile phase with a flow rate of 1.0 mL min^{-1}, and molecular weight data was collected using the refractive index peak. GPC data was collected by Dr Seán McMahon and Dr Patrick Duffy at Ashland Specialties Ireland Ltd., and analysed by the author.

4.2.3 Degradation study

Degradation studies were carried out by immersing individual disc-shaped (5 mm diameter, 600 µm thick) polymer samples in 5 mL PBS in bijou tubes, which were placed in an incubator at 37°C. pH measurements were taken at regular intervals using an HI 4222 pH meter (Hanna Instruments Ltd., UK), and PBS alone was used as a control for pH measurements. At desired timepoints the wet mass of the polymer samples was measured by dabbing them dry and weighing with a Sartorius Ultramicro balance, before returning them to the solution. A long-term (∼700 days) degradation study was carried out, as well as a shorter (30 days) study for more detailed analysis. After degradation, samples were dried at room temperature in a vacuum oven until reaching constant mass, before further analysis was carried out (except for mechanical testing, which was done without drying as described below).

4.2.4 Mechanical testing

Tensile testing was carried out using an H5KS Benchtop Tester (Tinius Olsen Ltd, UK) with a 250 N load cell, using filament grips (121-013, Tinius Olsen Ltd, UK), under a constant elongation rate of 2 mm min^{-1}. Dumbbell samples (5 mm gauge length, 600 µm thick) were tested in simulated body conditions (immersed in deionised water at 37℃) using a Saline Test Tank with Heater (Tinius Olsen Ltd, UK). To test mechanical properties after 30 days degradation, tensile specimens were incubated in PBS at 37℃ for 30 days, and removed immediately before testing. After loading samples into the grips and immersing them in water, they were left for approximately 10 minutes for the temperature to equilibrate. Strain was measured using a video extensometer and custom-built LabVIEW software, and dry transfer letters (black, approximately 1 mm squares, Chartpak Inc., USA) were used as strain markers. Yield strength (σ_y) for polymers was taken as the 0.2% offset yield point, and the elastic modulus (E) was calculated from the linear region of the stress-strain curve before yield.

4.3 Results

4.3.1 Long-term degradation

During long-term immersion degradation tests (Fig. 4.1), degradation of the polymer into lactic acid, causing pH reduction, was seen for all polymer and blend compositions. Pure PLLA degraded more slowly than all other blend compositions, requiring over 500 days for pH reduction to begin. Pure PLCL-PEG polymers showed rapid degradation, resulting in pH reduction after approximately 2 months. Blends containing PLLA and PLCL-PEG showed degradation behaviour in between that of the pure PLLA and PLCL-PEG components, with the addition of increasing amounts of PLCL-PEG accelerating degradation, demonstrating the ability to controllably accelerate PLLA degradation via blending with PLCL-PEG. PLCL(70:30)-PEG degraded faster than

PLCL(80:20)-PEG due to the higher CL content, and therefore also accelerated the blend degradation to a greater extent. The degradation time showed the same trend, and suggests that the dependence on composition is not linear (Fig. 4.2), with small initial PLCL-PEG additions causing a large increase in the degradation rate.

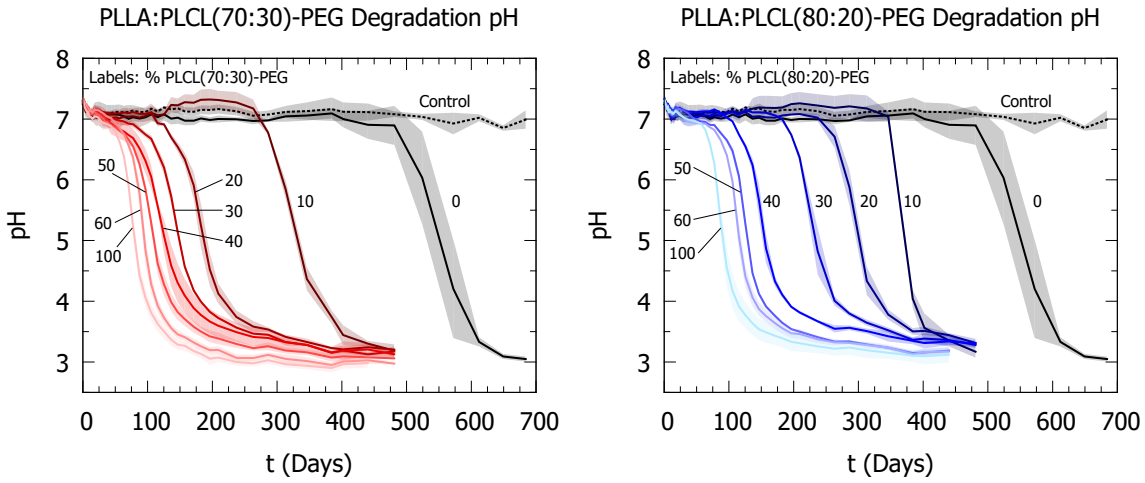

Fig. 4.1: Solution pH during long-term degradation test of PLLA:PLCL-PEG blends in PBS at 37°C. Shaded region denotes standard deviation, n = 3.

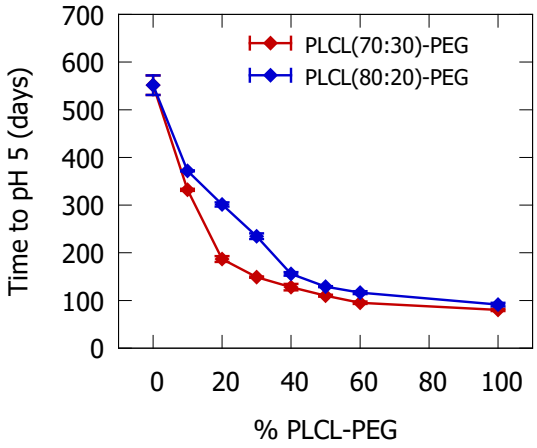

Fig. 4.2: Time taken to reach a solution pH = 5 during degradation, giving an indication of the relative degradation rate.

Examining the polymer morphology (Fig. 4.3) can also reveal information about the degradation behaviour. Fragmentation of the polymers was seen at advanced stages dur-

ing degradation, and the onset of fragmentation roughly corresponded to the speed of degradation. Fragmentation appeared to begin slightly earlier for PLLA:PLCL(80:20)-PEG blends than for PLLA:PLCL(70:30)-PEG, even though the former degraded more slowly, which may be a result of the more brittle nature of the higher LA copolymer. All the polymers were also seen to turn from transparent to opaque during degradation, which could indicate crystallisation or other processes resulting in light scattering.

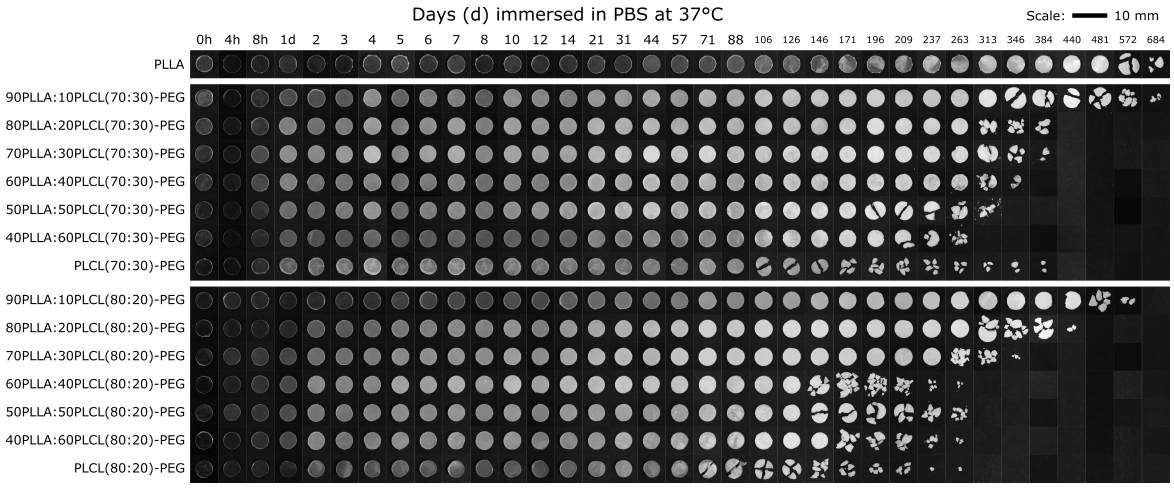

Fig. 4.3: Composite image showing photographs of polymer blend disc morphology during degradation.

The wet mass during degradation was also measured, this is shown in Fig. 4.4. In general the trends for mass loss followed those for degradation pH, with blend compositions that were seen to degrade faster by pH decrease also showing earlier onset of mass loss. In the first few days of degradation, all polymers displayed a small mass increase, reaching 100.5 - 101% of original mass. This suggests a low level of water absorption or hydration. Later on a consistent trend was observed for every blend composition except pure PLCL(70:30)-PEG, where a peak in mass at about 105 - 120% of original mass (suggesting significant water absorption) occurred just before the onset of mass loss and degradation. The lack of this increase in mass for pure PLCL(70:30)-PEG may be a result of the rapid onset of degradation for this polymer, beginning immediately. After this water absorption peak, polymer blends were seen

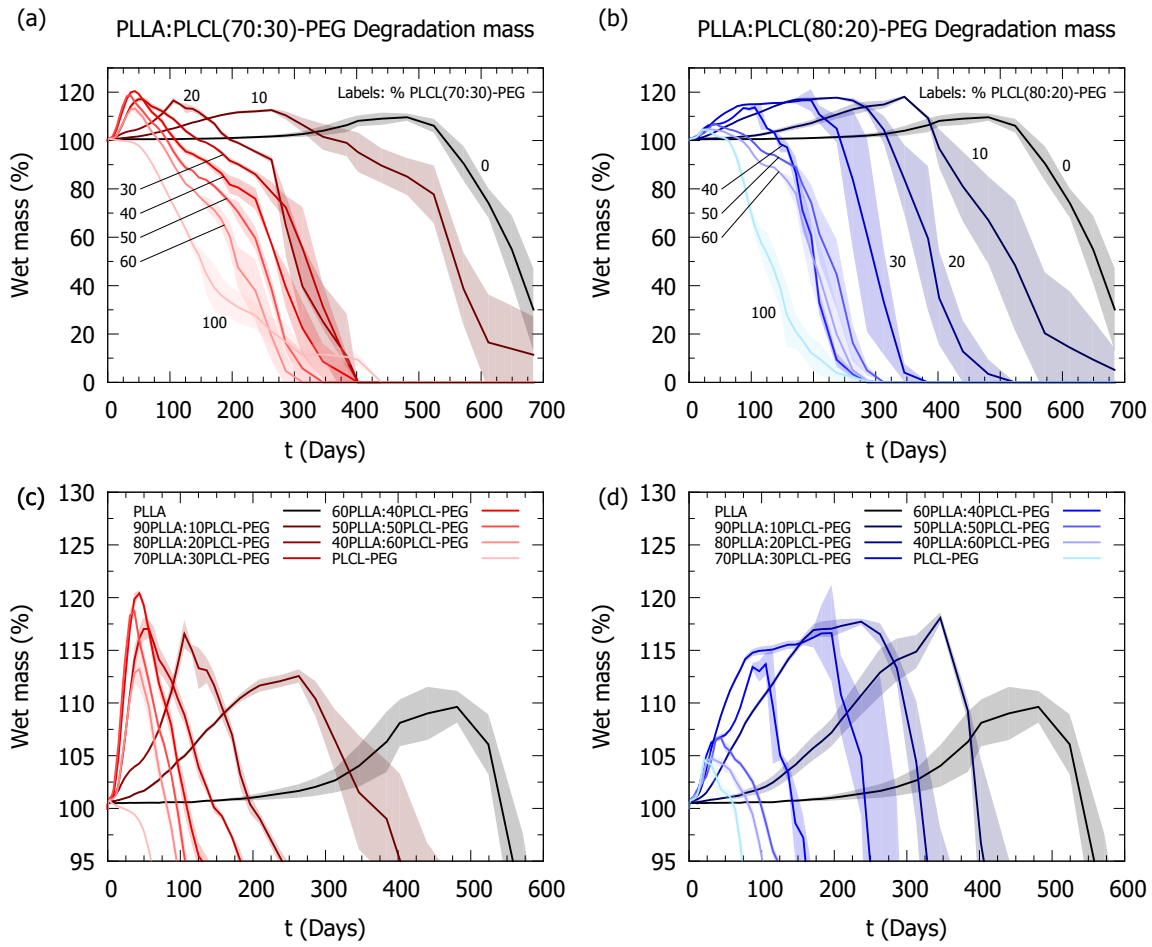

Fig. 4.4: Wet mass (as % of original dry mass) measured during long-term degradation test of PLLA:PLCL-PEG blends in PBS at 37°C. Shaded region denotes standard deviation, n = 3. (a) and (b) show blends of PLLA with PLCL(70:30)-PEG and PLCL(80:20)-PEG respectively, while (c) and (d) show the same data focusing on the mass gain region.

to slowly lose mass. The data in the region of significant mass loss ($\lesssim$90% wet mass) should be interpreted with caution, as in this region the polymers began to undergo fragmentation (Fig. 4.3), making accurate wet mass measurement difficult and subject to error, as shown by the large standard deviation.

4.3.2 Structure after short-term degradation

After 30 days degradation, GPC showed varying levels of molecular weight reduction, as seen in Table 4.1 and Fig. 4.5. Pure PLLA displayed a small amount of degradation,

with a degradation rate comparable with previous works [131, 287], while the addition of PLCL-PEG copolymers to the blend significantly increased the degradation rate. As expected, this increase was greater for addition of the less stable PLCL(70:30)-PEG copolymer, consistent with similar results seen by pH measurement during long term degradation.

Table 4.1: Molecular weights of PLLA:PLCL-PEG blends before (reproduced from Table 3.3, on page 70) and after 30 days degradation, along with calculated degradation rate according to $ln\ M_n(t_2) = ln\ M_n(t_1) - kt$. Error shown is the standard deviation from three measurements. Reproduced from Oosterbeek et al. [273].

	M_w,*t0* (kg mol^{-1})		M_w,*t30* (kg mol^{-1})		k (10^{-3} day^{-1})	
wt% PLCL-PEG	PLCL(80:20)-PEG	PLCL(70:30)-PEG	PLCL(80:20)-PEG	PLCL(70:30)-PEG	PLCL(80:20)-PEG	PLCL(70:30)-PEG
0	184 (±8)		156 (±2)		7.9 (±1.9)	
20	190 (±5)	173 (±6)	121 (±4)	85 (±3)	16.7 (±3.0)	28.2 (±1.8)
50	181 (±2)	159 (±2)	62 (±2)	58 (±1)	41.9 (±0.9)	54.7 (±1.3)
100	188 (±4)	129 (±4)	53 (±2)	27.7 (±0.6)	48.6 (±1.9)	58.7 (±1.4)

Examining the molecular weight distributions (Fig. 4.5), it is clear that there was a significant difference between the measured distribution and those calculated from individually degrading components (using Eq. 3.3 on page 69). This is shown by the large difference plot and associated p-value, indicating strong evidence of a difference between the distributions (chi-squared test $p < 0.05$, H_1 = difference between distributions exists). In all cases, after degradation the measured molecular weight distribution showed a lower amount of high molecular weight components than would be expected from degradation of PLLA, indicating that not only did the PLCL-PEG component degrade, but that this also caused accelerated degradation of the PLLA component when compared with how PLLA degraded on its own. When examining polymer blends by SEM before and after degradation, the appearance of voids within the

structure was observed (Fig. 4.6), although care must be taken in interpreting such images because of the potential effect of dehydration before imaging on the microstructure.

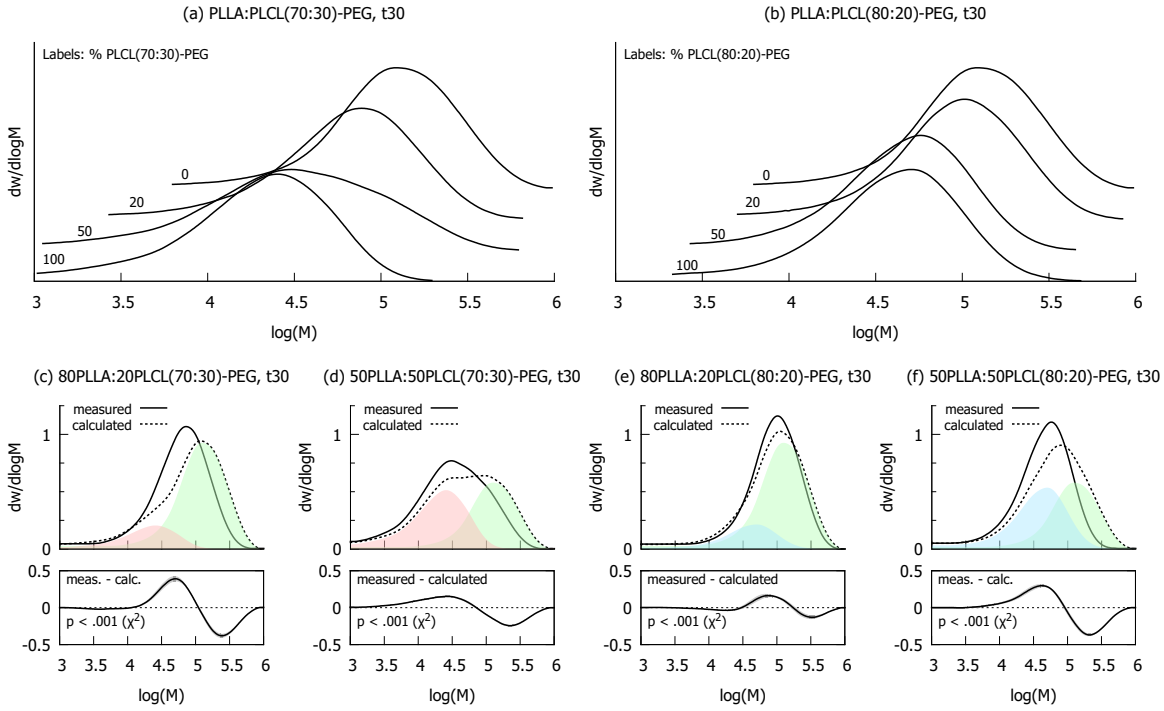

Fig. 4.5: GPC molecular weight distributions for PLLA:PLCL(70:30)-PEG blends (a) and PLLA:PLCL(80:20)-PEG blends (b) after 30 days degradation in PBS; curves are offset for clarity. Bottom row (c-f) shows measured and calculated distributions, based on a linear combination of the individual components (green = PLLA, red = PLCL(70:30)-PEG, blue = PLCL(80:20)-PEG). Shaded region in difference plot denotes standard deviation, n = 3. Reproduced from Oosterbeek et al. [273].

After the short degradation experiment, drying of polymer blend samples allowed the dry mass and water uptake to be calculated, as shown in Fig. 4.7. All blends except the pure PLCL-PEG copolymers showed no reduction in dry mass after 30 days degradation, while pure PLCL-PEG copolymers showed a small reduction in dry mass due to their faster degradation. The wet mass (sum of dry mass and water uptake) was consistent with long-term experiments at this time-point (Fig. 4.4), showing low water uptake for pure PLLA and PLCL-PEG copolymers, and a maximum water uptake for moderate PLCL-PEG additions (30 - 40% PLCL-PEG) reaching ∼5% water for PLLA:PLCL(80:20)-PEG and ∼20% water for PLLA:PLCL(70:30)-PEG.

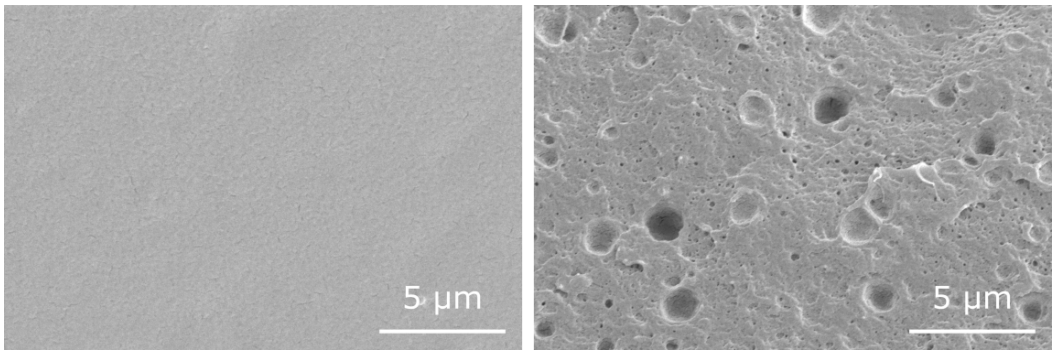

Fig. 4.6: SEM images of cross-sections of 80PLLA:20PLCL(70:30)-PEG before (left) and after (right) 30 days degradation, showing voids appearing after degradation. Reproduced from Oosterbeek et al. [273].

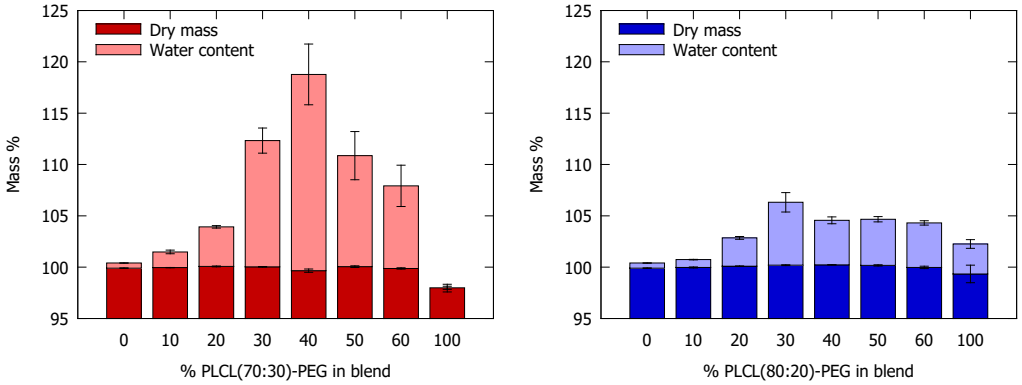

Fig. 4.7: Measured dry mass and water uptake (as % of original dry mass) for PLLA:PLCL-PEG blends after 30 days degradation in PBS at 37°C, showing PLLA:PLCL(70:30)-PEG blends (left) and PLLA:PLCL(80:20)-PEG blends (right). Error bars denote standard deviation, n = 3.

DSC analysis (Fig. 4.8) revealed several changes to the polymer blend structure that had occurred during 30 days degradation in PBS. While the PLLA:PLCL(80:20)-PEG blends showed unchanged miscibility behaviour, that of the PLLA:PLCL(70:30)-PEG blends had changed, with an increased region of miscibility now up to $\leq$ 40 wt% PLCL(70:30)-PEG. Changes were also seen in the enthalpy relaxation behaviour, where the associated peak (endothermic peak after the glass transition - ΔH_R) significantly increased after degradation for pure PLLA and blends with low PLCL-PEG content (Fig. 4.8). Examples of the glass transition region of the DSC curves are also shown in Fig 4.8, where the increase in the endothermic enthalpy relaxation peak after the glass transition can be seen for pure PLLA and 10 wt% PLCL-PEG blends, but not for blends with higher PLCL-PEG content. In addition to the increased endothermic peak

after the glass transition, blends that displayed significant enthalpy relaxation also showed increased glass transition temperatures compared to their as-fabricated state.

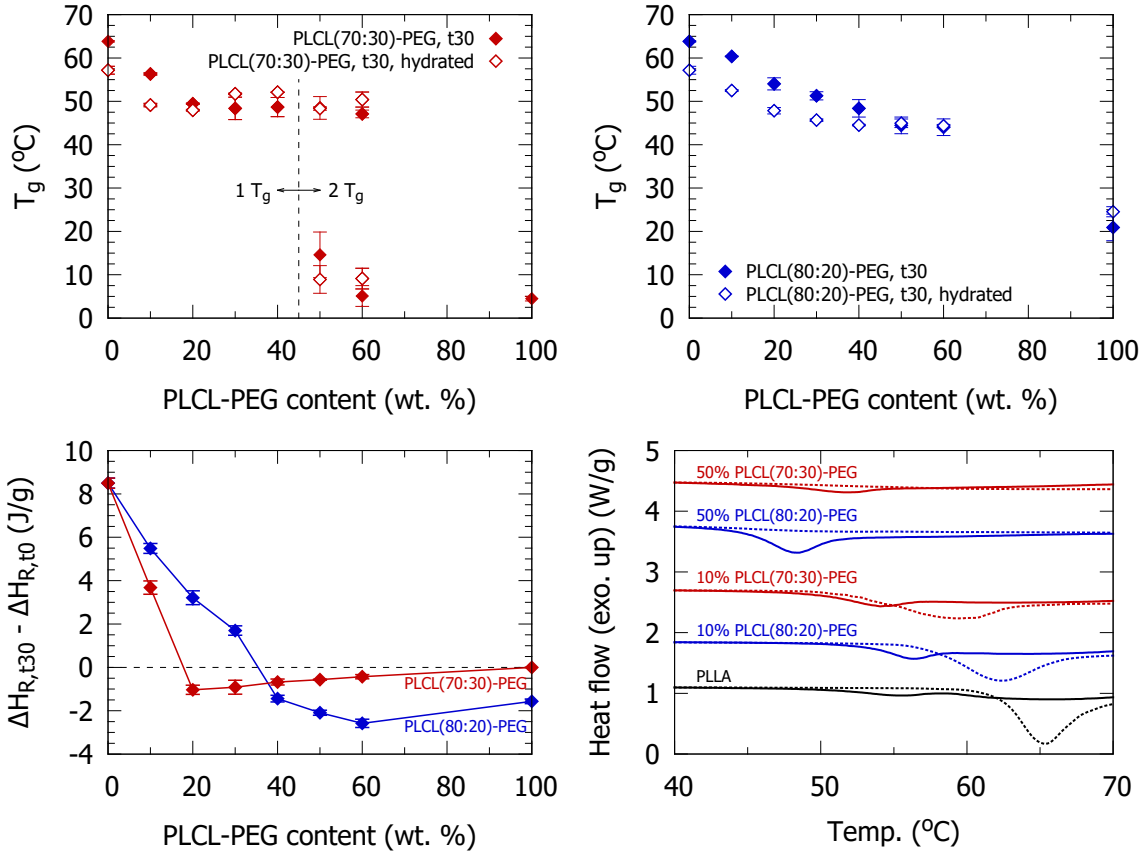

Fig. 4.8: Thermal properties of PLLA:PLCL-PEG blends measured after 30 days degradation in PBS at 37°C. Glass transition temperature (T_g) of PLLA:PLCL(70:30)-PEG blends (top left) and PLLA:PLCL(80:20)-PEG blends (top right) in dry and hydrated conditions. The change in enthalpy relaxation peak area during degradation (bottom left), and examples of the glass transition region of DSC curves (bottom right) are also shown. For DSC curves, solid lines denote measurements before degradation, and dotted lines denote measurements after 30 days degradation. Error bars denote standard deviation, n = 3. Reproduced from Oosterbeek et al. [273].

XRD was used to determine whether the initially amorphous polymer blends had crystallised during degradation. The crystalline content and representative diffraction patterns are shown in Fig. 4.9. For pure PLLA and blends with low PLCL-PEG content, little to no crystallisation was seen. At higher PLCL-PEG content, a step change was seen, where a large increase in crystallinity took place, increasing to a plateau at around 60% crystallinity. Observed peaks are consistent with the α form of the PLLA unit cell [140, 288].

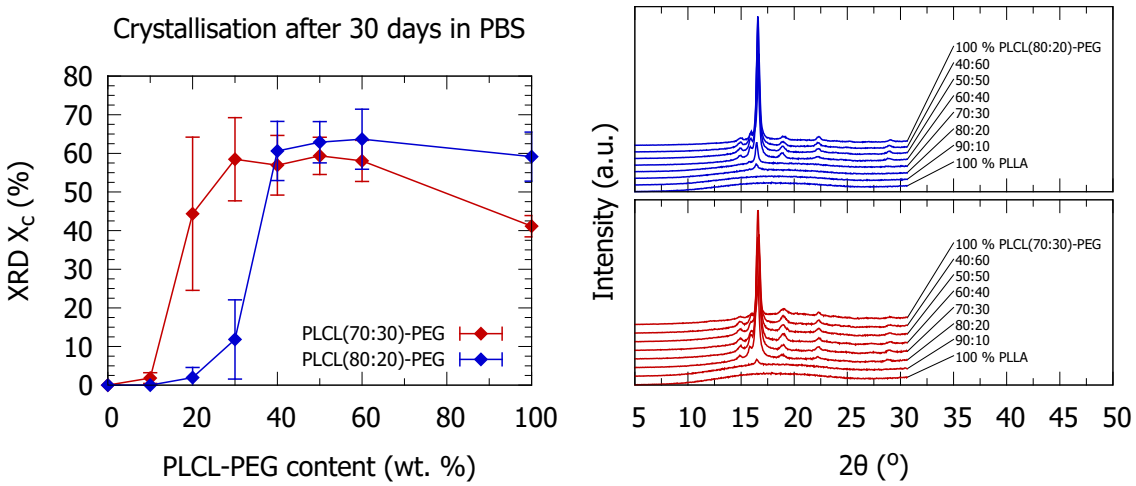

Fig. 4.9: Left: XRD crystallinity of initially amorphous polymer blends after 30 days degradation in PBS. Error bars denote standard deviation, n = 3. Right: representative diffraction patterns for PLLA:PLCL-PEG blends after degradation, labels denote PLLA:PLCL-PEG blend ratio, and datasets are offset for clarity. Reproduced from Oosterbeek et al. [273].

4.3.3 Mechanical properties after short-term degradation

Representative stress-strain curves, and a summary of mechanical properties are given in Figs. 4.10 and 4.11. When testing in simulated body conditions, these blends all displayed ductile behaviour initially as discussed in the previous chapter. After 30 days degradation in PBS at 37°C, several significant changes were seen in the mechanical properties of the polymer blends compared with those measured under the same conditions (in 37°C water) before degradation. Firstly, pure PLLA and 90PLLA:10PLCL(80:20)-PEG were strengthened but embrittled, with an increase in stiffness and strength, and large reduction in ductility. Blends with $\geq$ 20% PLCL(70:30)-PEG or $\geq$ 40% PLCL(80:20)-PEG also displayed significant embrittlement. Finally, the group of blends of PLLA with 10% PLCL(70:30)-PEG or 20 - 30% PLCL(80:20)-PEG constitute a compositional "sweet spot", where the polymers retained a significant amount of ductility after 30 days degradation, as well as maintaining comparable strength and stiffness.

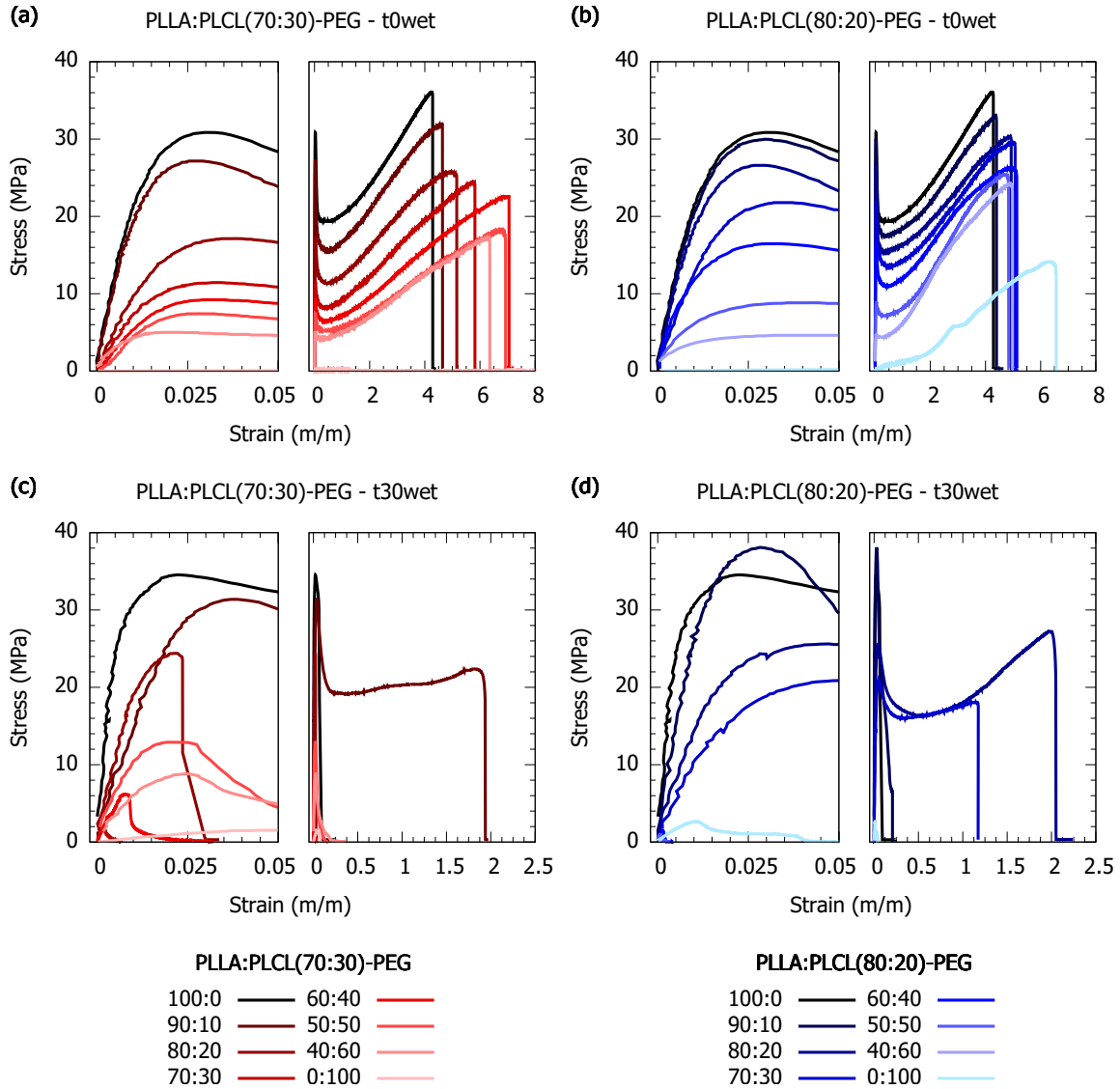

Fig. 4.10: Representative stress-strain curves for tensile testing of PLLA:PLCL-PEG blends under various conditions. As-fabricated PLLA:PLCL(70:30)-PEG blends (a) and PLLA:PLCL(80:20)-PEG blends (b) tested immersed in 37°C water (reproduced from Fig. 3.8), and PLLA:PLCL(70:30)-PEG blends (c) and PLLA:PLCL(80:20)-PEG blends (d) tested immersed in 37°C water, after 30 days degradation in PBS.

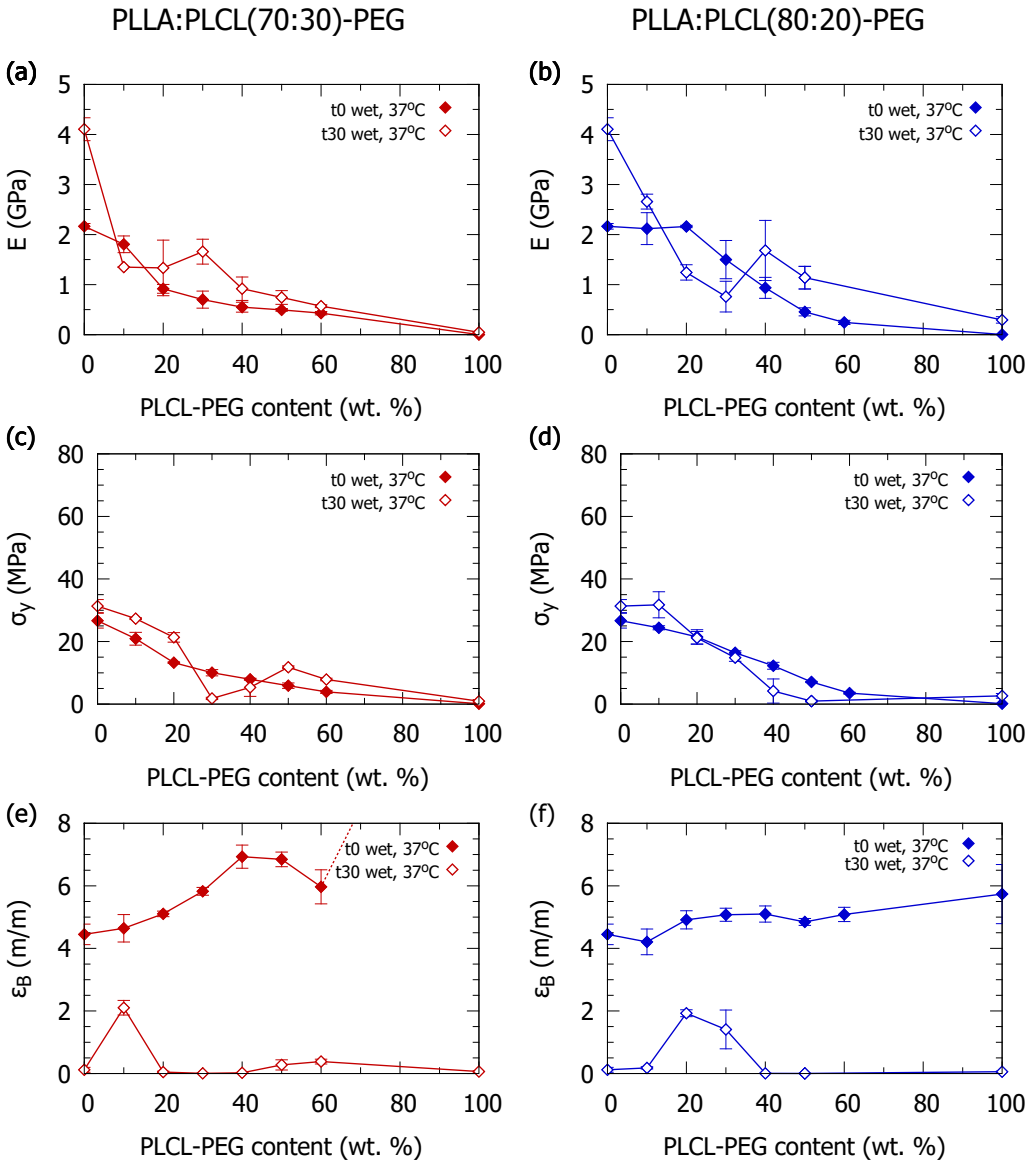

Fig. 4.11: Mechanical properties measured by tensile testing for PLLA:PLCL-PEG blends under various conditions. **t0 wet, 37°C** denotes as-fabricated samples tested immersed in 37°C water (reproduced from Fig. 3.9), and **t30 wet, 37°C** denotes samples tested immersed in 37°C water, after 30 days degradation in PBS. Top row: elastic modulus (a, b), middle row: yield strength (c, d), bottom row: elongation at break (e, f). Left column: PLLA:PLCL(70:30)-PEG blends (a, c, e), right column: PLLA:PLCL(80:20)-PEG blends (b, d, f). Error bars denote standard deviation, n = 3.

4.4 Discussion

During degradation, pH reduction was only seen for pure PLLA after more than 500 days. This is as expected as it is known to require over a year for resorption [35, 36, 62, 284, 285]. PLCL copolymers have been shown to degrade faster than either homopolymer [75], and this rapid degradation was seen here after approximately 2 months. After 30 days GPC measurements of degradation indicated that the addition of PLCL-PEG to PLLA accelerated degradation of the polymer blend. This can be attributed to auto-catalytic behaviour [130, 134] - as the faster degrading PLCL-PEG breaks down, there is an accumulation of catalytic oligomers formed by hydrolysis, which then catalyse degradation of PLLA as well as further degradation of PLCL-PEG. This is consistent with SEM observations, where the voids seen may correspond to areas where significant auto-catalysis has occurred, resulting in pockets of low molecular weight oligomers which diffuse slowly out through the polymer matrix [134, 138]. The non-linear dependence of the degradation time on composition (Fig. 4.2) also corroborates this autocatalytic mechanism.

Structural changes in polymer blends after degradation include increased miscibility, enthalpy relaxation, and crystallisation. The increased miscibility of PLLA:PLCL(70:30)-PEG blends can be attributed to the molecular weight reduction that occurred during degradation, making mixing more thermodynamically favourable. The increase in the enthalpy relaxation peak (ΔH_R) for pure PLLA and blends with low PLCL-PEG content indicates that these blends have undergone rearrangement into a denser, more thermodynamically stable configuration. This has also resulted in an increased T_g due to the reduced free volume in the densified structure [51]. The chain cleavage resulting from the hydrolysis reaction provided additional mobility for the polymer to rearrange into a crystalline structure [139], leading to those blends that degraded faster (greater PLCL-PEG content, and greater CL content in copolymer) having higher crystalline content. After the step transition ($\geq$ 20% PLCL(70:30)-PEG or $\geq$ 40% PLCL(80:20)-PEG) the blends showed a similar degree of crystallinity, indicating that

some maximum extent of crystallisation has been reached. Pure PLCL(70:30)-PEG showed a slightly lower crystallinity however, probably due to the difficulty of packing the less homogeneous copolymer. The appearance of the polymer discs during the long term degradation study (Fig. 4.3) is also consistent with crystallisation, where even the blends with low crystalline content show some opacity, while pure PLLA which has not crystallised after 30 days degradation remains transparent. It must be acknowledged however, that opacity could also arise as a result of cracking that may occur during degradation, or formation of clusters of absorbed water within the polymer.

These structural changes had a direct result on the mechanical properties. Pure PLLA and 90PLLA:10PLCL(80:20)-PEG samples experienced significant enthalpy relaxation, leading to densification, increased stiffness and strength, but lower ductility [51]. Blends with $\geq$ 20% PLCL(70:30)-PEG or $\geq$ 40% PLCL(80:20)-PEG displayed reduced molecular weight and high crystallinity as described above, resulting in increased stiffness and variable gains in yield strength, along with severe brittleness. The presence of a small amount of PLCL-PEG in blends of PLLA with 10% PLCL(70:30)-PEG or 20 - 30% PLCL(80:20)-PEG reduced the enthalpy relaxation during this timeframe (Fig. 4.8), due to the difficulty of structural rearrangement when two different polymers are present. Also, the amount of PLCL-PEG present was not sufficient to cause significant chain cleavage which leads to crystallisation (Fig. 4.9), resulting in a structure that was more resistant to enthalpy relaxation and crystallisation, and therefore retained much of its original ductility.

Based on the results discussed above, I suggest the following theoretical framework to summarise and explain the evolution of mechanical properties during degradation, specifically the embrittlement that occurs during degradation, resulting in the initially ductile polymers (when tested in 37°C water) becoming brittle. This embrittlement has been shown to be the result of two different structural changes, which occur for different blend ratios: enthalpy relaxation, and crystallisation. These are both exothermic

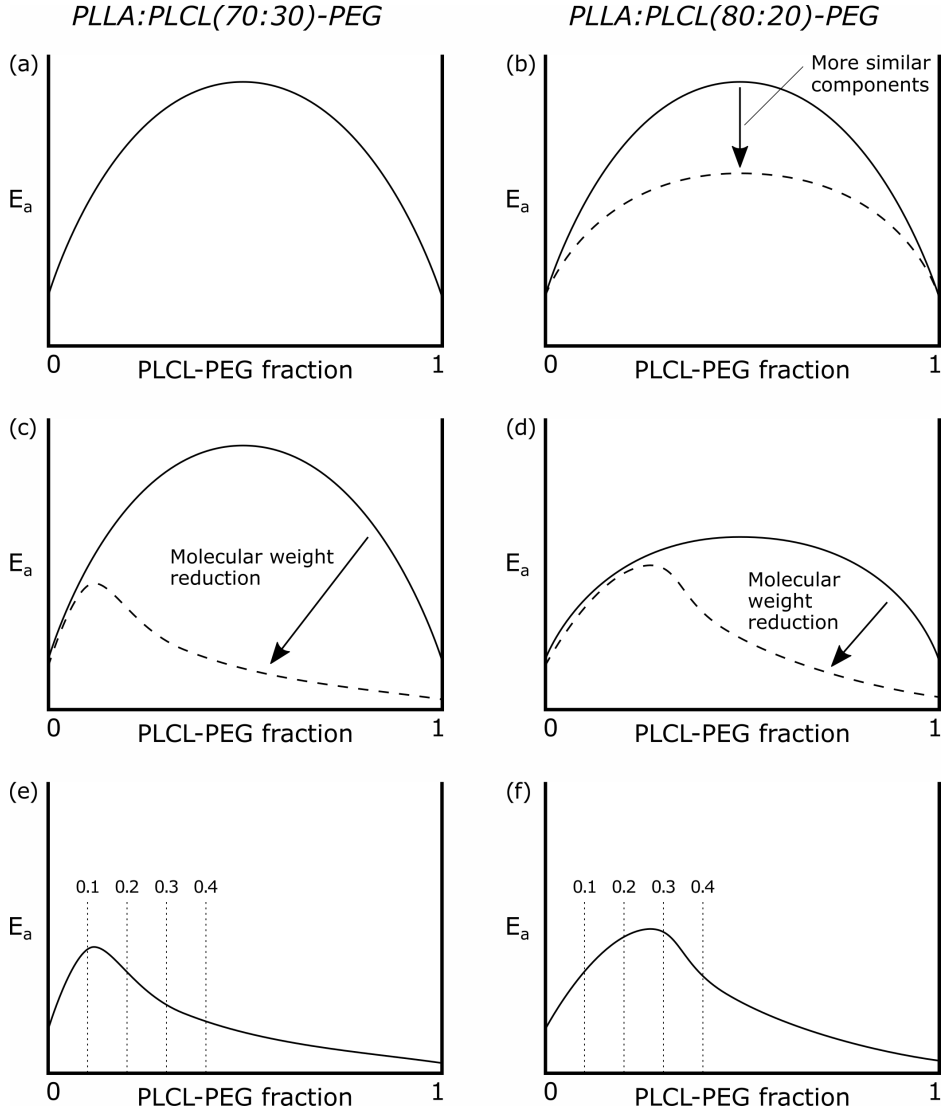

Fig. 4.12: Schematic diagrams showing the activation energy (E_a) for the general structural changes across blend compositions, showing the effect of polymer composition (a, b) and molecular weight reduction (c, d). (e, f) shows the combined effect of polymer composition and degradation, resulting in a maximum activation energy at certain compositions. Reproduced from Oosterbeek et al. [273].

transformations which have an associated activation energy, which governs the rate of transformation [51, 289]. In general for polymer blends, like-like interactions are favoured over interactions between different polymers, i.e. the Flory-Huggins interaction parameter χ is generally positive. It then follows that the activation energy for the general structural relaxation which increases intermolecular interactions will be greatest for a 50:50 blend, and lowest for the pure polymers. This is shown schematically in

Fig. 4.12a for PLLA:PLCL-PEG blends. By the same reasoning, if one of the blend components is exchanged for one that is chemically more similar to the other (e.g. exchanging PLCL(70:30)-PEG for PLCL(80:20)-PEG, which is more similar to PLLA), the magnitude of the activation energy will be decreased overall, as seen in Fig. 4.12b.

The activation energy for structural relaxation is also dependent on the molecular weight of a polymer, with a lower molecular weight known to reduce the activation energy and accelerate both enthalpy relaxation and crystallisation [51, 289, 290]. This is relevant to this work due to the effect of degradation, which reduces the molecular weight. This molecular weight reduction is asymmetric however, as discussed above, with high PLCL-PEG blends degrading significantly more than blends with lower PLCL-PEG content. This is reflected in Fig. 4.12c-d, where the activation energy for structural relaxation is reduced significantly for high PLCL-PEG blends, but only slightly for blends with low PLCL-PEG content.

The combination of these effects, as summarised in Fig. 4.12e-f, results in a maximum activation energy for low PLCL-PEG content. With increasing PLCL-PEG, the activation energy increases due to interactions between dissimilar polymer chains. As the PLCL-PEG content is increased further however, the activation energy decreases again due to molecular weight reduction caused by the accelerating effects of degrading PLCL-PEG. This can therefore provide an explanation of the changes in mechanical properties seen in Fig. 4.11, where a "sweet spot" of low PLCL-PEG content was seen, which retained some of its ductility during degradation. Higher or lower concentrations of PLCL-PEG resulted in stiffer but more brittle materials due to the aforementioned structural changes. This theoretical framework can provide a useful approach to explaining the evolution of the mechanical properties of polymer blends during degradation, as well as providing a basis for rational design of blends to engineer desired properties. These effects are summarised in Fig. 4.13, where degradation is shown to result in densification by either enthalpy relaxation or crystallisation, resulting in a corresponding embrittlement.

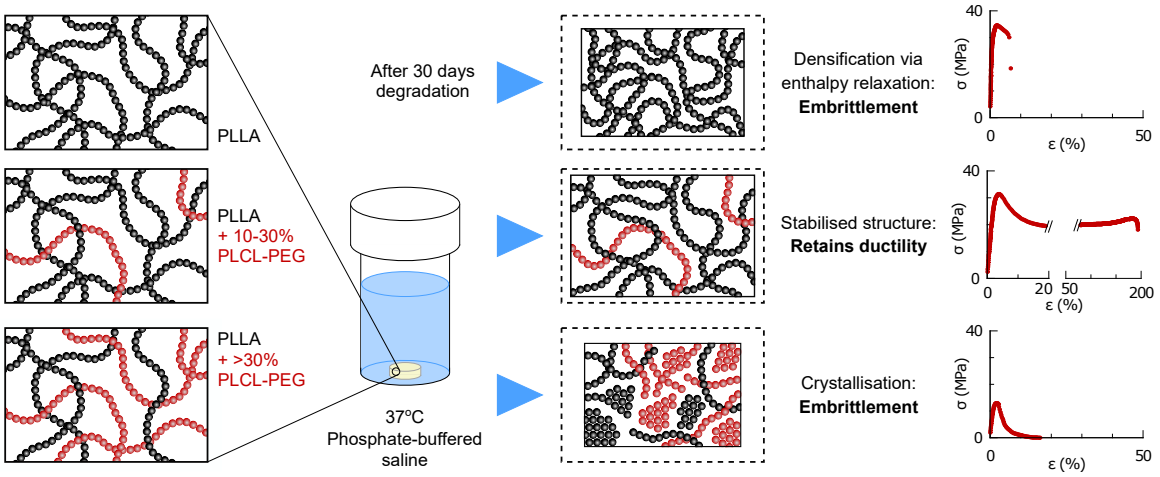

Fig. 4.13: Schematic diagram showing the initial structure of polymer blends with significant free volume (left), followed by densification during degradation by enthalpy relaxation or crystallisation, resulting in a more tightly packed or crystallised structure (middle). The effect on mechanical properties is shown (right), where greater densification leads to embrittlement.

When considering the design of materials for bioresorbable stents, these materials show significant promise. The phase separation that occurs within the blends significantly increases the ductility of the dry polymer, allowing plastic deformation during the crimping process, while the hydration-induced plasticisation would allow expansion *in vivo* with reduced risk of fracture. The accelerated degradation achieved here compared with pure PLLA is a promising result, allowing faster resorption on timescales that more closely resemble healing times, and the ability to prevent embrittlement during degradation is another crucial benefit. These results together provide a number of methods for designing resorbable stent materials with improved mechanical properties, faster resorption time, and retention of favourable mechanical properties during degradation.

4.5 Conclusions

A blending strategy has been developed which facilitated fine-tuning of performance with respect to polymer ductility, strength and stiffness while also offering broadened flexibility and perspective to bioresorbable polymer degradation profiles.

Degradation tests indicated that the presence of PLCL-PEG in the blend accelerates degradation; not only did the PLCL-PEG phase degrade, but the degradation products released accelerated degradation of both components via auto-catalysis. This approach demonstrates the ability to tune the degradation rate of these bioresorbable materials by controlling the PLLA:PLCL-PEG blend composition.

The evolution of the mechanical properties during degradation is governed by the structural changes that take place. Pure PLLA and blends with 10% PLCL(80:20)-PEG display densification via enthalpy relaxation, leading to increased strength and stiffness, along with embrittlement. Slightly higher amounts of PLCL-PEG (10% PLCL(70:30)-PEG, or 20-30% PLCL(80:20)-PEG) reduce this tendency for enthalpy relaxation, decreasing the extent of embrittlement that takes place during degradation. Larger amounts of PLCL-PEG ($\geq$ 20% PLCL(70:30)-PEG, or $\geq$ 40% PLCL(80:20)-PEG) begin to cause extensive molecular weight reduction, enhancing chain mobility and allowing crystallisation. This also leads to increased strength and stiffness, along with embrittlement. These mechanisms, and the resulting compositional "sweet spot" have been explained in terms of an activation energy for structural relaxation, where the chemical similarity of the blend components, and changes in molecular weight, are the main controlling factors.

Chapter 5

P_2O_5-CaO-Na_2O glasses: production and characterisation

5.1 Background and aims

Phosphate glasses are potentially promising materials for addressing the deficiencies of polymers and polymer blends for cardiac stents, in particular their mechanical properties, as discussed in sections 2.3 and 2.4. Phosphate-based glasses modified with calcium are of particular interest for biomedical applications, due to their chemical similarity to natural bone [159]. Even for applications in polymer composites for cardiac stents, where this similarity is of less concern, their ability to slowly dissolve in aqueous environments is a crucial advantage.

There are a number of techniques used for production of phosphate glasses. Sol-gel processing is a wet chemical method that involves reaction of precursors to form colloidal particles, and further condensation reactions develop the network. This results in an inorganic network containing a liquid phase, which is then removed by drying to form a porous material [291]. Sol-gel processing is a popular technique due to the low temperatures used, allowing inclusion of biologically active molecules, as well as the method's versatility of form (e.g. powders, films, coatings, porous scaffolds, and

bulk monoliths can all be fabricated). Unfortunately this method can be technically challenging, and it can be difficult to successfully achieve glassy gels with the desired composition [159, 292].

Melt processing techniques are the more traditional method for production of glass, and have been used since antiquity to create silica-based glasses, but are equally well suited to modern biomedical phosphate glasses. Here the glass precursors are melted at high temperature (over 1000℃) to form a homogeneous and degassed melt, before being rapidly quenched to below the glass transition temperature (T_g), and then slowly cooled to room temperature to remove residual stresses [159, 293]. Provided that a sufficiently fast cooling rate can be achieved, a large range of glass compositions can be successfully vitrified. The high temperatures used however, prevent incorporation of temperature-sensitive biological molecules, and the top-down approach makes production of nanoparticles or nanoscale pores challenging [220].

Unlike crystalline materials, the properties of melt-quenched glasses can be heavily dependent on their particular thermal history. The glass melt contracts as it cools, however if the melt is cooled rapidly, structural rearrangement to a denser structure cannot take place and the structure becomes fixed. For slower cooling, equilibrium between cooling and rearrangement can be maintained to a lower temperature, so a denser glass forms, with less free volume [293]. The glass density, and resulting free volume, can have profound effects on the transport properties, requiring greater energy for diffusion of ions through the glass as the density increases [294]. Due to the role of diffusion in phosphate glass dissolution [203, 205], the thermal history can therefore affect the glass dissolution behaviour in turn. In addition to the thermal history of the glass, the glass composition and the resulting network structure also have a significant effect on the final glass properties, from density and transport properties, to *in vitro* dissolution behaviour [160, 165, 178].

This chapter describes the production of a range of P_2O_5-CaO-Na_2O glasses, and the characterisation of their physical and chemical structure and properties. The glasses, in the range $(P_2O_5)_{90\text{-}x}(CaO)_x(Na_2O)_{10}$, where x = 40, 45, 50, were produced using melt quenching. Melt quenching allows the range of glass compositions used here, which can be challenging to produce using sol-gel methods, to be fabricated in a relatively straightforward manner. It also enables quenched glass to be further processed into bulk discs, which are convenient for certain experiments, or into powder suitable for incorporation into polymer-glass composites.

Accurate characterisation of the glass structure and properties is critical to understanding and explaining their dissolution behaviour, where factors such as ionic crosslinking and glass density can have an appreciable impact on the dissolution mechanics. This in turn can determine the degradation behaviour of polymer-glass composites that utilise these glasses, where the dissolution of the glass component is thought to play a major role in composite degradation [253–255]. In order to design polymer-glass composite materials suitable for bioresorbable cardiac stents, the degradation time must be within the body's natural healing timeframe, and controllable by composite composition. This chapter therefore aims to achieve a thorough understanding of the structure and properties of the phosphate glasses produced for later incorporation into polymer-glass composites, in particular those properties that are relevant for determining the dissolution behaviour. Polymer-glass composites utilise glass in powder form rather than the discs used for more comprehensive investigations here, therefore another key aim is to examine the differences between glasses with these two differing thermal histories, and assess the impact on their resulting properties.

5.2 Materials and Methods

5.2.1 Glass preparation

Glasses were prepared from precursors of sodium carbonate (Na_2CO_3), calcium carbonate ($CaCO_3$) and monoammonium phosphate ($NH_4H_2PO_4$). These were mixed and placed in a vitreous silica crucible, and heated in a kiln (SBSC-1500L, Kilns and Furnaces Ltd., Stoke-on-Trent, UK) to allow removal of H_2O and CO_2 gases. The powders were melted at the temperatures described in Table 5.1, and then either dry quenched by pouring the molten glass onto a cooled steel plate, or wet quenched by pouring into a bucket of water. Glass that was wet quenched was quickly removed from the water and placed in an oven at 120℃ to dry overnight, to reduce the effect of any moisture incorporated from water quenching. Wet quenching was required for one glass composition due to its tendency to crystallise at the lower cooling rate associated with dry quenching. Feed and target compositions, melt temperatures, and quench methods are listed in Table 5.1. Using this method, glass frit with size of several millimetres was obtained.

Some of this glass frit was then used to cast small discs, which are a more convenient form for some experiments. Glass frit was melted in a platinum crucible, in a Carbolite BLF1700 furnace, with casting temperatures of 1100℃ for P50Ca40 and P45Ca45 glasses, and 1230℃ for P40Ca50 glass. The molten glass was poured into a graphite mould (10 mm disc diameter, 2 mm thickness) that was preheated to 390℃ in a kiln (SBSC-1500L, Kilns and Furnaces Ltd., Stoke-on-Trent, UK). After a few seconds for the glass to solidify, the disc was removed from the mould and placed in the kiln at 390℃ to anneal. The discs were then left to cool to room temperature overnight in the kiln.

The preparation of glasses carried out in this section was done with the assistance of Mr. Ian Campbell, at Lucideon Ltd., Stoke-on-Trent, UK, and I am extremely thankful for his expertise and assistance in this area.

Table 5.1: Feed and target compositions, melt temperatures, and quench methods for the glasses produced.

Code		P50Ca40	P45Ca45	P40Ca50
Feed compositions (wt. %)	Na_2CO_3	6.3	6.7	6.5
	$CaCO_3$	24.1	28.8	32.9
	$NH_4H_2PO_4$	69.6	64.5	60.6
Target compositions (mol. %)	P_2O_5	50	45	40
	CaO	40	45	50
	Na_2O	10	10	10
Melt temperature (℃)		1230	1250	1360
Quench method		Dry	Dry	Wet
Disc casting temperature (℃)		1100	1100	1230

5.2.2 Powder milling

The glass frit that was not used for casting discs was milled to produce a coarse powder for later experiments. The glass frit was crushed by hand with a mortar and pestle, to fit through a 3.15 mm aperture sieve. A Fritsch Pulverisette 6 planetary ball mill was then used to mill this to a coarse powder. The glass frit (approximately 170 g) was added to the grinding bowl, along with 25 zirconia balls (20 mm diameter). This was milled at 550 rpm for 5 minutes, after which the powder was sieved through a 500 µm sieve and stored in glass jars.

5.2.3 Characterisation

5.2.3.1 Particle size analysis

Particle size was measured using a laser diffraction particle size analyser - Malvern Mastersizer 2000, with Hydro MU 2000 (A) pumping attachment (Malvern Instruments

Ltd., UK). The refractive index of the glasses was assumed to be constant at 1.543, with absorption coefficient of 0.02 [295], and the samples were dispersed in acetone (as the phosphate glasses are hygroscopic). Pumping speed was kept constant at 2000 rpm, and ultrasonication was carried out prior to analysis to break up agglomerates, by sonicating for 60 seconds with an amplitude of 10 µm. After sonication analysis was delayed by 60 seconds to allow bubbles caused by sonication to be removed. Five measurements were carried out for each sample. Reported median ($d_{0.5}$) and other diameters for fractions of the particle size distribution ($d_{0.1}$, $d_{0.9}$) are based on the particle volume distribution, unless otherwise specified.

5.2.3.2 Density

The density of the glass powders and discs was measured using an AccuPyc 1330 gas pycnometer (Micromeritics Instrument Corporation, USA). A 1 cm^3 chamber was used, calibrated with a 0.718522 cm^3 standard. Measurements were carried out until the standard deviation of the last five measurements was less than 0.1% of the mean.

5.2.3.3 DSC/TGA

DSC (Differential Scanning Calorimetry) and TGA (Thermogravimetric Analysis) were carried out on the glass samples using a TA Instruments SDT Q600 (SDT - Simultaneous DSC and TGA). Glass powder samples (10 - 25 mg) were contained in an alumina pan, and heated from 25 to 1000℃ at 20℃/min, under 100 mL/min flow of N_2 gas. A single heating run was used to measure the properties of the as-quenched glasses. The data was baseline corrected by subtracting the response of an empty alumina pan. Glass powder samples could be analysed directly, while cast discs were crushed by hand with a mortar and pestle before SDT analysis. Thermal properties were analysed using the TA Universal Analysis software, all characteristic temperatures were taken as onset temperatures except for glass transitions, which were taken as the inflection point.

5.2.3.4 SEM/EDS

SEM (Scanning Electron Microscopy) and EDS (Energy Dispersive X-Ray Spectroscopy) were carried out on the glass samples using a CamScan MX2600 FEGSEM, with EDS detector. INCA software (Oxford Instruments) was used to calculate atomic composition from EDS spectra, and measurements of elemental mol. % were converted to oxide mol. % by assuming oxidation states and stoichiometry. Prior to analysis samples were mounted on carbon tape and coated with 10 - 20 nm of Au/Pd, using an Emitech K550 sputter coater (40 mA deposition current for 2 minutes, under an argon atmosphere). Glass powder samples could be analysed directly, while cast discs were crushed by hand with a mortar and pestle before SEM/EDS analysis.

5.2.3.5 XRD

XRD (X-ray diffraction) was carried out on phosphate glass samples using a Bruker D8 Advance diffractometer with Cu Kα radiation. A 2θ range of 10-60° was used, with a 0.02° step size and dwell time of 0.5 s step^{-1}. X-ray diffraction patterns were analysed using profile analysis in HighScore Plus (Malvern Panalytical). Any crystalline material in the produced glasses was quantified by adding 5 wt.% NaCl powder, and determining the ratio of crystalline material to added NaCl.

5.2.3.6 FTIR

FTIR (Fourier Transform Infrared Spectroscopy) was carried out on phosphate glass samples using a Bruker Tensor 27 FTIR Spectrometer, in ATR configuration (Attenuated Total Reflectance). A background scan was obtained before each sample scan, and three replicates were analysed for each sample. Spectra were collected over the range 520 - 4000 cm^{-1}, with a resolution of 8 cm^{-1}, and 16 scans were collected for each sample. Coarse glass powder samples could be analysed directly, while cast discs were crushed by hand with a mortar and pestle before FTIR analysis.

5.2.3.7 NMR

The Q^n distribution in the glass network of phosphate glass powders was measured by ^{31}P solid-state magic angle spinning nuclear magnetic resonance (MAS-NMR), using a Bruker Avance 300 spectrometer at 121 MHz and a 4 mm MAS probe. Acquisition of NMR spectra was carried out by Dr Abil Aliev at University College London, and I am very grateful for his support with these experiments. Data analysis of NMR spectra was carried out by the author, here 1D spectra were fitted using TopSpin 4.0.5 (Bruker Ltd.) to quantify the Q^n species present.

5.3 Results

5.3.1 Physical and chemical properties

The composition of the glasses produced was measured by EDS, and is shown in Fig. 5.1 and Table 5.2. The CaO and P_2O_5 content is very close to the target compositions, which range from 40 - 50 mol. %. The Na_2O content is significantly lower than the target composition (about 7 mol. % compared with 10 mol. %), and appears to have been replaced by SiO_2. This is likely a result of diffusion of silica from the fused silica crucible into the melt during melting. Silicon replaces sodium, as alkali oxides such as sodium are known to be prone to volatilisation losses due to their high vapour pressure at elevated temperature [293]. In all cases there is negligible difference between the glass powder samples and the cast discs, indicating that the casting process did not alter the concentration or introduce any new impurities. This is to be expected, as a platinum crucible was used for remelting and casting rather than the silica crucible used for melting of the initial batch.

The glass densities were measured, and are presented in Fig. 5.2 and Table 5.3. The values measured here are broadly comparable to those seen in the literature for similar

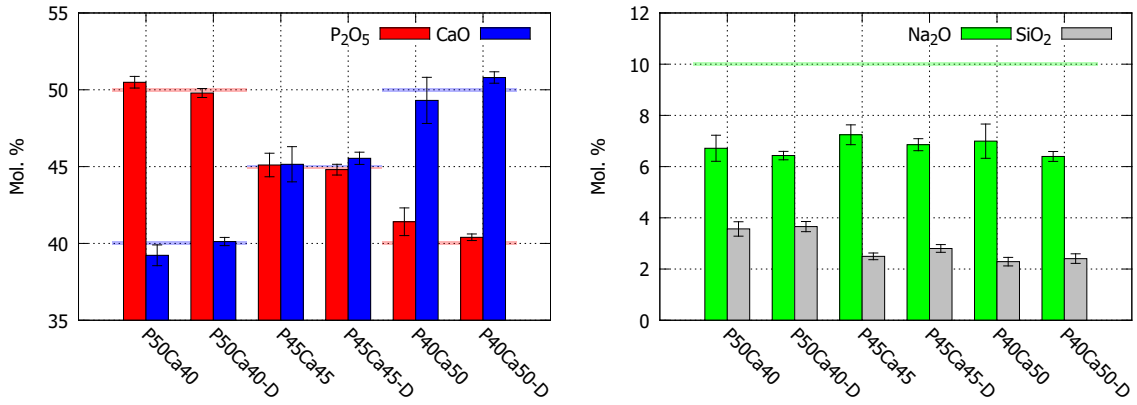

Fig. 5.1: Compositions of the glass samples measured by EDS, -D denotes the cast discs. Transparent lines show the target compositions for each glass. EDS spectra taken at 15 kV.

Table 5.2: Composition of the phosphate glass samples measured by EDS, with standard deviations. -D denotes cast discs.

Sample Code	P_2O_5 (mol.%)	CaO (mol.%)	Na_2O (mol.%)	SiO_2 (mol.%)
P50Ca40	50.5 ± 0.4	39.2 ± 0.7	6.7 ± 0.5	3.6 ± 0.3
P50Ca40-D	49.8 ± 0.3	40.1 ± 0.3	6.4 ± 0.2	3.7 ± 0.2
P45Ca45	45.1 ± 0.8	45.2 ± 1.1	7.2 ± 0.4	2.5 ± 0.1
P45Ca45-D	44.8 ± 0.3	45.5 ± 0.4	6.9 ± 0.2	2.8 ± 0.2
P40Ca50	41.4 ± 0.9	49.3 ± 1.5	7.0 ± 0.7	2.3 ± 0.2
P40Ca50-D	40.4 ± 0.2	50.8 ± 0.4	6.4 ± 0.2	2.4 ± 0.2

glass compositions [161, 167, 175, 176]. There is a clear increase in density as the CaO content increases. This is to be expected, and is the result of the increased amount of alkali oxide (glass network modifier CaO) filling interstitial spaces in the glass network, thereby increasing mass without increasing volume [293]. The free volume, a measure of the interstitial spaces present in a glass, was calculated from the measured densities and EDS compositions (according to Shelby [293]), and demonstrates the effect of alkali oxide filling these interstitial spaces.

There is also a difference in density observed between the powder and cast disc samples, with the discs displaying a consistently lower density. In this case the only

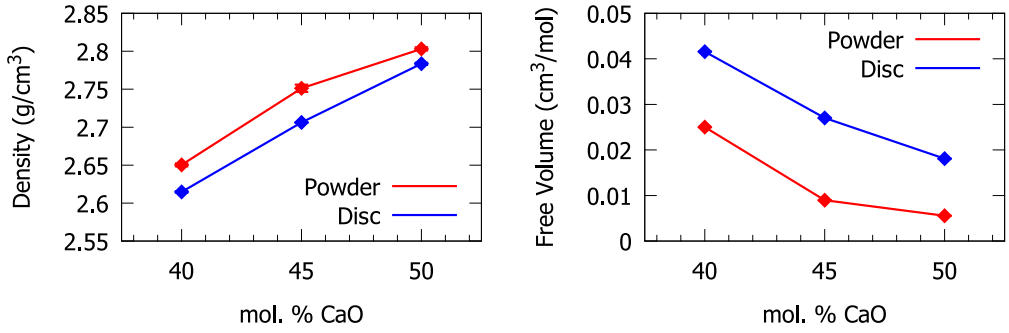

Fig. 5.2: Left: measured density for phosphate glasses. Right: free volume of phosphate glasses, calculated from measured densities and EDS compositions. Error bars (denoting standard deviation) are shown, but may be smaller than the point marker.

Table 5.3: Measured density for phosphate glass samples, with standard deviations.

Sample Code	Powder	Disc
P50Ca40	2.650 ± 0.002 g/cm^3	2.6147 ± 0.0009 g/cm^3
P45Ca45	2.751 ± 0.005 g/cm^3	2.7062 ± 0.0003 g/cm^3
P40Ca50	2.803 ± 0.002 g/cm^3	2.784 ± 0.001 g/cm^3

difference between the two is their thermal history, with the powders being prepared directly from quenched glass, while the discs were cast from remelted glass frit. The lower density of the discs indicates that they experienced faster cooling during casting, leaving them with a lower density (and therefore higher free volume) and higher fictive temperature [293].

XRD patterns of the phosphate glasses are shown in Fig. 5.3, for both powder and cast disc samples. All of the samples show a broad peak at around 25 - 27°, consistent with an amorphous material. No sharp diffraction peaks are observed for almost all samples, indicating that the glass fabrication process has successfully vitrified the glasses and avoided crystallisation. Some small diffraction peaks are observed however, for P40Ca50 glass powder, indicating a small amount of residual crystallinity. This was quantified by spiking the glass with 5 wt.% NaCl before measurement, and using profile analysis to calculate the ratio of crystallised material to added NaCl. Using this

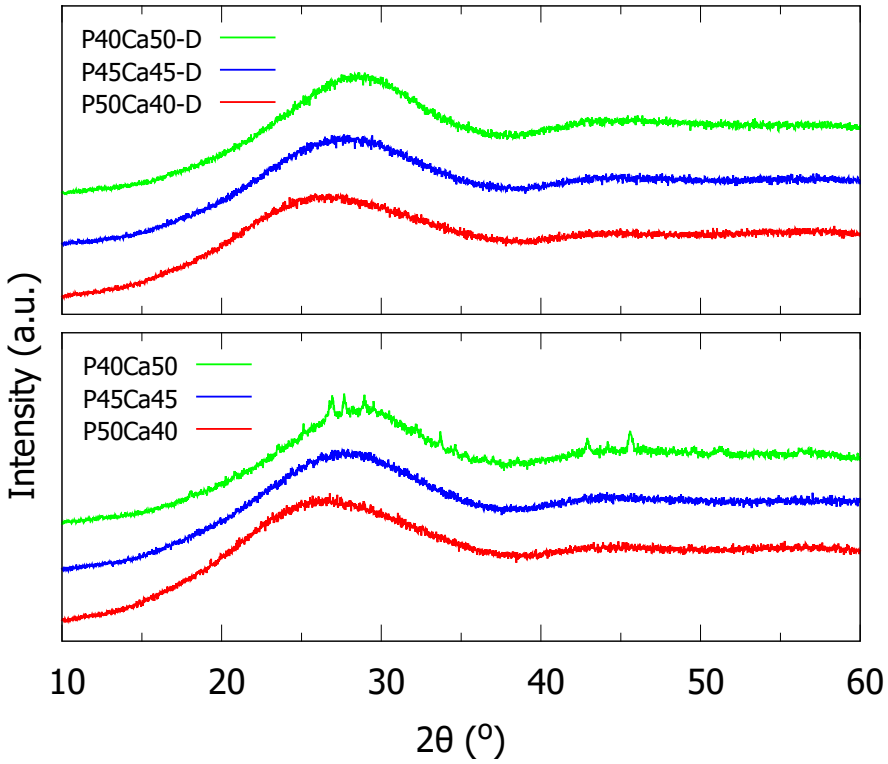

Fig. 5.3: XRD patterns for phosphate glasses, showing the crushed discs (denoted -D, top), milled glass powder (bottom).

method the crystallised material, $Ca_2P_2O_7$ (ICDD PDF file 01-073-0440), was found to be present at a level of 2.0 ±0.4 wt.%.

The broad, amorphous peak observed in the XRD patterns can also be observed to shift slightly depending on the glass composition, with higher Ca content resulting in a higher diffraction angle. A higher diffraction angle indicates smaller average atomic separation, therefore this shift in peak position suggests that increased Ca content leads to a smaller interatomic distance. This is consistent with density and free volume measurements above (Fig. 5.2 and Table 5.3).

The particle size distributions of the coarsely milled glass powder and crushed glass discs are shown in Fig. 5.4. The milled glass powder samples all have fairly similar distributions which is to be expected for a controlled process such as this. The

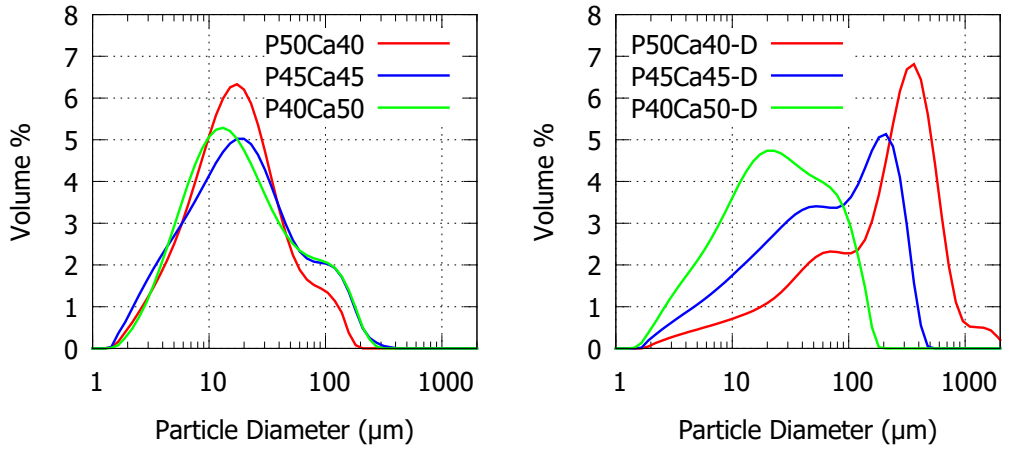

Fig. 5.4: Particle size distributions for phosphate glasses, showing the milled glass powder (left) and crushed discs (right).

mechanical properties of the glasses can be expected to be similar, so it is unsurprising that there is little significant difference in particle size between the different glass compositions. This coarse powder with $d_{0.5}$ around 15 - 17 µm is useful for handling and further analysis, however for eventual incorporation into composites, the size will need to be reduced further. The powders obtained by crushing glass discs show more variable results, which is to be expected from a manual process such as this. Because of the non-systematic nature of the process, little can be concluded from the differences between different compositions, however it is clear that the crushed glass discs have a larger particle size than the equivalent milled powders.

FTIR spectroscopy was also used to examine the chemical structure of the glasses produced, with a particular focus on the connectivity and network structure of the glass, as well as presence of impurities. FTIR spectra are shown in Fig. 5.5, and peak assignments are given in Table 5.4.

In general it is clear that the spectra for the glass discs and glass powder are very similar, however the disc spectra have a consistently lower absorbance than the powder. This can be attributed to the difference in sample preparation for FTIR - the glass powder was analysed as-produced (after dry milling to a coarse powder), while the glass

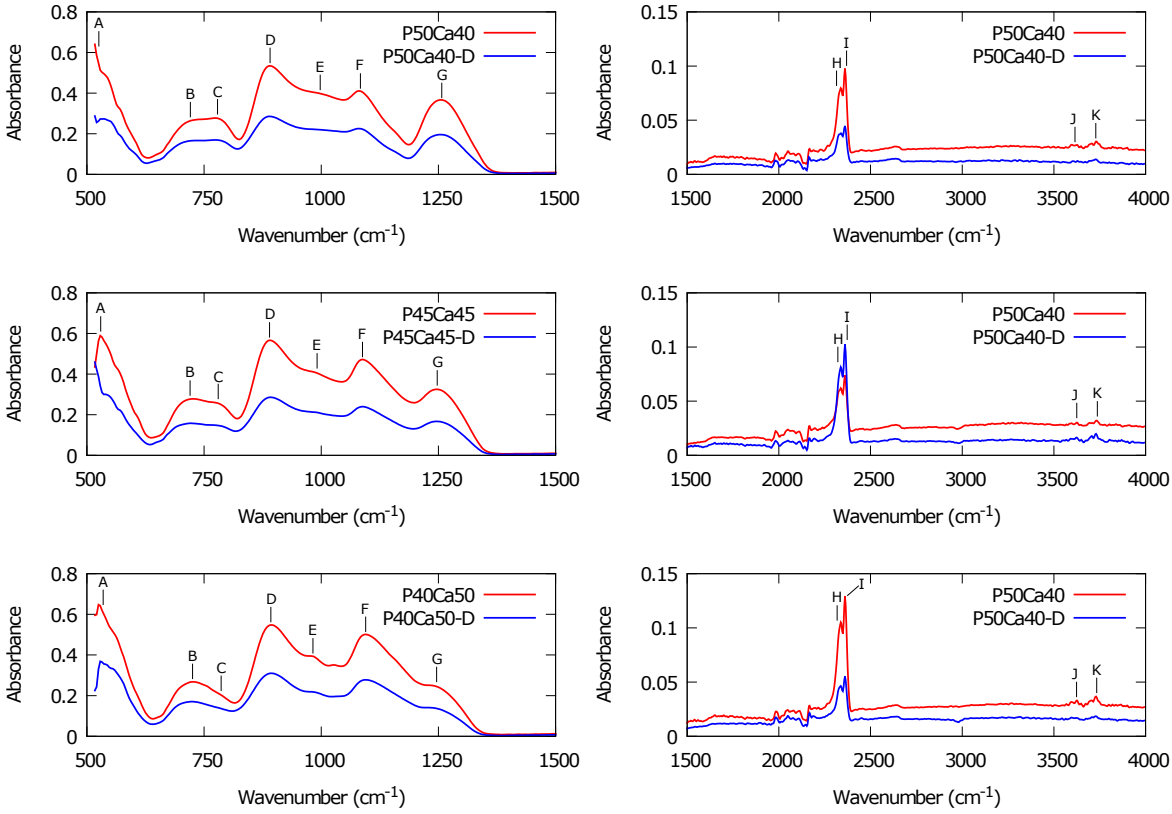

Fig. 5.5: FTIR spectra of the different glasses, -D denotes the cast disc samples. Peaks labelled A-K are described in Table 5.4.

discs were crushed by hand with a mortar and pestle. This resulted in the crushed disc samples having a larger particle size (see above), leading to poorer packing and less contact between the powder sample and internal reflection element of the spectrometer, leading to decreased absorbance, as reported previously by Udvardi et al. [296].

In general, the FTIR spectra are similar to those seen in literature for similar glass compositions. In particular, the results seen by Knowles et al. with a glass composition identical to the P50Ca40 glass validate the results seen here [299]. The only peaks observed from the glass components are from P-O bonds, which is to be expected as in this system P_2O_5 is the network forming oxide. Additions of CaO and Na_2O result in the alkali ions occupying interstitial space in the glass network, rather than forming covalent bonds with bridging oxygen atoms. This is typical behaviour for a phosphate glass and is confirmed by the FTIR spectra.

Table 5.4: Peak assignments for the labelled peaks in the FTIR spectra of phosphate glasses.

Label	Peak Position (cm^{-1})	Assignment	Symbol	Reference
A	500 - 550	P-O-P bend	δ(P-O-P)	[190, 297, 298]
B	720 - 740	P-O-P symmetric stretch	ν_s(P-O-P)	[190, 298]
C	770 - 780	P-O-P symmetric stretch	ν_s(P-O-P)	[190, 298]
D	890 - 900	P-O-P asymmetric stretch	ν_{as}(P-O-P)	[190, 297, 299, 300]
E	980 - 1000	$(PO_3)^{2-}$ terminal symmetric stretch	$\nu_s(PO_3)^{2-}$	[190, 297, 300]
F	1080 - 1100	$(PO_3)^{2-}$ terminal asymmetric stretch	$\nu_{as}(PO_3)^{2-}$	[190, 297, 300, 301]
G	1230 - 1260	O-P-O asymmetric stretch	ν_{as}(O-P-O)	[190, 202, 299, 300]
H	2335 - 2345	Gaseous CO_2 stretch	$\nu_{as}(CO_2)$	[302]
I	2355 - 2365	Gaseous CO_2 stretch	$\nu_{as}(CO_2)$	[302]
J	3600 - 3630	H_2O symmetric stretch	$\nu_s(H_2O)$	[303]
K	3725 - 3735	H_2O asymmetric stretch	$\nu_{as}(H_2O)$	[303]

The changes in peak height between different glass samples were also analysed. Most peaks show no significant changes, however peaks labelled C, F, and G (ν_s(P-O-P), $\nu_{as}(PO_3)^{2-}$, and ν_{as}(O-P-O) respectively) did show noticeable trends. These are shown in Fig. 5.6. The ν_s(P-O-P) and ν_{as}(O-P-O) peaks both involve only bridging oxygen species, and are seen to decrease as the P_2O_5 content of the glass decreases, while the $\nu_{as}(PO_3)^{2-}$ peak involves a terminal group and increases as the P_2O_5 content of the glass decreases. This is a result of the decreasing proportion of the network forming oxide P_2O_5, leading to a glass with a lower degree of connectivity, evidenced by lower concentration of bridging oxygens and higher concentration of terminal groups.

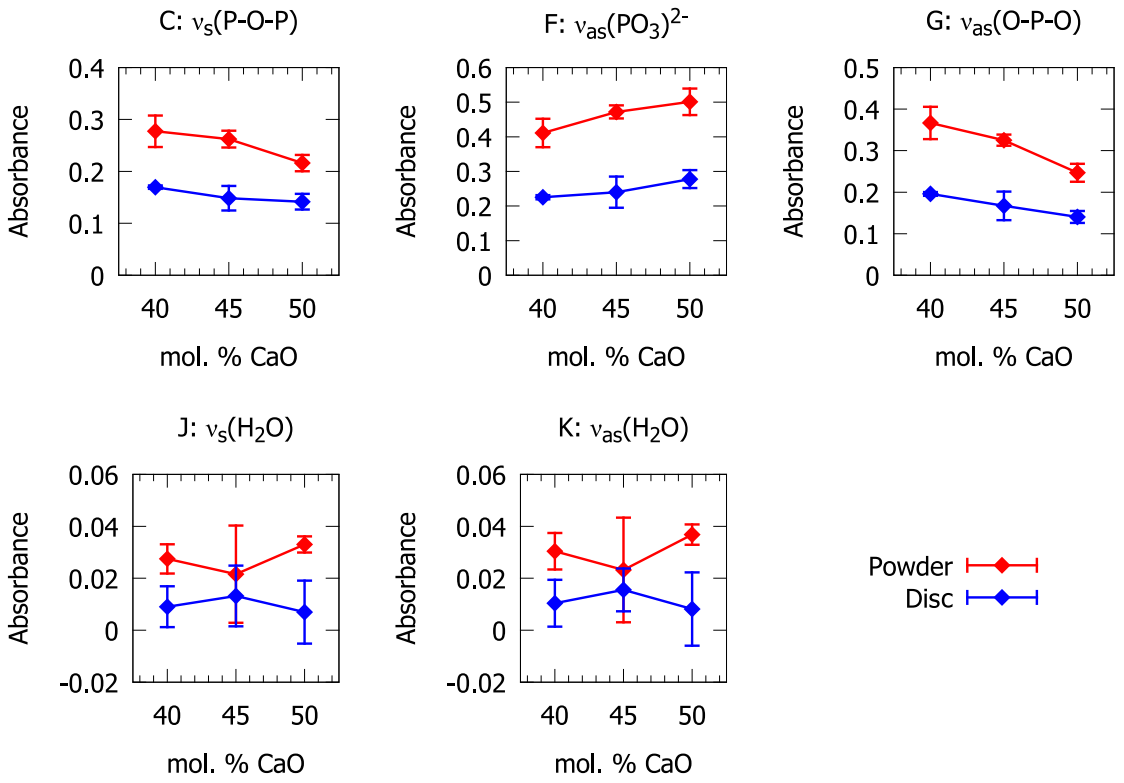

Fig. 5.6: Changes in the height of different FTIR absorbance peaks for the glass samples investigated, for as-produced powder, and cast discs. Peak labels correspond to those in Fig. 5.5, and Table 5.4.

Peaks corresponding to gaseous CO_2 are seen at around 2350 cm^{-1}, resulting from atmospheric CO_2 present in the air in voids between glass particles. This signal displayed high variability and was also seen in some background scans, demonstrating that it arose from atmospheric CO_2 rather than a component present in the glass.

The hydroxyl content of glasses is also of high importance, and is of interest in this case as one of the glass compositions (P40Ca50) was water quenched, which may have influenced its hydroxyl content. For calcium metaphosphate glasses $(P_2O_5)_{50}(CaO)_{50}$, hydroxyl content is seen to give rise to three main bands; band 1 in the range 3390 - 3640 cm^{-1} (OH-groups that are not involved in hydrogen bonding), band 2 in the range 2600 - 3000 cm^{-1} (OH-groups that interact with bridging oxygens via hydrogen bonding), and band 3 at around 2350 cm^{-1} (OH-groups interacting with each other via hydrogen bonds)[304, 305]. Any presence of band 3 would be obscured by the CO_2

signal (peaks H and I), however bands 1 and 2 are not seen either, therefore there is little evidence from this data for significant hydroxyl content in the glass. Peaks associated with water are seen however, at 3600 - 3630 and 3725 - 3735 cm^{-1}. These are related to H_2O symmetric and asymmetric stretches respectively (peaks J and K), and indicate the presence of physisorbed water rather than hydroxyl incorporated into the structure. No significant trends are seen for these peaks with respect to glass composition (Fig. 5.6 J and K), indicating that the water quenching process has not resulted in significantly different levels of water or hydroxyl incorporation compared to dry quenching.

Solid-state NMR was also used to quantitatively assess the chemical structure and network connectivity of the glass powder. From ^{31}P MAS-NMR (Fig. 5.7 and Table 5.5) only Q^1 and Q^2 phosphate tetrahedra (1 and 2 bridging oxygens respectively - see Fig. 2.10 on page 32) were seen, at positions from -7.7 to -10.8 ppm for Q^1, and from -22.9 to -25.5 ppm for Q^2 [161, 306]. Additional peaks at 50 to 100 ppm and -100 to -150 ppm can be attributed to spinning sidebands.

The glass with the highest phosphate content, P50Ca40, is composed mainly of Q^2 co-ordinated phosphate tetrahedra. No Q^3 tetrahedra are seen which is unsurprising due to the high (50%) amount of modifying oxides. As the Ca content increased the Q^1/Q^2 ratio increased, indicating depolymerisation of the network and replacement of chain forming Q^2 groups with chain terminating Q^1 groups. The Q^1 peak of the P40Ca50 glass displays two sharp peaks in addition to the single broad peak. This may be due to the presence of the small amount of crystalline $Ca_2P_2O_7$ also observed by XRD [307].

Using a simple structural model consisting of Q^2 and Q^1 tetrahedra, and the nominal glass composition, a theoretical estimate of the relative amounts of different Q species can be obtained. When using the nominal glass composition (Fig. 5.8, left), there is some discrepancy between the theoretical and experimental values. Previous measurements of these phosphate glasses with EDS show the presence of approximately

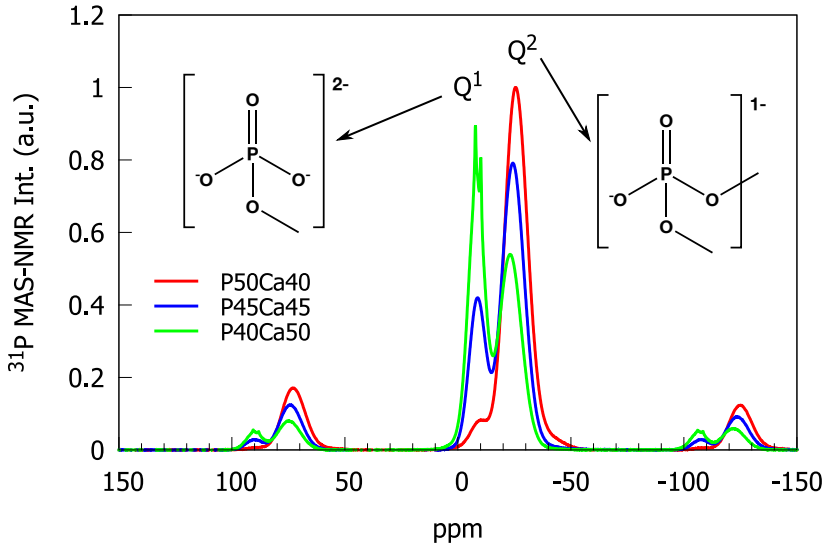

Fig. 5.7: ^{31}P MAS-NMR spectra of phosphate glass powder samples.

Table 5.5: NMR peak positions and area ratios for phosphate glass powder, with standard deviations.

Sample Code	Q^1 position (ppm)	Q^2 position (ppm)	Q^1/Q^2
P50Ca40	-10.782 ± 0	-25.54 ± 0.05	0.052 ± 0.002
P45Ca45	-9.26 ± 0.04	-24.17 ± 0.06	0.462 ± 0.01
P40Ca50	-7.667 ± 0.007	-22.89 ± 0.01	1.98 ± 0.02

3 mol. % SiO_2, resulting from substitution of Na with Si from the fused silica crucible. By incorporating the network disrupting effect of SiO_2 on phosphate glass [308] into the composition used for calculations, much closer agreement between theoretical and experimental values is achieved (Fig. 5.8, right). For the 50 mol. % CaO glass, there is still some difference between measured and predicted Q^1/Q^2 composition. This may be a result of hydroxyl incorporated into the structure as a result of the wet quenching process used for this glass composition (the other two compositions were quenched dry). This would have a depolymerising effect, increasing the relative amount of Q^1 species from the theoretical value, as seen in the results. Incorporated hydroxyl was not observed in FTIR, but the wet quenching process and these NMR results suggest that a small amount may be present.

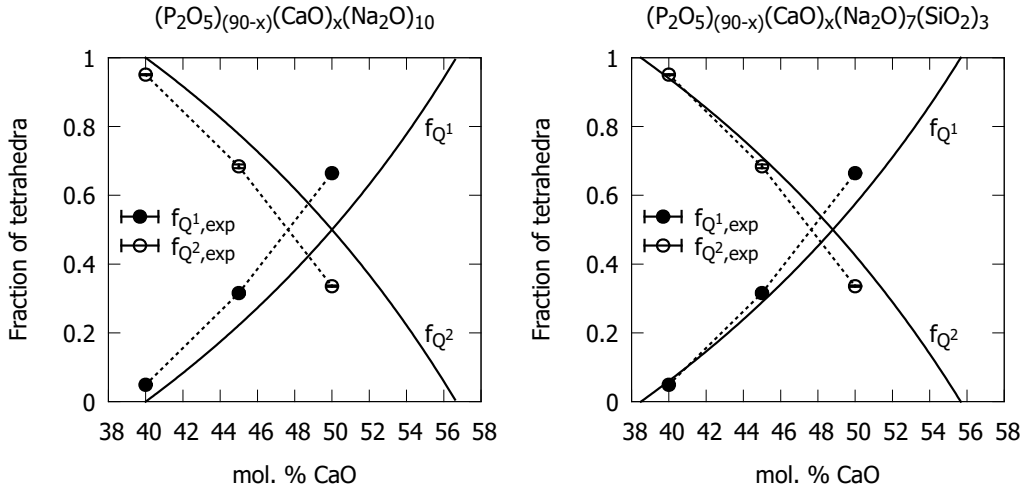

Fig. 5.8: Effect of CaO concentration on the relative theoretical and experimental concentrations of Q^n units in the phosphate glass, using a structural model based on Q^1 and Q^2 tetrahedra, and either the nominal glass composition (left) or with addition of SiO_2 (right).

5.3.2 Thermal properties

The thermal properties of the glasses were investigated by SDT (Simultaneous DSC and TGA) to give information on the possible thermal transformations and glass structure. Mass loss measured during TGA from 25 to 1000°C revealed a negligible change in mass - less than 0.3 wt. % in all cases. This small mass loss could be attributed to adsorbed water on the glass surface - significant mass loss of the glass would not be expected at these temperatures, as the melting temperature of the glasses was higher than 1000°C. Thermal decomposition or boiling would not be anticipated until even higher temperatures.

DSC data was also recorded during SDT analysis of phosphate glasses, and an example DSC curve is shown in Fig. 5.9. Transitions recorded from different glass compositions are summarised in Figs. 5.11 and 5.12, and Table 5.6. The DSC curves for all glass samples appear fairly typical for this type of phosphate glass, with a single glass transition, and one or more crystallisation and melting peaks [176, 206, 309–311].

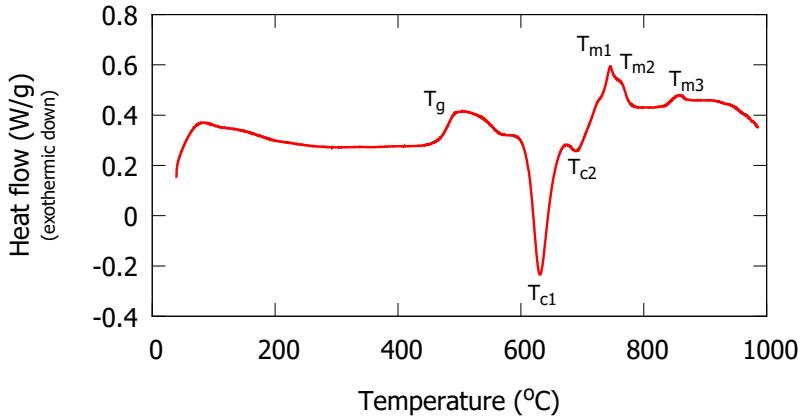

Fig. 5.9: Representative DSC curve for phosphate glass, showing the glass transition, and various crystallisation and melting peaks. This particular curve is for P45Ca45 glass powder.

Fig. 5.11 summarises the effects of composition on the thermal transitions of the phosphate glasses. It is clear that for both powder and cast discs, increasing Ca content increases the T_g; this is consistent with the work of Knowles et al. and can be attributed to an increased number of cross-links between the phosphate glass chains [206, 310, 311]. Formation of cross-links occurs when divalent ions are added - P-O-P bridging oxygen bonds are broken, however the Ca^{2+} ion creates an ionic cross-link between glass chains as demonstrated in Fig. 5.10 [201, 312].

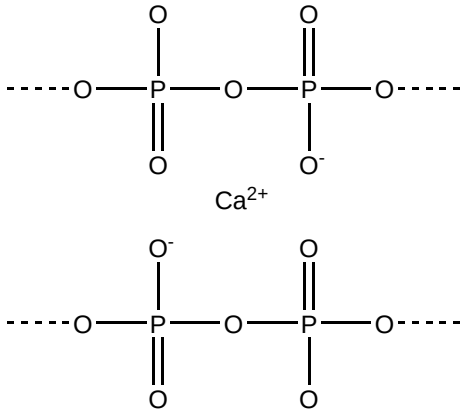

Fig. 5.10: Cross-linking of phosphate glass chains by a divalent cation (Ca^{2+}) as suggested by Van Wazer [312].

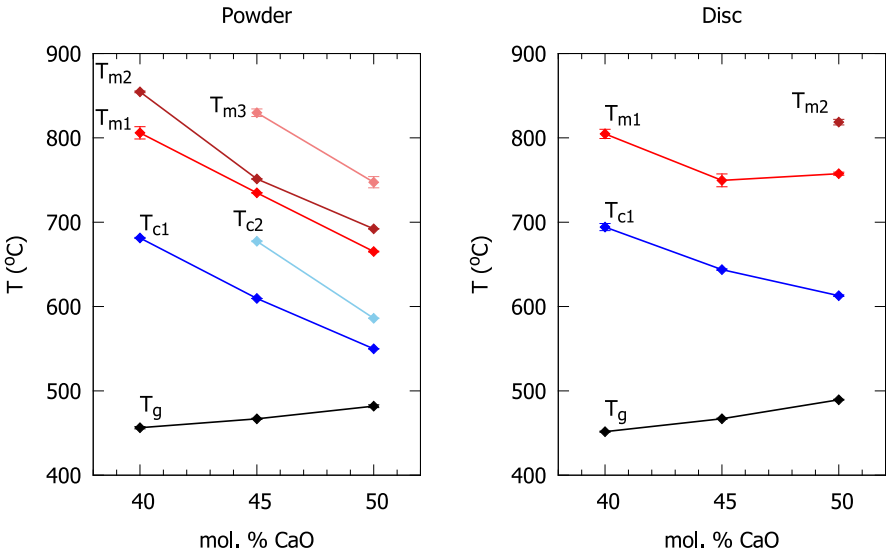

Fig. 5.11: Thermal transitions for different phosphate glass compositions, for powders and cast discs. Error bars (denoting standard deviation) are shown, but may be smaller than the point marker.

Table 5.6: Measured thermal transitions for different phosphate glass compositions, with standard deviations. -D denotes cast discs.

Sample Code	T_g (°C)	T_c (°C)	T_m (°C)
P50Ca40	456 ± 1	681.3 ± 0.7	806 ± 7,
			855 ± 1.0
P50Ca40-D	451.6 ± 0.7	694 ± 4	805 ± 5
P45Ca45	466.8 ± 0.7	609.57 ± 0.04,	734.8 ± 0.2,
		677.4 ± 0.5	751.3 ± 0.2,
			830± 4
P45Ca45-D	466.9 ± 0.7	644 ± 1	750 ± 8
P40Ca50	482 ± 2	549.87 ± 0.08,	665.2 ± 0.6,
		586.1 ± 0.4	692.14 ± 0.03,
			747 ± 7
P40Ca50-D	489.5 ± 0.5	613 ± 1	758 ± 2,
			819 ± 3

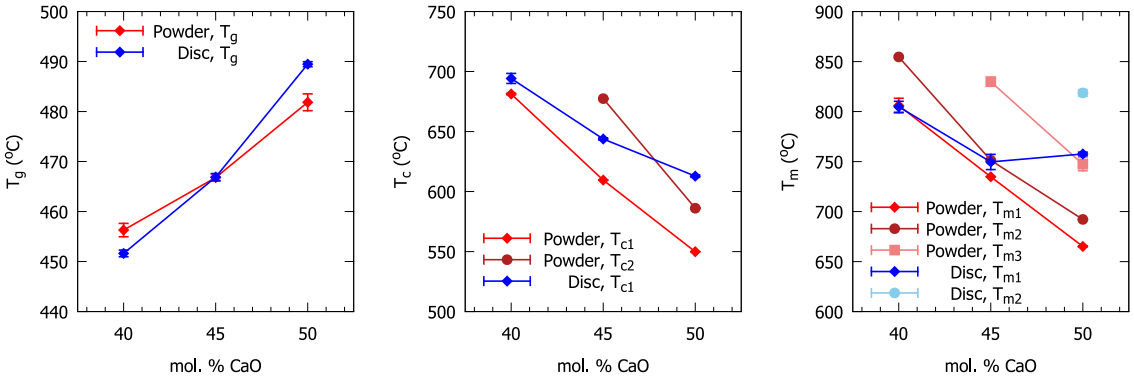

Fig. 5.12: Thermal transitions for different phosphate glass compositions, showing the same data as Fig. 5.11, but focusing on the comparison between powder and cast disc samples. Graphs show the glass transition (left), crystallisation (middle) and melting (right) transitions.

In addition to the effect of composition on thermal properties, the sample preparation method also appears to alter the transition temperatures, as shown in Fig. 5.12. The onset temperature of crystallisation for the powder sample is consistently lower than that for the cast disc samples, while the behaviour of the melting temperatures of the crystalline phases is not clear. It appears that the cast disc samples may have higher melting points, although without information on the exact phases present (i.e. XRD) it is difficult to fully explain this.

The increase in T_g with increasing Ca content has been discussed above, and it is seen to occur for both powder and cast disc samples. Interestingly, the Ca content appears to have a greater effect on the T_g of the cast disc than the powder. The exact reason for this is unclear, but may be related to the increased free volume of the cast discs, which could reduce T_g at low cross-linking density by increasing chain spacing and therefore reducing interchain forces. When additional Ca^{2+} ions are added to the less dense glass, they would more easily find interstitial spaces where they can be effective cross-linkers, thus having a greater effect on the T_g than the same Ca^{2+} ions added to the more dense glass.

5.4 Discussion

5.4.1 Glass characterisation

The glasses produced were seen to be mostly successfully vitrified, resulting in fully amorphous glass discs and powder as observed from the XRD patterns. One of the glass compositions, P40Ca50, with the highest Ca content, showed a small amount of crystallised material in the milled powder, but not in the cast glass discs. This crystallised material was analysed by XRD and found to be a calcium phosphate phase ($Ca_2P_2O_7$), present at a low level of 2.0 ±0.4 wt.%. The presence of both Ca and P in this crystalline phase suggest that this is a result of crystallisation of melted material during cooling, rather than residual unmelted precursors. The glass composition, as measured by EDS, matched the intended P_2O_5 and CaO amounts to within experimental error, indicating successful formation of the desired set of phosphate glass compositions.

The Na_2O amount was appreciably lower than the 10 mol. % targeted, averaging around 7 mol. % across all the glass compositions produced. This was paired with the inclusion of approximately 3 mol. % SiO_2 in the glass, which was not a targeted glass constituent. This can be explained by volatilisation of alkali Na from the melt, and contamination with SiO_2 from the crucible. Volatilisation losses are known to be particularly significant for alkali oxides, due to their high vapour pressure at high temperatures. Melting and homogenisation of the glass for extended time at high temperature in an uncovered crucible can be expected to lead to some loss of Na that is not observed for the other oxides used (P_2O_5, CaO) [293], however fortunately this loss is constant across all the glass compositions, so should not be a significant variable in future studies. Contamination with SiO_2 from dissolution of the crucible is also a phenomenon known to occur at these high temperatures [293], and it has been shown that addition of SiO_2 to phosphate glasses can increase the dissolution rate [308]. With the glasses produced here however, the SiO_2 content is relatively consistent across the glass compositions at about 3 mol. %, so this is unlikely to be a contributing variable

to future studies based on these glasses, although their dissolution may be faster than similar glass compositions without SiO_2 content.

The chemical structure of the glasses was investigated using FTIR and NMR, where is was observed that Ca has a depolymerising effect on the glass network, as observed in previous work [299]. The depolymerising effect of Ca was confirmed, with addition of CaO from 40 up to 50 mol. % causing a transition from mostly Q^2 phosphate tetrahedra, to mostly Q^1. Based on the glass composition and known connectivity of the phosphate tetrahedra, a glass structural model can be developed. In order to explain the NMR results observed, in terms of the Q^1/Q^2 ratio, the presence of SiO_2 from the crucible must be included, resulting in the glass formula $(P_2O_5)_{90\text{-}x}(CaO)_x(Na_2O)_7(SiO_2)_3$. In this model the Si performs a network modifying role (i.e. depolymerising), rather than forming the network as in silica-based glasses. This model still does not completely explain the Q^1/Q^2 ratios observed, with the P40Ca50 glass displaying lower Q^2 content than predicted. This can be attributed to hydroxyl incorporation from the wet quenching process, which does not appear to be large enough to be significant in FTIR results, but could cause additional depolymerisation of the glass network. This hydroxyl incorporation can impact the dissolution properties of the glass which are critical for medical applications.

Formation of hydroxyl within the glass by reaction with water is described in Eq. 5.1:

$$P-O-P \; + \; H_2O \; \rightarrow \; P-OH \; + \; HO-P \tag{5.1}$$

In a similar way to addition of network modifying oxides, this reaction causes depolymerisation of the phosphate glass network. Unlike the addition of alkali ions such as Ca^{2+} however, there is no subsequent formation of ionic crosslinks (Fig. 5.10), as the hydrogen atoms bond directly to these terminal oxygen atoms. Therefore the incorporation of hydroxyl can be expected to reduce the chemical durability of the

glass, as it breaks network bonds (i.e. P-O-P), but contrary to Ca^{2+} does not replace them with stronger crosslinks.

The glass structure is also clearly influenced by the composition, specifically the Ca content. Addition of Ca to the glass increases the density, consistent with Ca ions being located at interstitial sites within the phosphate network, forming crosslinks between phosphate glass chains [167, 312]. This is also supported by XRD results, where the shift of the amorphous peak to higher angle as Ca content increases is consistent with decreasing interatomic distance. The effect of these crosslinks was seen in the increased T_g for higher Ca glasses - Ca crosslinks provided greater thermal resistance and so increased the T_g [167, 206]. These crosslinks are also known to provide greater chemical durability, so would be expected to lead to a slower dissolution rate.

There is also a clear difference in the glass stability - the temperature difference between the glass transition T_g and the onset of crystallisation T_c - across the composition range studied. Addition of Ca to the glass increases the glass transition temperature, while substantially reducing the onset of crystallisation. One factor affecting this is the thermodynamic driving force for crystallisation, characterised by the enthalpy of fusion (ΔH_f) for the crystalline phase, however without comprehensive information on the crystalline phases formed this is difficult to comment on. The interatomic separation distance in the glass is another important factor in determining crystal nucleation and growth, where a more densely packed glass will exhibit faster nucleation and growth at any given temperature [293]. The increase in density seen for higher Ca glasses can therefore explain this reduction in crystallisation temperature, and therefore the reduced glass stability. The implication of this is that hot working of phosphate glasses (e.g. melt drawing into fibres) is significantly more difficult for glasses with higher Ca content, as crystallisation must be avoided.

5.4.2 Glass discs vs. powder

Differences in properties are also observed due to changes in the thermal history (i.e. quenching or casting discs). Some of these can be attributed to differences in particle size, where cast discs were manually crushed for analysis, resulting in a larger particle size than the milled powders. This artefact can explain differences observed in the FTIR peak intensity, as described in section 5.3.1, and possibly the crystallisation temperature. The onset temperature of crystallisation for the milled powder sample is consistently lower than that for the cast disc samples, which can be attributed to the reduced density of the cast discs reducing the crystal nucleation and growth rates. The smaller particle size of the milled powder is another possible explanation for this difference. Crystallisation in phosphate glasses typically occurs by surface nucleation, therefore the increased surface/volume ratio of the finer milled powder results in an earlier onset of crystallisation [313, 314]. This effect could also explain why a greater number of different crystalline phases are observed in the milled powder sample.

Cast discs consistently display a lower density compared with the as-quenched glass powder, indicating that cast discs experienced a faster cooling rate resulting in a less dense glass with more free volume. This can also explain why the P40Ca50 glass powder contains some crystallised material, while the cast disc with the same composition does not - the faster cooling rate during casting prevented crystallisation.

These different thermal histories however, would not be expected to significantly affect the network properties of the glass, as characterised by NMR and FTIR. When accounting for differences in particle size, FTIR showed similar trends in different functional groups for both glass powder and cast discs. solid state NMR was only carried out on glass powder, but the remelting and casting process would not reasonably be expected to alter the network connectivity of the glass, only the arrangement of the network (i.e. density, or formation of crystalline phases). In addition, the incorporation of hydroxyl into the glass network discussed for the wet-quenched P40Ca50 glass occurs

during the initial quenching step, and will therefore affect the glass powder and cast discs equally.

Using glass discs to evaluate the dissolution of the glass powder that will be used in composites is expected to result in a small amount of inaccuracy. Although the discs have the same composition as the powder, there are some differences as a result of their differing thermal history, which have been discussed in previous sections. The glass powders are all denser than their disc counterparts, with lower free volume, therefore it is reasonable to expect that diffusion through the powder samples will occur more slowly, giving rise to slower dissolution when diffusion is the limiting step. Diffusion is not the only phenomenon controlling glass dissolution however, with the hydrolysis and hydration reactions playing a major role. The hydrolysis reaction itself, where covalent bridging oxygen bonds are broken, is unlikely to be affected by changes in glass density brought on by different thermal processing methods, however this is not necessarily the case for the hydration reaction. This involves replacement of the ionic cross-linker cations (Fig. 5.10), which sit at interstitial sites within the free volume of the phosphate glass network, with hydrogen ions. It is difficult to predict how changes in density will affect this hydration reaction, but the glass transition temperature T_g, which is heavily affected by these cross-links, can be used as an indirect measure. Based on the glass transition temperatures (Fig. 5.12), this suggests that for P50Ca40 glass the hydration of the glass powder will be slower than for the cast discs, approximately the same for P45Ca45 glass, and for the high calcium P40Ca50 glass dissolution may be faster for the glass powder than the cast discs, when the hydration reaction is the dominant factor.

The P40Ca50 glass powder is also seen to contain a small amount of crystallised material as a result of the slower cooling process when compared with the cast disc. The $Ca_2P_2O_7$ material formed is an insoluble salt, therefore dissolution of the P40Ca50 glass powder would not be expected to go to completion, resulting in a small amount (approximately 2 wt. %) of insoluble material.

5.5 Conclusions

A set of phosphate glasses, in the range $(P_2O_5)_{90\text{-}x}(CaO)_x(Na_2O)_{10}$, where x = 40, 45, 50, were successfully produced using melt quenching, and subsequent milling into powder, or casting into discs. The Ca content was seen to have a dominant effect on the glass properties, increasing the density, while also reducing the connectivity of the phosphate network. These Ca^{2+} ions form crosslinks between phosphate glass chains, increasing the T_g of the glass.

Differences in thermal history between the glass powder and cast discs are also seen to have an impact on the glass properties, with the faster-cooled discs displaying reduced density and greater glass stability. The differences in properties between the glass powder and cast discs have been explained in terms of the effect of their thermal histories on their structure, and the potential effects of this on the dissolution behaviour has been discussed. In Chapter 6 the cast glass discs will be used to explore the dissolution behaviour of these glass compositions, to inform investigations of polymer-glass composites in Chapters 7 and 8. These composites will utilise phosphate glass powder, so it is important to understand the differences between these and resulting limitations of the method.

This chapter has provided a thorough understanding of the structure of these phosphate glasses, and the role that composition and thermal history play in determining their properties. This will enable the dissolution behaviour of these glasses, both on their own and as a component in a polymer-glass composite, to be fully understood and explained. In particular the dissolution of the glass is critical to the degradation behaviour of these polymer-glass composites, which is one of the key limitations of current polymer bioresorbable stent technology. Incorporating these phosphate glasses has the potential to accelerate the degradation of the composite, and bring stent degradation into a more suitable range that matches the body's natural healing time.

Chapter 6

P_2O_5-CaO-Na_2O glasses: dissolution kinetics and mechanisms

6.1 Background and aims

Phosphate-based glasses are attractive materials for medical implants, due in part to their cytocompatibility and demonstrated potential for use in soft tissue applications such as ligament and muscle scaffolds, wound healing, and promoting angiogenesis [178, 220, 309, 315, 316]. However perhaps their greatest advantage is their solubility in aqueous solutions, and the ability to tune this solubility over many orders of magnitude by tailoring the glass composition, to match the degradation lifetime of the material with tissue repair [167]. Phosphate glasses have potential applications including hard tissue engineering, as well as controlled release and antimicrobial materials [159, 160], and can also be combined with polymers in fully degradable polymer-glass composites for hard or soft tissue implant materials such as bioresorbable stents [178–180, 227, 228, 264]. The biological response of these materials is often closely linked to the dissolution rate of the glass - in order to support cell adhesion and survival, the surface must dissolve slowly enough to allow physical bonding [178–181]. It is clear that in

any application, the degradation timescale of the material is of critical importance, therefore intimate knowledge of the dissolution behaviour of the phosphate glass is crucial.

Due to their similarity in composition to natural bone, calcium containing phosphate glasses are of particular interest for medical applications. Early work by Bunker et al. and Uo et al. [164, 201] found that Ca ions introduced within the glass form ionic crosslinks between non-bridging oxygens of two different glass chains [312], enhancing the chemical durability of the glass.

Despite having been the subject of research for several decades, some uncertainty still remains over the mechanisms in effect during different stages of phosphate glass dissolution. Several studies [160, 200, 201] have observed an initial dissolution stage with parabolic time dependence, in P_2O_5-CaO-Na_2O glasses, which Bunker et al. attributed to water diffusion and formation of a surface hydration layer [201]. This initial stage has also been observed in P_2O_5-FeO-Fe_2O_3-Na_2O glasses [205], however other works on P_2O_5-CaO-Na_2O glasses have not observed this initial non-linear stage [163, 165], suggesting that it may be related to the changing ionic strength of the solution rather than diffusion and ion exchange [317]. The later stage of dissolution, with linear time dependence, is considered to be controlled by the reaction of the hydrated layer at the glass-solution interface [200, 205, 317]. The cause of the transition between these stages is not yet well understood, but the transition time has been observed to be roughly correlated to the durability of the glass [201] (i.e. the overall resistance to dissolution).

The pH dependence of Ca-P glass dissolution has been previously characterised, with results indicating that the rate of dissolution increases in acidic or basic solutions [163, 201, 204], with acidic solutions accelerating dissolution by disrupting ionic crosslinks between phosphate chains. However, the interaction between solution pH

and the multi-stage dissolution behaviour, and the transition between these dissolution stages, has not been thoroughly investigated.

This chapter investigates the dissolution behaviour of a set of P_2O_5-CaO-Na_2O glasses in deionised (DI) water and phosphate-buffered saline (PBS). In order to gain insight into the mechanisms of dissolution a two-stage model is applied, similar to that used by Ma et al. [200, 205] to describe the mass loss of Na-Fe-P and Na-Ca-P glasses, based on an initial parabolic time dependence, followed by later linear dissolution. To the author's knowledge, this is the first work to quantitatively compare the non-linear mechanisms of P_2O_5-CaO-Na_2O glass dissolution in DI water and higher ionic strength PBS, across a range of pH values, and provides new insight into the two stages of dissolution, and the cause of the transition between them. The effect of pH is especially important when considering phosphate glasses as a component in polymer-glass composites, due to the acidification that can result from degradation of commonly used degradable polymers. To simulate the conditions phosphate glass may experience in a polymer-glass composite, dissolution experiments were conducted in PBS with added lactic acid (the acidic degradation product of common degradable polymers) to alter the solution pH, and determine the effect on the dissolution rate and mechanisms. Previous works have speculated that the transition between the two dissolution stages may be related to the nature of the conversion layer (also referred to as an alteration layer [205]); this work discusses how the formation of different conversion layer species across a range of solution conditions can affect the transition behaviour.

6.2 Materials and methods

6.2.1 Glass preparation

Glass discs were prepared and characterised as described in Chapter 5. These glass discs had nominal compositions in the range $(P_2O_5)_{90\text{-}x}(CaO)_x(Na_2O)_{10}$, where $x = 40$, 45, 50.

6.2.2 Dissolution testing

Dissolution tests were carried out in DI water (Type I, 18.2 MΩ.cm) and PBS (phosphate-buffered saline, pH = 7) (Gibco, Thermo Fisher Scientific Inc., USA), as well as PBS adjusted to pH = 3, and pH = 5 by adding lactic acid (≥85%, Sigma-Aldrich 252476). Glass discs were incubated at 37℃ in conical-bottomed vials (to ensure all surfaces were exposed to solution) containing in 15 mL of the chosen solution (surface area/volume ratio 15 m^{-1}). For all dissolution testing, this surface area/volume ratio (SA/V) was used unless otherwise specified. Selected testing was also carried out with a larger solution volume of 250 mL (surface area/volume ratio 0.88 m^{-1}). Solution pH was measured using a Hanna HI 4222 pH meter, and Ca^{2+} ion concentration was measured using an ISE (ion selective electrode - Sentek 361-75 Calcium Combination ISE), calibrated using a modified Nernst equation [318] with standard solutions diluted with DI water from a 0.1 mol L^{-1} calcium standard (Hanna HI 4004-01). To measure glass disc mass during dissolution, discs were removed from solution, rinsed with DI water, dabbed dry, and weighed, before being returned to the solution for further dissolution. Digital photographs were also taken to record visible changes in morphology. Before SEM imaging, partially dissolved discs were removed from solution, rinsed with DI water, dabbed dry, and stored in a desiccator to dry over several days.

Dissolution tests in PBS and pH-modified PBS (except those at SA/V = 0.88 m^{-1}) were carried out by Ms. Kalliope Margaronis as part of a final year undergraduate research project at the University of Cambridge, and I am very grateful for her collab-

oration on this work. Analysis and interpretation of the results in this chapter were all carried out by the author.

6.2.3 Characterisation

SEM (Scanning electron microscopy) and EDS (Energy dispersive X-ray spectroscopy) were performed on the glass samples after dissolution testing, using a CamScan MX2600 FEG-SEM and Phenom ProX SEM. INCA software (Oxford Instruments) was used to calculate atomic composition from EDS spectra. Prior to analysis samples were coated with 10 - 20 nm of Au/Pd, using an Emitech K550 sputter coater (40 mA deposition current for 2 minutes, under an argon atmosphere). XRD (X-ray diffraction) was carried out using a Bruker D8 Advance diffractometer with Cu Kα radiation, using a 2θ range of 20-50° with a 0.1° step size and dwell time of 10 s step^{-1} to maximise the signal/noise ratio. Any crystalline phases present were identified using HighScore Plus software (Malvern Panalytical).

As with the dissolution tests above, characterisation of glasses dissolved in PBS and pH-modified PBS (except those at SA/V = 0.88 m^{-1}) were carried out by Ms. Kalliope Margaronis. Interpretation of these results was carried out by the author.

6.3 Calculation

A two-stage dissolution model is used here to describe the glass mass loss in a similar fashion to the work of Ma et al. [205], however here this model is adapted for use in a disc geometry by considering the thickness of a dissolved layer x. In the initial diffusion controlled stage (before the transition time t_{trans} is reached, i.e. $t < t_{trans}$), dissolution occurs at the surface of the disc and the interface moves towards the centre, resulting in the unreacted core shrinking and decreasing the surface and hence reaction

area over time as shown in Fig. 6.1. In this stage a 3D diffusion model (DM) with parabolic time dependence applies [208, 209], such that:

$$x(t < t_{trans}) = k_{DM} t^{1/2} \tag{6.1}$$

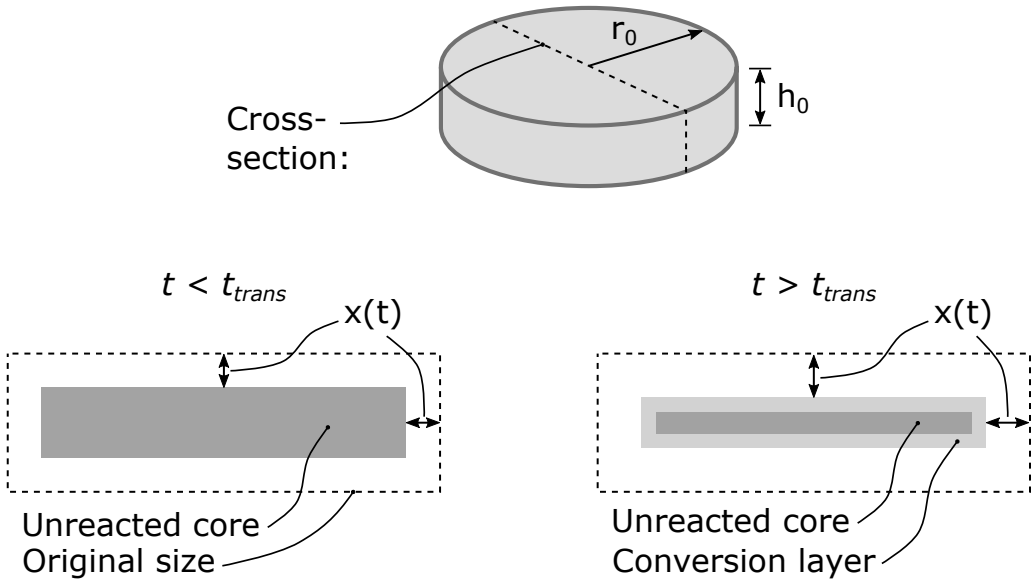

Fig. 6.1: Schematic showing the model geometry for glass dissolution, and two-stage dissolution model as described by Eqs. 6.3 and 6.4.

In later stages ($t > t_{trans}$) the surface reaction determines the dissolution rate, with conversion reactions progressing into the disc by diffusion (as shown in Fig. 6.1), while dissolution of the conversion layer occurs at the surface. Assuming linear reaction kinetics the dissolution progress can be described by a contracting volume model [208, 210] (CVM):

$$x(t > t_{trans}) = k_{CVM} t \tag{6.2}$$

Therefore the extent of the dissolved layer over the whole course of dissolution can be described by:

$$x(t) = H(t_{trans} - t)k_{DM}t^{1/2} + H(t - t_{trans})(k_{DM}t_{trans}^{1/2} + k_{CVM}(t - t_{trans})) \quad (6.3)$$

where H is the Heaviside step function (half-maximum convention). Applying the disc geometry, the mass fraction dissolved (α) can be given by:

$$\alpha(t) = 1 - \frac{(r_0 - x(t))^2(h_0 - x(t))}{r_0^2 h_0} \quad (6.4)$$

where r_0 and h_0 are, respectively, the initial radius and height of the disc, as shown in Fig. 6.1. Eqs. 6.3 and 6.4 were used to model the mass loss of phosphate glasses, using non-linear least squares regression in Matlab.

6.4 Results

6.4.1 Dissolution in DI water

The changes in solution pH and Ca^{2+} ion activity as the glasses dissolve in DI water are seen in Fig. 6.2. The control solution (DI water only) suffered a rapid decrease in pH to around 4.7 due to dissolution of atmospheric CO_2 and subsequent formation of carboxylic acid, followed by a gradual increase to about 5.6. This gradual increase can be attributed to contamination of the solution with residual ions from the electrodes used for pH and Ca^{2+} ion measurement. In spite of thorough washing between samples, some transfer and contamination was unavoidable, and resulted in a pH increase for the control solution which has very low ionic concentration and therefore is very sensitive to changes.

Changes in measured Ca^{2+} ion activity indicate that the level of Ca released from the glass (Fig. 6.2) was the inverse of Ca content, with the lowest Ca glass (P50Ca40) releasing Ca the fastest. This indicates that Ca release is clearly more closely linked

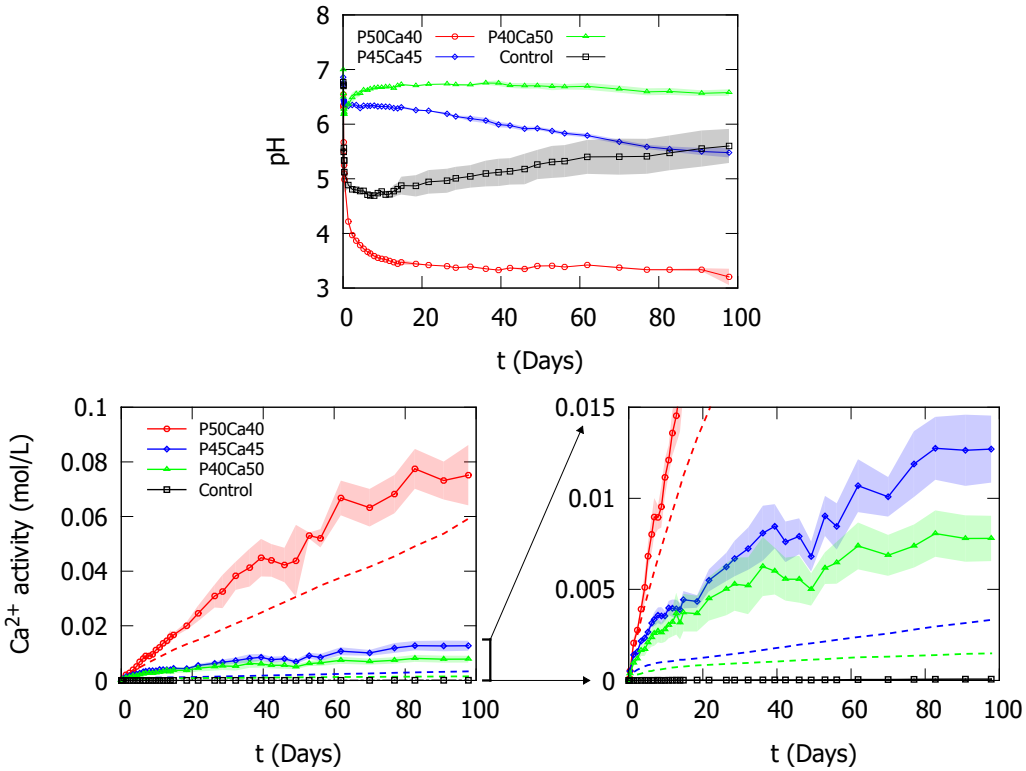

Fig. 6.2: Solution pH (top) and Ca^{2+} activity (bottom) for phosphate glasses dissolving in DI water at 37°C. Solid lines indicate Ca^{2+} activity measured using an ISE, while dotted lines indicate Ca^{2+} activity calculated based on measured mass loss assuming congruent dissolution. Shaded region denotes standard deviation for n = 3 measurements.

to the dissolution behaviour (see below) than actual Ca content. Dotted lines in this graph indicate the Ca^{2+} activity calculated from the mass loss data (using the Truesdell-Jones model [319–321]) in Fig. 6.3, assuming congruent dissolution. In all cases the measured Ca release was significantly higher than that expected from the mass loss, indicating Ca was leached from the bulk glass.

The mass loss of phosphate glasses during dissolution in DI water (Fig. 6.3) shows that glasses with higher Ca content dissolved more slowly. It can also be seen that linear dissolution models (inset plots) did not describe this data adequately, underestimating the initial stages of dissolution, and not accounting for slower dissolution in the later stages. By contrast the two-stage model, incorporating a diffusion stage (DM) and contracting volume stage (CVM), fitted the data well, with parameters given in Table

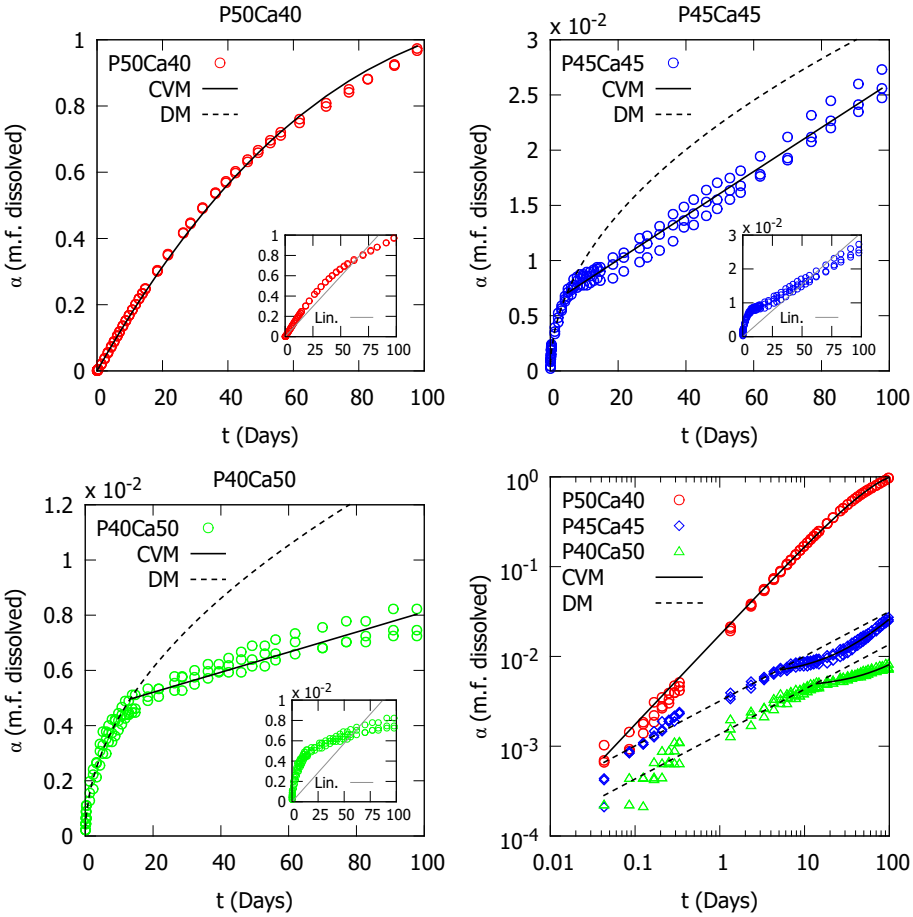

Fig. 6.3: Mass fraction dissolved during dissolution in DI water at 37°C for phosphate glasses, fitted to two-stage model with diffusion stage (dotted line - DM) and contracting volume stage (solid line - CVM). Inset plots show the same data fitted to a linear dissolution rate. Bottom right shows the same data combined onto a log-log scale for comparison.

6.1 and Fig. 6.5. Rate constants (k_{DM}, k_{CVM}) decreased with increasing Ca, consistent with slower dissolution, while the transition time t_{trans} increased. The initial diffusion limited stage was not observed for the P50Ca40 glass, therefore t_{trans} can only be given as lower than the first non-zero timepoint (one hour).

The morphology of the phosphate glasses after dissolution in DI water is shown in Fig. 6.4. After 98 days a layer (denoted as type B) was observed on the surface of the P45Ca45 and P40Ca50 glasses. The morphology of this layer is difficult to interpret, as the cracks seen may be caused by the drying process, however the composition of this

layer is of principal interest. EDS revealed this to be dominated by Ca and P, with a P:Ca:Na:Si ratio of 100:71:2:0 measured, regardless of the actual glass composition. A similar layer (B) with comparable composition was also seen partially covering the surface of the P50Ca40 glass, with the remaining area (denoted as type A) displaying etch pits. Areas where etch pits were found (only on P50Ca40) had a similar composition to the starting glass, however were depleted in Ca, with P:Ca:Na:Si ratio of 100:33:15:4, compared with a ratio of 100:40:13:4 before dissolution. This layer was also seen in macro-scale images of the glass discs, where it turned the transparent glass opaque (Fig. 6.4e). The time at which this layer appeared roughly corresponded to the transition time between the two stages of mass loss (Table 6.1) for the medium and high Ca glass (P45Ca45 and P40Ca50), however for the low Ca glass P50Ca40 transition occurred very early on, while the layer was only visible well into the dissolution process.

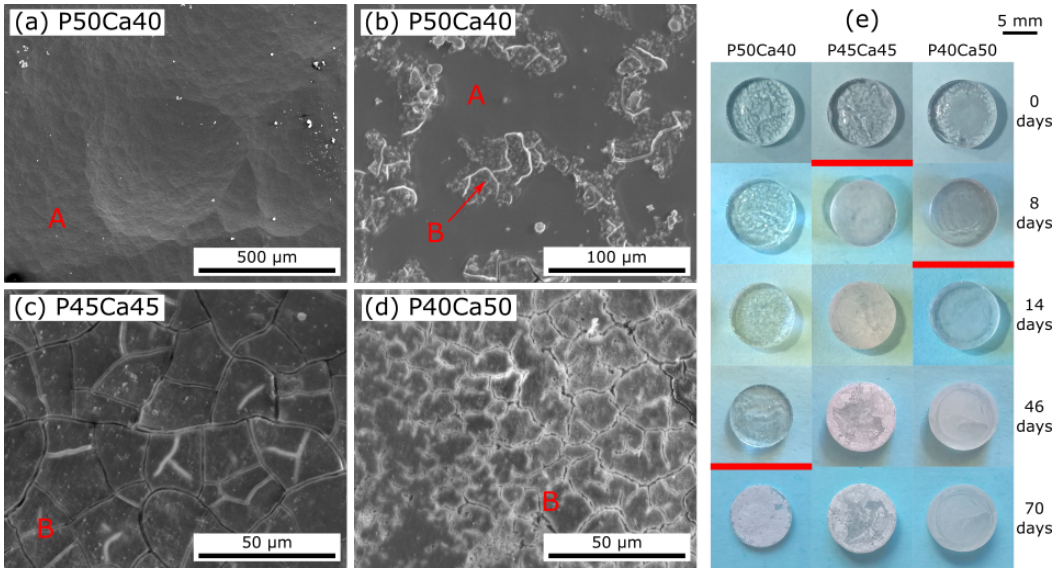

Fig. 6.4: Morphology of glass discs during and after dissolution, showing SEM images after 98 days in DI water at 37°C for P50Ca40 (a, b), P45Ca45 (c), P40Ca50 (d), and digital photographs of glass discs at various dissolution timepoints (e). Red lines indicate the time taken for observation of an opaque layer.

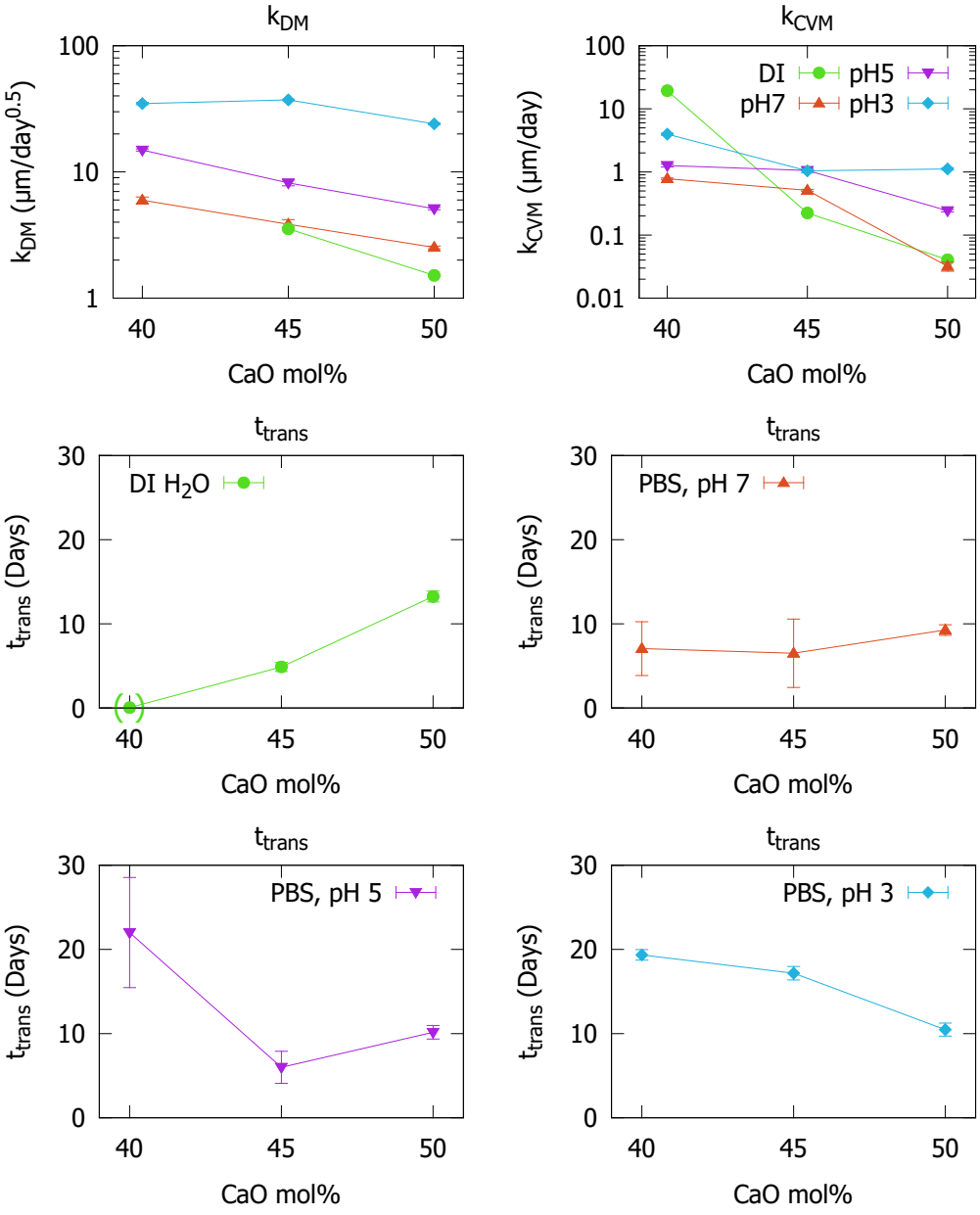

Fig. 6.5: Fitted parameters (k_{DM}, k_{CVM}, t_{trans}) for the two-stage model for phosphate glass dissolution in DI water, PBS, or lactic acid-adjusted PBS at pH 3 or 5, all at 37°C. Error bars denote standard deviation for n = 3 measurements, brackets () denote transition occurring immediately, with no diffusion-limited stage observed.

Table 6.1: Fitted reaction rate parameters for two-stage models for phosphate glass dissolution.

Glass code	Solution	k_{DM} (µm/day$^{0.5}$)	k_{CVM} (µm/day)	t_{trans} (days)	R^2
P50Ca40	DI H_2O	-	19.4 (±0.3)	< 0.04	0.999
P45Ca45	DI H_2O	3.5 (±0.1)	0.224 (±0.003)	4.9 (±0.5)	0.989
P40Ca50	DI H_2O	1.52 (±0.02)	0.041 (±0.002)	13.2 (±0.7)	0.982
P50Ca40	PBS pH 7	6.0 (±0.3)	0.78 (±0.2)	7 (±3)	0.963
P45Ca45	PBS pH 7	3.9 (±0.3)	0.51 (±0.02)	7 (±4)	0.938
P40Ca50	PBS pH 7	2.52 (±0.06)	0.032 (±0.005)	9.3 (±0.6)	0.873
P50Ca40	PBS pH 5	14.9 (±0.3)	1.26 (±0.06)	22 (±7)	0.970
P45Ca45	PBS pH 5	8.2 (±0.4)	1.06 (±0.02)	6 (±2)	0.983
P40Ca50	PBS pH 5	5.1 (±0.1)	0.24 (±0.01)	10.2 (±0.8)	0.959
P50Ca40	PBS pH 3	34.8 (±0.8)	4.0 (±0.2)	19.4 (±0.6)	0.971
P45Ca45	PBS pH 3	37.2 (±0.5)	1.04 (±0.08)	17.2 (±0.8)	0.973
P40Ca50	PBS pH 3	24.0 (±0.5)	1.12 (±0.05)	10.5 (±0.8)	0.964
P40Ca50	PBS pH 7 SA/V 0.88 m^{-1}	12.9 (±0.2)	0.2 (±0.1)	32 (±0.2)	0.983

6.4.2 Dissolution in PBS

The evolution of solution pH during phosphate glass dissolution in PBS and pH-adjusted PBS is shown in Fig. 6.6. The trend observed for different glass compositions is consistent with that seen for dissolution in DI water (Fig. 6.2), with higher Ca glasses leading to higher solution pH. In general, regardless of initial pH, the dissolution of the glass in PBS appeared to result in a slow convergence of the solution pH towards a similar value for each glass composition, as the glass dissolution slowly dominated over the initial solution conditions. The pH of the empty solution (PBS) was measured to be stable at pH $\approx$ 7 over the experimental timescale used.

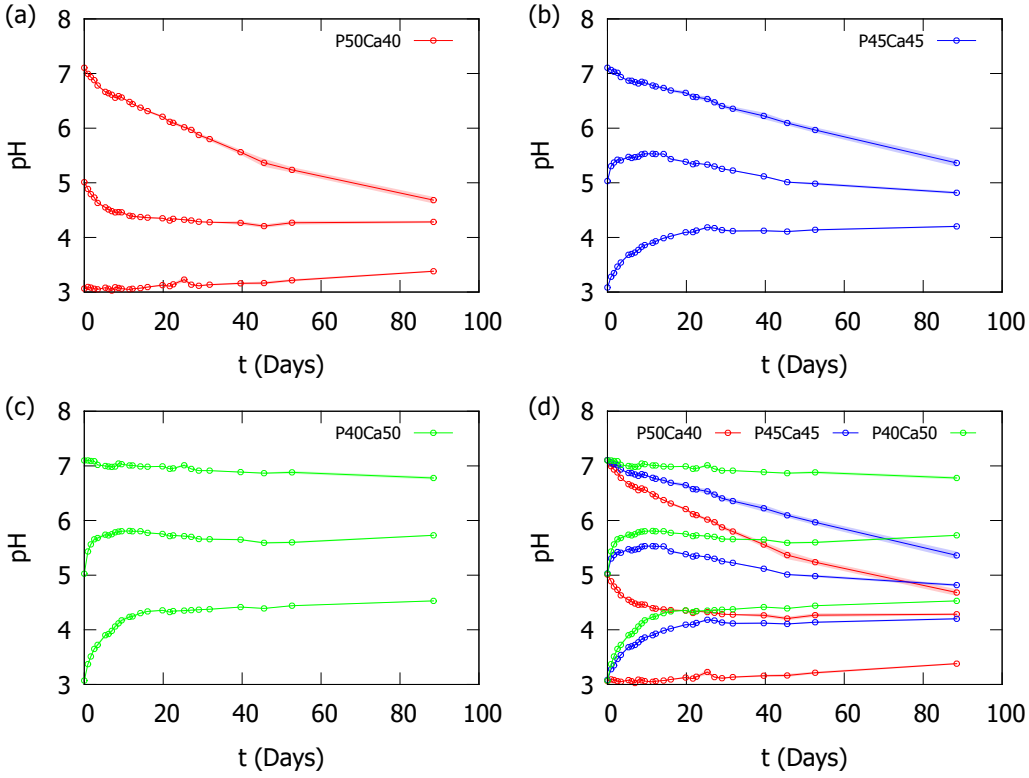

Fig. 6.6: Solution pH for phosphate glasses dissolving in PBS, or lactic acid-adjusted PBS at pH 3 or 5, at 37°C, showing P50Ca40 (a), P45Ca45 (b), P40Ca50 (c), and all three glasses together for comparison (d). Shaded region denotes standard deviation for n = 3 measurements.

The mass loss of phosphate glasses during dissolution in PBS and pH-adjusted PBS is shown in Fig. 6.8, with fitted curves from the two-stage model in Table 6.1. Again it is clear that glasses with higher Ca content dissolved more slowly, in accordance with earlier results in DI water. The effect of pH on the general mass loss trend is also clear; reduced pH accelerated mass loss for all glass compositions. Fig. 6.7 shows the mass loss of P40Ca50 glass in the same PBS solution, but at different surface area/volume ratios. It can be seen that dissolution occurs significantly faster in a greater volume of solution.

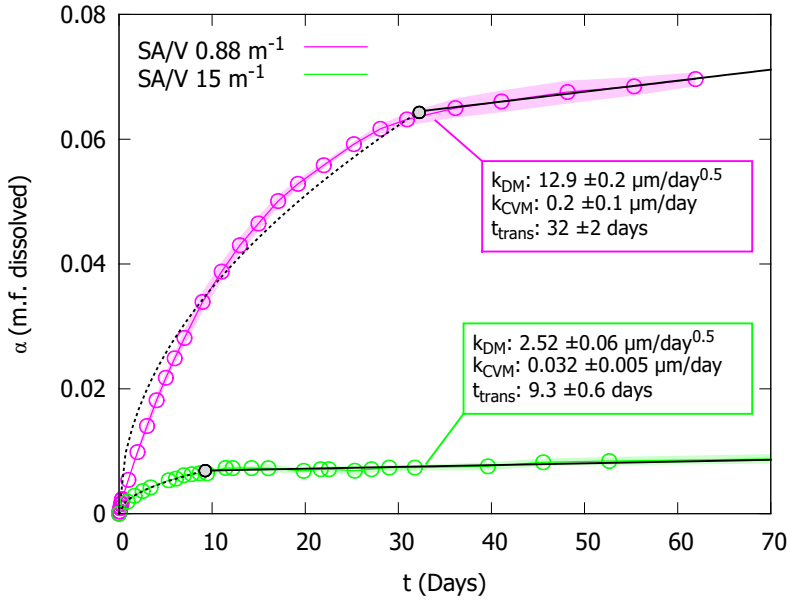

Fig. 6.7: Mass fraction dissolved during dissolution of P40Ca50 glass in PBS at 37°C, for surface area/volume ratios of 15 and 0.88 m^{-1}. Shaded region denotes standard deviation for n = 3 measurements.

The fitted parameters for the two-stage model (Table 6.1 and Fig. 6.5) showed significant variation across glass composition and solution conditions. The rate constant for the diffusion controlled stage (k_{DM}) showed a clear decreasing trend for increasing Ca content, and also increased significantly as the solution pH decreased. Similar trends, although less clear, were also seen for the rate constant for the reaction controlled stage (k_{CVM}). Variation in the transition time (t_{trans}) between the two stages was also seen across different glass compositions and solution conditions. In DI water, t_{trans} increased with increasing Ca content, however this trend was absent in PBS with a similar t_{trans} observed for all glass compositions, and reversed in pH-adjusted PBS, with a decreasing t_{trans} with increasing Ca content. The effect of surface area/volume ratio on dissolution rate parameters is also clear from Table 6.1 and Fig. 6.7, where it can be seen that increasing the volume of solution increases the dissolution rate constants for both dissolution stages, while also increasing the time required for transition between these two stages (t_{trans}).

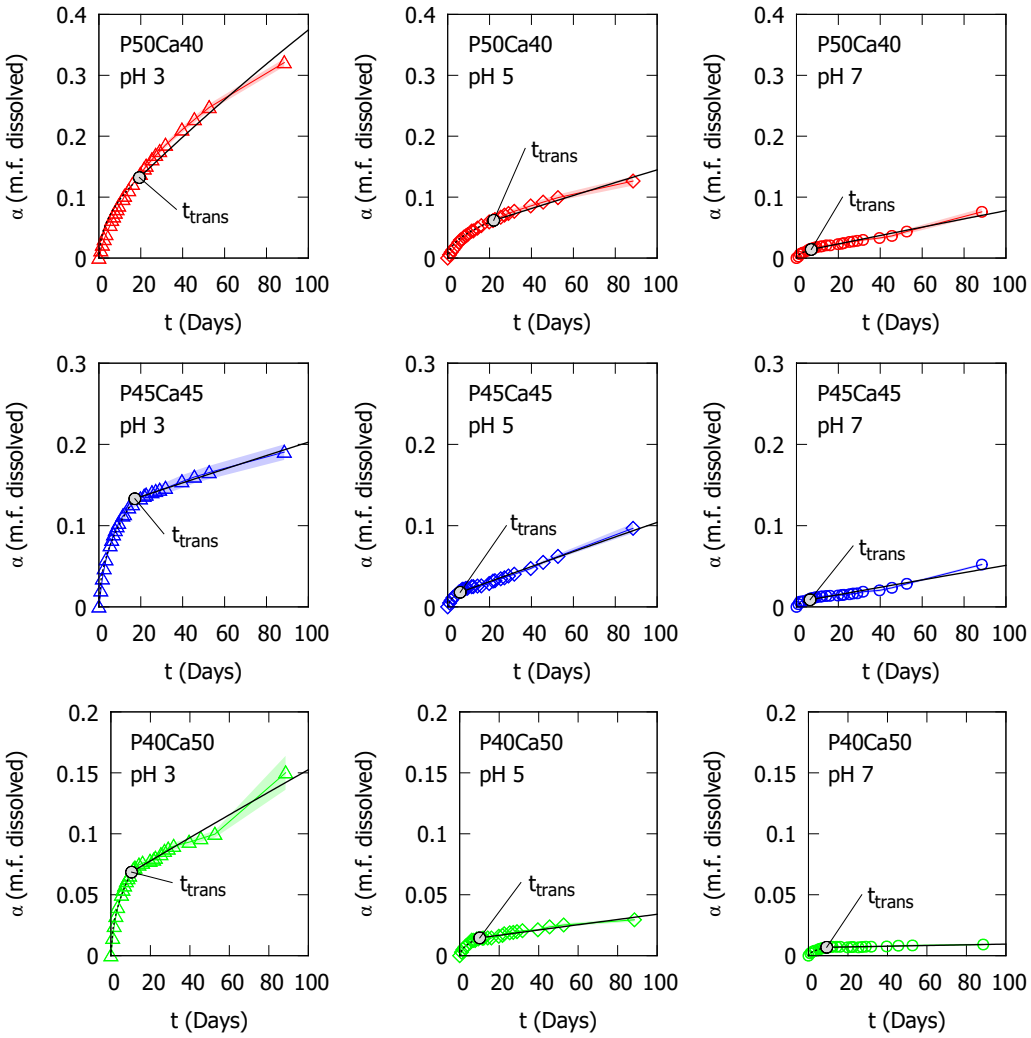

Fig. 6.8: Mass fraction dissolved during dissolution in PBS, or lactic acid-adjusted PBS at pH 3 or 5, at 37°C. Shaded region denotes standard deviation for n = 3 measurements. Black line shows fitted model according to Eq. 6.4, with dotted and solid regions denoting the diffusion and contracting volume stages respectively.

The macro-scale morphology of glass discs during dissolution is shown in Fig. 6.9, where the formation of an opaque layer was observed for all glasses except for P50Ca40 in pH 3 and pH 5. The time taken for observation of this layer is also shown plotted against the fitted t_{trans} parameter in Fig. 6.10. Data points for P50Ca40 in DI water and PBS at pH 3 and 5 were excluded from this plot as transition occurred immediately in DI water, and no layer was observed in PBS at pH 3 and 5 within the duration of the experiment. Good correlation can be observed between these two values, giving an

R^2 value of 0.86. A more detailed view of the morphology is shown by SEM analysis in Fig. 6.12, where several types of dissolution behaviour can be seen.

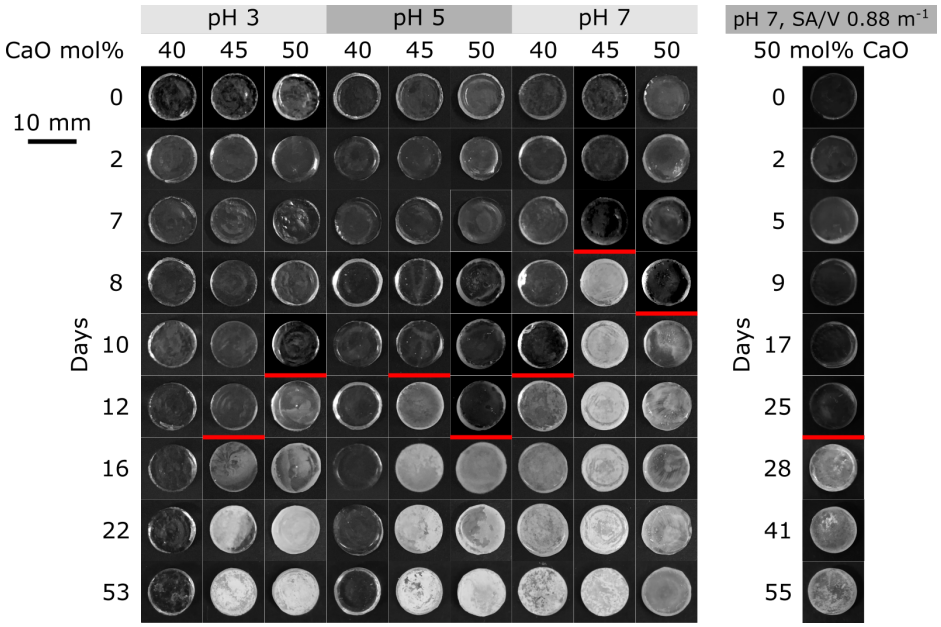

Fig. 6.9: Composite image of photographs showing the morphology of glass discs during and after dissolution in PBS, or lactic acid-adjusted PBS at pH 3 or 5, at 37°C. Red lines indicate the time taken for observation of an opaque layer.

Type A dissolution (Fig. 6.12a) consisted of the formation of etch pits in the glass surface, and was seen by EDS to be depleted in Ca compared with the original glass. Type A dissolution was observed at dissolution times below t_{trans}, as well as at the end of the study (88 days) for P50Ca40 glass in pH 3 or 5. Type B dissolution (Fig. 6.12c-f) consisted of formation of a layer rich in Ca but also K, and depleted in Na. This layer was identified by EDS but could not be detected by XRD (Fig. 6.11), suggesting that the layer had very little long-range crystalline order [165]. The presence of K in this layer was attributed to the PBS used, the original glasses did not contain any, however the solution was rich in potassium. The cross section shown in Fig. 6.12e revealed some information about the morphology of this layer, where a dense initial portion was seen, below a more porous section. Fig. 6.12f is also interesting to note, as the remnants of type A etch pits (lighter lines across the surface) were visible below the

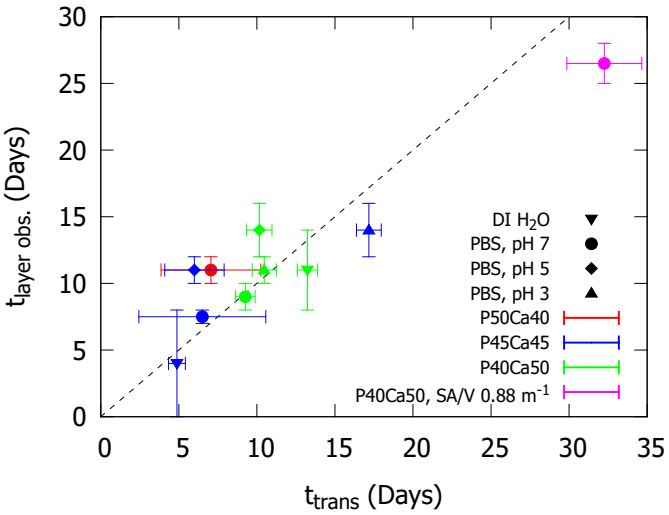

Fig. 6.10: Comparison of fitted t_{trans} parameter, and the time taken to observe formation of an opaque layer on the glass surface. Colours denote glass compositions, and symbols denote the dissolution media, as described in the key. Dotted line represents $t_{trans} = t_{layer\ obs}$.

more porous type B layer. Type C dissolution (Fig. 6.12b) consisted of formation of a NaCl layer on the glass surface, which could be identified by EDS and XRD (Fig. 6.11). This NaCl layer was only observed at dissolution times slightly above t_{trans}, but not at the end of the study (88 days).

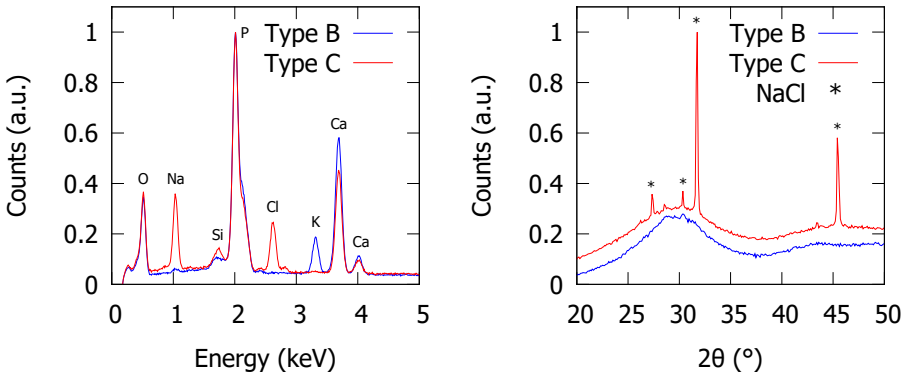

Fig. 6.11: EDS spectra (left), and XRD patterns (right), for representative samples displaying type B (CaP layer formation) and type C (NaCl layer formation) behaviour. XRD patterns are offset vertically for clarity.

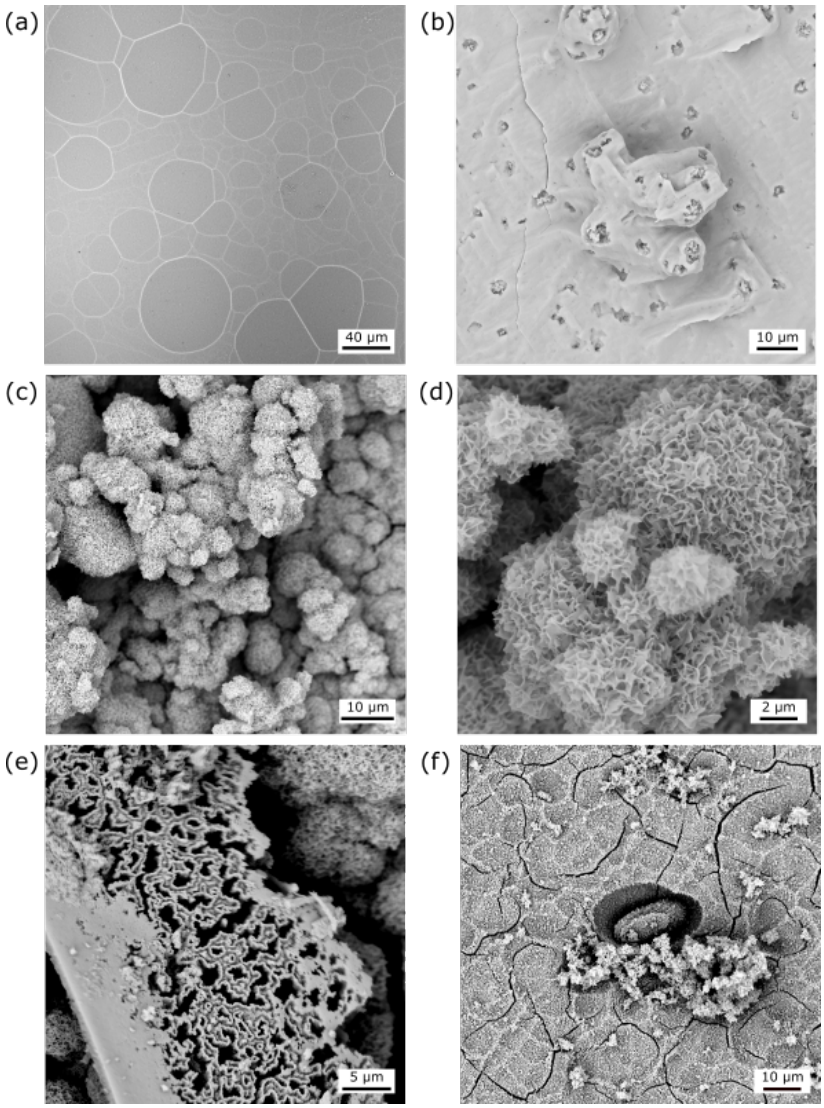

Fig. 6.12: SEM images of phosphate glasses during dissolution showing (a) type A behaviour (etch pits) on P45Ca45 in pH 3 below t_{trans}, and (b) type C behaviour (NaCl layer formation) on P40Ca50 in pH 7 above t_{trans}. (c-f) show type B behaviour (CaP layer formation): on P45Ca45 in pH 3 after 88 days (c, d), on P40Ca50 in pH 3 after 88 days (e), and on P40Ca50 in pH 7 above t_{trans} (f).

6.5 Discussion

6.5.1 Dissolution kinetics

Although phosphate glasses have been researched for several decades now, the mechanisms in effect during different stages of their dissolution are still a source of uncertainty [200], and it is hoped that the results described here can provide some additional insight into these mechanisms. Here I propose the following explanation for the observed dissolution behaviour, which can be broadly broken down into two main categories of reaction. Firstly the idea of the formation of a conversion layer is introduced, which can include hydration among other reactions. Secondly, layer dissolution reactions encompass dissolution of the various products of conversion layer formation, involving release of ions into solution. It must be noted that both of these reaction categories take place simultaneously throughout the dissolution process, however at various points one or other of these may be rate-limiting. A summary of this mechanism scheme is shown in Fig. 6.13.

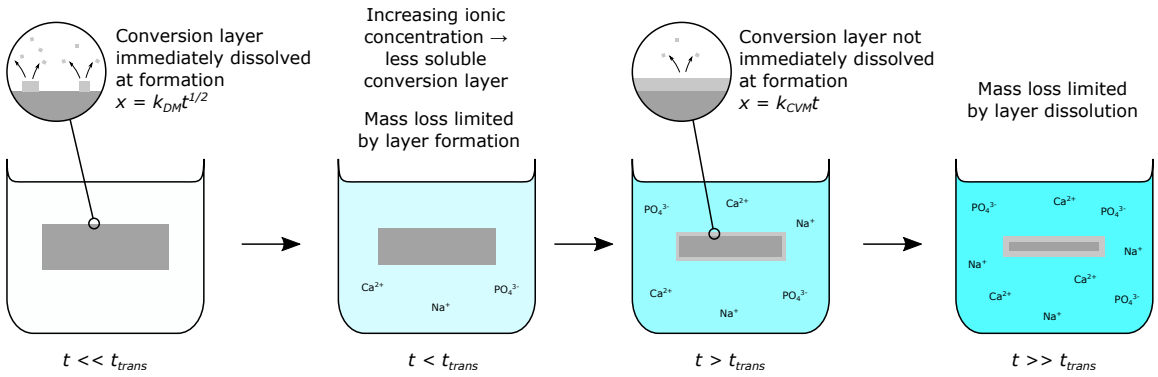

Fig. 6.13: Schematic diagram illustrating dissolution mechanism, showing diffusion limited dissolution before t_{trans}, and surface reaction limited dissolution after t_{trans} when the conversion layer is stable.

Conversion layer formation involves reaction of crosslinked phosphate glass anions to form other solid species, usually including hydration but possibly other reactions as well. The hydration reaction (Eq. 6.5) has been described by Ma et al. [200], defining the hydration of crosslinks between metal cations and two phosphate

anions (with n and m phosphate tetrahedra). This is adequate for dissolution in DI water, however the situation is more complex for solutions such as PBS where various other ions are present in solution. Formation of metal hydroxides can be replaced by, or occur in conjunction with, reactions to form solid metal chlorides as described in Eq. 6.6. This is particularly significant given the much greater solubility in water of $CaCl_2$ compared with $Ca(OH)_2$.

$$\begin{aligned}(P_nO_{3n+1})(Ca,Na_2)_{(n+m+4)/2}(P_mO_{3m+1}) + (n{+}m{+}4)H_2O \rightarrow H_{2+n}P_nO_{3n+1} \\ + H_{2+m}P_mO_{3m+1} + (n{+}m{+}4)/2(Ca,Na_2)(OH)_2\end{aligned} \tag{6.5}$$

$$\begin{aligned}&(P_nO_{3n+1})(Ca,Na_2)_{(n+m+4)/2}(P_mO_{3m+1}) \\ &\quad + (n{+}m{+}4)H^+ + (n{+}m{+}4)Cl^- \rightarrow H_{2+n}P_nO_{3n+1} \\ &\quad + H_{2+m}P_mO_{3m+1} + (n{+}m{+}4)/2(Ca,Na_2)Cl_2\end{aligned} \tag{6.6}$$

The reaction front for these conversion layer formation reactions progresses into the glass, following a parabolic time dependence ($t^{1/2}$) due to the diffusive mass transport required to transport reactants to the reaction front. This is supported by the observed formation of a NaCl layer during dissolution, as well as Ca-rich layers (Figs. 6.12 and 6.11).

Layer dissolution is the second reaction stage, involving surface dissolution of the solid species formed during the conversion layer formation stage, described in Eqs. 6.7-6.9. As shown in Eq. 6.9, orthophosphoric acid (n=1) can dissolve directly, while polyphosphates can undergo further hydrolysis. Nevertheless, it is well known that polyphosphates can be released into solution without further hydrolysis [176, 200].

$$(Ca,Na_2)(OH)_2 \rightarrow (Ca,Na_2)^{2+} + 2OH^- \tag{6.7}$$

$$(Ca,Na_2)Cl_2 \rightarrow (Ca,Na_2)^{2+} + 2Cl^- \tag{6.8}$$

$$H_{2+n}P_nO_{3n+1} + (n-1)H_2O \rightarrow (3n)H^+ + nPO_4^{3-} \tag{6.9}$$

The reaction front for these layer dissolution reactions progresses into the conversion layer, following a linear time dependence (t) due to the reaction controlled process. The dissolution of solid species via these reactions will be sensitive to solution conditions, not only pH but various ion concentrations, which can themselves change over time as the glass dissolves. Depending on ion concentrations, reverse reactions can also occur in a highly saturated solution, involving reaction of solution ions to form a precipitate on the glass surface. This is especially important for metal phosphates, as shown in Eq. 6.10, where metal and phosphate ions (resulting from glass dissolution, or already present in PBS) form metal phosphates. Eq. 6.10 shows formation of simple phosphates, but more complex forms such as octacalcium phosphate, calcium pyrophosphate, or hydroxyapatite are also possible, as suggested by the morphology of the Ca-rich layer observed (Figs. 6.12 and 6.11) [165, 322].

$$3(Ca, Na_2, K_2)^{2+} + 2PO_4^{3-} \rightarrow (Ca, Na_2, K_2)_3(PO_4)_2 \tag{6.10}$$

These two reaction categories can explain the multi-stage dissolution behaviour observed here and elsewhere. Initially the conversion layer formation reactions, which must occur first to produce soluble salts, are rate-limiting due to fast dissolution of the small amounts of hydrated phosphates and metal hydroxides or chlorides produced. As this reaction is limited by mass transport of reactants to the reaction front, this leads to the initial $t^{1/2}$ dependence of the reaction progress x. As the conversion layer dissolves as fast as it is formed, there is no stable conversion layer present on the surface. In later stages ($t > t_{trans}$) the layer dissolution reactions determine the glass dissolution rate, giving rise to the linear t dependence due to assumed linear reaction kinetics. Here the conversion layer is produced faster than it can be dissolved, leading to buildup of the layer on the surface, as illustrated in Fig. 6.1. Despite encompassing dissolution of several layer species (Eqs. 6.7-6.9), as well as deposition reactions (Eq. 6.10), glass dissolution controlled by dissolution of the conversion layer can be adequately described by Eq. 6.2 of the model. Assuming Eqs. 6.7-6.10 proceed via linear reaction kinetics, k_{CVM} is simply the sum of equivalent parameters for individual reactions. k

for deposition reactions will be negative, and if deposition outweighs mass loss, k_{CVM} will be negative, leading to overall mass gain.

The effect of Ca on the dissolution rate in the initial conversion layer formation stage seen here is consistent with multiple previous works, where increased Ca content reduced the dissolution rate [159, 160, 206]. Higher Ca glasses were shown to have higher density (Table 5.3), indicating that Ca ions were located at interstitial sites between phosphate glass chains, reducing the free volume [293]. In this diffusion controlled stage, this resulted in reduced dissolution (lower k_{DM}) by blocking of interstitial diffusion pathways. The greater strength of the Ca-O-P crosslinks compared with P-O-P bonds is another reason for the reduced dissolution rate of higher Ca glasses [201]. The rate constant governing this diffusion stage (k_{DM}) was shown to have a significant dependence on the starting solution pH (Fig. 6.5), with large increases in k_{DM} observed as the pH of the solution was reduced. This is consistent with a diffusion mechanism involving H^+ diffusion into the glass, which would be increased by a larger H^+ concentration in the solution. A diffusion limited mechanism such as this would be expected to show strong dependence on solution concentration, as a concentration gradient is the driving force for diffusion. This is consistent with observations shown in Fig. 6.7, where the P40Ca50 glass shows faster dissolution in the initial layer formation stage when dissolving in a larger volume of solution (lower surface are/volume ratio).

The later stages of dissolution are limited by the surface reactions (Eqs. 6.7-6.10), leading to the formation of a stable conversion layer, which persists as it is formed faster than it dissolves. The effect of Ca on the reaction rate here also results in reduced dissolution with increasing Ca content. This can be explained in terms of the hydration reaction (Eq. 6.5), which indicates that production of the less soluble $Ca(OH)_2$ would dominate over NaOH as the Ca/Na ratio increases. Similarly, when PO_4^{3-} concentration is sufficient, precipitation of phosphates according to Eq. 6.10 dominates, resulting in production of the less soluble calcium phosphates and further

reducing the mass loss. The effect of pH in this layer dissolution stage is complex, however in general lower pH increases the reaction rate constant k_{CVM}, which can be attributed to increased solubility of the conversion layer species in more acidic conditions. Dissolution limited by reaction of the surface layer would also be expected to be dependent on the solution concentration, with a lower ionic concentration in the solution leading to faster dissolution during this stage (i.e. higher k_{CVM}). This was confirmed during dissolution testing with different solution volumes (Fig. 6.7), where faster dissolution in the later layer dissolution stage was observed when dissolving in a larger solution volume (lower surface area/volume ratio).

The transition time between these two stages is perhaps the least well understood component of the non-linear dissolution of phosphate glasses. Bunker et al. described a rough correlation between glass durability and transition time, also noting that it was also sensitive to pH [201], while Ma et al. found that the transition time only varied for glasses with short phosphate chains (i.e. higher O/P and Q^1/Q^2 ratios), finding a similar correlation to Bunker et al., but also commenting that it may be related to the nature of the surface layer [205]. In this work a similar correlation to Bunker et al. was observed for dissolution in DI water (more soluble glasses have a shorter transition time), however this trend was absent in PBS and was reversed in pH-adjusted PBS (pH = 3 or 5).

Under the mechanism proposed here, the transition from the conversion layer formation stage to the layer dissolution stage is controlled predominantly by the nature of the conversion layer (i.e. the combination of solid species formed by Eqs. 6.5-6.6) and its solubility in the surrounding solution, which will be heavily dependent on pH and ion concentrations. As the solution chemistry changes during dissolution, increases in dissolved metal (Ca, Na), hydroxide, and phosphate ions will reduce the dissolution rate of the conversion layer. Once the dissolution rate is lower than the formation rate, the conversion layer is stabilised, and the rate limiting reaction will become

the layer dissolution, leading to a change from parabolic ($t^{1/2}$) to linear (t) reaction kinetics. This mechanism predicts therefore, that dissolution of the same glass in a larger volume of solution would result in a higher t_{trans}, as more dissolved ions will be required to achieve the concentration necessary to stabilise the conversion layer. This is validated by the results seen in Fig. 6.7, where the transition time is much longer when the P40Ca50 glass is dissolved in a large volume of solution (at 0.88 m^{-1} surface area /volume ratio) compared with a smaller volume of solution (15 m^{-1} surface area/volume ratio).

When this stable layer is dominated by $(Ca,Na_2)(OH)_2$ or $(Ca,Na_2)Cl_2$, or deposited phosphates (Eq. 6.10), it would be expected to be optically opaque as observed in Fig. 6.9, explaining the correlation between t_{trans} and the time for observation of an opaque layer (Fig. 6.10). The behaviour of P50Ca40 glass seemed to contradict this however, displaying transition to the linear layer dissolution kinetics in DI water, and PBS at pH 3 or 5, without formation of an opaque layer. This can be explained by differences in the phosphate anions present. Based on the glass composition, the number average chain length can be calculated [201]; for P50Ca40, P45Ca45, and P40Ca50 the average chain length (n) is 2.5, 1.64, and 1.14 respectively. This means that in acidic conditions, layer dissolution from P50Ca40 may be limited by the hydrolysis reaction of longer phosphate chains (Eq. 6.9, where $n \geq 2$) rather than dissolution of other solid species. Transition to this stage would then not result in a visible opaque layer, as the hydrated phosphate anions ($H_{2+n}P_nO_{3n+1}$) that make up the conversion layer are not forming a new crystalline solid but rather their cation crosslinkers are simply being exchanged for H^+ ions.

6.5.2 Implications for polymer-glass composites

Understanding the dissolution behaviour of phosphate glasses is an important step in rationalising the degradation behaviour of polymer-glass composites, and designing

composites with a degradation profile suited to application as a bioresorbable cardiac stent.

The pH dependence of glass dissolution revealed here is particularly relevant for composite applications. Degradation tests of bioresorbable polymers (Chapter 4) indicated significant pH reduction during degradation, reaching a plateau at around pH 3 after extended degradation. Similar reductions in starting solution pH were observed here to result in significantly faster glass dissolution. Incorporation of glass powder into a polymer composite can also be expected to affect the dissolution behaviour in other ways. From the results in this chapter it is clear that glass dissolution is affected, in both the conversion layer formation and layer dissolution stages, by mass transport of reactants and products to and from the reaction surface or interface. This is especially true for the conversion layer formation stage, which is limited by mass transport (diffusion) even when directly immersed in water as in these experiments. Dispersing glass powder within a polymer matrix would clearly slow these mass transport phenomena, reducing the dissolution rate especially in the early conversion layer formation stages.

The use of glass powder in a composite rather than bulk glass discs would also have a significant effect on the dissolution behaviour. Assuming a 2 µm diameter spherical particle, this would result in a 2,000-fold increase in specific surface area compared with the glass discs. Given that both the conversion layer formation and dissolution reactions occur across this surface, the use of glass powder would result in a greatly increased dissolution rate.

Another important effect to consider when incorporating these glass particles into a polymer composite is the local buildup of dissolution products in the immediate vicinity of the dissolving glass particle, due to slow diffusive mass transfer of reaction products out of the composite. This could result in a region with significantly increased ionic concentration compared with the bulk solution. As discussed above, this would

impact the mechanisms of glass dissolution, bringing about a faster transition from the conversion layer formation stage to conversion layer dissolution. It would also reduce the dissolution rate in both regimes. The effect of localised product buildup would also have a large effect on the pH, with increased concentration of phosphoric acid resulting in lower pH.

As discussed in section 2.1.3.1, a lower solution pH leads to faster hydrolytic degradation of lactide-based bioresorbable polymers [133]. This suggests that the local acidification caused by phosphate glass dissolution could accelerate polymer hydrolysis in the local region, leading to subsequent autocatalysis of polymer degradation. When combined with the effect pH has on accelerating glass dissolution, these two effects may create a positive feedback loop. Glass dissolution, which is at its fastest early in the dissolution process, could cause the initial pH reduction by production of phosphoric acid. This could then accelerate polymer degradation and further pH reduction by production of lactic acid. It remains to be seen however, whether the pH decrease brought about by glass dissolution is sufficient to accelerate polymer degradation to a fast enough timescale to take part in a positive feedback loop such as the one described.

6.6 Conclusions

These results offer new insight into the mechanism of phosphate glass dissolution in various media, in particular the origin of the parabolic time dependence and transition time between the two stages. Understanding the dissolution behaviour of these glasses is of importance when considering their dissolution in medical applications, and the pH dependence of this is particularly of interest in polymer composite applications, where polymer degradation results in formation of lactic acid and acidification.

The dissolution behaviour of a range of P_2O_5-CaO-Na_2O glasses was measured in deionised water, PBS, and pH-adjusted PBS at pH 3 or 5. In accordance with previous studies in DI water, increased Ca was observed to significantly reduce the dissolution rate in all conditions. Two-stage behaviour was seen in DI water, PBS, and pH-adjusted PBS, with an initial parabolic time dependence, followed by later linear time dependent reaction progression. A two-stage model similar to those reported previously was adapted for use with the disc-shaped glass samples here.

Based on these results, a new dissolution mechanism was proposed to explain the two-stage dissolution behaviour, that takes into account more complex dissolution media. The initial stage involves diffusion of water or ions into the glass, with $t^{1/2}$ dependence, forming a conversion layer consisting of hydrated phosphate anions, and metal hydroxides or chlorides. Once the solution conditions slow the layer dissolution reactions enough so that the conversion layer is stabilised, the layer dissolution reaction becomes rate-limiting and results in linear t dependence. Under this mechanism, the transition time t_{trans} is sensitive both to the nature of the conversion layer, and the solution conditions.

These results demonstrate that the pH reduction as a result of polymer degradation will accelerate glass dissolution in a polymer-glass composite. This also suggests that, given the faster dissolution/degradation of both polymer and glass components in more acidic solutions, their acidic products could result in formation of a positive feedback loop leading to accelerated degradation. The dissolution mechanisms revealed here also allow the behaviour of glass within a composite to be anticipated, with local concentration buildup slowing dissolution and causing faster transition beween stages, while the increased specific surface area of the glass powder will also have a major effect.

Chapter 7

Polymer-glass composites: production and characterisation

7.1 Background and aims

To address the inherent limitations of polymeric materials, in particular their mechanical properties, inorganic fillers are often used to create polymer composites, which offer a combination of the properties of their constituent materials. Typically the elastic modulus of a material is improved by addition of inorganic particles to a polymer matrix, due to the higher stiffness of the inorganic phase. The upper and lower bounds of the elastic modulus (Voigt-Reuss bounds) can therefore be calculated assuming iso-strain and iso-stress conditions as follows:

$$E_c^{upper} = E_f\phi_f + E_m(1-\phi_f) \tag{7.1}$$

$$E_c^{lower} = \frac{E_f E_m}{E_f(1-\phi_f) + E_m\phi_f} \tag{7.2}$$

where subscripts c, f, and m denote the composite, filler, and polymer matrix respectively. These give upper and lower bounds for the composite modulus, and the modulus of the composite material typically lies between these two bounds [323, 324].

A more detailed prediction can be given by the model proposed by Counto [325], which assumes perfect bonding between the particle and matrix, and gives good agreement with a variety of measured data [326, 327]. The elastic modulus of the composite is given by:

$$E_{Counto} = \frac{1-\sqrt{\phi_f}}{E_m} + \frac{1}{\left(\frac{1-\sqrt{\phi_f}}{\sqrt{\phi_f}}\right)E_m + E_f} \tag{7.3}$$

The composite yield strength is also heavily influenced by the addition of filler particles to the polymer matrix. For micro-particle composites, stress transfer between the matrix and filler is a key consideration and is determined by the interfacial adhesion between the two phases - if stress can be effectively transferred to the stronger filler particle, the yield strength of the composite can be improved. In addition, dispersed particles can also function as barriers to crack propagation, again improving the yield strength. This must be balanced against the weakening effect that can arise from stress concentration in the polymer matrix around the filler particle [326].

The effects of stress concentration and transfer within a particle-filled polymer composite were assessed by Nicolais et al., to determine upper and lower bounds for the composite yield strength [328, 329]. In the case of perfect adhesion between polymer matrix and filler, the composite yield strength will simply be equal to the yield strength of the polymer [328–330], giving the upper bound:

$$\sigma_{y,c}^{upper} = \sigma_{y,m} \tag{7.4}$$

The lower bound can then be found by assuming no adhesion between the polymer and matrix, and that load is carried only by the polymer matrix [328, 329], giving:

$$\sigma_{y,c}^{lower} = \sigma_{y,m}(1 - 1.21\phi_f^{2/3}) \tag{7.5}$$

In a ductile matrix, the addition of brittle filler materials such as phosphate glass can significantly increase the brittleness of the composite due to stress concentration. However, if interfacial adhesion is good, the ductility can be maintained or even increased, as a result of toughening mechanisms such as crack deflection, blunting, or pinning, as well as interfacial debonding, all of which increase the energy required for failure [326, 327].

The elastic modulus of the composite is typically independent of the particle size, provided it is above a critical value that depends on the particle, matrix, and interfacial adhesion. Below this critical value (often in the range of tens of nm) reducing the particle size increases the modulus, but above the critical value the modulus is insensitive to particle size [326]. The yield strength does not display a similar critical value, with yield strength significantly increasing as particle size is decreased due to the larger surface area, giving more efficient stress transfer [331, 332]. The particle size is also a key consideration for applications of composites as cardiovascular stent materials, where strut sizes are often on the order of 100 µm. Here large particles are unacceptable due to the deviation from bulk properties that could occur at these small scales. In order to achieve a sufficiently small particle size with phosphate glasses, numerous techniques can be used, including "bottom-up" sol-gel processing methods [291, 292]. However, when using a "top-down" approach starting from bulk melt-quenched glass, mechanical milling methods must be employed. Techniques such as ball milling or planetary milling are commonplace, but to achieve a fine particle size within a short time, high energy methods such as attritor milling are preferred, especially for pharmaceutical applications where contamination (typically dependent on milling time) is a critical issue [333, 334].

Dispersion of these small particles within the polymer matrix to create a polymer composite can be challenging. Melt blending is commonly used industrially but requires expensive, specialised equipment and can cause chemical changes to the

polymer, resulting in deterioration of mechanical properties [220, 224, 225]. Solvent-based methods, where the filler is dispersed into a dissolved polymer, can avoid these issues but can be affected by residual solvent and agglomeration of filler particles, both of which have a detrimental effect on mechanical or biological properties [219, 220].

This chapter aims to:

- Develop an attritor milling method to produce suitable phosphate glass microparticles for incorporation into polymer-glass composites
- Develop a method for production of well dispersed polymer-glass composites, and characterise the structural properties of these composites
- Assess the mechanical properties of these composite materials, and explain these in terms of interactions between different components of the composite

7.2 Materials and methods

7.2.1 Materials

Commercial PLLA (Ingeo 2500 HP) was supplied by Natureworks LLC, USA. PEG-functionalised PLCL was synthesised and supplied by Ashland Specialties Ireland Ltd. (Dublin, Ireland), here the copolymer molar ratio (LA:CL) used was 70:30. This polymer contained a singular PEG end-group of length 550 g mol^{-1}. The presence of PEG was confirmed by the supplier by utilising ^{1}H-NMR to determine the chemical composition of the copolymers. Characterisation and testing of these polymers and blends is described in Chapters 3 and 4. Phosphate glass powders, with nominal composition $(P_2O_5)_{90\text{-}x}(CaO)_x(Na_2O)_{10}$, where x = 40, 45, 50, were produced as described in sections 5.2.1 and 5.2.2. Characterisation and testing of these glasses is described in Chapters 5 and 6. Composite production is described in sections 7.2.2-7.2.5, and summarised in Figure 7.1.

DCM was supplied by Merck KGaA, Germany, acetone and ethanol were purchased from Sigma Aldrich, UK, and Gibco phosphate-buffered saline (PBS), pH = 7.4, was supplied by Thermo Fisher Scientific Inc., USA.

7.2.2 Final milling

To produce glass powder with a fine particle size for incorporation into composite materials, the coarse glass powder produced earlier (see section 5.2.2, with $d_{0.5}$ around 15 - 17 µm) was further milled using attritor milling. A Netzsch PE 075 attritor mill was used, with 400 g of milling media (0.5 mm ZrO_2 beads, Netzsch ZetaBeads Plus 0.5), 40 g glass powder, and 40 g acetone as a lubricant. The media and slurry were milled at 1000, 1500, or 2000 rpm for a total of 60 minutes, with 15 minutes rest every 5 minutes (to prevent temperature buildup). Additional acetone was added periodically to replace acetone evaporated during milling. After milling, the glass and ZrO_2 media were rinsed with acetone through a 200 µm sieve, to remove the media and produce a dilute glass/acetone slurry. A small sample of the slurry was pipetted into a petri dish and left to dry, to measure the slurry concentration (approximately 60 mg mL^{-1}).

7.2.3 Composite film casting

Composite films were produced by solvent casting. Polymers (pure PLLA or a 90:10 w/w mixture of PLLA and PLCL(70:30)-PEG) were dissolved in DCM (0.1 g mL^{-1}), and then glass slurry (milled glass dispersed in acetone, milled for 60 mins at 1500 rpm) was added to give the desired polymer/glass ratio. After 15 minutes stirring and 15 minutes sonication, the polymer/glass/DCM/acetone mixture was cast into petri dishes to dry in ambient conditions. After 24 hours drying in ambient conditions, films were dried under vacuum at 50°C for 10 days to remove any residual solvent.

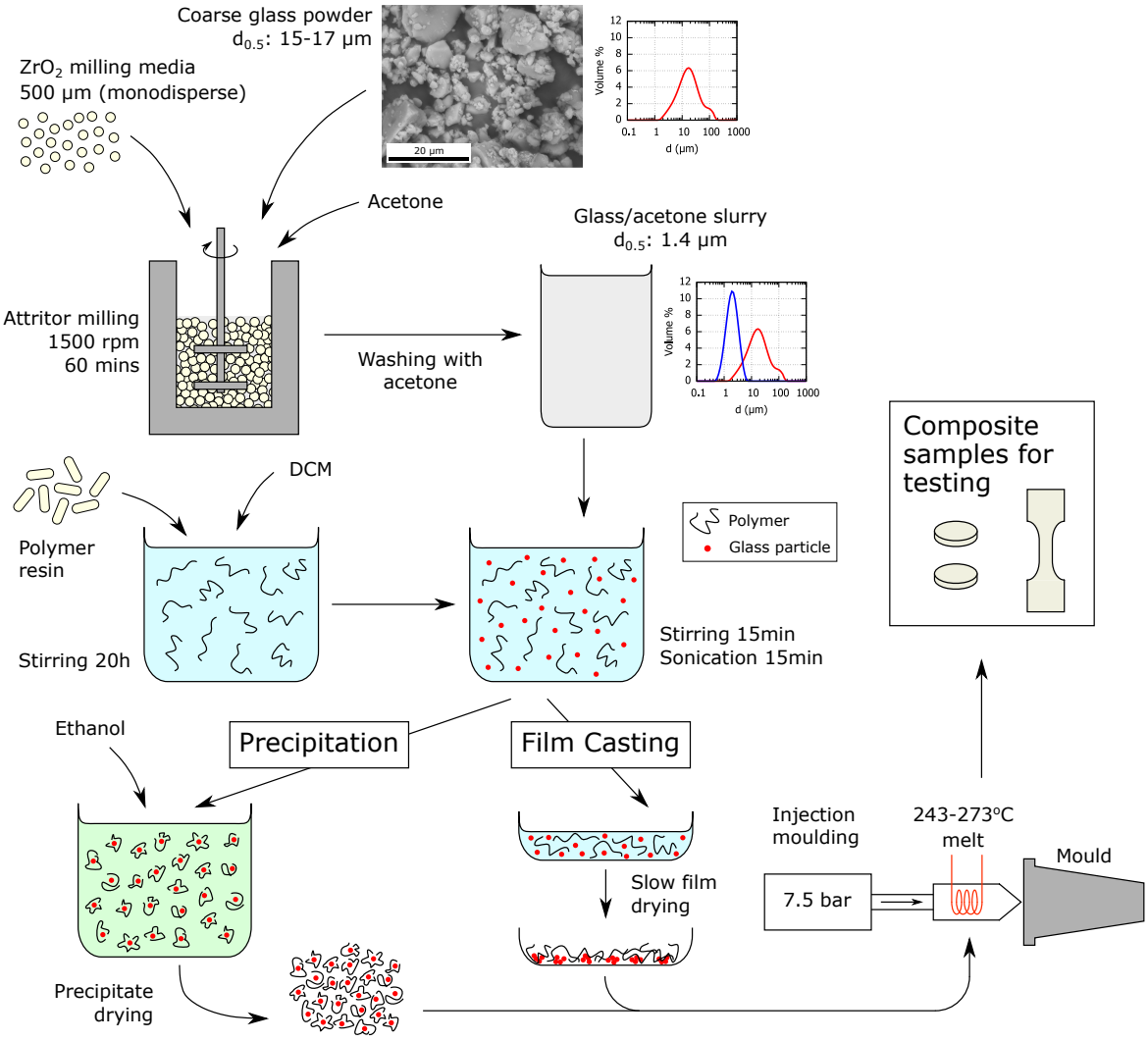

Fig. 7.1: Schematic of composite production workflow, showing final glass powder milling stage, composite production by precipitation or film casting, and then injection moulding of composite parts.

7.2.4 Composite precipitation

In addition to casting composite films, polymer glass composites were fabricated via a novel precipitation method. Polymers (pure PLLA or a 90:10 w/w mixture of PLLA and PLCL(70:30)-PEG) were dissolved in DCM (0.1 g mL^{-1}), and then glass slurry (milled glass dispersed in acetone, milled for 60 mins at 1500 rpm) was added to give the desired polymer/glass ratio. The polymer/glass/DCM/acetone mixture was then stirred for 15 minutes and sonicated for 15 minutes. Ethanol was then added to the mixture while stirring, in a 3:1 ethanol/DCM ratio. This reduces the solvent power

of the liquid, causing the polymer to precipitate onto the glass particles. This results in a clear solution with a solid composite precipitate, which was poured into a steel drying tray for the solvent to evaporate. The precipitate was then dried under vacuum at 50°C for 10 days to remove any residual solvent. The set of composites produced is described in Table 7.1.

Table 7.1: Compositions of the composites produced, showing weight fractions of different polymers within the polymer matrix component, as well as the amount of glass filler used as a weight fraction of the total composite mass.

Sample code	Matrix Composition (w/w in matrix)		Filler Composition (w/w of total)	
	PLLA	PLCL(70:30)-PEG	P45Ca45	P40Ca50
PLA	1	-	-	-
PLA-CL	0.9	0.1	-	-
PLA-0.15P45Ca45	1	-	0.15	-
PLA-CL-0.15P45Ca45	0.9	0.1	0.15	-
PLA-0.3P45Ca45	1	-	0.3	-
PLA-CL-0.3P45Ca45	0.9	0.1	0.3	-
PLA-0.15P40Ca50	1	-	-	0.15
PLA-CL-0.15P40Ca50	0.9	0.1	-	0.15
PLA-0.3P40Ca50	1	-	-	0.3
PLA-CL-0.3P40Ca50	0.9	0.1	-	0.3

7.2.5 Injection moulding

Composite films or precipitates were then processed into dumbbell (19 mm length, 5 mm gauge length, 0.6 mm thick) or disc shaped (5 mm diameter, 0.6 mm thick) samples using micro-injection moulding (IM 5.5, Xplore Instruments BV, The Netherlands) and custom-made moulds in ambient conditions. Micro-injection moulding was carried out at the minimum (nominal) melt temperature required for complete mould filling and uniform sample appearance, which ranged from 243 - 273°C depending on glass content, with the mould held at ambient temperature. A pressure of 7.5 bar was applied and held for 60 s to fill the mould and minimise shrinkage during cooling.

7.2.6 Characterisation

7.2.6.1 Particle size analysis

The particle size of phosphate glass powders was measured using a laser diffraction particle size analyser - Malvern Mastersizer 2000, with Hydro MU 2000 (A) pumping attachment (Malvern Instruments Ltd, UK). The refractive index of the glasses was assumed to be constant at 1.543, with absorption coefficient of 0.02 [295], and the samples were dispersed in acetone (as the phosphate glasses are hygroscopic). Pumping speed was kept constant at 2000 rpm, and ultrasonication was carried out prior to analysis to break up agglomerates, by sonicating for 60 seconds with an amplitude of 10 µm. After sonication analysis was delayed by 60 seconds to allow bubbles caused by sonication to be removed. Five measurements were carried out for each sample. Reported median ($d_{0.5}$) and other diameters for fractions of the particle size distribution ($d_{0.1}$, $d_{0.9}$) are based on the particle volume distribution, unless otherwise specified.

7.2.6.2 ICP-OES

Trace element analysis was conducted on milled phosphate glass samples to determine Zr levels using ICP-OES (Inductively Coupled Plasma - Optical Emission Spectrometry). A microwave assisted acid digest was performed using hydrochloric acid, nitric acid, and hydrofluoric acid to completely dissolve the glass sample. After sealing, the temperature was ramped to 220°C over 20 minutes, and then held for a further 20 minutes. Once cooled, any unreacted hydrofluoric acid was complexed with boric acid (to form fluoroboric acid). The solution was then analysed using a Varian 720-ES ICP-OES instrument, calibrated with four matrix-matched calibration points and a blank. ICP-OES experiments were carried out by technician(s) at Lucideon Ltd, Stoke-on-Trent, UK, in order to determine the trace Zr concentration of samples supplied by the author, and I am very grateful for their assistance.

7.2.6.3 SEM/EDS

SEM (Scanning Electron Microscopy) and EDS (Energy Dispersive X-Ray Spectroscopy) were carried out on the glass samples using a CamScan MX2600 FEGSEM, with EDS detector, using a 20 kV accelerating voltage. Prior to analysis a few drops of glass slurry (glass particles in acetone) were dropped onto a glass slide, and the solvent was allowed to evaporate before coating with 10 - 20 nm of Au/Pd, using an Emitech K550 sputter coater (40 mA deposition current for 2 minutes, under an argon atmosphere). Composite samples were imaged using an FEI Nova NanoSEM, using an accelerating voltage of 5 kV. Samples were prepared by cryo-fracturing in liquid nitrogen to view the cross-section, and then sputter coating with 10 - 20 nm of Au, using an Emitech K550 sputter coater (20 mA deposition current for 4 minutes, under an argon atmosphere).

7.2.6.4 µCT

X-ray micro-computed tomography (µCT) analysis was carried out using a Skyscan 1172 system (Bruker), to image injection moulded dumbbell samples of polymer-glass composites. Images were taken with X-ray voltage and current of 59 kV and 167 µA respectively, with 0.2° rotation steps, 2.58 s acquisition time, averaged over two frames. The pixel size was set at 1.49 µm. Image projections were reconstructed into 3D datasets using the NRecon software (Bruker). 3D datasets were analysed using CTAn software (Bruker); global thresholding and despeckling were applied before individual object analysis was used to generate a size distribution of filler particles.

7.2.6.5 DSC

DSC (Differential scanning calorimetry) was carried out using a DSC Q2000 (TA Instruments, USA), in Al hermetic pans at a heating rate of 20℃ min^{-1}, from -20 to 230℃ under 50 mL min^{-1} N_2 gas flow. A single heating run was used to measure the properties of the composites after processing. TA Universal Analysis software was used

for data analysis, and the glass transition temperature T_g was taken at the inflection point.

7.2.6.6 Ash testing

The actual weight fraction of glass particles in polymer composites was determined by ashing. A known mass of composite was fixed onto a borosilicate glass cover slip using DCM, and weighed, before heating in a ventilated furnace at 300℃ h^{-1} to 650℃. The temperature was held at 650℃ for 1 h to ensure complete burn off of the polymer. After cooling to room temperature overnight the glass cover slip and remaining ash was weighed to determine the mass loss. Polymer-only samples with no glass added were also tested to ensure the validity of the method. These temperatures were chosen based on previous TGA data on polymers (Fig. 3.2, on page 67), as well as knowledge of the softening point of the glass slip (>800℃). The ashing temperature must be sufficient for complete polymer burn off, but not allow significant viscous flow of the glass slip.

Using this method, the glass weight fraction (w_{pg}) can be calculated according to Eq. 7.6:

$$w_{pg} = \frac{m_{sample+slip,f} - m_{slip}}{m_{t_0}} \tag{7.6}$$

where $m_{sample+slip,f}$ is the mass of the glass cover slip and residual ash after burn off, m_{slip} is the mass of the glass cover slip which is assumed to stay constant, and m_{t_0} is the initial composite sample mass.

7.2.6.7 XRD

XRD (X-ray diffraction) was carried out using a Bruker D8 Advance diffractometer with Cu Kα radiation, using a 2θ range of 5-50°, with a 0.05° step size and dwell

time of 1.0 s step^{-1}. Line profile analysis was used to quantify the amorphous and crystalline content using Match! (Crystal Impact GbR) software, and unknown phases were identified using the Crystallography Open Database [335–340].

7.2.7 Mechanical testing

Tensile testing was carried out using a 1ST Benchtop Tester (Tinius Olsen Ltd, UK) with a 1 kN load cell, using miniature vice grips (HT54, Tinius Olsen Ltd, UK), under a constant elongation rate of 1 mm min^{-1}. Dumbbell samples (5 mm gauge length) were tested in simulated body conditions (immersed in deionised water at 37°C) using a Saline Test Tank with Heater (Tinius Olsen Ltd, UK). After loading samples into the grips and immersing them in water, they were left for approximately 10 minutes for the temperature to equilibrate. Strain was measured using a video extensometer and custom-built LabVIEW software, and dry transfer letters (black, approximately 1 mm squares, Chartpak Inc., USA) were used as strain markers. Yield strength (σ_y) was taken as the 0.2% offset yield point, and the elastic modulus (E) was calculated from the linear region of the stress-strain curve before yield.

7.2.8 Short-term water uptake

The short-term water uptake of composites injection moulded from composite precipitate was tested by immersing composite samples in deionised water at 37°C (using a surface area/volume ratio of 10 m^{-1}). At desired timepoints 10, 30, and 90 minutes) the wet mass of the composite samples was measured by dabbing them dry and weighing with a Sartorius Ultramicro balance.

7.3 Results and Discussion

7.3.1 Glass microparticle production

7.3.1.1 Results

The particle size of phosphate glass powder milled by attritor milling is shown in Figs. 7.2 and 7.3. The maximum particle size (d_{max}) should be interpreted carefully as this is prone to variability. It does however offer information useful to assessing the suitability of these milled particles for use in composite materials for cardiac stents, as the material should be reasonably homogeneous across the length scale of a stent strut (approximately 100 µm). Excessively large particles would concentrate stresses and increase the likelihood of strut fracture and should therefore be avoided. It is clear that to completely avoid excessively large particles (about 10 µm) longer milling times of about 60 minutes are required.

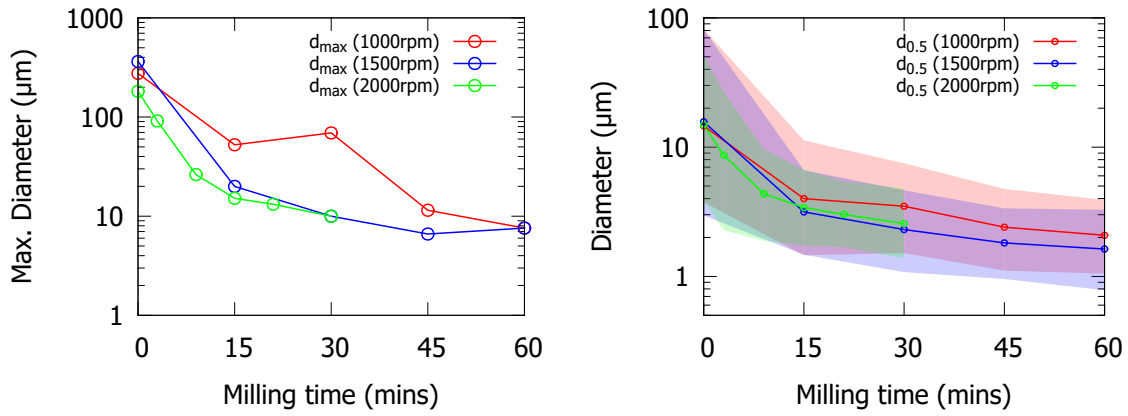

Fig. 7.2: Particle size distribution of phosphate glass milled at 1000, 1500, or 2000 rpm for up to 60 minutes. Left: maximum particle size measured for different milling conditions. Right: lines show the $d_{0.5}$ (50% by volume) value, while shaded regions indicate the range $d_{0.1}$ - $d_{0.9}$.

For the median particle size (by volume, $d_{0.5}$) and particle size range ($d_{0.1}$ - $d_{0.9}$) there was a significant decrease in size for longer milling times as expected, and this reduction plateaued over time. There was an observable difference in particle size between the different milling speeds, showing greater particle size reduction achieved with higher milling speed.

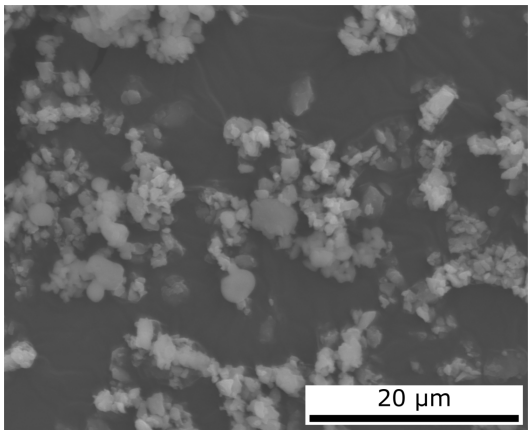

Fig. 7.3: SEM image showing P45Ca45 glass particles after milling for 60 minutes at 1500 rpm.

One issue encountered early on in optimisation of this milling procedure was contamination of the slurry with wear debris from the zirconia milling media, which caused discolouration of the slurry from white to dark grey (Fig. 7.4). This problem was solved by reducing the amount of acetone used for lubrication, thereby concentrating the slurry and reducing the effective ball-to-powder ratio, known to reduce contamination [333]. This is due to the increased glass particle-zirconia collisions compared with zirconia-zirconia collisions which are more likely to generate debris. No discolouration of the slurry was observed when using a concentrated slurry (method described in section 7.2.2) as seen in Fig. 7.4, however ICP-OES analysis provided a more sensitive way to quantify the amount of contamination present. Fig. 7.5 shows Zr levels measured by ICP-OES, along with particle size information useful for selecting a milling method for further use. Zr contamination increased with longer milling time, as well as with higher milling speed. In all cases Zr levels remained between 150 - 250 ppm.

As a result of the observed differences between glass microparticles produced using different milling process parameters, a milling speed of 1500 rpm and milling time of 60 minutes were chosen as the optimised settings for further testing. The reasons for this are discussed further in section 7.3.1.2. Further results in sections 7.3.2 and 7.3.3 therefore all refer to composites fabricated using glass milled under these milling parameters.

Fig. 7.4: Photographs showing dried milled glass before the final attritor milling stage (left), after the trial milling method (middle), and after the optimised milling method (right). Note: these dried powders display significant agglomeration that is not present in the glass/acetone slurry.

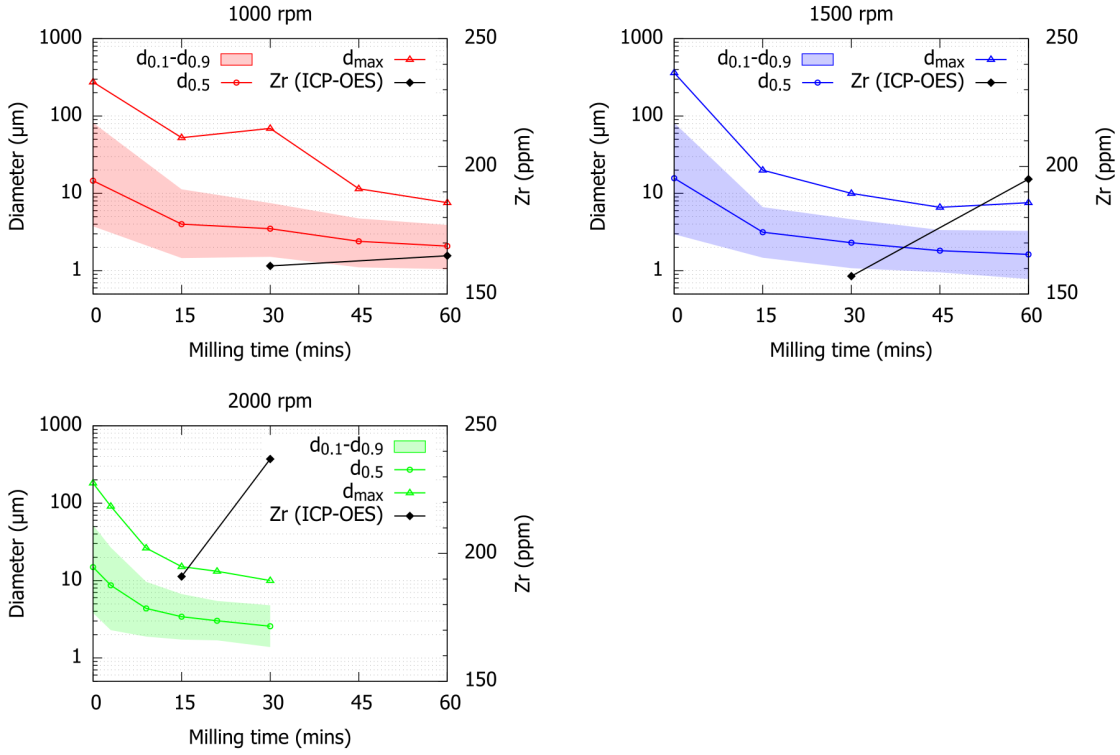

Fig. 7.5: Particle sizes of phosphate glass, and Zr contamination levels measured by ICP-OES, after milling at 1000, 1500, or 2000 rpm for up to 60 minutes. Shaded regions indicate the range $d_{0.1}$ - $d_{0.9}$.

7.3.1.2 Discussion

Trialling of different milling parameters has allowed an optimised method to be chosen for production of glass microparticles for incorporation into polymer-glass composites. The chosen method must balance the need for small particle size with avoiding contamination by wear debris, both of which increase with longer milling time and faster milling speed. These two effects are not equivalent however, results in Figs. 7.2 and 7.5 indicate that longer milling times significantly reduce particle size, while increases in milling speed have a much smaller effect. The milling speed does however have a large effect on the amount of contamination, especially when coupled with increased milling time. For these reasons, a milling speed of 1500 rpm and milling time of 60 minutes were chosen for production of microparticles for composites, as this provides good particle size reduction while keeping contamination levels relatively low. The typical properties of phosphate glass milled using this method are summarised in Table 7.2.

With a Zr content in the phosphate glass of about 200 ppm, the total amount of Zr in a typical cardiac stent could reach as high as 16 µg. For comparison, human blood typically contains about 6.2 µg/g Zr, and daily human uptake of Zr is usually around 125 mg [341]. Thus it is clear that any slow release of Zr from a polymer-glass composite stent will be negligible compared to baseline Zr levels and daily uptake.

Table 7.2: Typical particle properties for phosphate glass attritor milled at 1500 rpm for 60 minutes.

	Typical value
$d_{0.1}$ (µm)	0.5 (±0.3)
$d_{0.5}$ (µm)	1.4 (±0.3)
$d_{0.9}$ (µm)	3.0 (±0.5)
d_{max} (µm)	7.4 (±0.4)
Zr content (ppm)	195

7.3.2 Polymer-glass composite production

7.3.2.1 Results

Two different methods were investigated for production of polymer-glass composites. The composite film casting process (section 7.2.3) was used to produce thin composite films, followed by injection moulding to fabricate composite samples for subsequent testing. The composite precipitation process (section 7.2.4) was used to produce precipitated composite powder, again followed by injection moulding to fabricate composite samples for later testing.

µCT images of composite films before injection moulding (Fig. 7.6) showed segregation of glass particles to the bottom of the film. This indicated that the composite films used for subsequent injection moulding were not homogeneous. Representative µCT images are shown in Fig. 7.7 of composite samples produced by injection moulding of composite films and composite precipitate. Both large and small agglomerates were visible in the samples injection moulded from composite films, while those injection moulded from composite precipitate showed a smaller amount and size of agglomerates.

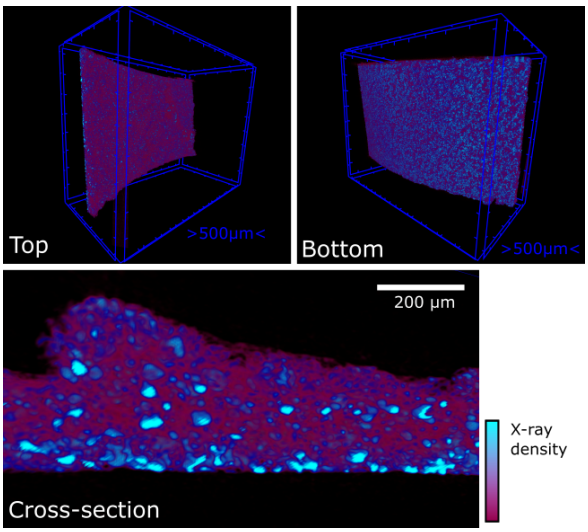

Fig. 7.6: Pseudo-coloured µCT X-ray density reconstructed images of composite films before injection moulding, coloured to show denser glass particles (blue) and less dense polymer matrix (purple).

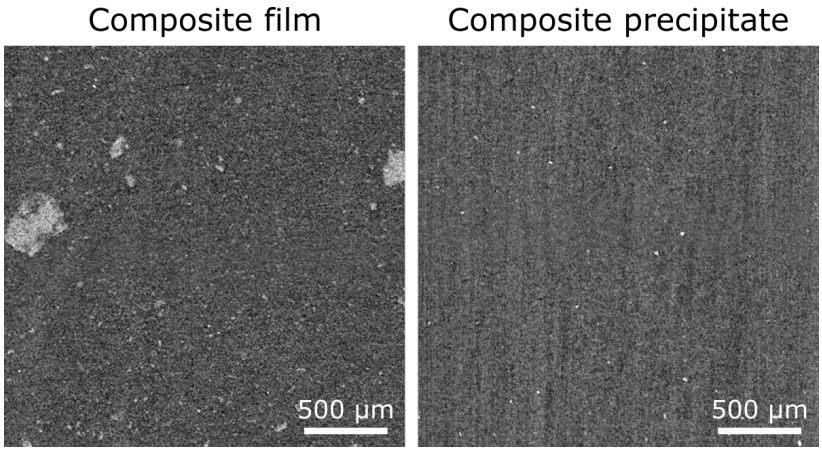

Fig. 7.7: µCT cross-sectional reconstructed images of composite samples (PLLA with 30 wt.% phosphate glass) injection moulded from composite films (left) and composite precipitate (right).

To quantify this difference 3D individual object analysis was used, to detect and measure individual agglomerate particles. These results are summarised in the distributions in Fig. 7.8. Volume percentages were normalised to the total scan volume so that the amount of detected agglomerates could also be assessed. The samples tested were PLLA with a high glass content (as these have the greatest tendency to agglomerate) of 30 wt.%, equivalent to 17 vol.%. In both cases the total vol.% of agglomerates detected (1.49 - 4%) was significantly lower than the actual glass content (17%). This was due to the individual particle size, as detailed in Table 7.2, being comparable to the pixel size (1.49 µm) - for detection particles need to be at least 3 times the pixel size. Therefore, well dispersed particles were not detected. The total vol.% of objects detected could therefore be used to assess the amount of glass forming agglomerates - for samples injection moulded from composite films, this was 4% of the total volume, so 24% of the phosphate glass. By contrast for samples injection moulded from composite precipitate, only 1.49% of volume was taken up by agglomerated glass, about 9% of the total glass - a clear reduction in agglomeration.

It is also important to assess not just the amount of agglomeration occurring, but also the size of these agglomerates. As the size distributions in Fig. 7.8 show, samples injection moulded from composite precipitates showed a significant reduction in the

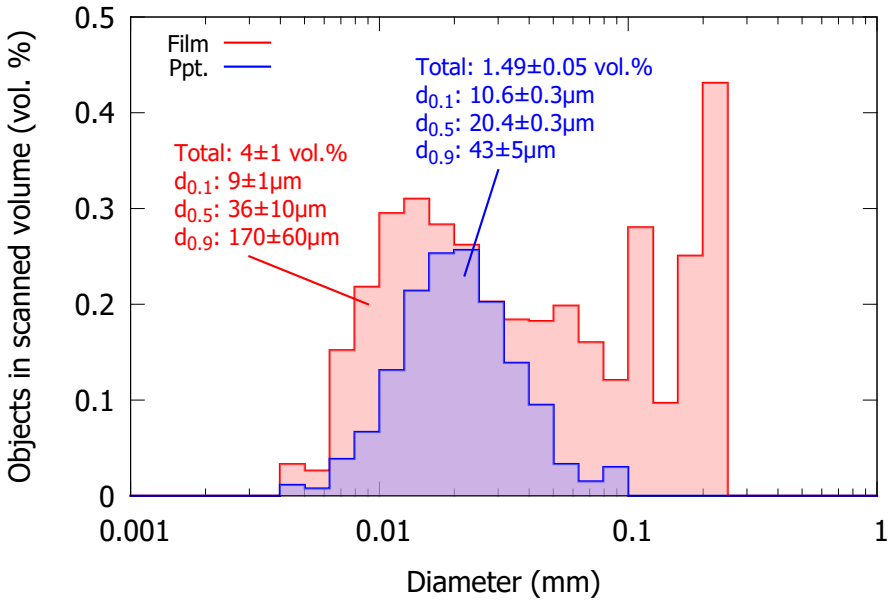

Fig. 7.8: Size distribution (by volume) of objects detected in µCT scans, normalised to the total scan volume, for PLLA with 30 wt.% (17 vol.%) phosphate glass, injection moulded from either composite films or composite precipitate (ppt.).

amount of large agglomerates, with a reduction in the $d_{0.9}$ value from 170 ±60 µm to 43 ±5µm. Composites moulded from films showed large amounts of agglomerates in the size range above 100 µm, while those moulded from composite precipitate completely eliminated agglomerates above 100 µm, with the bulk of agglomerates around 20 µm.

SEM results also show similar results to those observed by µCT. Composites produced by injection moulding of cast films displayed large agglomerates of glass particles, as seen in Fig. 7.9. Conversely, composites fabricated by injection moulding of composite precipitate showed even dispersion of glass particles throughout the polymer matrix, with few large agglomerates seen.

In order to assess the impact of these two different production methods, and in particular the effect of agglomeration, mechanical testing was carried out using composites of PLLA with 30wt.% phosphate glass. These tests were carried out with the samples immersed in 37°C water, to simulate conditions within the body. Mechanical testing

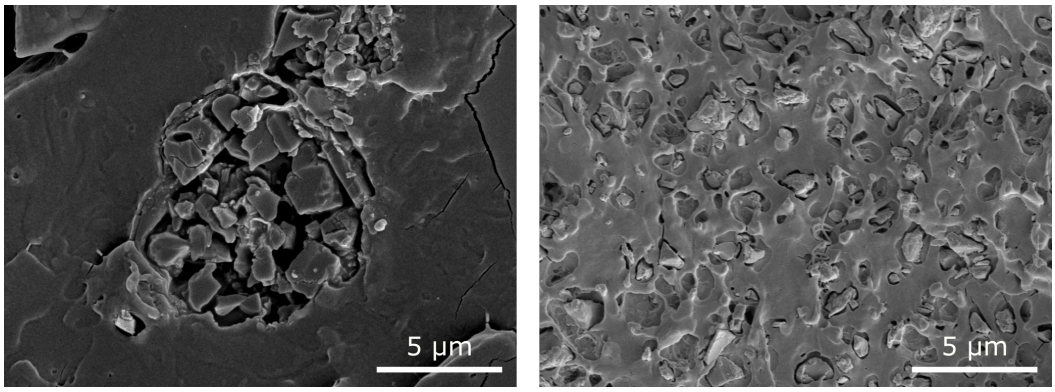

Fig. 7.9: SEM images of composite samples (PLLA with 30 wt.% phosphate glass) injection moulded from composite films (left) and composite precipitate (right).

results are shown in Fig. 7.10, where stress-strain curves can be seen, along with photographs of samples before and after tensile testing. Composite samples injection moulded from composite films and composite precipitate showed comparable strength and stiffness, with little significant differences seen between the measured E and σ_y for these two methods. However there was a large difference in the ductility of these materials, with composites moulded from films failing at 7% (±4) strain, while those moulded from composite precipitate showed extensive plastic deformation, eventually failing at 120% (±60) strain. These differences are also clear in photographs (Fig. 7.10b-e), where the samples moulded from composite films showed tearing and crack propagation, while the samples moulded from composite precipitate showed necking and drawing before failure.

As a result of the observed differences between polymer-glass composites fabricated by injection moulding from composite films or composite precipitate, the composite precipitation method was chosen as the final production method for polymer-glass composites for further testing. The reasons for this are discussed further in section 7.3.2.2. Further results in section 7.3.3 therefore all refer to composites fabricated by injection moulding from composite precipitate.

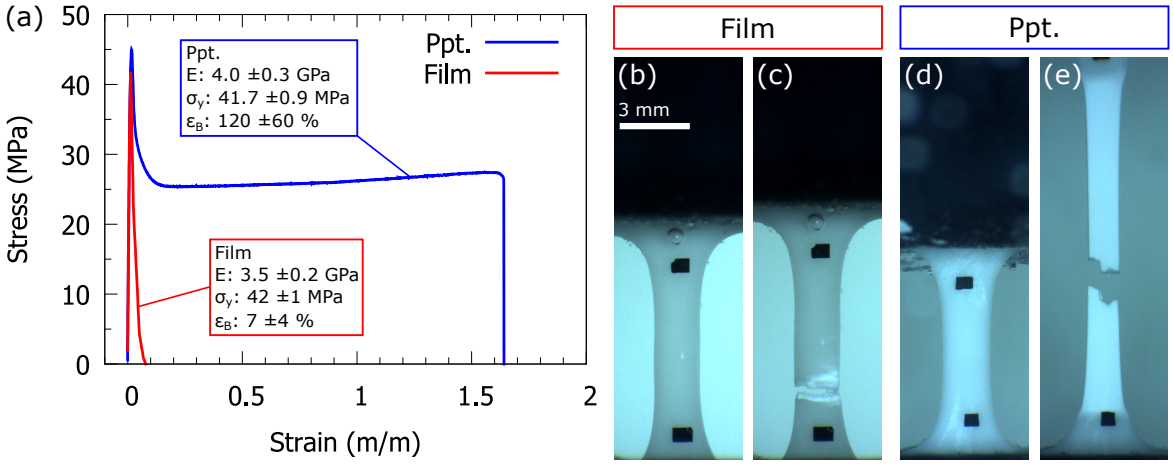

Fig. 7.10: Typical mechanical testing results of composite (PLLA with 30wt.% glass) samples injection moulded from composite films and composite precipitate, tested in deionised water at 37°C, showing stress-strain curves (a). Photographs of samples are also shown: samples injection moulded from composite films, before testing (b) and after tensile failure (c), and samples injection moulded from composite precipitate, before testing (d) and after tensile failure (e).

7.3.2.2 Discussion

Early trials of polymer-glass composites used the composite film casting process (section 7.2.3), followed by injection moulding to fabricate composite samples. µCT analysis showed significant agglomeration of glass particles in samples injection moulded from composite films, including a large proportion of agglomerates with particle size over 100 µm. This is similar or greater than the size of a typical stent strut, and therefore would result in inhomogeneity and increase the risk of strut fracture. This agglomeration arose due to the film casting process. During film casting, dissolved polymers and glass slurry mixture were left in petri dishes for the solvent to evaporate. This evaporation took several hours, allowing the denser glass particles to settle to the bottom of the film as evidenced in Fig. 7.6. During injection moulding, films were melted and then forced into a mould - there was little mixing of the molten composite carried out. Therefore agglomerates formed during production of composite films were carried through to the injection moulded sample as seen in Figs. 7.7 and 7.8.

To reduce this tendency the composite precipitation process was developed, as described in section 7.2.4, where composite samples were fabricated by production of

composite precipitate and subsequent injection moulding. This was observed to result in significantly less agglomeration, and agglomerates that did form were significantly smaller (Figs. 7.7 and 7.8), indicating improved dispersion for the precipitation method. µCT results indicated that 1.49 vol.% of the composite (or 9% of the glass) was made up of agglomerated glass, however this is likely to be a slight overestimate. All particles detected by µCT (minimum diameter of 4.5 µm) were assumed to be glass agglomerates, however given the glass particle size (Table 7.2), particularly the maximum particle size of 7.4 µm, it is clear that a small portion of these will in fact be single particles rather than agglomerates.

The composite precipitation method was able to achieve good dispersion of phosphate glass particles within the polymer matrix due to the fast formation of solid polymer on the surface of the glass particles. The glass particles were well dispersed in the slurry/dissolved polymer after sonication, and rather than transferring this to petri dishes for slow evaporation, ethanol was added to precipitate the polymer immediately. Once the solvent power of the solution was reduced enough for polymer precipitate to form, it nucleated on glass particles within the solution. Therefore, individual glass particles should be well covered by polymer precipitate, preventing agglomeration.

This novel method allows production of well dispersed composites, avoiding the agglomeration that can be experienced when using solvent casting. It provides a useful alternative to melt blending, where the two components are mixed with the polymer in its molten state [218]. This can result in significant polymer degradation and molecular weight reduction, owing to the extended processing time and high shear forces at high temperature [220, 224].

The effects of this improved dispersion are clear from the mechanical testing results in Fig. 7.10. The elastic modulus of the composite was unchanged, as this is typically a result of the amount of glass present rather than the particle size, and the loading

was kept constant at 30wt.%. Similarly, in the absence of strong interfacial bonding between the polymer and glass components of the composite, the agglomeration of glass particles would not be expected to significantly alter the yield strength, provided that agglomerates are not larger than the critical size for brittle failure by stress concentration [326]. The key difference between composites produced using these two methods was seen in the ductility, where the composites with more evenly dispersed glass (precipitation method) had a much greater toughness. One crucial toughening mechanism for inorganic particle reinforced polymer composites is the debonding of the matrix from the particle. In composites where significant agglomeration has taken place, the surface area for energy absorption by debonding will be significantly lower, reducing the toughness. In addition, the greater stress concentrating effect of the large agglomerate, as well as the weak inter-particle bonding within the agglomerate, may all contribute to the lower ductility of the composites produced from injection moulding of films [326, 342].

7.3.3 Composite properties and performance

7.3.3.1 Results

Polymer-glass composites produced using the precipitation method and subsequent injection moulding were characterised by ash testing, and the target and measured glass loading are shown in Table 7.3. Ash testing results showed that the measured phosphate glass weight fraction in the composite (w_{pg}) matched well with the target, demonstrating the effectiveness of this method. Polymer-only samples (PLA and PLA-CL) showed complete polymer burn off, with negligible residual ash content. This confirms the validity of this method for measuring the actual glass content, in particular the assumption in Eq. 7.6 that the glass slip mass (m_{slip}) is unchanged after polymer burn off.

Table 7.3: Ash testing results for the as-fabricated polymer-glass composites, showing the target and measured glass weight fraction.

Sample code	Target w_{pg} (wt.%)	w_{pg} (wt.%)
PLA	0	0.013 ± 0.007
PLA-CL	0	0.01 ± 0.01
PLA-0.15P45Ca45	15	14.3 ± 0.3
PLA-CL-0.15P45Ca45	15	14.0 ± 0.2
PLA-0.3P45Ca45	30	29.8 ± 0.1
PLA-CL-0.3P45Ca45	30	30.0 ± 0.1
PLA-0.15P40Ca50	15	15.8 ± 0.2
PLA-CL-0.15P40Ca50	15	16.1 ± 0.2
PLA-0.3P40Ca50	30	30.9 ± 0.1
PLA-CL-0.3P40Ca50	30	31.4 ± 0.1

XRD was carried out in order to assess the crystallinity of the as-fabricated polymer-glass composite samples, and representative diffraction patterns are shown in Fig. 7.11. Firstly it is clear that there were no sharp diffraction peaks observed, indicating that both the polymer and glass components were in an amorphous state. For the polymer component, this indicated that the fast cooling provided after injection moulding by the room temperature mould quenched the polymer into an amorphous state, as seen in Chapter 3 for polymer blends. In Chapter 5 the P40Ca50 glass powder was shown to contain a small amount of devitrified crystalline material ($Ca_2P_2O_7$) at a level of 2.0 ±0.4 wt.%. This was not observed here for composites containing this glass composition, possibly because the devitrified material formed a smaller proportion of the polymer-glass composite.

The shape of the diffraction pattern can also be explained in terms of the composition of the composite. Polymer-only samples displayed a broad peak at around 17°, equivalent to those observed in Chapter 3 (Fig. 7.11, and Fig. 3.6 on page 70). When glass was incorporated into the composite, this peak remained, but a second broad peak was observed at around 30°. This can be attributed to the broad amorphous peak observed for phosphate glasses (Fig. 5.3, on page 111) at around 27°, combined

with the second order of the initial broad amorphous polymer peak at around 33°. The ratio of these two broad peaks at 17° and 30° appeared to vary in accordance with the glass content in the composite.

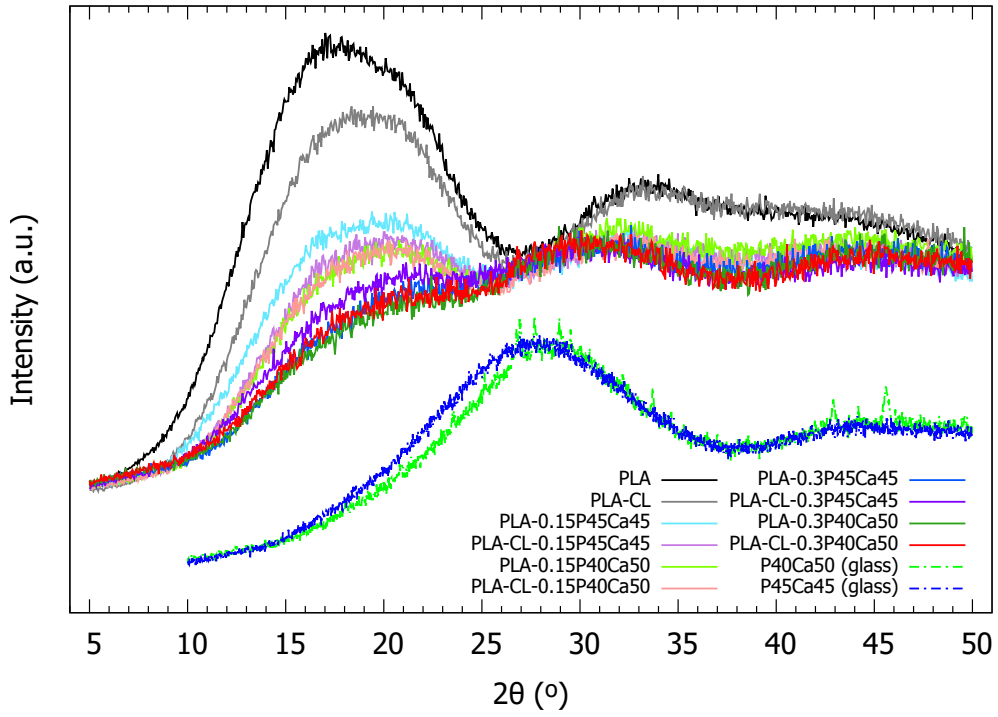

Fig. 7.11: XRD patterns of various as-fabricated polymer-glass composite samples, with phosphate glasses for comparison.

The thermal properties of the polymer-glass composites were also characterised in their as-fabricated state, with the glass transition temperature T_g shown in Fig. 7.12. There was little evidence of a significant difference in the glass transition temperature when glass particles were incorporated into the composite - the T_g appeared approximately constant as the glass content increases. There was however a difference observed depending on the polymer matrix composition. As observed in Chapter 3 (Fig. 3.5, on page 69), the addition of PLCL(70:30)-PEG to PLLA reduced the glass transition temperature in the single phase composition region. Only one T_g was detected here within the temperature range studied, indicating that this addition of

10wt.% PLCL(70:30)-PEG to PLLA formed a single phase polymer blend, as expected from previous results seen in section 3.3.3 on page 68.

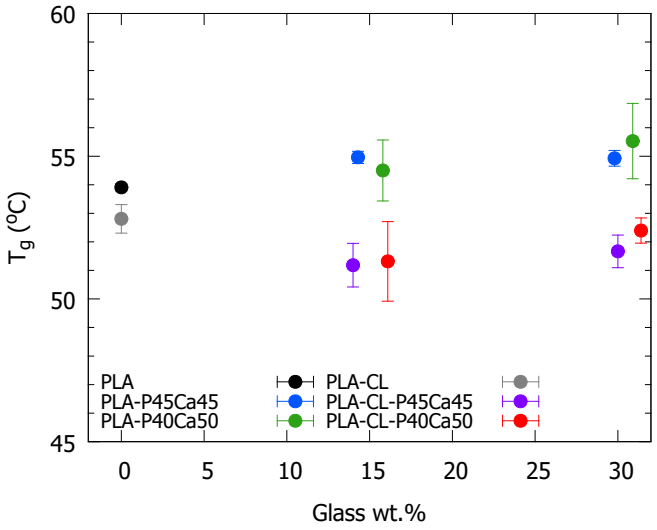

Fig. 7.12: Glass transition temperatures (T_g) of various as-fabricated polymer-glass composite samples, according to measured glass content (wt.%).

The short-term water absorption behaviour of the composites was also assessed, in order to understand the differences in behaviour between dry and wet conditions, before any degradation had occurred, results are shown in Fig. 7.13. The addition of phosphate glass to the polymer component had a significant effect on the water absorption, even on a short timescale, with polymer-only samples showing low water uptake of around 0.3wt.%, while for composites this reached as high 2 wt.% within 90 minutes. Increasing the amount of glass in the composite led to a corresponding increase in the water uptake, with composites containing 30wt.% glass absorbing approximately twice as much water as those with 15wt.% glass.

The chemical composition of the different components also played a role in the amount of water absorbed. The addition of PLCL(70:30)-PEG to PLLA was seen (in sections 4.3.1 and 4.3.2 on pages 86 and 89) to increase the water absorbed during degradation for polymer blends. This phenomenon was reproduced here with the

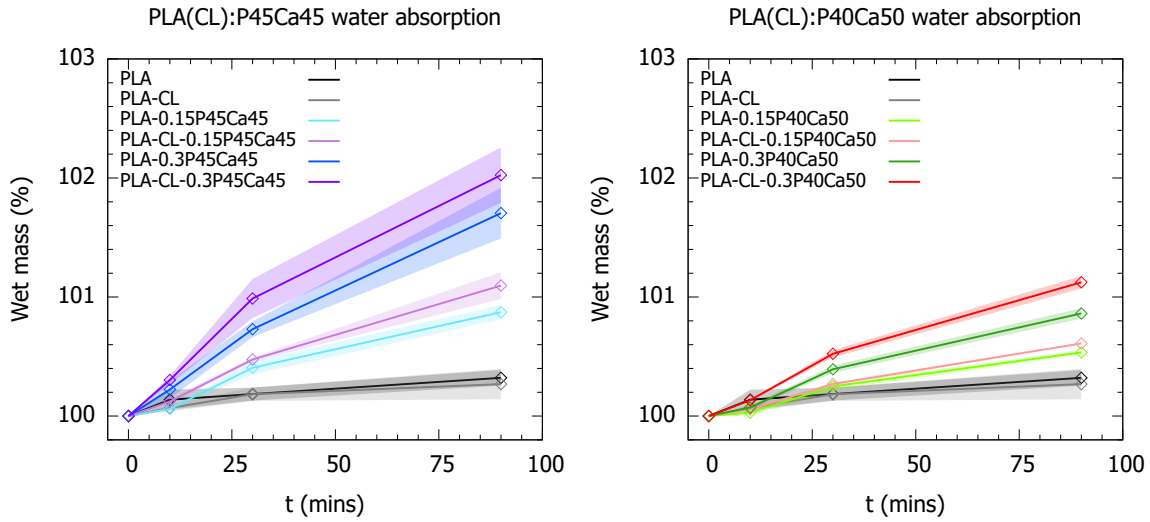

Fig. 7.13: Wet mass of polymer-glass composites during short-term water absorption, showing composites with the P45Ca45 glass (left) and P40Ca50 glass (right). The wet mass is given as a % of the original dry mass, and the shaded region shows the standard deviation for n = 3 measurements.

composite materials, where composites with PLCL(70:30)-PEG in the polymer matrix displayed slightly greater water absorption than the equivalent composites without this copolymer. The glass composition was also seen to have a strong effect on the amount of water absorbed, where an increase in the glass CaO content (from 45 mol% to 50 mol%, with a corresponding reduction in P_2O_5 content from 45 mol% to 40 mol%) consistently reduced the water absorption by half.

The timescale of this water absorption is also important to consider. The significant differences observed between different composite compositions were only observed after slightly longer immersion times (30 - 90 minutes). For shorter immersion times (10 minutes) the differences between materials were limited, and the level of water uptake was low at <0.3wt.%.

Representative stress-strain curves, and a summary of the mechanical properties of the composites produced (compositions from Table 7.1) are shown in Figs. 7.14 and 7.15. These show the mechanical properties of composites with 0, 15, and 30 wt.% glass, in ambient and simulated body conditions.

Under dry conditions, the addition of phosphate glass was seen to provide significant mechanical reinforcement, increasing the elastic modulus from approximately 3 GPa for the polymers, to approximately 4 GPa with 15wt.% glass and approximately 5 GPa with 30 wt.% glass. The same was not the case for the yield strength however, which showed a modest decrease as phosphate glass was added to the composite. The polymers, and composites with lower (15wt.%) glass content showed similar deformation behaviour, with a small amount of plastic deformation after yield. The addition of 15wt.% glass did not appear to have affected the elongation at break significantly, however when the glass content was increased to 30wt.% the ductility decreased noticeably, with failure occurring shortly after yield.

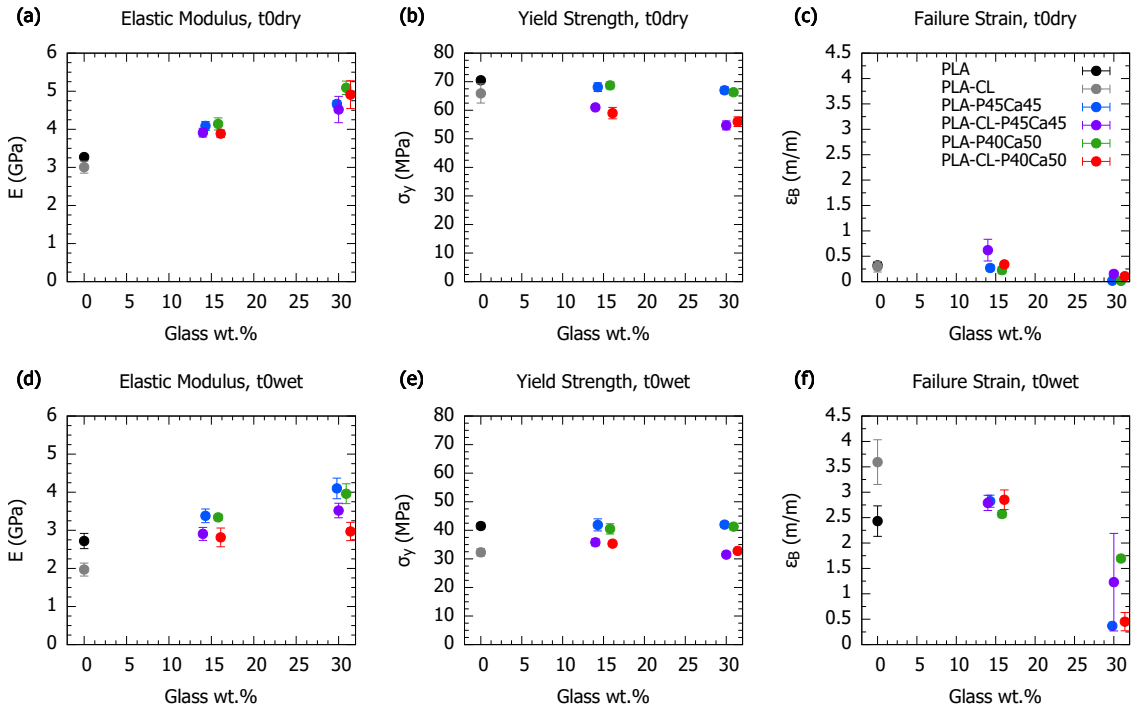

Fig. 7.14: Mechanical properties measured by tensile testing for polymer-glass composites under various conditions, according to measured glass content. (a, b, c): As-fabricated composites tested dry at room temperature (**t0dry**), showing the elastic modulus (a), yield strength (b), and elongation at break (c). (d, e, f): As-fabricated composites tested immersed in 37°C water (**t0wet**), showing the elastic modulus (d), yield strength (e), and elongation at break (f). Error bars denote standard deviation, n = 3.

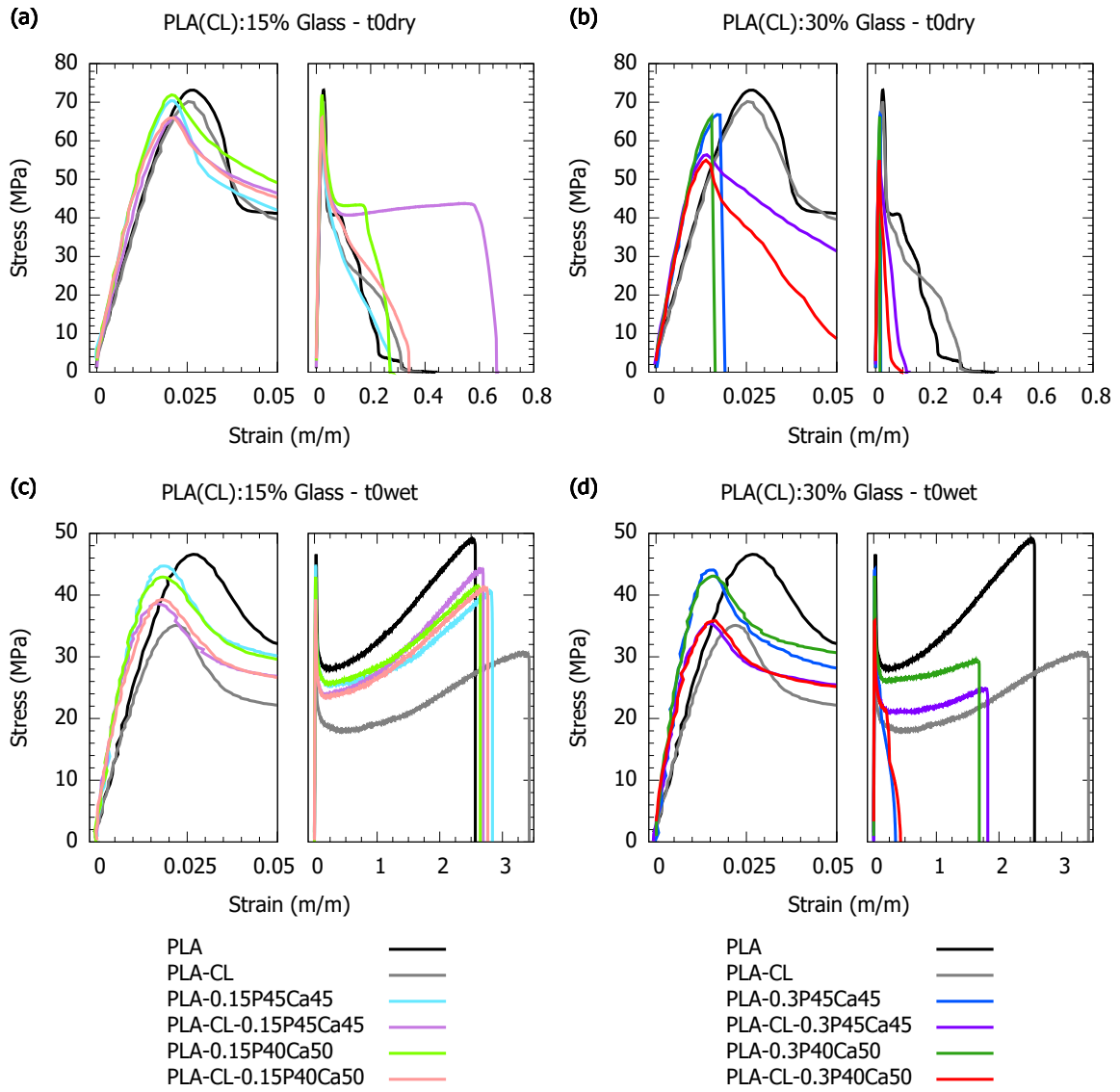

Fig. 7.15: Representative stress-strain curves for tensile testing of polymer-glass composites under various conditions. (a, b): As-fabricated composites with 15wt.% glass (a) and 30wt.% glass (b) tested dry at room temperature (**t0dry**). (c, d): As-fabricated composites with 15wt.% glass (c) and 30wt.% glass (d) tested immersed in 37°C water (**t0wet**).

The addition of the PLCL(70:30)-PEG copolymer to PLLA in the polymer matrix component of the composite was also observed to impact the composite mechanical properties under ambient conditions. There was a slight decrease in the elastic modulus across all compositions, as well as a reduction in yield strength. The yield strength results also suggest there was an interaction between the effects of PLCL(70:30)-

PEG addition and phosphate glass addition, with the addition of glass decreasing yield strength more when the matrix contained PLCL(70:30)-PEG. The addition of PLCL(70:30)-PEG to the polymer matrix also appeared to increase the elongation at break slightly, but did not lead to a large scale change in the deformation behaviour. Two different glass compositions have been used with this set of composites (P45Ca45 and P40Ca50), but this did not have an impact on the mechanical properties of the composite under ambient conditions.

Significant changes were seen in these mechanical properties when tested in simulated body conditions (immersed in deionised water at 37°C). For all compositions the elastic modulus significantly reduced, although composites containing more glass still displayed a higher modulus than those without glass reinforcement. The yield strength also decreased significantly. In addition, the slight reduction in yield strength observed in ambient conditions when glass was incorporated was no longer present under simulated body conditions. Instead, the main variation in yield strength seen when testing in wet conditions at 37°C was the reduction arising from addition of PLCL(70:30)-PEG to the polymer matrix.

When carrying out tensile tests in simulated body conditions, the elongation at break observed was significantly higher than when tested in ambient conditions. Large scale plastic deformation was seen for the polymer-only samples and composites with 15wt.% glass, where at least 200% elongation was observed before failure. Composites with 30wt.% glass also showed more ductile behaviour than in ambient conditions, however the large scale plastic deformation seen for composites with lower glass content was not consistently achieved, and the elongation at break was lower and more variable. Addition of the PLCL(70:30)-PEG to the polymer matrix was found to increase the elongation at break here, once large scale plastic deformation began, however this effect was only seen for the polymer-only samples and not the composites. As seen for testing in ambient conditions, the glass composition (P45Ca45 or P40Ca50) again did not

have a noticeable effect on the mechanical properties when tested under immersion in 37℃ water.

7.3.3.2 Discussion

The characterisation of composites produced by injection moulding of composite precipitate demonstrated that this method is effective for producing well dispersed polymer-glass composites with controllable glass filler loading. The targeted glass loading is accurately reflected in that measured by ashing, and the composites were X-ray amorphous due to the fast cooling of the polymer and glassy nature of the phosphate glasses. The short term water absorption behaviour of the composites demonstrated a low level of water uptake at short times of around 10 minutes, which is approximately the same as the immersion time allowed for temperature equilibration before starting mechanical testing. This water absorption, along with the increased temperature under simulated body conditions (immersed in 37℃ water), reduces the inter-chain bonding within the polymer [50] leading to the differences seen in the mechanical properties of samples measured in ambient conditions and simulated body conditions.

Fig. 7.16 compares the measured elastic moduli of the composites to that calculated by the Counto model (Eq. 7.3). For a given value of E_{Counto}, equivalent Voigt-Reuss bounds (Eqs. 7.1 and 7.2) can also be calculated, based on the glass volume fraction and elastic moduli of the glass and matrix, these are also shown in Fig. 7.16. In this analysis the elastic modulus of the phosphate glass was taken as 48 GPa (from Sglavo et al. [343]), assumed to be constant with respect to the glass compositions tested here, and different testing conditions (dry at room temperature, wet at 37℃). The measured composite moduli are seen to fall within the relevant Voigt-Reuss bounds, and closely match the moduli calculated using the Counto model ($R^2 = 0.90$). This indicates that the main factors affecting the composite modulus before degradation, in both ambient and simulated body conditions, are the glass loading and the polymer matrix stiffness

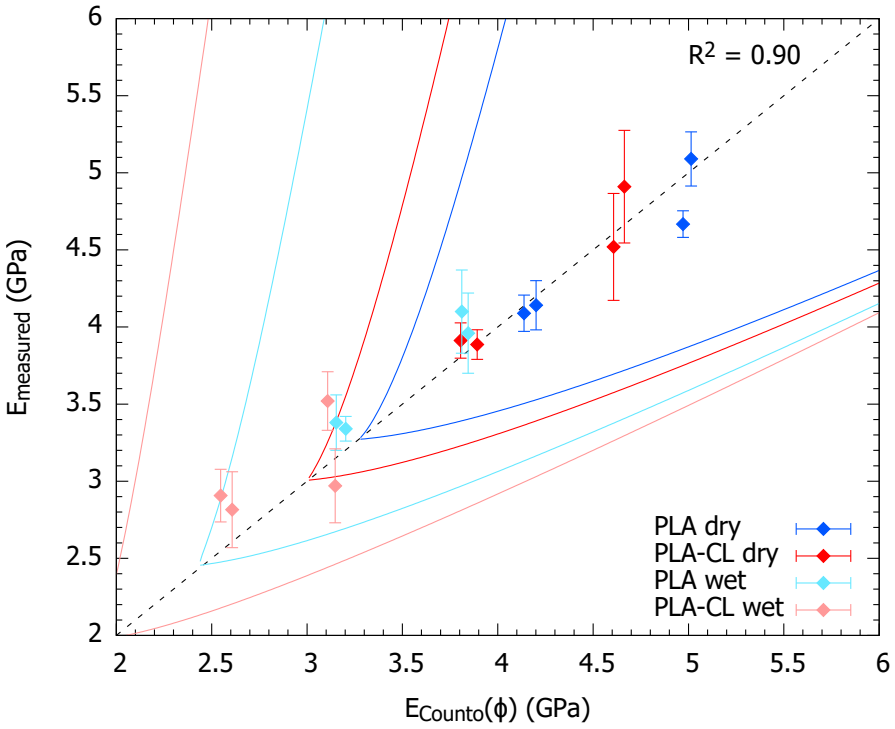

Fig. 7.16: Measured elastic modulus vs. elastic modulus calculated from the matrix properties, glass properties, and loading fraction, using the Counto model (Eq. 7.3). Data is shown for composites based on PLA and PLA-CL polymer matrices, in wet (at 37°C) and dry conditions. Solid lines shown are the upper and lower bounds for the modulus (Voigt-Ruess bounds, Eqs. 7.1 and 7.2), and the dotted line represents $E_{measured} = E_{Counto}$.

(which is in turn dependent on matrix composition and the temperature/hydration state). Other factors such as the glass composition, interfacial bonding, or deviation from the model at high ϕ_f are not seen to be significant. During deformation in the elastic region, there is insufficient extension to separate the interface between inorganic particles and the polymer matrix, therefore the elastic modulus is not significantly affected by the interfacial strength [326]. The elastic modulus is thus a function of the matrix stiffness, the stiffness of the inorganic phase, and the loading volume fraction.

Under ambient conditions, the yield strength of the polymer-glass composites tested was seen to fall between the bounds defined by Nicolais and Nicodemo (Eqs. 7.4 and 7.5) for no adhesion (lower bound) and perfect adhesion (upper bound), as seen in Fig. 7.17. This indicated that some stress transfer occurred and the load was not borne

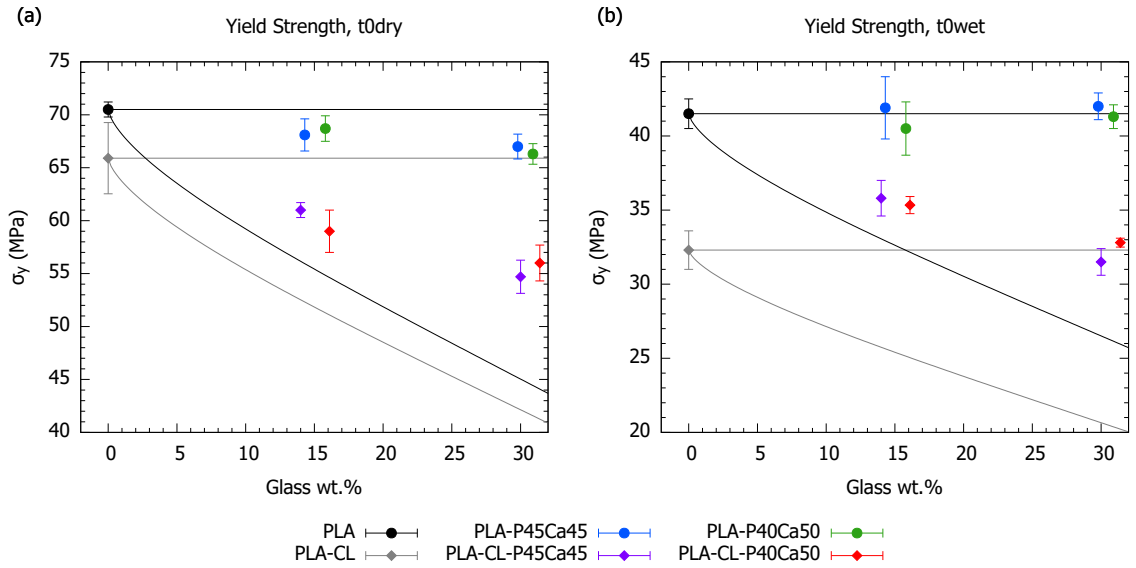

Fig. 7.17: Yield strength for polymer composites tested (a) dry at room temperature (**t0dry**), and (b) immersed in 37°C water (**t0wet**) - data from Fig. 7.14. Solid lines show the upper and lower bounds for the yield strength, according to Eqs. 7.4 and 7.5.

solely by the polymer matrix, however due to imperfect adhesion yield was initiated by separation at the polymer-glass interface. This led to stress concentration in the matrix and subsequent bulk yield. The reduction in yield strength as the filler amount increased appeared to be more severe for composites with the PLA-CL matrix than the PLA matrix, suggesting that the PLA-phosphate glass interface had superior interfacial adhesion than the PLA-CL-phosphate glass interface, under ambient conditions.

The behaviour of the yield strength was different when tested in simulated body conditions (immersed in 37°C water), generally following the upper bound predicted by Eq. 7.4. This could be interpreted as a strengthening of the interfacial adhesion, but it is more likely to be a result of the reduced strength of the polymer matrix under these non-ambient conditions. The effect of increased temperature and hydration reduced the yield strength of the polymer matrix, which may have led to to bulk yield in the polymer matrix before reaching sufficient stress to cause separation at the polymer-glass interface. For composites with 15wt.% glass in a PLA-CL matrix, there did appear to be a modest increase in strength above the upper limit when tested

in simulated body conditions, indicating strong matrix-particle interfacial bonding between both glass compositions and the PLA-CL matrix. This may suggest an increase in dipole-dipole interactions between the matrix and glass in the higher temperature, hydrated state, however a marginal change such as this should be interpreted with caution.

The dependence of the measured composite ductility on the testing conditions can mainly be attributed to the behaviour of the polymer matrix, which becomes significantly more ductile when tested in simulated body conditions as discussed in Chapters 3 and 4. Under both testing conditions the variation in ductility with regards to particle loading is similar, where the ductility stayed relatively unchanged upon addition of 15wt.% glass, and decreased for the higher 30wt.% glass loading. This suggests that the stress concentrating effect of the filler particles was somewhat counteracted by toughening mechanisms (such as interfacial debonding, or crack deflection, blunting, or pinning) for the lower 15wt.% filler loading. For the composites with 30wt.% glass, the increased brittleness may be a result of greater stress concentration, or an effect of particle agglomeration, which is more likely for higher filler loading.

7.3.4 Implications for cardiac stents

These mechanical testing results can give an indication of the suitability of these materials for bioresorbable cardiac stent applications, in particular during the implantation procedure where deformation under ambient conditions occurs during crimping, and further deformation occurs during expansion *in vivo*, before significant degradation has taken place. The ability to incorporate 15wt.% glass without loss of ductility is encouraging, allowing filler to be utilised without significantly increasing the tendency for brittle failure during crimping or expansion. The increased modulus achieved by addition of phosphate glass is a promising result, which could reduce the elastic recoil observed after stent expansion, in turn reducing the risk of restenosis [47]. In terms of yield strength, the properties under simulated body conditions are of most relevance;

here composites with phosphate glass achieve comparable yield strength to the unfilled polymer.

7.4 Conclusions

These results demonstrate the effectiveness of a method for production of micron-size phosphate glass particles, and incorporation of these particles into polymer-glass composites. Phosphate glass particles with $d_{0.5} = 1.4$ µm and minimal contamination with zirconia were produced using attritor milling, and were then incorporated into well dispersed polymer-glass composites using a precipitation method followed by injection moulding. Composites produced using this method demonstrated reduced agglomeration and therefore reduced brittleness compared with composites produced using solvent film casting.

Mechanical testing of these composites in ambient and simulated body conditions demonstrated that addition of the glass particles provides effective reinforcement, increasing the elastic modulus. The elastic modulus corresponded well with the Counto model, demonstrating that composite stiffness variation was a result of changes in matrix stiffness and filler loading. The yield strength indicated the presence of some interfacial adhesion between the polymer matrix and phosphate glass, which was higher for composites with the PLA matrix than the PLA-CL matrix, but independent of glass composition. In ambient conditions yield was initiated by separation at the polymer glass interface, while in simulated body conditions, the reduced strength of the polymer matrix in the higher temperature, hydrated state led to yield in the bulk polymer matrix before sufficient stress for matrix-particle debonding was reached.

Incorporation of up to 15wt.% phosphate glass into polymer-glass composites was able to improve the elastic modulus without reduction in the ductility, suggesting that

these materials can reduce the stent elastic recoil and risk of restenosis, without risking brittle material failure. The presence of some interfacial polymer-glass adhesion in the composites resulted in comparable yield strength to the unfilled polymer, demonstrating that the composites are noninferior to existing polymers in terms of yield strength and the resulting strut size required.

Chapter 8

Polymer-glass composites: mechanical and degradation behaviour

8.1 Background and aims

Bioresorbable stents have the potential to be the 4th revolution in interventional cardiology [52], reducing rates of restenosis, late thrombosis, and other long-term complications [59, 344]. To date however, this promise has not been realised, with some of the first bioresorbable stents brought to market subsequently experiencing safety issues and being withdrawn from sale [31]. Many of these issues arise from the mechanical properties of the material used for these stents, PLLA (poly-L-lactide, or polylactic acid). PLLA has a significantly lower yield strength than the metals currently used for stents, necessitating much thicker struts to provide sufficient device strength. This in turn leads to problems with device size, causing issues for surgeons navigating the devices through tortuous vessels. Thicker struts also increase blood flow turbulence, which can negatively affect the endothelialisation of the stent and increase the risk of thrombosis [35, 345]. The relatively low elastic modulus of PLLA is also an issue when considering the elastic recoil of a stent after implantation, which must be

minimised to prevent restenosis or stent dislodgement [35]. It is clear that to overcome issues with existing bioresorbable stent technologies, improvements in material yield strength and elastic modulus are necessary [36].

Fabrication of polymer composites is a popular technique for improving the mechanical properties of polymeric materials. In fact, polymer composites have been widely investigated for use as orthopaedic implants [346, 347]. Polymer composites incorporating hydroxyapatite or α-TCP are prominent in this area, due to the similarity of these ceramics to natural bone mineral, and give substantial improvements in mechanical properties [218, 348–351]. Composites incorporating bioactive glasses have also been investigated, and are attractive due to the exceptional tunability of the dissolution rate and ion release properties that can be achieved by engineering the glass composition [160, 317, 352]. For applications as bioresorbable stent materials however, these composites have not been frequently studied. The use of Ca-containing bioceramic fillers may appear to pose a risk of arterial calcification, however when the small amount of material, extended timescale of release, and relatively large volume of blood flow through coronary arteries are considered [353], the increase in blood Ca levels is negligible compared with the baseline concentration.

To date most strategies for tuning the mechanical behaviour of stent materials rely on altering the polymer chemistry (i.e. copolymerisation ratio etc.) or polymer structure (orientation, crystallisation), however these methods cannot be applied without altering the degradation behaviour of the material [35, 139]. By incorporating bioactive glass however, results have shown that the degradation of the composite can be tuned by varying the glass composition [248, 253–255]. This occurs via several mechanisms. Increased water absorption at the polymer/glass interface, especially for continuous glass fibres where wicking plays a large role, can accelerate the degradation rate [230]. There are also chemical effects resulting from dissolution of the inorganic filler. α-TCP particles are seen to slow polymer degradation due to the buffering effect of the ions

released as the ceramic dissolves [217, 249]. Similar effects can occur in polymer-glass composites, where ion exchange can occur at the glass surface resulting in a buffering effect at the interface [252].

These phenomena lead to the idea that polymer-glass composites can allow decoupling of mechanical and degradation properties, whereby incorporation of glass particles can provide mechanical reinforcement, and changing the glass composition can tune the degradation profile, with minimal impact on the mechanical properties. This degradation profile is another key issue with current stents based on PLLA that must be addressed. PLLA is well known to experience very slow degradation *in vivo*, requiring several years for full resorption [35, 62, 284, 285], while healing after stent deployment is typically complete after around six months [282, 283]. Developing materials with accelerated rates of resorption would therefore be highly advantageous for stent device manufacture [36].

The work described in this chapter aims to assess the composite materials developed in Chapter 7 for use as cardiac stents, in terms of their degradation behaviour, and development of mechanical properties during degradation. Polymer matrix compositions of pure PLLA and 90PLLA:10PLCL(70:30)-PEG were chosen to observe the effect of blend composition on composite properties, with PLLA as a control and a small amount of PLCL-PEG added to improve ductility and accelerate degradation, without causing rapid loss of mechanical integrity.

8.2 Materials and methods

8.2.1 Composite production

Composites of PLLA and PLCL(70:30)-PEG polymers with P_2O_5-CaO-Na_2O glasses were produced using the precipitation method and injection moulding as detailed in

Chapter 7 (sections 7.2.2, 7.2.4, and 7.2.5), with compositions as described in Table 7.1. Briefly, phosphate glass powder (produced in Chapter 3) was milled to a fine particle size using attritor milling. Phosphate glass slurry was then added to dissolved polymers, and ethanol was added to precipitate the polymer onto dispersed glass particles, producing a composite precipitate. This precipitate was moulded to create dumbbell or disc shaped samples for further testing using micro-injection moulding.

8.2.2 Degradation testing

Degradation studies were carried out by immersing individual disc-shaped (5 mm diameter, 600 µm thick) composite samples in 5 mL PBS in bijou tubes, which were placed in an incubator at 37℃. pH measurements were taken at regular intervals using an HI 4222 pH meter (Hanna Instruments Ltd., UK), and Ca^{2+} ion concentration was measured using an ISE (ion selective electrode - Sentek 361-75 Calcium Combination ISE), calibrated using a modified Nernst equation [318] with standard solutions diluted with DI water from a 0.1 mol L^{-1} calcium standard (Hanna HI 4004-01). PBS alone was used as a control for pH and Ca^{2+} ion measurements. At desired timepoints the wet mass of the composite samples was measured by dabbing them dry and weighing with a Sartorius Ultramicro balance, before returning them to the solution. A long-term (∼300 days) degradation study was carried out, as well as a series of shorter studies (5, 30, 120 days) for more detailed analysis. After degradation, samples were dried at room temperature in a vacuum oven until reaching constant mass, before further analysis was carried out (except for mechanical testing, which was done without drying as described below).

8.2.3 Mechanical testing

Tensile testing was carried out using a 1ST Benchtop Tester (Tinius Olsen Ltd, UK) with a 1 kN load cell, using miniature vice grips (HT54, Tinius Olsen Ltd, UK), under a constant elongation rate of 1 mm min^{-1}. Dumbbell samples (5 mm gauge length) were tested in simulated body conditions (immersed in deionised water at 37°C) using a Saline Test Tank with Heater (Tinius Olsen Ltd, UK). To test mechanical properties after 5, 30 or 120 days degradation, tensile specimens were incubated in PBS at 37°C for the desired amount of time, and removed immediately before testing. After loading samples into the grips and immersing them in water, they were left for approximately 10 minutes for the temperature to equilibrate. Strain was measured using a video extensometer and custom-built LabVIEW software, and dry transfer letters (black, approximately 1 mm squares, Chartpak Inc., USA) were used as strain markers. Yield strength (σ_y) was taken as the 0.2% offset yield point, and the elastic modulus (E) was calculated from the linear region of the stress-strain curve before yield.

8.2.4 Characterisation

8.2.4.1 SEM

SEM (Scanning Electron Microscopy) was carried out on the composite samples using an FEI Nova NanoSEM, using an accelerating voltage of 5 kV. Samples were prepared by cryo-fracturing in liquid nitrogen to view the cross-section, and then sputter coating with 10 - 20 nm of Au, using an Emitech K550 sputter coater (20 mA deposition current for 4 minutes, under an argon atmosphere). Degraded samples were dried at room temperature in a vacuum oven until reaching constant mass, before sputter coating.

8.2.4.2 DSC

DSC (Differential scanning calorimetry) was carried out using a DSC Q2000 (TA Instruments, USA), in Al hermetic pans at a heating rate of 20℃ min^{-1}, from -20 to 230℃ under 50 mL min^{-1} N_2 gas flow. A single heating run was used to measure the properties of the composites after processing and degradation. TA Universal Analysis software was used for data analysis, and the glass transition temperature T_g was taken at the inflection point. Degraded samples were dried at room temperature in a vacuum oven until reaching constant mass, before testing.

8.2.4.3 XRD

XRD (X-ray diffraction) was carried out using a Bruker D8 Advance diffractometer with Cu Kα radiation, using a 2θ range of 5-50°, with a 0.05° step size and dwell time of 1.0 s $step^{-1}$. Line profile analysis was used to quantify the amorphous and crystalline content using Match! (Crystal Impact GbR) software, and unknown phases were identified using the Crystallography Open Database [335–340]. Degraded samples were dried at room temperature in a vacuum oven until reaching constant mass, before testing.

8.2.4.4 Drying and ash testing

The weight fraction of different components within the composite was determined before and after degradation by drying and ashing. After short-term degradation studies, the water uptake was measured by drying. Composite samples were removed from the degradation solution and dabbed dry, before being weighed using a Sartorius Ultramicro balance. The total wet mass (as a fraction of initial mass) can then be given by Eq. 8.1:

$$w_{total} = \frac{m_{t_i,wet}}{m_{t_0}} \tag{8.1}$$

where $m_{t_i,wet}$ is the wet mass of the composite (after i days degradation) and m_{t_0} is the initial composite mass. Samples were then dried at room temperature in a vacuum oven until reaching constant mass, when they were weighed again. The water uptake could then be calculated according to Eq. 8.2:

$$w_{water} = \frac{m_{t_i,wet} - m_{t_i,dry}}{m_{t_0}} \tag{8.2}$$

where $m_{t_i,dry}$ is the mass after vacuum drying. After drying the fraction of glass particles remaining in polymer composites was determined by ashing. A known mass of composite was fixed onto a borosilicate glass cover slip using DCM, and weighed, before heating in a ventilated furnace at 300℃ h^{-1} to 650℃. The temperature was held at 650℃ for 1 h to ensure complete burn off of the polymer. After cooling to room temperature overnight the glass cover slip and remaining ash were weighed to determine the mass loss. These temperatures were chosen based on previous TGA data on polymers (Fig. 3.2, on page 67), as well as knowledge of the softening point of the glass slip (>800℃). The ashing temperature must be sufficient for complete polymer burn off, but not allow significant viscous flow of the glass slip. Using this method, the glass weight fraction (w_{pg}) can be calculated according to Eq. 8.3:

$$w_{pg} = \frac{m_{sample+slip,f} - m_{slip}}{m_{t_0}} \tag{8.3}$$

where $m_{sample+slip,f}$ is the mass of the glass cover slip and residual ash after burn off, and m_{slip} is the mass of the glass cover slip which is assumed to stay constant. If the mass loss during ashing is assumed to be solely composed of burnt-off polymer, polymer weight fraction in the composite can also be calculated, according to Eq. 8.4:

$$w_{poly} = \frac{m_{t_i,dry} - (m_{sample+slip,f} - m_{slip})}{m_{t_0}} \tag{8.4}$$

8.3 Results

8.3.1 Long-term degradation behaviour

Results from long-term degradation tests of the range of samples given in Table 7.1 are shown in Figs. 8.1 and 8.2. Measurements of solution pH during degradation showed no change for PLA over this time period, which was as expected due to the slow degradation of this polymer. The degradation behaviour of PLA-CL was consistent with results on this same composition (90PLLA:10PLCL(70:30)-PEG) from Chapter 4 (Fig. 4.1, on page 84), showing no change and then reduction to pH 6 after about 300 days. Significant differences were seen for the glass-containing composites, with those with 30wt.% glass demonstrating a fast pH reduction to around pH 6 before plateauing, as a result of glass dissolution.

The plateau pH was dependent on the phosphate glass composition, with the higher P_2O_5 glass resulting in a lower pH, consistent with results from Chapter 6. Composites with lower glass content of 15wt.% showed a slightly delayed response, before also displaying pH reduction as a result of glass dissolution, and again the higher P_2O_5 glass resulted in a lower pH. Although the addition of PLCL-PEG had a major effect on the degradation of the unfilled matrix, the same cannot be said of the composite materials. For most of the degradation experiment no differences were observed based on the matrix composition, however after around 200 days composites with low glass content (15wt.%) and a matrix that contains PLCL-PEG did appear to show additional pH reduction compared with the equivalent composite without PLCL-PEG, however this difference was relatively small.

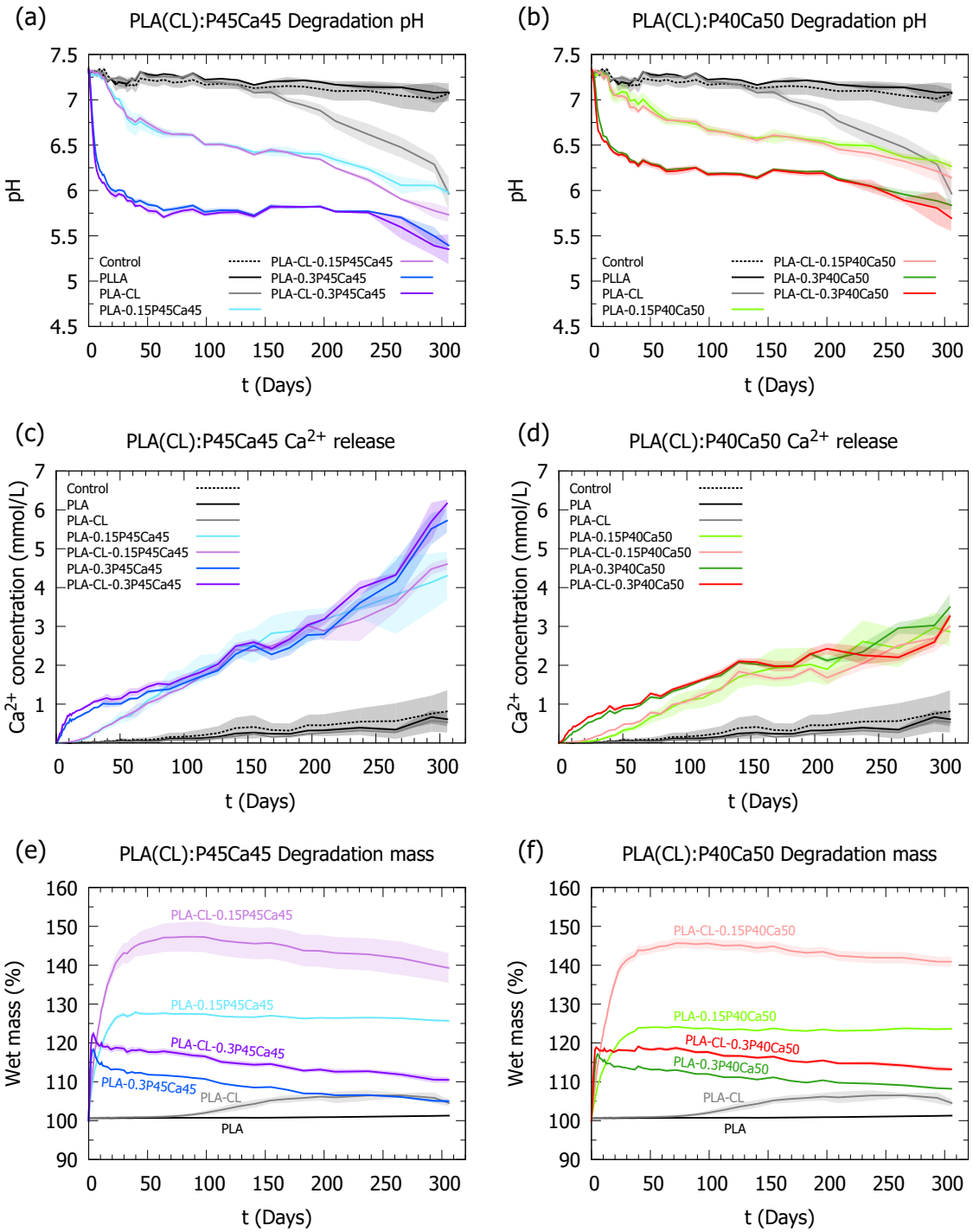

Fig. 8.1: Degradation behaviour of composite samples in PBS at 37°C, with sample codes from Table 7.1. Graphs show solution pH for composites with P45Ca45 glass (a) and P40Ca50 glass (b), solution Ca^{2+} concentration for composites with P45Ca45 glass (c) and P40Ca50 glass (d), and wet mass (% of original mass) for composites with P45Ca45 glass (e) and P40Ca50 glass (f). Shaded regions denote standard deviation, n = 3.

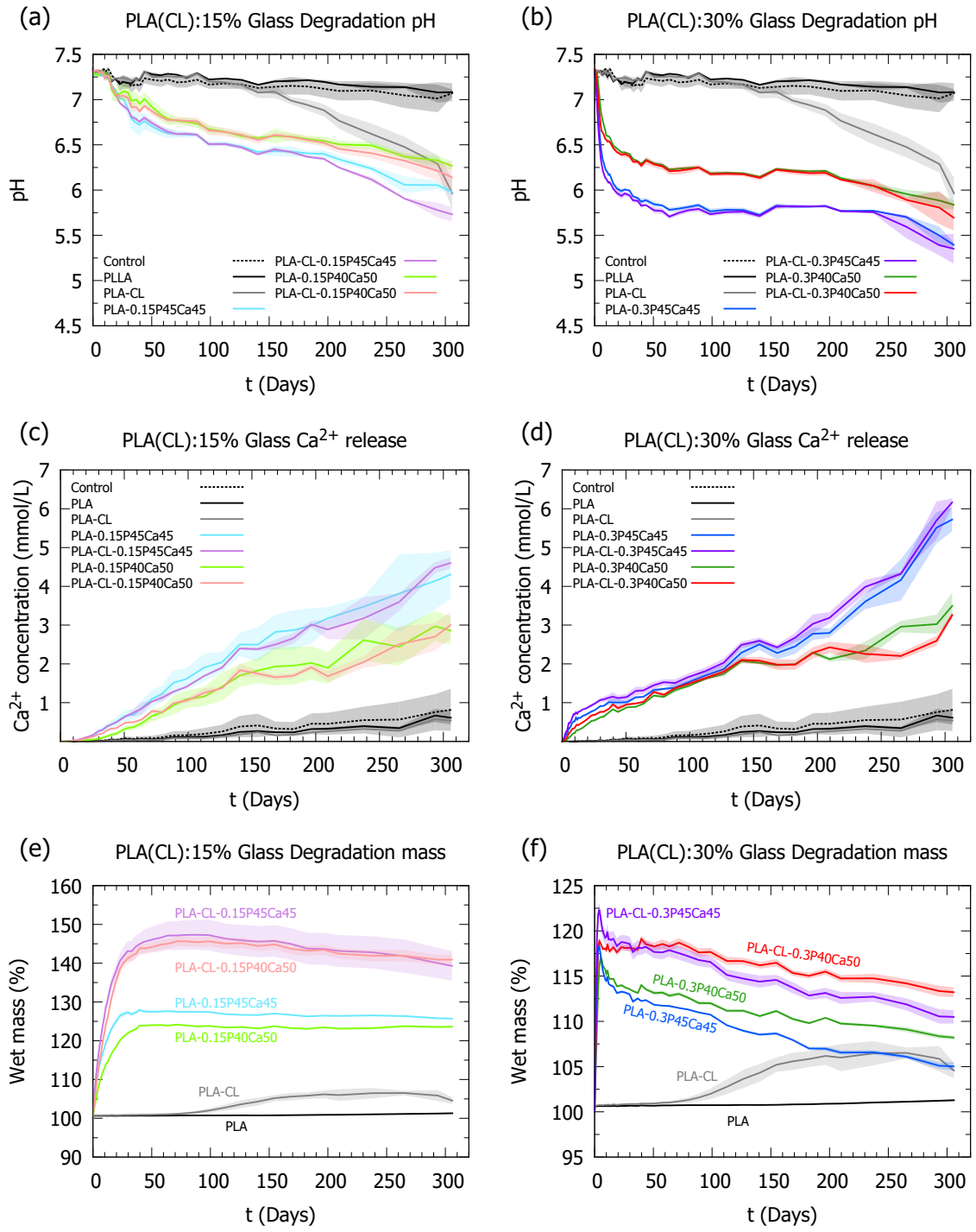

Fig. 8.2: Degradation behaviour of composite samples in PBS at 37°C, with sample codes from Table 7.1. This is the same data as Fig. 8.1, grouped instead by glass filler content. Graphs show solution pH for composites with 15wt.% glass (a) and 30wt.% glass (b), solution Ca^{2+} concentration for composites with 15wt.% glass (c) and 30wt.% glass (d), and wet mass (% of original mass) for composites with 15wt.% glass (e) and 30wt.% glass (f). Shaded regions denote standard deviation, n = 3.

Measurements of Ca^{2+} release from the composites also revealed interesting similarities and differences between composite samples. A slow but consistent increase in measured Ca^{2+} content was observed for the PLA and PLA-CL samples, despite the fact that these unfilled polymer matrices did not contain any glass. This can be attributed to contamination of the solution with residual ions from the electrodes used for pH and Ca^{2+} ion measurement. In spite of thorough washing between samples, some transfer and contamination was unavoidable, and resulted in a Ca^{2+} concentration increase for the polymer only samples. This is corroborated by a similar increase observed for the control solution (PBS alone). Similar to the solution pH, the Ca^{2+} concentration showed significant dependence on the composite composition. As seen in Chapter 6 for the dissolution of the glasses alone, composites containing glasses with higher P_2O_5 content displayed higher Ca^{2+} release despite their lower CaO content, due to their faster dissolution. Composites with higher glass content also displayed higher Ca^{2+} release initially, however over time this difference disappeared, suggesting that some equilibrium was reached between the dissolving glass and the solution. Few differences were observed between composites with the PLA and PLA-CL matrices.

By contrast, the matrix composition played a large role in the mass gain seen for all the composites, which can be attributed to water absorption. The pure polymers displayed low water absorption of around 1% initially, with the PLA-CL sample later showing an increase of about 6%, due to the increased water absorption that precedes bulk degradation (as observed in Fig. 4.4 on page 86). Composite samples demonstrated significantly higher wet mass during degradation, and the presence of PLCL-PEG in the matrix dramatically increased this in all cases. The most significant factor determining the wet mass increase however, appeared to be the glass content. Composites with 30wt.% glass displayed a fast initial mass increase, followed by a peak and slow decrease, which can be attributed to fast water absorption and subsequent glass dissolution. Composites with 15wt.% glass demonstrated similar behaviour, however the initial absorption was slower but reached a higher mass. The initial absorption

stage did not appear to be heavily influenced by the glass composition, however in the later mass loss stage composites containing the faster dissolving P45Ca45 glass (see Chapter 6) lost mass more quickly.

8.3.2 Structure changes during degradation

8.3.2.1 Composite components

Changes in the relative proportion of different composite components during degradation were assessed by weighing after degradation, drying, and ashing at different timepoints, and results are shown in Figs. 8.3 and 8.4. The total wet mass appeared consistent with results from similar measurements during long-term degradation experiments, but it is difficult to interpret these results due to the overlap of multiple different effects. The drying and ashing procedures allowed these effects to be separated into changes in water, glass, and polymer mass.

The water content within the composites (w_{water}) demonstrated a gradual increase as a result of water absorption, slowing over time. Composites with a higher glass content experienced faster water absorption initially (up to 5 days), which can be attributed to the increased glass/polymer interfacial area providing additional area for wicking [230, 242]. Later on (after 30 days or more) composites with lower glass content were seen to exceed the water absorption of their higher glass content counterparts, due in part to the greater proportion of the polymer component, suggesting that although the interface promotes water absorption, the water is stored within the polymer. Other factors that led to increased water absorption were greater hydrophilicity of the components; composites containing a PLA-CL matrix or P45Ca45 glass consistently showed increased water absorption compared with equivalent composites containing a PLA matrix or P40Ca50 glass.

Changes in the glass mass were also observed, as the composites absorbed water leading to dissolution of the glass. As expected, the faster dissolving P45Ca45 glass (see Chapter 6) showed faster mass loss, while the polymer matrix composition (PLA or PLA-CL) did not appear to have an impact on glass dissolution. The amount of glass present altered the glass dissolution behaviour, where a delayed start to glass mass loss was observed for composites with lower glass content (minimal mass loss after 5 days), compared with the composites with higher glass content. The slower initial water absorption of the 15wt.% glass composites is one explanation for this, restricting the water available for dissolution of glass.

During the timescale of these tests (up to 120 days) no change in the polymer mass for PLA samples was observed, while PLA-CL samples displayed a small mass loss, as expected from previous results (Chapter 4) for these slowly degrading polymers. Within the initial 5 days, these results showed an increase in the polymer mass for all composite compositions, however this is likely to be an artefact of the drying and ashing technique. Vacuum drying at room temperature was necessary to remove water without further alteration to the composite, however this is unlikely to have completely removed all absorbed water. Upon ashing, this retained water was removed, along with the polymer, resulting in an erroneously high measurement of polymer mass.

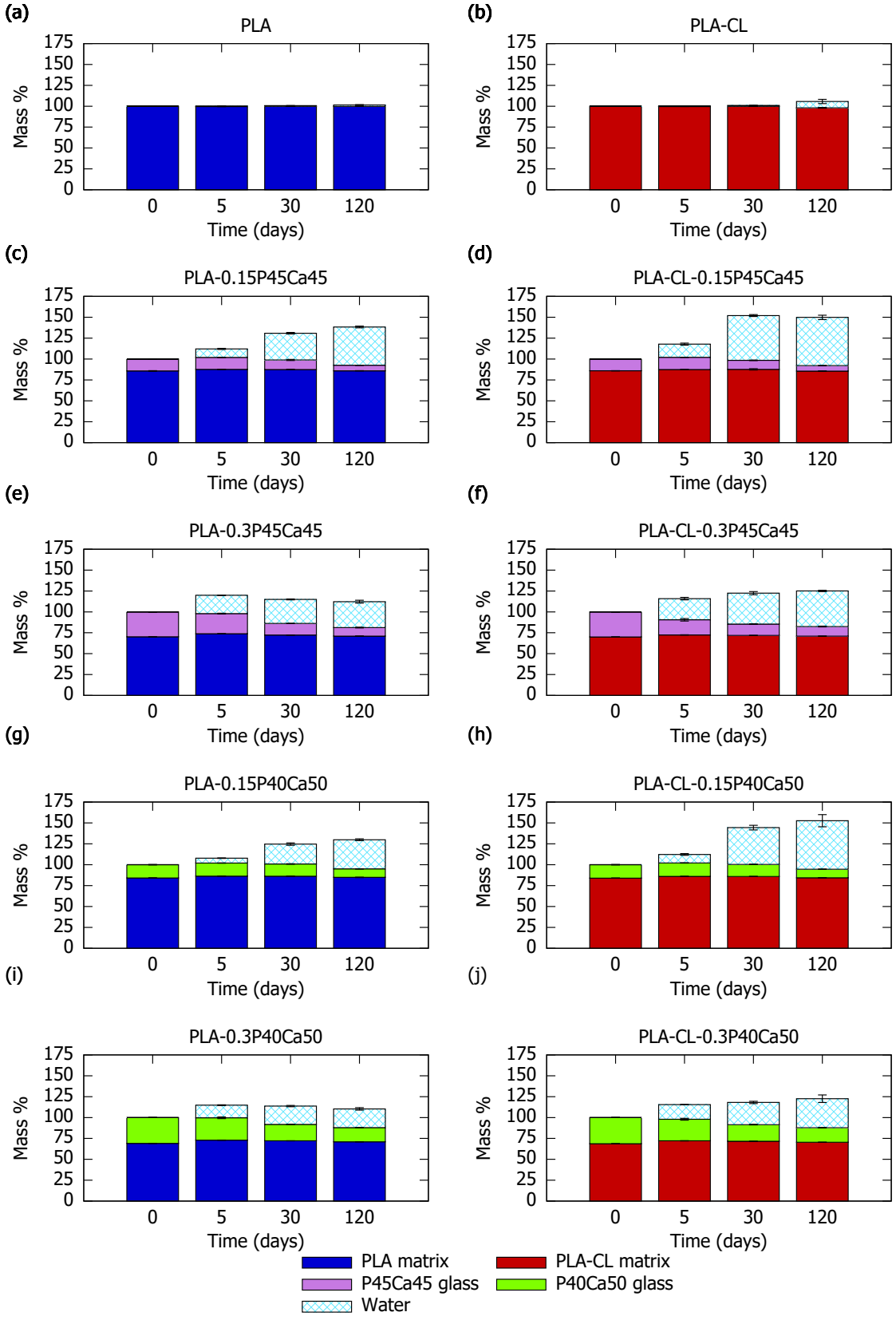

Fig. 8.3: Results of drying and ashing tests, showing how the mass of different components within a composite material changes during degradation. Shown are the water mass, glass mass, and polymer mass, according to Eqs. 8.1 - 8.4.

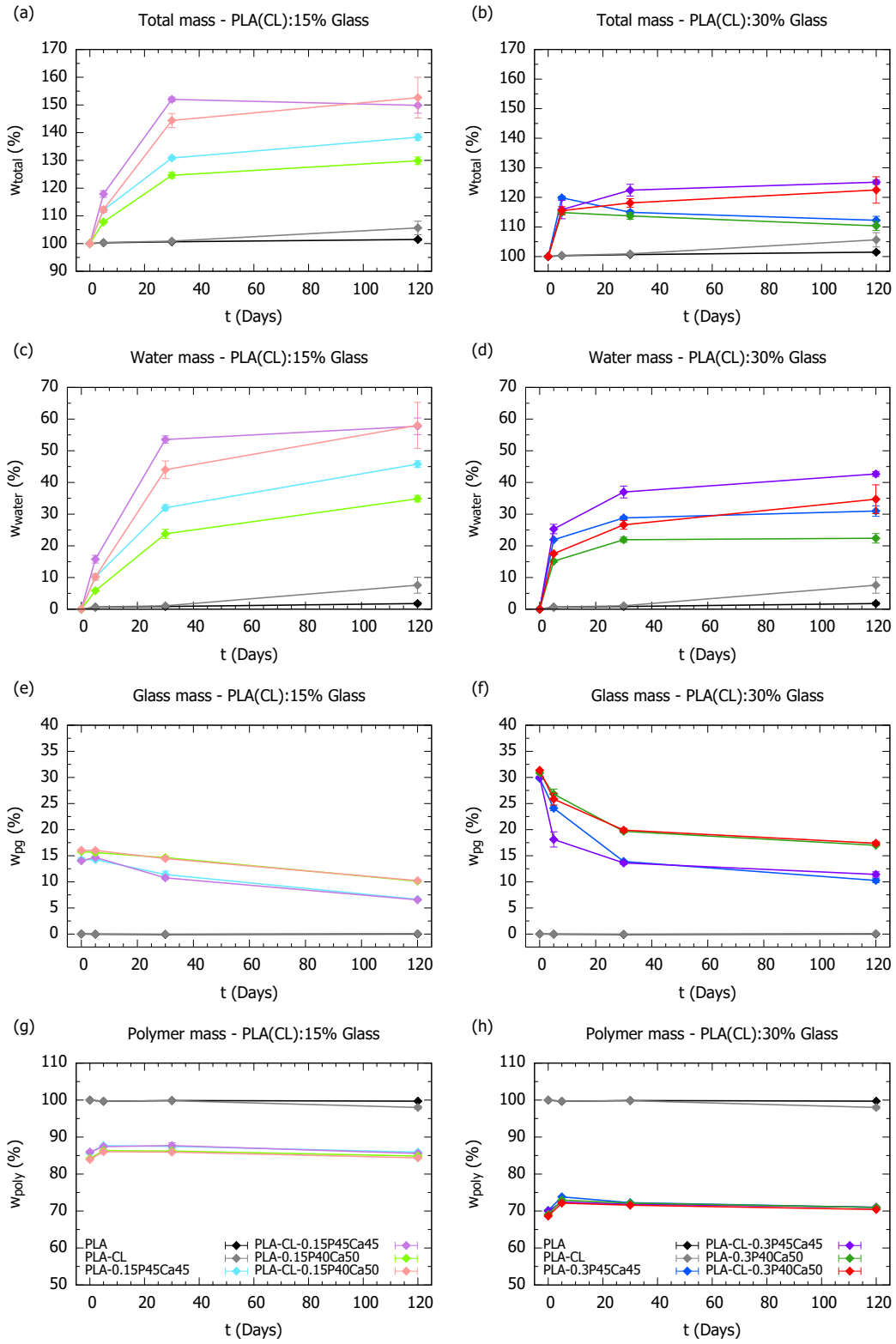

Fig. 8.4: Results of drying and ashing tests, showing how the mass of different composite components changes during degradation. Samples are grouped by composites with 15wt.% glass (a, c, e, g) and 30wt.% (b, d, f, h), showing the total mass (a, b), water mass (c, d), glass mass (e, f) and polymer mass (g, h), according to Eqs. 8.1 - 8.4. These graphs show the same data as Fig. 8.3, replotted to reveal differences between different compositions.

8.3.2.2 Polymer structure

Significant changes were seen in the structure of the polymer within the composite as a result of degradation. Crystallisation of the polymer matrix was observed, as shown in Fig. 8.5. Crystallisation was seen for both the PLA and PLA-CL polymer samples, with significantly more crystallisation occurring in the PLA-CL sample due to the faster degradation of the PLCL-PEG copolymer and greater mobility of the resulting short chain polymers (as discussed in Chapter 4). The addition of phosphate glass to the composite was seen to result in suppression of crystal formation within the polymer matrix, preventing any polymer crystallisation in composites based on a PLA matrix, and limiting it to <20% in composites based on a PLA-CL matrix. The observed XRD peaks for the polymer crystallites (example in Fig. 8.6) were consistent with the the α form of the PLLA unit cell [140, 288].

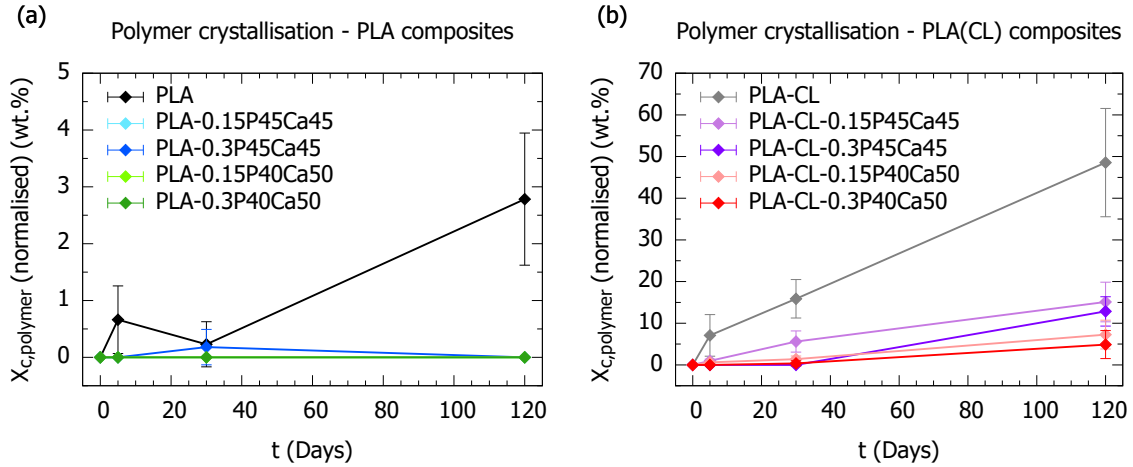

Fig. 8.5: XRD polymer crystallinity (normalised to nominal polymer content) of initially amorphous polymer-glass composites after 0, 5, 30, and 120 days degradation in PBS at 37°C. Shown are composites with a PLLA matrix (a) and 90PLLA:10PLCL(70:30)-PEG matrix (b), error bars denote standard deviation for n = 3 samples. Note the different y-axis scale for (a) and (b).

The thermal properties measured by DSC can also reveal information about the polymer structure. For composites with both PLA and PLA-CL matrices, the T_g increased significantly during degradation, with most of this increase occurring within the first 5 days (Fig. 8.7). The addition of phosphate glass did not have a significant

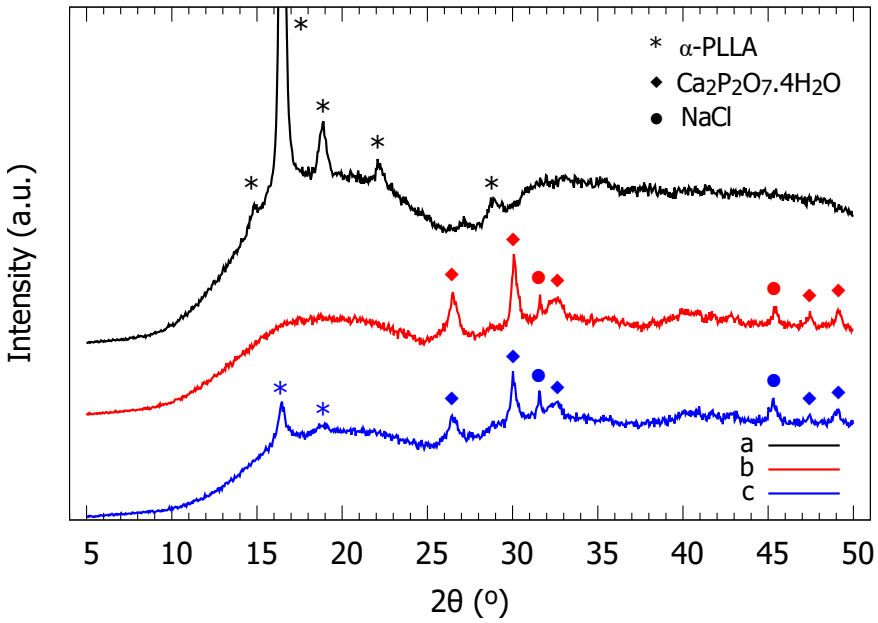

Fig. 8.6: Example X-ray diffraction patterns demonstrating polymer crystallisation (a), inorganic crystallisation (b), and a mixture of polymer and inorganic crystallisation (c). Samples shown are PLA-CL (a), PLA-0.15P40Ca50 (b), and PLA-CL-0.15P40Ca50, all after 120 days degradation in PBS at 37°C.

effect on the T_g of PLA matrices, while for PLA-CL matrices increased glass addition resulted in a lower T_g (but still higher than the T_g before degradation). Enthalpy relaxation of the amorphous polymer was also seen to occur during degradation, with the change in the enthalpy relaxation peak from the initial state ($\Delta H_{R,t} - \Delta H_{R,t_0}$) shown in Fig. 8.8. An initial increase in the enthalpy relaxation measured during degradation was observed for all compositions, as a result of increased mobility at the degradation temperature (37°C) allowing structural relaxation and densification. This was greater for the pure PLA than the PLA-CL blend due to unfavourable interactions between dissimilar polymers as discussed in detail in Chapter 4. The addition of glass reduced the amount of enthalpy relaxation that occurred, while composites with the PLA-CL matrix experienced a reduction in enthalpy relaxation after a peak after 5 days, with this reduction greater for composites than the unfilled matrix.

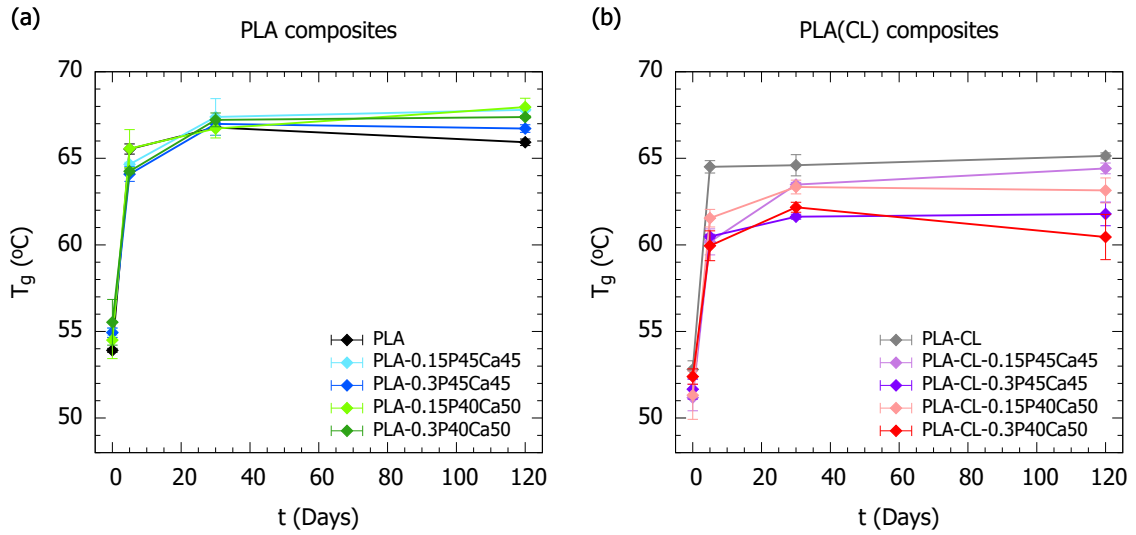

Fig. 8.7: Glass transition temperature T_g measured by DSC for dry composites after 0, 5, 30, and 120 days degradation in PBS at 37°C. Shown are composites with a PLLA matrix (a) and 90PLLA:10PLCL(70:30)-PEG matrix (b), error bars denote standard deviation for n = 3 samples.

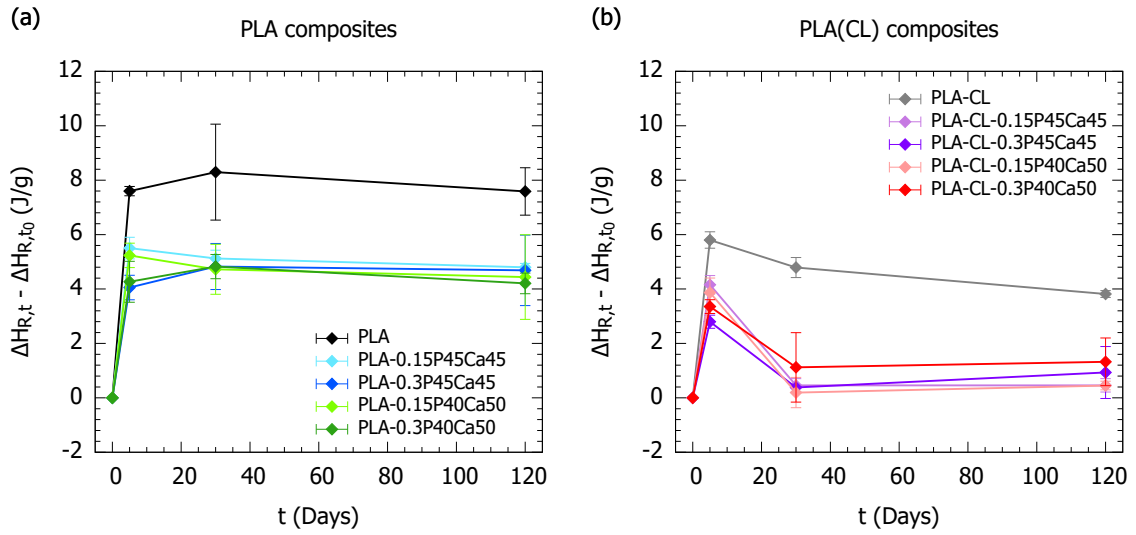

Fig. 8.8: Change in the enthalpy relaxation peak ΔH_R for dry composites measured by DSC between the initial value, and after 5, 30, and 120 days degradation in PBS at 37°C. Shown are composites with a PLLA matrix (a) and 90PLLA:10PLCL(70:30)-PEG matrix (b), error bars denote standard deviation for n = 3 samples.

8.3.2.3 Composite structure

XRD of degraded composite samples also revealed that formation of inorganic crystallites had occurred, as shown in Fig. 8.6. These are the result of glass dissolution via the mechanisms discussed in Chapter 6, namely formation of a conversion layer, and dissolution (or deposition) of conversion layer species, leading to formation of NaCl and $Ca_2P_2O_7.4H_2O$ crystallites. This crystallisation was observed for all the composite samples, reaching a maximum of 3 - 18% after 120 days degradation as shown in Fig. 8.9.

SEM images of the composite samples at various stages of degradation are shown in Figs. 8.10 and 8.11. Minor morphological changes were observed for the polymer only samples PLA and PLA-CL, with an increase in small voids observed. With the addition of phosphate glass, this increase in void volume over time increased significantly. The increased void volume was also noticeably higher for the composites with 15wt.% glass compared with composites with 30wt.% glass. No significant differences between composites with PLA and PLA-CL matrices could be detected by SEM. Care must be taken in interpreting such images however, because of the potential effect of dehydration before imaging on the microstructure. The results of inorganic crystallisation could also be observed with SEM. Glass particles within the composite that were originally smooth, after degradation showed a roughened surface with crystallite nodules, demonstrating crystal growth or deposition.

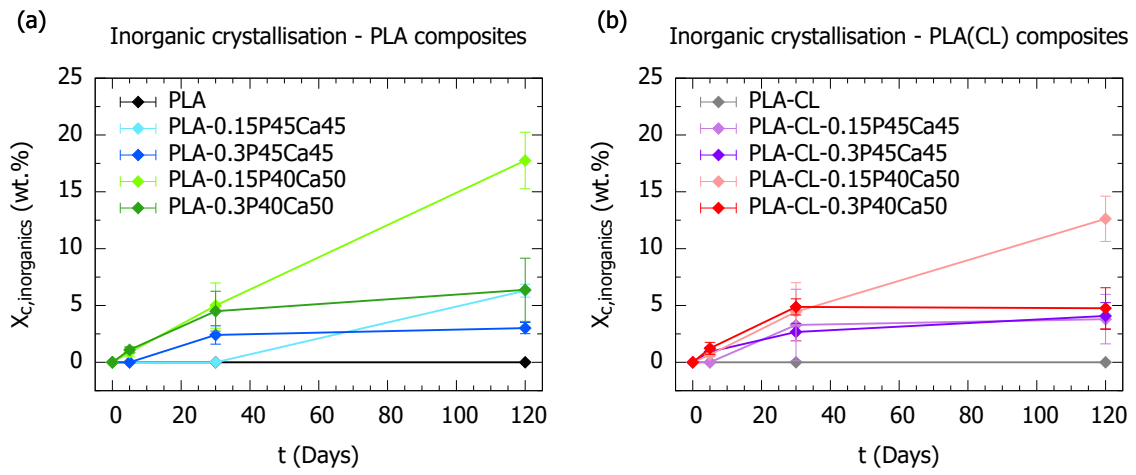

Fig. 8.9: XRD crystallinity (inorganic components only) of initially amorphous polymer-glass composites after 0, 5, 30, and 120 days degradation in PBS at 37°C. Shown are composites with a PLLA matrix (a) and 90PLLA:10PLCL(70:30)-PEG matrix (b), error bars denote standard deviation for n = 3 samples.

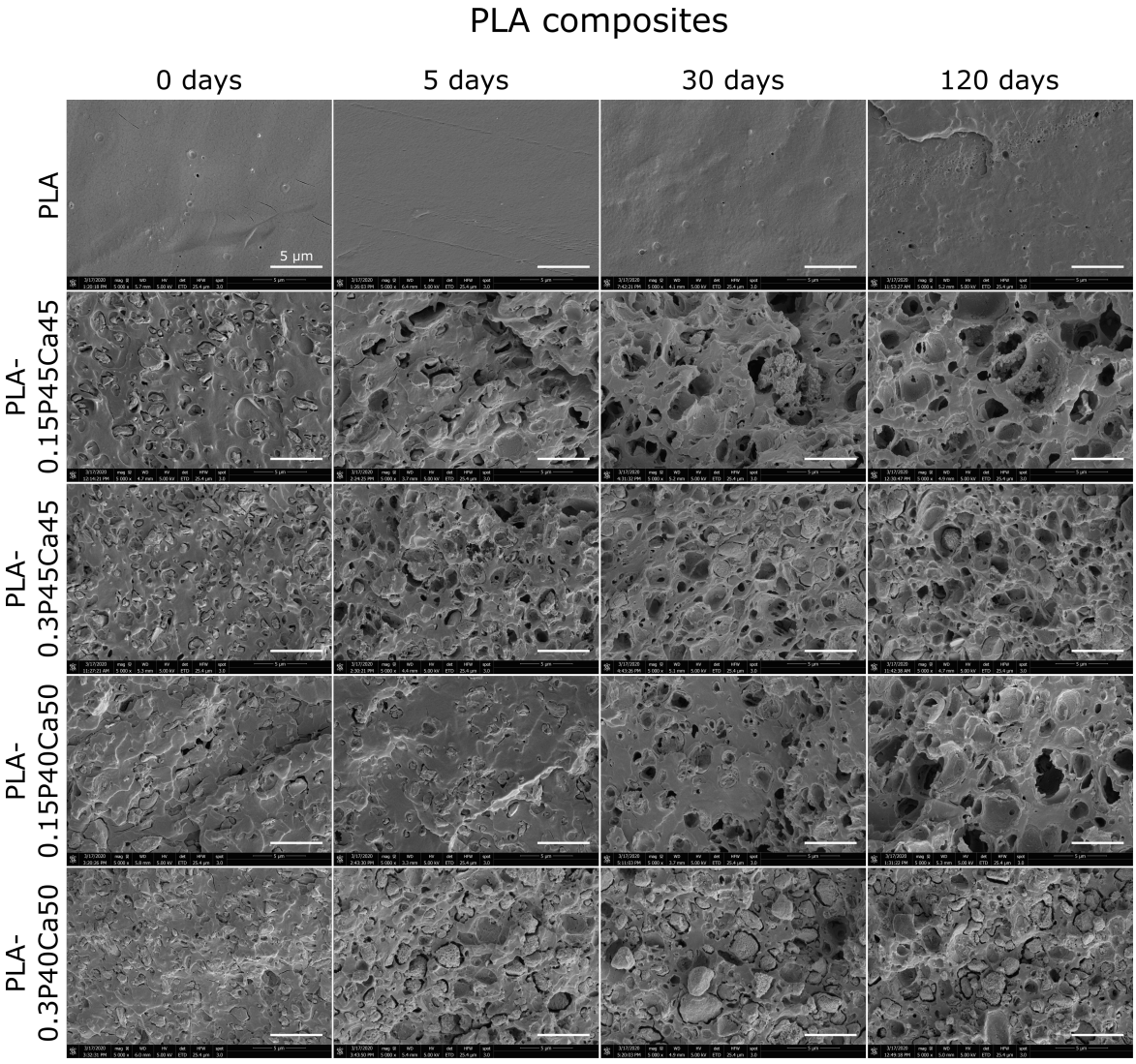

Fig. 8.10: SEM images showing changes in the composite microstructure during degradation in PBS at 37°C for 0, 5, 30, and 120 days, for composites based on a PLLA matrix. Scale bar shown is 5 µm.

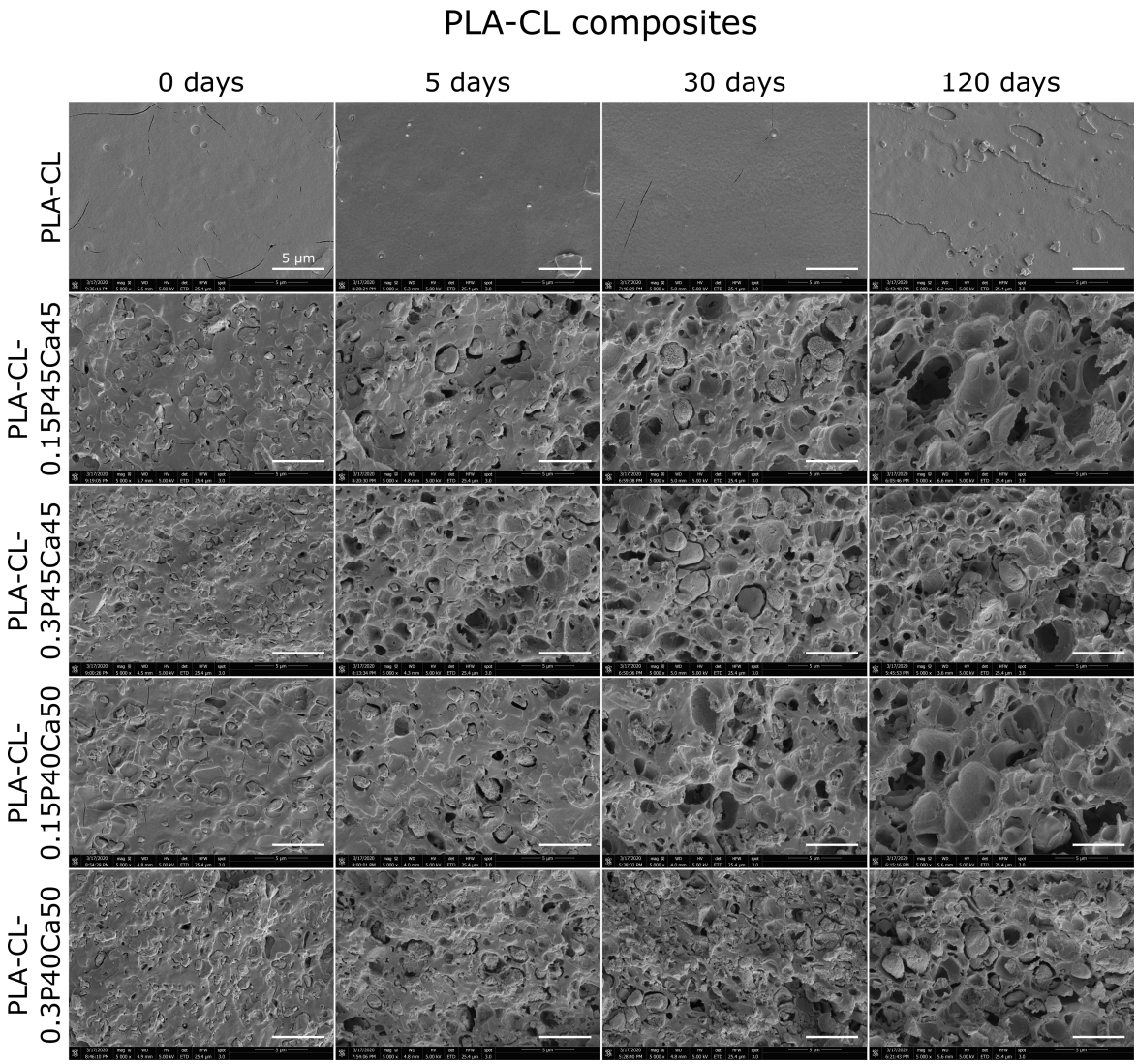

Fig. 8.11: SEM images showing changes in the composite microstructure during degradation in PBS at 37℃ for 0, 5, 30, and 120 days, for composites based on a 90PLLA:10PLCL(70:30)-PEG matrix. Scale bar shown is 5 µm.

8.3.3 Evolution of mechanical properties

The mechanical properties of the composite samples evolved significantly over time during degradation, as shown in Fig. 8.12. The effects of composition (in terms of matrix polymer composition and glass content and composition) on the initial mechanical properties under these testing conditions (immersed in 37℃ water) have already been discussed in Chapter 7 so will not be repeated here. As degradation progresses, both unfilled polymer samples (PLA and PLA-CL) were seen to undergo an increase in elastic modulus until 30 days, followed by a gradual decrease. Composites with glass added showed the opposite effect, with the modulus decreasing significantly within the first 5 days. This decrease was greater for composites with a higher 30wt.% glass content, which had a higher elastic modulus initially, but fell to lower than the 15wt.% glass composites after this decrease. A similar set of trends was observed for the yield strength, with an initial increase followed by reduction for unfilled polymers. Composites with 15wt.% glass showed a more gradual loss of strength, while those with higher glass content again suffered a larger strength decrease.

Large changes in the elongation at break (ϵ_B) were also observed during degradation. Unfilled polymers experienced a large reduction in ductility within the first 5 days of degradation, with this reduction more severe for the pure PLA polymer. Composites with 15wt.% glass showed negligible changes within the first 5 days, however experienced a gradual loss of ductility for longer degradation times, but remained more ductile than the unfilled polymers. Composites with 30wt.% glass, which initially showed lower and more variable ductility than the 15wt.% glass composites, generally maintained or increased their ductility over the first 5 days, before also showing a gradual loss of ductility for longer degradation times.

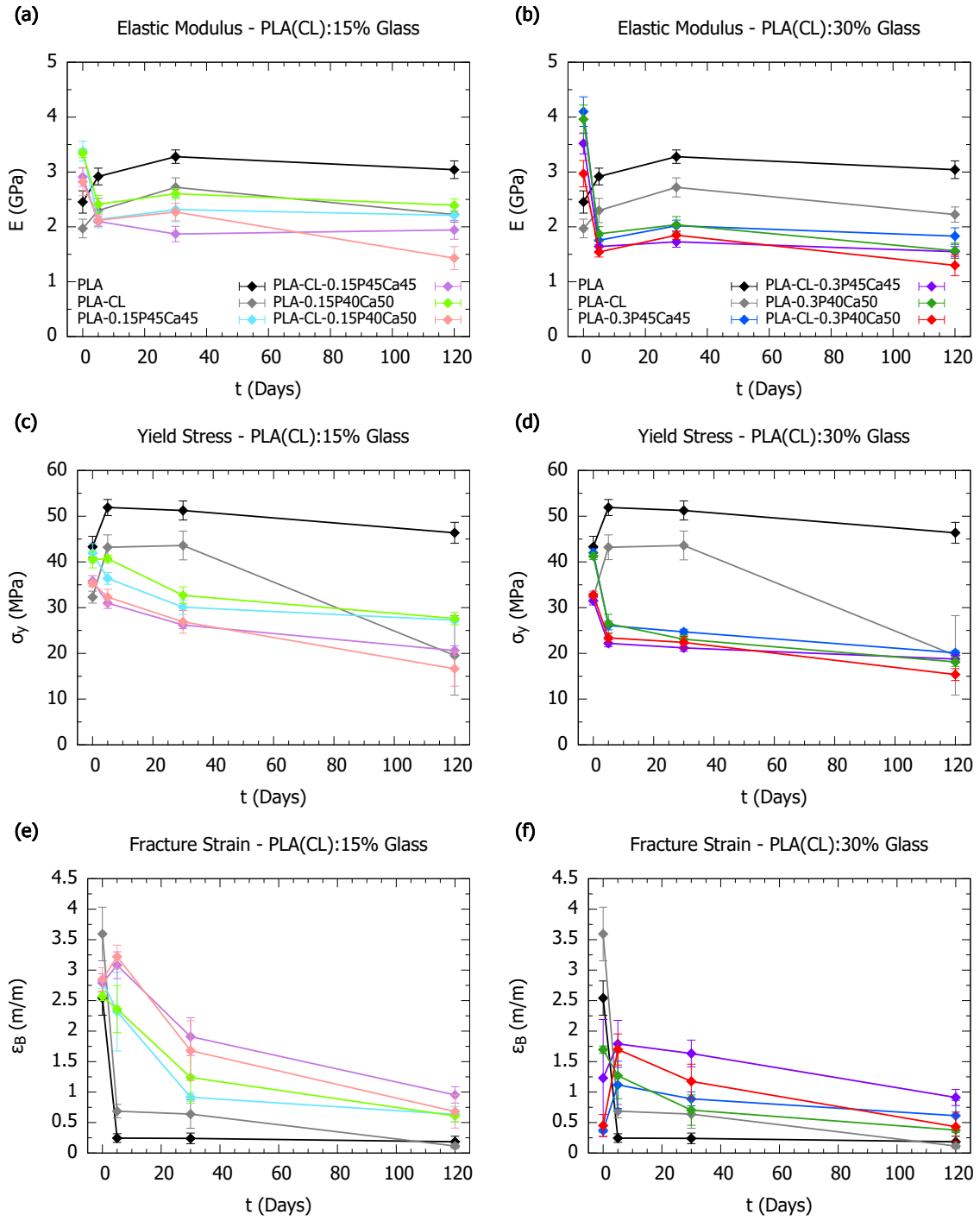

Fig. 8.12: Mechanical properties as measured by tensile testing for polymer-glass composites in 37°C water, measured after 0, 5, 30, and 120 days degradation in PBS at 37°C. Graphs show elastic modulus E for composites with 15wt.% glass (a) and 30wt.% glass (b), yield stress σ_y for composites with 15wt.% glass (c) and 30wt.% glass (d), and fracture strain ϵ_B for composites with 15wt.% glass (e) and 30wt.% glass (f).

8.4 Discussion

8.4.1 Degradation behaviour

By assessing the degradation behaviour of a range of composite materials (listed in Table 7.1 on page 163), the effects of different components can be understood. The degradation lifetime can be broadly broken down into two regimes, firstly an initial stage where water absorption is dominant and wet mass increases to a maximum, before the second regime begins, which is dominated by glass dissolution and results in slow mass loss. For composites with 30 wt.% glass this transition occurs at about 5 days, while for composites with 15 wt.% glass this takes up to about 90 days.

During the first stage the wet mass increases significantly by water absorption. The glass composition affects the water absorption, with composites containing the more hydrophilic P45Ca45 glass [164] absorbing more water. The polymer matrix plays an even larger role here, with composites where the matrix contains 10 wt.% of the more hydrophilic PLCL-PEG [101] showing significantly higher water absorption. It is clear that in the water absorption stage, the hydrophilicity of both components plays a role in the amount of water absorbed. All the composite samples show much higher mass increases than the polymers, suggesting that water absorption mainly occurs due to, and along, the interface between the two components [230, 234]. Composites containing more glass will have a greater interfacial area, explaining the faster water absorption experienced by 30 wt.% glass composites during the initial stage. During this initial stage the Ca^{2+} release and pH change appear to be mainly influenced by the glass dissolution - in spite of the large difference in water absorption caused by addition of PLCL-PEG to the polymer matrix, this only has a small effect on the solution pH and Ca^{2+} concentration. These changes in ionic concentration in the solution can be attributed to the dissolution of the glass component, with composites containing a greater amount of glass causing greater changes in solution concentrations. The effect of glass composition is in accordance with results seen in Chapter 6 - the slower dissolution of the higher Ca glass P40Ca50 results in a smaller pH reduction and lower Ca^{2+} release.

Different behaviour is seen in the second regime where the sample mass change is dominated by glass dissolution. Composites containing 15 wt.% glass show only slight reduction in mass from their peak after about 300 days degradation, so it is difficult to comment on trends here. Composites with 30 wt.% glass on the other hand, are clearly losing mass after peaking at around 5 days, which can be mainly attributed to glass dissolution - significant polymer mass loss would not be expected within this timeframe as indicated by the lack of mass loss for PLA and PLA-CL samples, as well as drying and ashing tests. During this regime the glass composition is the dominant factor, with composites containing the faster dissolving P45Ca45 glass losing mass significantly faster than those containing P40Ca50 glass. The addition of PLCL-PEG to the polymer matrix does not appear to have a significant effect on the mass loss behaviour in this second regime, as the mass loss is mainly glass dissolution and the pH reduction caused by glass dissolution has not triggered significant polymer degradation. Within the timescale of the long term degradation experiment, reduction in wet mass by polymer degradation of PLA-CL is only just observable after 300 days. As a result it is difficult to determine whether PLCL-PEG-related mass loss in the composites is counteracted by glass addition, or whether it is not yet observable.

Although differences in solution ionic concentration (pH and Ca^{2+}) are observed depending on PLCL-PEG content in the matrix in the first regime, once glass dissolution becomes dominant these ionic concentrations begin to converge. Again this indicates that glass dissolution is the dominant factor here. Furthermore, the solution Ca^{2+} concentration appears to be converging for all different composite compositions (irrespective of glass composition, matrix composition, or glass filler content), suggesting that some equilibrium is being approached between the glass dissolving in the composite, and the solution concentration. This is not a situation that would occur in clinical use of these materials, and represents a limitation of the static degradation test used here.

The time taken for transition between these two regimes is clearly different between composites containing 15 and 30 wt.% glass. The higher glass content results in faster water absorption due to the greater interfacial area, hastening the onset of glass dissolution. The larger amount of glass present also means that once glass dissolution begins, it will have a larger impact and quickly become dominant over other factors.

Although increased solution acidity is known to accelerate the rate of PLLA hydrolysis, the modification of solution pH by glass dissolution does not appear to have significantly accelerated the rate of degradation of the polymer component. This suggests that the size of the pH change here, which is relatively small when compared with the work of Tsuji and Ikarashi [133] (who observed acceleration of hydrolysis when reducing pH from 7.4 to 0.2), was insufficient to trigger catalysis of PLLA hydrolysis.

8.4.2 Structure evolution

Multiple structural changes occur within the polymer-glass composites during degradation, and these are summarised in Fig. 8.13. Enthalpy relaxation was observed to occur early on during degradation as a result of increased mobility at the degradation temperature (37°C) allowing structural relaxation and densification [51]. This in turn leads to increased intermolecular interactions and increased T_g. As discussed in Chapter 4 and elsewhere [273], the addition of PLCL-PEG to PLLA polymer reduces this tendency for enthalpic relaxation due to unfavourable interactions between dissimilar polymer chains. The addition of phosphate glass particles also reduces the enthalpic relaxation, due to reduced mobility of the amorphous polymer in the immediate vicinity of a filler particle [354, 355]. For longer degradation times, crystallisation of polymer chains becomes more significant. This is more pronounced for composites where the matrix contains PLCL-PEG, due to the chain cleavage resulting from the hydrolysis reaction. This provides additional mobility for the polymer to rearrange into a crystalline structure [139]. The addition of phosphate glass particles also reduces the polymer crystallisation,

by reducing the mobility of the polymer chains in the vicinity of the filler particles, in a similar fashion to how enthalpic relaxation is affected.

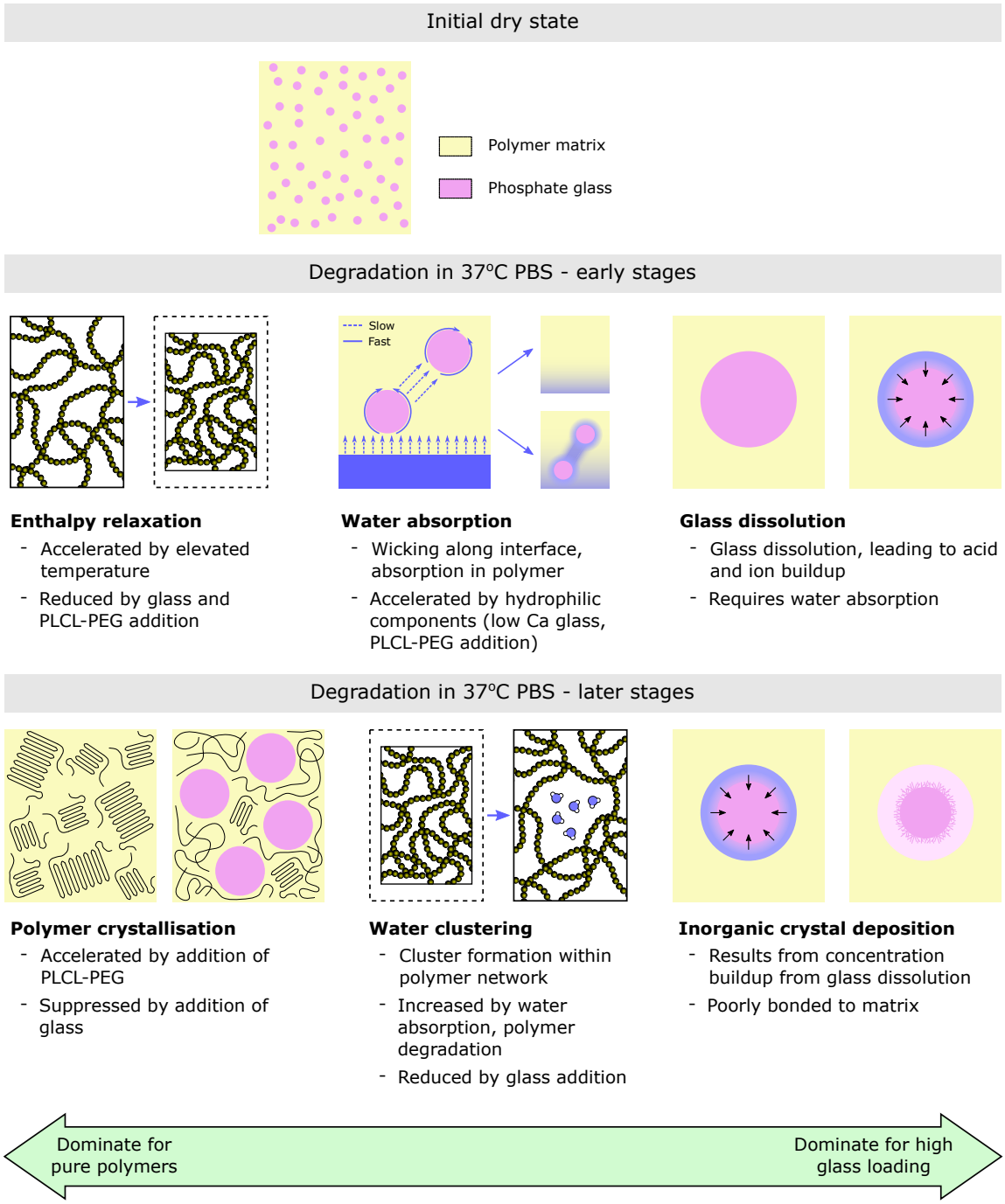

Fig. 8.13: Summary of the mechanisms of structural changes that occur in polymer-glass composites during degradation over different timescales.

Water absorption is a key phenomenon determining the structure and properties of these polymer-glass composites during degradation. According to purely Fickian diffusion behaviour, the presence of particulate filler would be expected to reduce the rate and level of water absorption by diffusion, due to immobilisation of diffusing molecules on or near the particle surface [356]. However this is not always observed in practice, and anomalous absorption is often seen as a result of factors such as defects such as voids or micro-cracks introduced by the composite, or interactions between the particles and penetrant (i.e. water) [356]. In this case the increased absorption rate for particulate-filled composites can be attributed to surface interactions of water with the phosphate glass particles. As hydrophilic materials [164] the phosphate glass will be easily wetted by absorbed water and contribute to accelerating water transport into the composite by wicking. Absorption in this manner thus increased for higher glass content, as well as for more hydrophilic components (polymer matrix that includes PLCL-PEG, and lower Ca content in the glass).

At later stages of degradation, water absorption was observed to lead to void formation, which was greater for 15wt.% glass composites than for composites with 30wt.% glass. These can be explained as the result of water clustering and subsequent formation of voids. Due to the reduced mobility of polymer chains within a composite with greater filler content, the equilibrium void content reduces as more glass is added [356], explaining the lower water content seen for 30wt.% glass composites when compared with 15wt.% glass composites. However, due to the faster absorption observed for composites, they are able to reach a higher water content than the unfilled polymers within the timeframe of this experiment.

Dissolution of glass particles is another key structural change, which dominates for composites with high glass loading. Glass dissolution requires supply of water to the glass particle, and is therefore dependent on water absorption. The reduced interfacial area of 15wt.% glass composites compared with 30wt.% glass composites reduces their

initial water absorption rate, explaining the initial delay in glass mass loss seen for 15wt.% glass composites. Mass transport of dissolution products out of the composite will be limited, leading to buildup of ions in the region around the dissolving glass. Although this would be expected to lead to significant acidification, above the level seen in the bulk solution, this was apparently still insufficient to significantly affect polymer hydrolysis. This buildup of concentration does seem to impact the glass dissolution behaviour, allowing stabilisation of the conversion layer and triggering the transition from diffusion limited to surface reaction limited glass dissolution. The formation and deposition of conversion layer species (here NaCl and $Ca_2P_2O_7.4H_2O$) was observed in XRD and SEM results, and is responsible for the reduction in glass dissolution rate observed in mass loss measurements.

8.4.3 Effects on mechanical properties

The evolution of the mechanical properties of the unfilled polymers can be understood in terms of the changes to the polymer structure. Enthalpy relaxation and crystallisation are the dominant effects, and both act to increase the elastic modulus and yield strength, at the expense of ductility [51]. The later reduction in the elastic modulus and yield strength of PLA-CL (and to a lesser extent PLA) after 120 days can be attributed to greater water absorption, and for PLA-CL, hydrolytic degradation as well.

The changes in the mechanical properties of the composites will be a combination of multiple different effects involving the polymer matrix, glass particles, and water absorption. The decrease in elastic modulus and yield strength for all composites is interesting to analyse. The decrease is more severe and faster for composites with 30wt.% glass, and results in inferior mechanical properties compared with composites with 15wt.% glass, despite their superior starting point. This suggests that water absorption is the dominant effect, acting more quickly for composites with higher glass content, and causing a physical separation between the glass and polymer ma-

trix (as observed in SEM images). This results in transfer of stress from the glass filler to the polymer matrix, reducing the elastic modulus and yield strength, and for composites with higher glass content and lower polymer content, this effect is even more pronounced. The reduction seen however, is greater than the reduction that would be expected from simple debonding of the matrix from the filler, and can also be attributed to hydration of the polymer chains by the increased water content of the composites, increasing chain mobility and reducing the elastic modulus and yield strength [50]. The enthalpy relaxation and polymer crystallisation seen for composites would be expected to counteract this somewhat and lead to increases in the elastic modulus and yield strength, however these effects appear to be small relative to the water absorption and hydration effects.

The ductility of the composite materials also gradually decreases as degradation time increases - except for composites with 30wt.% glass in the early stages, where water absorption increases the ductility of those composites that are initially relatively brittle. The gradual loss of ductility is unlikely to be a result of enthalpy relaxation or crystallisation, as these effects are reduced by the presence of glass particles. Instead this is again an effect of absorbed water, causing clustering and void formation, which can act as defects that initiate crack growth [356]. Hydrolytic degradation of the polymer will also play a role in reducing the ductility, and is more significant for composites containing the PLCL-PEG copolymer.

8.4.4 Implications for cardiac stents

The results here, in particular the evolution of mechanical properties over time, give some indication of the suitability of these materials and strategies for bioresorbable cardiac stent applications. The large reduction in elastic modulus and yield strength observed for composites with 30wt.% glass that occurs within the first 5 days is potentially problematic and could contribute to elastic stent recoil and increase the

risk of restenosis [47]. By contrast composites with 15wt.% glass display a more gradual loss of mechanical properties which could be advantageous for a stent and allow gradual transfer of mechanical support to newly healed tissue. Although there is no evidence of glass addition accelerating polymer degradation within the timescale of these experiments, the addition of the PLCL-PEG copolymer to the polymer matrix does accelerate degradation compared with PLLA, allowing the stent to degrade within a more suitable timeframe [17, 34–36].

8.5 Conclusions

Degradation testing of polymer-glass composites based on PLLA, PLCL-PEG and P_2O_5-CaO-Na_2O glasses demonstrated a two-stage mechanism, where water absorption dominates initially, while later stages are dominated by glass dissolution. Although pH reduction was observed as a result of glass dissolution, this was not observed to accelerate degradation of the polymer matrix component within the timescale of these experiments ($\sim$1 year).

Structural changes that occur during composite degradation were seen to depend on time and composition. For unfilled polymers, chain rearrangements including enthalpy relaxation and polymer crystallisation are critical, while the presence of glass particles suppresses these processes. For composites the glass-polymer interface accelerates water absorption, leading to significant water uptake and cluster formation. This water absorption leads to dissolution of the glass component of the composite, which dominates for high glass loading, leading to debonding of the glass particles from the matrix.

These structural changes have significant effects on the mechanical properties of the composites during degradation, with unfilled polymers becoming stronger and stiffer, but less ductile. The evolution of mechanical properties is more favourable for cardiac stent applications for composites with 15wt.% glass, which demonstrate a more gradual

loss of mechanical properties during degradation. This could allow gradual transfer of loading to newly healed tissue, and reduce the risk of catastrophic brittle device fracture.

The results provide valuable new understanding of the range of structural changes that can occur during degradation of polymer-glass composites, and how the composition of the composite affects which of these mechanisms are dominant. This allows the evolution of mechanical properties during degradation to be understood, which is crucial to designing effective bioresorbable cardiac stent devices.

Chapter 9

Overall summary

This thesis investigated polymer blends and polymer-glass composites as potential materials for bioresorbable stents for treatment of cardiovascular disease.

A review of the literature in this area revealed significant scope for improvement in materials for bioresorbable stent applications. Current stents based on PLLA degrade too slowly and have inadequate mechanical properties. They can experience brittle failure either during deployment or during degradation, and have lower elastic modulus and yield strength than the metals currently used for permanent stents. This requires thicker struts, making the device bulkier and at risk of inducing thrombosis. Polymer-glass composites were found to have been heavily investigated for applications in bioresorbable orthopaedic implants, where similar mechanical strength is required. These works showed that the mechanical and degradation properties of a base polymer such as PLLA can be tuned by incorporation of other polymers in a blend, and by fabricating polymer-glass composites.

The objective of this thesis was to investigate and optimise the properties of these polymer blends and polymer-glass composites for new applications as bioresorbable cardiac stent materials. Tunable acceleration of the degradation lifetime was desired, in order to produce stents that more closely match the body's natural

healing time. Controllable mechanical reinforcement was also a key aim; to provide increased yield strength and stiffness, while retaining ductility both before and after degradation, to avoid catastrophic brittle failure. Throughout these studies, a mechanistic understanding of these materials was constantly sought, because if the material processing-structure-property relationships can be well understood, the desired device performance can be engineered effectively.

9.1 PLLA/PLCL-PEG blends

Chapters 3 and 4 described investigations into blends of PLLA with PLCL(80:20)-PEG and PLCL(70:30)-PEG. This blending strategy facilitated tuning of polymer properties such as ductility, strength, and stiffness, while also allowing control of bioresorbable polymer degradation profiles. Blends with low PLCL-PEG content were brittle in their dry state, due to the solubility of PLCL-PEG polymers in PLLA. Once enough PLCL-PEG was added to the blend to form a PLCL-PEG-rich phase (either by phase separation or bulk composition change) then blends became ductile. When tested in simulated body conditions however, the temperature and hydration had a plasticising effect, reducing interchain bonding, leading to reduced strength and stiffness as well as high ductility for all blend compositions. The degradation lifetime of the polymers was able to be controlled by tuning blend composition, with addition of PLCL-PEG accelerating degradation in a controllable manner. Crucially, rather than the faster degrading PLCL-PEG component simply degrading independently of the PLLA component, results showed significant interaction between these two components, resulting in accelerated degradation of the blend as a whole.

The evolution of the mechanical properties during degradation can be understood in terms of the structural changes that occur over time. Pure PLLA and blends with 10 wt.% PLCL(80:20)-PEG content displayed densification via enthalpy relaxation.

Due to the chemical similarity between individual polymer chains, when the blend is plasticised by water absorption, a thermodynamically driven enthalpy relaxation occurs, to minimise free volume. This densification results in improved strength and stiffness, but significant embrittlement as well, which could be dangerous for a cardiac stent strut. Blends with high PLCL-PEG content (>20% PLCL(70:30)-PEG or >40% PLCL(80:20)-PEG) showed different behaviour, with the rapid degradation caused by high PLCL-PEG content resulting in extensive molecular weight reduction, encouraging crystallisation of the polymer. As with enthalpy relaxation, this led to improved strength and stiffness, but also serious embrittlement, again posing a risk if used as a cardiac stent material. Between these two compositional ranges, a "sweet spot" was found at low PLCL-PEG concentration (10% PLCL(70:30)-PEG, or 20-30% PLCL(80:20)-PEG). These compositions reduced the tendency for enthalpy relaxation by adding more of a dissimilar polymer to the blend, making densification less thermodynamically favourable due to greater interactions between dissimilar chains. They also reduced the propensity of the polymer blend to crystallise, by slowing the degradation rate and reducing production of more easily crystallised short chain polymers.

The polymer blend formulations developed here provide an improved set of properties useful for applications in cardiac stents. Specifically, blends of PLLA with 10 wt.% PLCL(70:30)-PEG provide accelerated degradation on a timescale comparable to wound healing times. This blend composition also retains ductility more effectively during degradation, reducing the risk of stent strut fracture, with only small reductions in strength and stiffness. In order to improve these mechanical properties to the level necessary for use as a bioresorbable cardiac stent, phosphate glasses were later incorporated as a reinforcing phase in polymer-glass composites. In addition to developing blend formulations with improved properties, and understanding how these properties are controlled, the mechanistic understanding discovered here provides a useful template for understanding the changes in structure and mechanical properties of other bioresorbable polymer blends in the future. Bioresorbable polymers are an

increasingly important technology, especially in medical materials, and therefore the importance of properly understanding their changes in properties during degradation cannot be overstated.

9.2 Phosphate glasses

Chapters 5 and 6 described the synthesis, characterisation, and dissolution testing of a range of P_2O_5-CaO-Na_2O glasses. In the context of bioresorbable cardiac stents, phosphate glasses are of interest as a reinforcing phase in polymer-glass composites, that can also have the ability to further tune the degradation behaviour. When incorporated into a polymer-glass composite, phosphate glasses can experience significantly different solution conditions to when they are dissolving on their own, due to acidification from polymer degradation products (lactic acid). Therefore, dissolution tests in a variety of dissolution media were carried out, including solutions containing lactic acid to simulate polymer degradation.

Phosphate glasses, with composition $(P_2O_5)_{90-x}(CaO)_x(Na_2O)_{10}$ where x = 40, 45, 50, were synthesised by melt quenching and either milling to produce glass powder, or casting to produce glass discs. Increasing CaO content in the glass depolymerised the glass network, reducing connectivity and replacing bridging oxygen (P-O-P) bonds with Ca^{2+} cationic crosslinks. These Ca^{2+} cations were located in the interstitial spaces, increasing glass density.

Dissolution tests in a variety of dissolution media indicated that increased CaO concentration in the glass significantly reduced the dissolution rate, while dissolution was accelerated by more acidic solution conditions. Two-stage dissolution behaviour was seen, with initial parabolic mass loss, followed by later linear dissolution. A shrinking-core model from the literature was adapted to describe the different sample

geometry (glass discs) in this work. A new dissolution mechanism was proposed to describe the two-stage dissolution observed here, that takes into account the more complex dissolution media used, compared with previous works focusing on dissolution in deionised water only. An initial stage involves diffusion of water or ions into the glass, with $t^{1/2}$ dependence, which forms a conversion layer consisting of hydrated phosphates, and metal hydroxides or chlorides. This layer dissolves quickly initially, however as the solution concentration increases the dissolution reaction slows, stabilising the conversion layer. The dissolution of the conversion layer then becomes rate-limiting, resulting in linear t dependence of mass loss. This mechanism also allows the behaviour of the transition time (t_{trans}) between these two stages to be understood, where this is responsive to both the solution conditions and the nature of the conversion layer (i.e. the specific hydrated phosphates, metal hydroxides, and chlorides present).

The investigation into the dissolution behaviour of these phosphate glasses has provided insight into how these glasses dissolve in a variety of different media. Due to the changes in solution conditions locally within a polymer-glass composite, this knowledge will help to explain their degradation behaviour, and how the degradation products of glass dissolution and polymer degradation interact and affect bulk degradation. As well as informing the design and study of polymer-glass composites, this knowledge of glass dissolution behaviour is of interest more broadly. Phosphate glasses are an emerging technology, of interest to the biomaterials community as they can provide more versatile dissolution behaviour than existing glass/ceramic materials such as Bioglass or hydroxyapatite. They have been investigated as components in composites (such as in this work) for various soft tissue applications, and also as glass monoliths or porous glass scaffolds for bone regeneration. In any such applications, a detailed knowledge of the dissolution behaviour is essential if the material is to be used clinically with confidence.

9.3 Polymer-glass composites

Finally, Chapters 7 and 8 described the production and testing of polymer-glass composites, based on the polymer blends developed in Chapters 3 and 4, and phosphate glasses synthesised and tested in Chapters 5 and 6. Firstly, a production method was developed and optimised to fabricate the desired polymer-glass composites. Starting from the coarse glass powder produced in Chapter 4, an attritor millling method was developed to produce small microparticles ($d_{0.5}$ = 1.4 ±0.3 µm) of phosphate glass for incorporation into composites, while avoiding excess contamination with wear debris from ZrO_2 milling media. Trials of composite production by solvent casting and injection moulding showed significant glass agglomeration, with negative effects on mechanical and degradation properties. This would also be a significant risk for stent materials, where glass agglomeration within stent struts, with sizes of around 100 µm, could result in catastrophic failure. Subsequently, a new composite production method utilising polymer precipitation onto glass particles, followed by injection moulding, was developed. This new method allowed production of well-dispersed composites, while avoiding the drawbacks of alternative methods such as melt blending, namely the excessive polymer degradation that can result from high shear forces at high temperature.

Mechanical testing of composites injection moulded from composite precipitate indicated that addition of phosphate glass can provide significant improvements in the elastic modulus, consistent with the Counto model for particulate composites. For a cardiac stent material this would provide greater resistance against elastic recoil, which is a significant concern with current bioresorbable stents. Interfacial adhesion between the polymer matrix and phosphate glass particles provided some stress transfer in ambient conditions, while in simulated body conditions the reduced strength of the polymer matrix resulted in bulk yield before debonding at the glass-polymer interface was initiated. Although the composite stiffness was improved by glass addition, the composite materials still retained some ductility, which is crucial for allowing plastic

deformation during stent deployment. Up to 15wt.% glass could be incorporated into the composite without significant reduction in the ductility, while a higher glass loading of 30wt.% resulted in a reduced and more variable ductility.

Degradation studies on composites injection moulded from composite precipitate were performed, using the two slower dissolving glasses studied in Chapter 4 (P45Ca45 and P40Ca50). The degradation studies reveal two distinct regimes of degradation; an initial stage where water absorption is controlling, and a later stage where glass dissolution is dominant. In the initial water absorption stage, mass gain is controlled by the hydrophilicity of the glass and polymer components, with the addition of PLCL-PEG to the matrix having a greater effect than the glass composition. The increased interfacial area found in composites with higher glass content also significantly accelerates water absorption. In the second regime, degradation is dominated by glass dissolution, and slow mass loss occurs as a result. This is controlled mainly by the glass composition, with composites containing the higher Ca glass losing mass more slowly, as expected from results in Chapter 4. Glass dissolution during degradation led to release of acidic dissolution products and reduction in solution pH, however this was not seen to impact the degradation rate of the polymer component, and no difference was observed in the degradation of the polymer component as a result, within the timescale of these experiments.

A range of structural changes occurred during degradation, depending on the composite composition, and the degradation time, which in turn determined the resulting mechanical properties. For unfilled polymers densification via enthalpy relaxation and crystallisation dominated, leading to strengthening and embrittlement, however these processes were suppressed by addition of phosphate glass particles. The interface created by this glass addition accelerated water absorption into the polymer, leading to glass dissolution and debonding from the matrix. This limits the stress transfer that can occur from the polymer matrix to the stronger glass particles, reducing the

composite strength and stiffness. Both composites and unfilled polymers showed an eventual reduction in strength and ductility over time during degradation, however the gradual loss of support from the composites may allow more gentle transfer of loading to the newly healed tissue around an implanted cardiac stent.

9.4 Parameter space

The map of the parameter space shown in Fig. 9.1 shows the key deficiencies of materials in different regions of the glass filler loading and polymer matrix composition parameter space. At low glass loading, polymer embrittlement during degradation is the key issue, with structural rearrangements such as enthalpy relaxation for low PLCL-PEG content, and polymer crystallisation at high PLCL-PEG content influencing the evolution of mechanical properties during degradation. Addition of phosphate glass suppresses these changes, however the fast degradation of polymers with high PLCL-PEG content will probably still result in significant crystallisation. Despite PLCL-PEG addition promoting crystallisation, which can have negative implications, the presence of a low or moderate level of PLCL-PEG is required to accelerate polymer degradation above the very slow rate seen for pure PLLA.

The addition of phosphate glass is advantageous to provide mechanical reinforcement to the weaker polymer matrix, however excessive glass addition can have negative effects on the mechanical properties. Stress concentration and particle agglomeration can lead to reduction in the initial ductility, however this can be counteracted by increased PLCL-PEG addition. The increased water absorption caused by glass addition also impacts the change in mechanical properties during degradation, with wicking and glass dissolution leading to significant loss of composite mechanical properties due to debonding at the particle-matrix interface. This is magnified by an increase in PLCL-PEG content, which also serves to increase the water absorption.

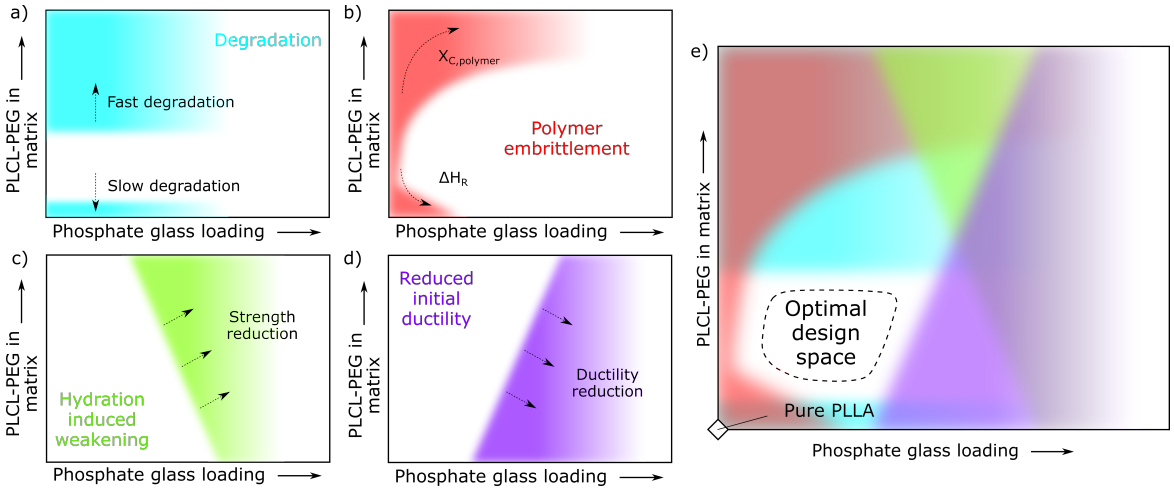

Fig. 9.1: Map of glass filler loading and polymer matrix composition parameter space, showing the key deficiencies of materials in different regions. The shaded region denotes the most promising set of compositions.

The effects of phosphate glass composition and PLCL-PEG copolymer ratio are not reflected in this diagram, however they can also affect the composite behaviour. Increasing the lactide content in the copolymer from PLCL(70:30)-PEG to PLCL(80:20)-PEG reduces the hydrophilicity and degradation rate, as well as making the polymer blend components more compatible. As demonstrated in Chapter 4, this would shift the range of polymer embrittlement towards higher PLCL-PEG content. The slower degradation of this copolymer would also alter the position of the region of optimal degradation rate, again towards higher PLCL-PEG content. Due to the lower ductility of the PLCL(80:20)-PEG copolymer, the border of the region of reduced initial ductility would have a higher gradient, as PLCL-PEG addition would be less effective in retaining ductility, while the gradient of the hydration-induced weakening region would decrease (become more negative) due to the reduced water absorption experienced by the more hydrophobic PLCL(80:20)-PEG copolymer. The glass composition will also have an impact on the evolution of composite properties. A more hydrophilic, faster dissolving glass (i.e. lower CaO content) would accelerate water absorption into the composite, moving the boundary of the hydration-induced weakening region to lower values of phosphate glass loading.

9.5 Overall outcomes

The materials developed in this thesis show considerable promise for applications as bioresorbable cardiac stents. A key issue with current bioresorbable polymer stents is their slow degradation, and this work has demonstrated that this can be accelerated to a more suitable degradation rate by blending with PLCL-PEG, allowing the degradation of these materials to more closely match the body's natural healing time. The change in stent mechanical properties during degradation is another key consideration, and this work has developed strategies to provide more gradual loss of strength and ductility by blending with PLCL-PEG, and addition of phosphate glass particles within a composite. This addition of phosphate glass also provides mechanical reinforcement to the polymer matrix, reducing the risk of stent recoil after implantation (which can lead to restenosis). The improved mechanical properties also allow the stent strut size to be reduced, reducing blood flow turbulence and again reducing the risk of restenosis.

In addition to advances in development of stent materials, this thesis has also resulted in new scientific insights regarding the behaviour of these materials. Investigations of PLLA/PLCL-PEG blends revealed how the blend ratio of miscible and semi-miscible blends determines the structural rearrangements that occur during degradation, with important implications for the resulting properties. The role of the faster degrading PLCL-PEG component in catalysing PLLA degradation was also confirmed. New understanding of the dissolution behaviour of phosphate glasses was also gained, revealing that the transition from diffusion-controlled layer formation to reaction-controlled layer dissolution is dependent on the nature of the conversion layer, and solution conditions. For polymer-glass composites, changes in the solution conditions as a result of glass dissolution were not seen to accelerate PLLA degradation, in contrast to previous experiments with other bioresorbable polymers. Glass particles were found to play a crucial role in suppressing structural changes within the polymer, while also enhancing water absorption, which has a strong effect on the

composite properties. This knowledge is essential for understanding the mechanical and degradation behaviour of polymers and polymer-glass composites, and allows for more effective design of bioresorbable stent materials.

Chapter 10

Future work

This work has developed new polymer blend and polymer-glass composite materials which show promise for application as bioresorbable cardiac stent materials. In addition, a thorough mechanistic understanding of these materials has been devised, allowing control of mechanical and degradation properties. There are however, still further tests required to conclusively assess the suitability of these materials for cardiac stents, including dynamic mechanical and degradation testing, as well as assessment of the biological response. Furthermore, in order to close the gap in mechanical properties between polymer-based bioresorbable stents and the current standard metallic stents, greater improvements in strength are needed, and suggested methods for achieving this are discussed below.

10.1 Dynamic testing

The mechanical testing carried out on these materials so far has all been under static loading conditions, however this is not the case when these devices are in service. Stents are crimped (i.e. compressed) onto a catheter, and later expanded again during deployment, before being subjected to cyclic loading (at about 1 Hz due to blood being pumped around the body) for the entirety of their service life. Mechanical testing under

non-static loading conditions would provide an informative complement to existing static loading results. Simulated crimping and deployment tests could be carried out, where the material is plastically deformed and unloaded, before being tested to failure. This would reveal the effects of the deployment procedure and changes to the material microstructure, on the subsequent mechanical properties. Fatigue testing, where the material is subjected to a load significantly below its yield strength for many cycles, could also provide useful information about the mechanisms and factors affecting fatigue failure. However, performing accelerated fatigue testing (i.e. cycling load at >1 Hz) could prove challenging as the interaction with material degradation is crucial, and this is challenging to accurately accelerate due to the multitude of different mechanisms (water absorption, glass dissolution, inorganic crystallisation, polymer hydrolysis, and polymer crystallisation) occurring concurrently. In addition, the well-known strain rate dependence of PLLA mechanical properties [49] would provide additional complications for accelerated testing.

The dissolution and degradation testing carried out so far has all been under static conditions, which are convenient and easy to interpret. This does not mirror *in vivo* conditions, where fresh fluid is constantly passing over the material. Dynamic testing, where fresh solution is constantly flowed over the degrading sample, is more challenging to conduct but could provide more representative information about how these materials would behave during implantation. This is especially important considering that, as this work has demonstrated, phosphate glass dissolution and the transition between dissolution stages is heavily dependent on surrounding solution conditions. In addition, acid buildup from glass dissolution or polymer degradation can affect further polymer degradation, so continual refreshing of the solution could also alter polymer degradation behaviour. These experiments could also be conducted in a semi-dynamic way, by refreshing the degradation solution regularly rather than having a continuous flow.

Alongside these dynamic testing methods, further µCT analysis of polymer-glass composite samples at various stages of degradation would allow certain aspects of the degradation process to be investigated. Formation of voids within the polymer matrix has been attributed to clustering of absorbed water, and µCT analysis would allow these voids to be imaged without the complicating effects of additional processing (i.e. drying). This technique would also allow inorganic precipitation within the composite to be studied in more detail, to determine when inorganic phases are formed, and whether they nucleate on the glass or polymer surfaces.

10.2 Biological response

The biological response to any implanted material is of crucial importance, and here interactions at the material surface are a key concern. For stent materials an inflammatory reaction caused by the material can lead to excessive growth of the neointima (the newly forming tissue layer that covers the implant), which can contribute to restenosis (recurring narrowing of the artery after stenting) [357]. Most bioresorbable polymeric stents under development therefore incorporate, on top of the structural base material, a thin polymer coating (around 4 µm thick PDLLA) loaded with antiproliferative drugs such as everolimus or sirolimus [35]. This reduces immune cell proliferation on the material in order to reduce restenosis rates, therefore any new composite materials used for biological testing should also incorporate this coating that will be in contact with the biological environment.

Stent placement within the artery can induce platelet adhesion and stimulate coagulation, which can result in potentially fatal thrombosis. This requires patients to adhere to dual antiplatelet therapy, however this is not feasible for all patients [358]. As thrombus formation is a key shortcoming of stent implantation, the thrombogenicity of any new stent material should be carefully assessed. *In vitro* testing of platelet

adhesion on these materials should be carried out in order to determine the material's thrombogenicity and ensure they are no worse than current stent materials. Although coating stents with a drug-eluting layer to reduce immune cell proliferation is effective, growth and proliferation of endothelial cells to form the endothelium is essential to restore homeostasis. *In vitro* cell proliferation assays could be carried out using human vascular smooth muscle cells and human vascular endothelial cells, to ensure that the stent material can be appropriately re-endothelialised, without the excessive proliferation of muscle cells that can result in neointimal hyperplasia (thickening of arterial walls and decreased arterial lumen space) and consequent restenosis.

In addition to cell proliferation and platelet adhesion testing methods that are often used for stent materials, the presence of phosphate glass within these composite stents makes further *in vitro* testing desirable. Due to the slow release of calcium ions as the glass dissolves arterial calcification may be a concern, however this may be counteracted by the large volume of blood flow through the artery (making any increase in Ca concentration above the baseline negligible) or the calcification-suppressing effect of pyrophosphate release from the dissolving glass. *In vitro* testing with human vascular smooth muscle cells could determine whether ion release from polymer-glass composite stents has any impact on the likelihood of vascular calcification. This is a key concern as increased calcification could lead to additional atherosclerotic lesions, requiring further stenting to treat.

10.3 Material development

Despite the advances made in this work, further material development is still necessary in order to improve material strength and allow stent strut size reduction. As demonstrated in this work, addition of phosphate glass microparticles can effectively increase the elastic modulus, but other techniques are necessary if the yield strength is

to be significantly improved to allow comparable polymer strut sizes to metallic stents. Recent work has demonstrated the ability of advanced polymer processing techniques such as solid die-drawing and microfibre filament formation to significantly improve the yield strength of PLLA by orientation of the polymer chains [35, 359]. This is a promising technique that could also be applied to the polymer blends and polymer-glass composites studied here, however the effects of this orientation on the degradation behaviour, and the changes in mechanical properties during water absorption and degradation are essential to characterise and understand.

Despite using two relatively slowly dissolving phosphate glasses for incorporation into composites, a noticeable drop in pH is observed during degradation of all the composites tested, within the first month. This acidification could have negative effects on the surrounding tissue *in vivo*. In addition, the dissolution of the glass at the polymer-glass interface plays a role in the fast loss of mechanical properties for composites with high filler loading. Changing the glass composition is one way that this issue could be addressed, by reducing the glass dissolution rate further, by addition of Fe_2O_3 or TiO_2 [167, 175, 176]. Alternatively, glasses with a higher Na_2O content, although they dissolve more quickly, can result in a pH increase due to the ions released as they dissolve [165], which may counteract some of the potential negative biological effects of local acidification.

The high water absorption seen for the polymer-glass composites is seen to reduce the mechanical properties, as absorbed water along the interface disrupts bonding between the two components and dissolves the glass at the interface, reducing the mechanical strength [230]. Interfacial coupling agents have been investigated with some success [238, 360], however this has not resulted in suitable mechanical properties over the course of the degradation lifetime. Other potential methods to reduce water absorption along the interface include use of sol-gel derived hybrids, with covalent bonds between inorganic and organic components, or melt-blended combinations of low-T_g phosphate

glass with organic polymers [361, 362]. Detailed study and engineering of the surface chemistry of the two components, in terms of the hydrophilicity and different surface energy components, is another promising method for controlling water absorption and therefore the reduction in mechanical strength. If the surface chemistry of the polymer and glass components can be tuned to be hydrophobic (while maintaining desired degradation characteristics), and reduce the interfacial energy of the polymer-glass interface, this could make polymer-glass contact more thermodynamically favourable than contact with water, discouraging wicking along the interface.

* * *

This thesis represents an original investigation of polymer-glass composites for application as bioresorbable cardiac stent materials. These findings provide new understanding of the essential mechanisms that determine the mechanical properties, degradation behaviour, and evolution of mechanical properties during degradation, and how these can be customised by engineering the structure and composition of the composite. The materials developed here show encouraging results, and this, along with the more broadly applicable concepts generated here, demonstrates that polymer-glass composites are a promising material for the next generation of bioresorbable cardiac stents.

References

[1] British Heart Foundation. *Heart and Circulatory Disease Statistics 2019*. Tech. rep. April. 2019, pp. 94–96.

[2] World Health Organisation. *Preventing chronic diseases: a vital investment: WHO global report*. Tech. rep. World Health Organisation, 2005.

[3] World Health Organisation. *Cardiovascular diseases (CVDs)*. 2017. URL: https://www.who.int/news-room/fact-sheets/detail/cardiovascular-diseases-(cvds) (visited on 04/15/2020).

[4] World Health Organisation. *WHO: The top 10 causes of death*. 2017. URL: http://www.who.int/mediacentre/factsheets/fs310/en/ (visited on 04/05/2017).

[5] Institute for Health Metrics and Evaluation (IHME). *Rethinking Development and Health: Findings from the Global Burden of Disease Study*. Tech. rep. Seattle, WA: IHME, 2016.

[6] E. Wilkins, L. Wilson, K. Wickramasinghe, P. Bhatnagar, J. Leal, R. Leungo-Fernandez, R. Burns, M. Rayner, and N. Townsend. *European Cardiovascular Disease Statistics 2017*. Tech. rep. 2017.

[7] E. A. Martin. *Concise Medical Dictionary*. Oxford University Press, 2010.

[8] *Creative Commons — Attribution 3.0 Unported — CC BY 3.0*. URL: https://creativecommons.org/licenses/by/3.0/deed.en (visited on 06/22/2020).

[9] Blausen Medical. *Medical gallery of Blausen Medical 2014*. 2014. URL: https://en.wikiversity.org/wiki/WikiJournal_of_Medicine/Medical_gallery_of_Blausen_Medical_2014 (visited on 04/06/2017).

[10] *Creative Commons — Attribution-ShareAlike 4.0 International — CC BY-SA 4.0*. URL: https://creativecommons.org/licenses/by-sa/4.0/deed.en (visited on 06/22/2020).

[11] Blausen Medical. *Angioplasty*. 2016. URL: https://commons.wikimedia.org/wiki/File:Angioplasty_-_Balloon_Inflated_with_Stent.png (visited on 04/06/2017).

[12] T. Simard, B. Hibbert, F. D. Ramirez, M. Froeschl, Y.-X. Chen, and E. R. O'Brien. "The Evolution of Coronary Stents: A Brief Review". *Canadian Journal of Cardiology* 30.1 (2014), pp. 35–45.

[13] *Creative Commons — Attribution-NonCommercial-ShareAlike 4.0 International — CC BY-NC-SA 4.0*. URL: https://creativecommons.org/licenses/by-nc-sa/4.0/ (visited on 06/22/2020).

[14] K. Milewski, P. Gasior, S. Samborski, P. P. Buszman, A. Blachut, A. Wojtaszczyk, A. Mlodziankowski, A. Mendyk, W. Wojakowski, and P. E. Buszman. "Evaluation of safety and efficacy of NexGen-an ultrathin strut and hybrid cell design cobalt-chromium bare metal stent implanted in a real life patient population-the Polish NexGen Registry". *Postepy w Kardiologii Interwencyjnej* 12.3 (2016), pp. 217–223.

[15] T. Palmerini, C. Barozzi, L. Tomasi, D. D. Riva, M. Marengo, G. Cicoria, A. G. Bruno, M. L. Bacchi-Reggiani, M. Naldi, M. Bartolini, S. Fanti, N. Galiè, and G. W. Stone. "In vitro thrombogenicity of drug-eluting and bare metal stents". *Thrombosis Research* 185 (2020), pp. 43–48.

[16] A. Mattesini, S. Bartolini, C. S. Dini, S. Valente, G. Parodi, M. Stolcova, F. Meucci, and C. Di Mario. "The DESolve novolimus bioresorbable Scaffold: from bench to bedside". *Journal of Thoracic Disease* 9.S9 (2017), S950–S958.

[17] J. Foerst, M. Vorpahl, M. Engelhardt, T. Koehler, K. Tiroch, and R. Wessely. "Evolution of Coronary Stents: From Bare-Metal Stents to Fully Biodegradable, Drug-Eluting Stents". *Combination Products in Therapy* 3.1 (2013), pp. 9–24.

[18] G. Sarno, B. Lagerqvist, O. Fröbert, J. Nilsson, G. Olivecrona, E. Omerovic, N. Saleh, D. Venetzanos, and S. James. "Lower risk of stent thrombosis and restenosis with unrestricted use of 'new-generation' drug-eluting stents: a report from the nationwide Swedish Coronary Angiography and Angioplasty Registry (SCAAR)". *European Heart Journal* 33.5 (2012), pp. 606–613.

[19] G. Nakazawa, A. V. Finn, M. Vorpahl, E. R. Ladich, F. D. Kolodgie, and R. Virmani. "Coronary Responses and Differential Mechanisms of Late Stent Thrombosis Attributed to First-Generation Sirolimus- and Paclitaxel-Eluting Stents". *Journal of the American College of Cardiology* 57.4 (2011), pp. 390–398.

[20] G. Nakazawa, F. Otsuka, M. Nakano, M. Vorpahl, S. K. Yazdani, E. Ladich, F. D. Kolodgie, A. V. Finn, and R. Virmani. "The Pathology of Neoatherosclerosis in Human Coronary Implants: Bare-Metal and Drug-Eluting Stents". *Journal of the American College of Cardiology* 57.11 (2011), pp. 1314–1322.

[21] J. Iqbal, J. Gunn, and P. W. Serruys. "Coronary stents: historical development, current status and future directions". *British Medical Bulletin* 106.1 (2013), pp. 193–211.

[22] U.S Food and Drug Administration. *FDA News Release: FDA approves first absorbable stent for coronary artery disease*. 2016. URL: https://www.fda.gov/newsevents/newsroom/pressannouncements/ucm509805.htm (visited on 04/10/2017).

[23] D. Fornell. "FDA Approves First Totally Bioresorbable Stent". *Diagnostic and Interventional Cardiology* (2016).

[24] P. W. Serruys, J. Ormiston, R.-J. van Geuns, B. de Bruyne, D. Dudek, E. Christiansen, B. Chevalier, P. Smits, D. McClean, J. Koolen, S. Windecker, R. Whitbourn, I. Meredith, L. Wasungu, D. Ediebah, S. Veldhof, and Y. Onuma. "A polylactide bioresorbable scaffold eluting everolimus for treatment of coronary stenosis 5-year follow-up". *Journal of the American College of Cardiology* 67.7 (2016), pp. 766–776.

[25] C. Lu, K. B. Filion, and M. J. Eisenberg. "The Safety and Efficacy of Absorb Bioresorbable Vascular Scaffold: A Systematic Review". *Clinical Cardiology* 39.1 (2016), pp. 48–55.

[26] D. Brie, P. Penson, M.-C. Serban, P. P. Toth, C. Simonton, P. W. Serruys, and M. Banach. "Bioresorbable scaffold — A magic bullet for the treatment of coronary artery disease?" *International Journal of Cardiology* 215.April (2016), pp. 47–59.

[27] G. Sarno, N. Bruining, Y. Onuma, S. Garg, S. Brugaletta, S. De Winter, E. Regar, L. Thuesen, D. Dudek, S. Veldhof, C. Dorange, H. M. Garcia-Garcia, J. A. Ormiston, and P. W. Serruys. "Morphological and functional evaluation of the bioresorption of the bioresorbable everolimus-eluting vascular scaffold using IVUS, echogenicity and vasomotion testing at two year follow-up: a patient level insight into the ABSORB A clinical trial". *The International Journal of Cardiovascular Imaging* 28.1 (2012), pp. 51–58.

[28] H. Khamis, K. Shokry, A. Ramzy, and A. Samir. "Bioresorbable Vascular Scaffold (ABSORB BVS); first report in Egyptian patients with 6 month angiographic/IVUS follow up". *Egyptian Heart Journal* 66.3 (2014), pp. 227–232.

[29] Z. A. Ali, R. Gao, T. Kimura, Y. Onuma, D. J. Kereiakes, S. G. Ellis, B. Chevalier, M.-T. Vu, Z. Zhang, C. A. Simonton, P. W. Serruys, and G. W. Stone. "Three-Year Outcomes With the Absorb Bioresorbable Scaffold: Individual-Patient-Data Meta-Analysis From the ABSORB Randomized Trials." *Circulation* 137.5 (2018), pp. 464–479.

[30] P. W. Serruys, B. Chevalier, Y. Sotomi, A. Cequier, D. Carrié, J. J. Piek, A. J. Van Boven, M. Dominici, D. Dudek, D. McClean, S. Helqvist, M. Haude, S. Reith, M. de Sousa Almeida, G. Campo, A. Iñiguez, M. Sabaté, S. Windecker, and Y. Onuma. "Comparison of an everolimus-eluting bioresorbable scaffold with an everolimus-eluting metallic stent for the treatment of coronary artery stenosis (ABSORB II): a 3 year, randomised, controlled, single-blind, multicentre clinical trial". *The Lancet* 388.10059 (2016), pp. 2479–2491.

[31] D. Fornell. "Abbott Will End Sales of Absorb Bioresorbable Stent". *Diagnostic and Interventional Cardiology* (2017).

[32] S. Z. Rittersma, R. J. de Winter, K. T. Koch, M. Bax, C. E. Schotborgh, K. J. Mulder, J. G. Tijssen, and J. J. Piek. "Impact of strut thickness on late luminal loss after coronary artery stent placement". *The American Journal of Cardiology* 93.4 (2004), pp. 477–480.

[33] S. Bangalore, H. G. Bezerra, D. G. Rizik, E. J. Armstrong, B. Samuels, S. S. Naidu, C. L. Grines, M. T. Foster, J. W. Choi, B. D. Bertolet, A. P. Shah, R. Torguson, S. B. Avula, J. C. Wang, J. P. Zidar, A. Maksoud, A. Kalyanasundaram, S. J. Yakubov, B. M. Chehab, A. J. Spaedy, S. P. Potluri, R. P. Caputo, A. Kondur, R. F. Merritt, A. Kaki, R. Quesada, M. A. Parikh, C. Toma, F. Matar, J. DeGregorio, W. Nicholson, W. Batchelor, R. Gollapudi, E. Korngold, R. Sumar, G. S. Chrysant, J. Li, J. B. Gordon, R. M. Dave, G. F. Attizzani, T. P. Stys, O. S. Gigliotti, B. E. Murphy, S. G. Ellis, and R. Waksman. "The State of the Absorb Bioresorbable Scaffold". *JACC: Cardiovascular Interventions* 10.23 (2017), pp. 2349–2359.

[34] C. Collet, R. J. de Winter, Y. Onuma, and P. W. Serruys. "The Absorb bioresorbable vascular scaffold for the treatment of coronary artery disease". *Expert Opinion on Drug Delivery* 13.10 (2016), pp. 1489–1499.

[35] S. McMahon, N. Bertollo, E. D. O. Cearbhaill, J. Salber, L. Pierucci, P. Duffy, T. Dürig, V. Bi, and W. Wang. "Bio-resorbable polymer stents: a review of material progress and prospects". *Progress in Polymer Science* 83 (2018), pp. 79–96.

[36] D. Mukherjee. "Device Thrombosis with Bioresorbable Scaffolds". *New England Journal of Medicine* 376.24 (2017), pp. 2388–2389.

[37] D. Capodanno. "Bioresorbable scaffolds in coronary intervention: Unmet needs and evolution". *Korean Circulation Journal* 48.1 (2018), pp. 24–35.

[38] NatureWorks. "Ingeo™ Biopolymer 2500HP Technical Data Sheet" (2015).

[39] P. Barragan, R. Rieu, V. Garitey, P.-O. Roquebert, J. Sainsous, M. Silvestri, and G. Bayet. "Elastic recoil of coronary stents: A comparative analysis". *Catheterization and Cardiovascular Interventions* 50.1 (2000), pp. 112–119.

[40] T. Ota, H. Ishii, T. Sumi, T. Okada, H. Murakami, S. Suzuki, K. Kada, N. Tsuboi, and T. Murohara. "Impact of coronary stent designs on acute stent recoil". *Journal of Cardiology* 64.5 (2014), pp. 347–352.

[41] Y. Cheng, P. Gasior, M. Shibuya, K. Ramzipoor, C. Lee, E. A. Estrada, D. Dokko, J. C. McGregor, G. B. Conditt, G. L. Kaluza, and J. F. Granada. "Comparative Characterization of Biomechanical Behavior and Healing Profile of a Novel Ultra-High-Molecular-Weight Amorphous Poly-l-Lactic Acid Sirolimus-Eluting Bioresorbable Coronary Scaffold". *Circulation: Cardiovascular Interventions* 9.10 (2016).

[42] S. D. Washko and G. Aggen. "Wrought Stainless Steels". *Properties and Selection: Irons, Steels, and High-Performance Alloys, Vol 1, ASM Handbook* (1990), pp. 841–907.

[43] D. Hodgson, M. Wu, and R. Biermann. "Shape Memory Alloys". *Properties and Selection: Nonferrous Alloys and Special-Purpose Materials, Vol 2, ASM Handbook* (1990), pp. 897–902.

[44] J. B. Park and R. S. Lakes. *Biomaterials: an introduction*. 3rd ed. Springer, 2007, p. 267.

[45] A. Roguin and R. Beyar. "The acute effect of stenting with the nitinol self-expanding coil stent: preliminary experience." *International journal of cardiac imaging* 13.6 (1997), pp. 441–50.

[46] H. Y. Ang, H. Bulluck, P. Wong, S. S. Venkatraman, Y. Huang, and N. Foin. "Bioresorbable Stents: Current and Upcoming Bioresorbable Technologies". *International Journal of Cardiology* 228 (2016), pp. 931–939.

[47] J. Butany, K. Carmichael, S. W. Leong, and M. J. Collins. "Coronary artery stents: identification and evaluation." *Journal of clinical pathology* 58.8 (2005), pp. 795–804.

[48] Y. Sotomi, Y. Onuma, C. Collet, E. Tenekecioglu, R. Virmani, N. S. Kleiman, and P. W. Serruys. "Bioresorbable scaffold: The emerging reality and future directions". *Circulation Research* 120.8 (2017), pp. 1341–1352.

[49] A. C. Bobel, S. Lohfeld, R. N. Shirazi, and P. E. McHugh. "Experimental mechanical testing of Poly (l-Lactide) (PLLA) to facilitate pre-degradation characteristics for application in cardiovascular stenting". *Polymer Testing* 54 (2016), pp. 150–158.

[50] O. Vyavahare, D. Ng, and S. L. Hsu. "Analysis of Structural Rearrangements of Poly(lactic acid) in the Presence of Water". *The Journal of Physical Chemistry B* 118.15 (2014), pp. 4185–4193.

[51] P. Pan, B. Zhu, and Y. Inoue. "Enthalpy Relaxation and Embrittlement of Poly(L-lactide) during Physical Aging". *Macromolecules* 40.26 (2007), pp. 9664–9671.

[52] S. A. Wayangankar and S. G. Ellis. "Bioresorbable Stents: Is This Where We Are Headed?" *Progress in Cardiovascular Diseases* 58.3 (2015), pp. 342–355.

[53] M. Shibuya, C. A. Gongora, Y. Cheng, G. B. Conditt, J. McGregor, J. Granada, and G. L. Kaluza. "TCT-85 Factors Influencing Stent Recoil and Underexpansion In Vivo Independent of Atherosclerosis: A Multimodality Imaging Study in Normal Porcine Coronary Arteries". *Journal of the American College of Cardiology* 64.11 (2014), B25.

[54] K. Igaki, M. Iwamoto, H. Yamane, and K. Saito. "Development of the novel biodegradable coronary stent [1st report, poly (glycolic acid) as the stent material]". *Transactions of the Japan Society of Mechanical Engineers, Part A* 65.639 (1999), pp. 2379–2384.

[55] K. Kumar, R. S. Gill, and U. Batra. "Challenges and opportunities for biodegradable magnesium alloy implants". *Materials Technology* 33.2 (2018), pp. 153–172.

[56] S. Amani and G. Faraji. "Processing and Properties of Biodegradable Magnesium Microtubes for Using as Vascular Stents: A Brief Review". *Metals and Materials International* 25.5 (2019), pp. 1341–1359.

[57] D. I. Shin, P. J. Kim, K.-B. Seung, D. B. Kim, M.-J. Kim, K. Chang, S. M. Lim, D. S. Jeon, W. S. Chung, S. H. Baek, and M. Y. Lee. "Drug-Eluting Stent Implantation Could Be Associated With Long-Term Coronary Endothelial Dysfunction Comparison Between Sirolimus-Eluting Stent and Paclitaxel-Eluting Stent". *International Heart Journal* 48.5 (2007), pp. 553–567.

[58] J. M. Anderson, A. Rodriguez, and D. T. Chang. "Foreign body reaction to biomaterials". *Seminars in Immunology* 20.2 (2008), pp. 86–100.

[59] J. Iqbal, Y. Onuma, J. Ormiston, A. Abizaid, R. Waksman, and P. Serruys. "Bioresorbable scaffolds: rationale, current status, challenges, and future". *European Heart Journal* 35.12 (2014), pp. 765–776.

[60] L. S. Nair and C. T. Laurencin. "Biodegradable polymers as biomaterials". *Progress in Polymer Science* 32 (2007), pp. 762–798.

[61] T. H. Barrows. "Degradable implant materials: A review of synthetic absorbable polymers and their applications". *Clinical Materials* 1.4 (1986), pp. 233–257.

[62] P. B. Maurus and C. C. Kaeding. "Bioabsorbable implant material review". *Operative Techniques in Sports Medicine* 12.3 (2004), pp. 158–160.

[63] NatureWorks. *Ingeo Resin - Naturally Advanced Materials - Product Guide*. Tech. rep. 2017.

[64] CONMED Corporation. *Orthopedics*. URL: https://www.conmed.com/en/products/orthopedics/knee (visited on 07/01/2020).

[65] Arthrex Inc. *Interference Screws*. URL: https://www.arthrex.com/knee/interference-screws (visited on 07/01/2020).

[66] J. C. Middleton and A. J. Tipton. "Synthetic biodegradable polymers as orthopedic devices". *Biomaterials* 21.23 (2000), pp. 2335–2346.

[67] H. H. Lu, J. A. Cooper, S. Manuel, J. W. Freeman, M. A. Attawia, F. K. Ko, and C. T. Laurencin. "Anterior cruciate ligament regeneration using braided biodegradable scaffolds: in vitro optimization studies". *Biomaterials* 26.23 (2005), pp. 4805–4816.

[68] J. A. Cooper, H. H. Lu, F. K. Ko, J. W. Freeman, and C. T. Laurencin. "Fiber-based tissue-engineered scaffold for ligament replacement: design considerations and in vitro evaluation". *Biomaterials* 26.13 (2005), pp. 1523–1532.

[69] L. E. L. Perkins, M. B. Kossuth, J. C. Fox, and R. J. Rapoza. "Paving the way to a bioresorbable technology: Development of the absorb BRS program". *Catheterization and Cardiovascular Interventions* 88.September (2016), pp. 1–9.

[70] J. Bergsma, F. Rozema, R. Bos, G. Boering, W. de Bruijn, and A. Pennings. "In vivo degradation and biocompatibility study of in vitro pre-degraded as-polymerized polylactide particles". *Biomaterials* 16.4 (1995), pp. 267–274.

[71] K. L. Harrison and M. J. Jenkins. "The effect of crystallinity and water absorption on the dynamic mechanical relaxation behaviour of polycaprolactone". *Polymer International* 53.9 (2004), pp. 1298–1304.

[72] C. Pitt, M. Gratzl, G. Kimmel, J. Surles, and A. Schindler. "Aliphatic polyesters II. The degradation of poly (DL-lactide), poly (ϵ-caprolactone), and their copolymers in vivo". *Biomaterials* 2.4 (1981), pp. 215–220.

[73] A. Schindler, R. Jeffcoat, G. L. Kimmel, C. G. Pitt, M. E. Wall, and R. Zweidinger. "Biodegradable polymers for sustainable drug delivery". In: *Contemporary Topics in Polymer Science, Volume 2.* Ed. by E. M. Pearce and J. R. Schaefgen. New York, London: Plenum Press, 1977, pp. 251–289.

[74] M. Hiljanen-Vainio, T. Karjalainen, and J. Seppälä. "Biodegradable lactone copolymers. I. Characterization and mechanical behavior of e-caprolactone and lactide copolymers". *Journal of Applied Polymer Science* 59.8 (1996), pp. 1281–1288.

[75] M. Malin, M. Hiljanen-Vainio, T. Karjalainen, and J. Seppälä. "Biodegradable lactone copolymers. II. Hydrolytic study of e-caprolactone and lactide copolymers". *Journal of Applied Polymer Science* 59.8 (1996), pp. 1289–1298.

[76] T. Karjalainen, M. Hiljanen-Vainio, M. Malin, and J. Seppälä. "Biodegradable lactone copolymers. III. Mechanical properties of e-caprolactone and lactide copolymers after hydrolysis in vitro". *Journal of Applied Polymer Science* 59.8 (1996), pp. 1299–1304.

[77] W. P. Ye, F. S. Du, W. H. Jin, J. Y. Yang, and Y. Xu. "In vitro degradation of poly(caprolactone), poly(lactide) and their block copolymers: influence of composition, temperature and morphology". *Reactive & Functional Polymers* 32 (1997), pp. 161–168.

[78] S. K. Saha and H. Tsuji. "Effects of rapid crystallization on hydrolytic degradation and mechanical properties of poly(l-lactide-co-ϵ-caprolactone)". *Reactive and Functional Polymers* 66.11 (2006), pp. 1362–1372.

[79] S. K. Saha and H. Tsuji. "Enhanced Crystallization of Poly(L-lactide-co-e-caprolactone) in the Presence of Water". *Journal of Applied Polymer Science* 112.2 (2009), pp. 715–720.

[80] J. Fernández, A. Etxeberria, and J. R. Sarasua. "Synthesis, structure and properties of poly(L-lactide-co-ϵ-caprolactone) statistical copolymers". *Journal of the Mechanical Behavior of Biomedical Materials* 9 (2012), pp. 100–112.

[81] J. Fernández, A. Etxeberria, J. M. Ugartemendia, S. Petisco, and J. R. Sarasua. "Effects of chain microstructures on mechanical behavior and aging of a poly(L-lactide-co-ϵ-caprolactone) biomedical thermoplastic-elastomer". *Journal of the Mechanical Behavior of Biomedical Materials* 12 (2012), pp. 29–38.

[82] J. Fernández, A. Larrañaga, A. Etxeberria, W. Wang, and J. R. Sarasua. "A new generation of poly(lactide/ϵ-caprolactone) polymeric biomaterials for application in the medical field". *Journal of Biomedical Materials Research - Part A* 102.10 (2014), pp. 3573–3584.

[83] J. Fernández, E. Meaurio, A. Chaos, A. Etxeberria, A. Alonso-Varona, and J. Sarasua. "Synthesis and characterization of poly (l-lactide/ϵ-caprolactone) statistical copolymers with well resolved chain microstructures". *Polymer* 54.11 (2013), pp. 2621–2631.

[84] J. Fernández, A. Etxeberría, and J. Sarasua. "Effects of repeat unit sequence distribution and residual catalyst on thermal degradation of poly(l-lactide/ϵ-caprolactone) statistical copolymers". *Polymer Degradation and Stability* 98.7 (2013), pp. 1293–1299.

[85] X. L. Lu, Z. J. Sun, W. Cai, and Z. Y. Gao. "Study on the shape memory effects of poly(L-lactide-co-ϵ-caprolactone) biodegradable polymers". *Journal of Materials Science: Materials in Medicine* 19.1 (2008), pp. 395–399.

[86] L. N. Woodard, V. M. Page, K. T. Kmetz, and M. A. Grunlan. "PCL-PLLA Semi-IPN Shape Memory Polymers (SMPs): Degradation and Mechanical Properties". *Macromolecular Rapid Communications* 37 (2016), pp. 1972–1977.

[87] D. Cohn and H. Younes. "Biodegradable PEO/PLA block copolymers". *Journal of Biomedical Materials Research* 22.11 (1988), pp. 993–1009.

[88] L. Youxin and T. Kissel. "Synthesis and properties of biodegradable ABA triblock copolymers consisting of poly(l-lactic acid) or poly (l-lactic-co-glycolic acid) A-blocks attached to central poly (oxyethylene) B-blocks". *Journal of Controlled Release* 27.3 (1993), pp. 247–257.

[89] A. Reed and D. Gilding. "Biodegradable polymers for use in surgery — poly(ethylene oxide)/poly(ethylene terephthalate) (PEO/PET) copolymers: 2. In vitro degradation". *Polymer* 22.4 (1981), pp. 499–504.

[90] K. J. Zhu, L. Xiangzhou, and Y. Shilin. "Preparation and properties of D,L-lactide and ethylene oxide copolymer: A modifying biodegradable polymeric material". *Journal of Polymer Science Part C: Polymer Letters* 24.7 (1986), pp. 331–337.

[91] A. Hatefi and B. Amsden. "Biodegradable injectable in situ forming drug delivery systems". *Journal of Controlled Release* 80.1 (2002), pp. 9–28.

[92] X. Zhang, J. K. Jackson, W. Wong, W. Min, T. Cruz, W. L. Hunter, and H. M. Burt. "Development of biodegradable polymeric paste formulations for taxol: An in vitro and in vivo study". *International Journal of Pharmaceutics* 137.2 (1996), pp. 199–208.

[93] P. A. Davis, S. Cousins, and Davis. *Biodegradable injectable drug delivery polymer*. 1992.

[94] B. Jeong, Y. H. Bae, D. S. Lee, and S. W. Kim. "Biodegradable block copolymers as injectable drug-delivery systems". *Nature* 388.28 (1997), pp. 860–862.

[95] B. Jeong, Y. Choi, Y. Bae, G. Zentner, and S. Kim. "New biodegradable polymers for injectable drug delivery systems". *Journal of Controlled Release* 62.1 (1999), pp. 109–114.

[96] B. Jeong, Y. H. Bae, and S. W. Kim. "Thermoreversible Gelation of PEG-PLGA-PEG Triblock Copolymer Aqueous Solutions". *Macromolecules* 32.21 (1999), pp. 7064–7069.

[97] C. He, S. W. Kim, and D. S. Lee. "In situ gelling stimuli-sensitive block copolymer hydrogels for drug delivery". *Journal of Controlled Release* 127.3 (2008), pp. 189–207.

[98] H. Bramfeldt, P. Sarazin, and P. Vermette. "Characterization, degradation, and mechanical strength of poly(D,L-lactide-co-e-caprolactone)-poly(ethylene glycol)- poly(D,L-lactide-co-e-caprolactone)". *Journal of Biomedical Materials Research Part A* 83A (2007), pp. 503–511.

[99] D. S.-G. Hu and H.-J. Liu. "Structural analysis and degradation behavior in polyethylene glycol/poly(L-lactide) copolymers". *Journal of Applied Polymer Science* 51.3 (1994), pp. 473–482.

[100] J. H. Lee, A. K. Go, S. H. Oh, K. E. Lee, and S. H. Yuk. "Tissue anti-adhesion potential of ibuprofen-loaded PLLA–PEG diblock copolymer films". *Biomaterials* 26.6 (2005), pp. 671–678.

[101] Z. Azhari, S. McMahon, L. Pierucci, W. Wang, and R. E. Cameron. "Short poly(ethylene glycol) block initiation of poly(L-lactide) di-block copolymers: a strategy for tuning the degradation of resorbable devices". *Polymer International* 67.6 (2018), pp. 726–738.

[102] J. Kwon, Z. Azhari, P. Duffy, S. McMahon, W. Wang, and R. E. Cameron. *Biodegradable polymer platform for stent application*. Tech. rep. 2017.

[103] J. Kwon, Z. Azhari, P. Duffy, S. McMahon, W. Wang, and R. E. Cameron. "[PEG-functionalised PLCL copolymers, blends and composites: thermal, mechanical, and degradation properties]". *UNPUBLISHED RAW DATA* (2017).

[104] A. Hughes, H. Tai, A. Tochwin, and W. Wang. "Biodegradable and Biocompatible PDLLA-PEG1k-PDLLA Diacrylate Macromers: Synthesis, Characterisation and Preparation of Soluble Hyperbranched Polymers and Crosslinked Hydrogels". *Processes* 5.2 (2017), p. 18.

[105] H.-G. Elias. *An introduction to polymer science*. VCH, 1997.

[106] O. Olabisi, L. M. Robeson, and M. T. Shaw. *Polymer-polymer miscibility*. New York: Academic Press, 1979, p. 370.

[107] L. A. Utracki, P. Mukhopadhyay, and R. K. Gupta. "Polymer blends: Introduction". In: *Polymer Blends Handbook*. Springer Netherlands, 2014, pp. 3–170.

[108] C. Nakafuku and S.-y. Takehisa. "Glass transition and mechanical properties of PLLA and PDLLA-PGA copolymer blends". *Journal of Applied Polymer Science* 93.5 (2004), pp. 2164–2173.

[109] J. Ugartemendia, A. Larrañaga, H. Amestoy, A. Etxeberria, and J. Sarasua. "Tougher biodegradable polylactide system for bone fracture fixations: Miscibility study, phase morphology and mechanical properties". *European Polymer Journal* 98 (2018), pp. 411–419.

[110] S. Petisco-Ferrero, A. Etxeberria, and J. Sarasua. "Mechanical properties and state of miscibility in poly(racD,L-lactide-co-glycolide)/(L-lactide-co-ϵ-caprolactone) blends". *Journal of the Mechanical Behavior of Biomedical Materials* 71 (2017), pp. 372–382.

[111] T. Nardo, V. Chiono, P. Gentile, M. Tabrizian, and G. Ciardelli. "Poly(DL-lactide-co-ϵ-caprolactone) and poly(DL-lactide-co-glycolide) blends for biomedical application: Physical properties, cell compatibility, and in vitro degradation behavior". *International Journal of Polymeric Materials and Polymeric Biomaterials* 65.14 (2016), pp. 741–750.

[112] N. López-Rodríguez, A. López-Arraiza, E. Meaurio, and J. Sarasua. "Crystallization, morphology, and mechanical behavior of polylactide/poly(e-caprolactone) blends". *Polymer Engineering & Science* 46.9 (2006), pp. 1299–1308.

[113] F. S. Bates. "Polymer-Polymer Phase Behavior". *Science* 251.4996 (1991), pp. 898–905.

[114] P. Saini, M. Arora, and M. R. Kumar. "Poly(lactic acid) blends in biomedical applications". *Advanced Drug Delivery Reviews* 107 (2016), pp. 47–59.

[115] M. Hiljanen-Vainio, P. Varpomaa, J. Seppälä, and P. Törmälä. "Modification of poly(L-lactides) by blending: mechanical and hydrolytic behavior". *Macromolecular Chemistry and Physics* 197.4 (1996), pp. 1503–1523.

[116] H. Tsuji and Y. Ikada. "Blends of aliphatic polyesters. I. Physical properties and morphologies of solution-cast blends from poly(DL-lactide) and poly(ϵ-caprolactone)". *Journal of Applied Polymer Science* 60.13 (1996), pp. 2367–2375.

[117] S. Wachirahuttapong, C. Thongpin, and N. Sombatsompop. "Effect of PCL and Compatibility Contents on the Morphology, Crystallization and Mechanical Properties of PLA/PCL Blends". *Energy Procedia* 89 (2016), pp. 198–206.

[118] M. E. Broz, D. L. VanderHart, and N. R. Washburn. "Structure and mechanical properties of poly(d,l-lactic acid)/ poly(e-caprolactone) blends". *Biomaterials* 24 (2003), pp. 4181–4190.

[119] I. Navarro-Baena, V. Sessini, F. Dominici, L. Torre, J. M. Kenny, and L. Peponi. "Design of biodegradable blends based on PLA and PCL: From morphological, thermal and mechanical studies to shape memory behavior". *Polymer Degradation and Stability* 132 (2016), pp. 97–108.

[120] I. Fortelný, A. Ostafińska, D. Michálková, J. Jůza, J. Mikešová, and M. Šlouf. "Phase structure evolution during mixing and processing of poly(lactic acid)/ polycaprolactone (PLA/PCL) blends". *Polymer Bulletin* 72.11 (2015), pp. 2931–2947.

[121] A. Ostafinska, I. Fortelny, M. Nevoralova, J. Hodan, J. Kredatusova, and M. Slouf. "Synergistic effects in mechanical properties of PLA/PCL blends with optimized composition, processing, and morphology". *RSC Advances* 5.120 (2015), pp. 98971–98982.

[122] A. Ostafinska, I. Fortelný, J. Hodan, S. Krejčíková, M. Nevoralová, J. Kredatusová, Z. Kruliš, J. Kotek, and M. Šlouf. "Strong synergistic effects in PLA/PCL blends: Impact of PLA matrix viscosity". *Journal of the Mechanical Behavior of Biomedical Materials* 69 (2017), pp. 229–241.

[123] C.-H. Kim, K. Y. Cho, E.-J. Choi, and J.-K. Park. "Effect of P(lLA-co-ϵCL) on the compatibility and crystallization behavior of PCL/PLLA blends". *Journal of Applied Polymer Science* 77.1 (2000), pp. 226–231.

[124] N.-S. Choi, C.-H. Kim, K. Y. Cho, and J.-K. Park. "Morphology and hydrolysis of PCL/PLLA blends compatibilized with P(LLA-co-ϵCL) or P(LLA-b-ϵCL)". *Journal of Applied Polymer Science* 86.8 (2002), pp. 1892–1898.

[125] W. Wang, J. Hu, C. He, W. Nie, W. Feng, K. Qiu, X. Zhou, Y. Gao, and G. Wang. "Heparinized PLLA/PLCL nanofibrous scaffold for potential engineering of small-diameter blood vessel: Tunable elasticity and anticoagulation property". *Journal of Biomedical Materials Research Part A* 103.5 (2015), pp. 1784–1797.

[126] Y. H. Na, Y. He, X. Shuai, Y. Kikkawa, Y. Doi, and Y. Inoue. "Compatibilization effect of poly (ϵ-caprolactone)-b-poly(ethylene glycol) block copolymers and phase morphology analysis in immiscible poly(lactide)/poly(ϵ-caprolactone) blends". *Biomacromolecules* 3.6 (2002), pp. 1179–1186.

[127] J. H. Kim, H. Noh, J. H. Kang, B. S. Lee, J. Choi, K. Park, and D. K. Han. "Characteristics of PLLA films blended with PEG block copolymers as additives for biodegradable polymer stents". *Biomedical Engineering Letters* 1.1 (2011), pp. 42–48.

[128] M. Deroiné, A. Le Duigou, Y. M. Corre, P. Y. Le Gac, P. Davies, G. César, and S. Bruzaud. "Accelerated ageing of polylactide in aqueous environments: Comparative study between distilled water and seawater". *Polymer Degradation and Stability* 108 (2014), pp. 319–329.

[129] I. Grizzi, H. Garreau, S. Li, and M. Vert. "Hydrolytic degradation of devices based on poly(dl-lactic acid) size-dependence". *Biomaterials* 16.4 (1995), pp. 305–311.

[130] H. Tsuji. "Autocatalytic hydrolysis of amorphous-made polylactides: effects of l-lactide content, tacticity, and enantiomeric polymer blending". *Polymer* 43 (2002), pp. 1789–1796.

[131] H. Tsuji. "In vitro hydrolysis of blends from enantiomeric poly(lactide)s. Part 4: well-homo-crystallized blend and nonblended films". *Biomaterials* 24.4 (2003), pp. 537–547.

[132] H. Tsuji and K. Ikarashi. "In vitro hydrolysis of poly(L-lactide) crystalline residues as extended-chain crystallites: II. Effects of hydrolysis temperature". *Biomacromolecules* 5.3 (2004), pp. 1021–1028.

[133] H. Tsuji and K. Ikarashi. "In vitro hydrolysis of poly(L-lactide) crystalline residues as extended-chain crystallites: III. Effects of pH and enzyme". *Polymer Degradation and Stability* (2004).

[134] A. Gleadall, J. Pan, M.-A. Kruft, and M. Kellomäki. "Degradation mechanisms of bioresorbable polyesters. Part 1. Effects of random scission, end scission and autocatalysis". *Acta Biomaterialia* 10.5 (2014), pp. 2223–2232.

[135] Y. Wang, J. Pan, X. Han, C. Sinka, and L. Ding. "A phenomenological model for the degradation of biodegradable polymers". *Biomaterials* (2008).

[136] K. Sevim and J. Pan. "A model for hydrolytic degradation and erosion of biodegradable polymers". *Acta Biomaterialia* 66 (2018), pp. 192–199.

[137] H. Tsuji and Y. Ikada. "Properties and morphology of poly(L-lactide) 4. Effects of structural parameters on long-term hydrolysis of poly(L-lactide) in phosphate-buffered solution". *Polymer Degradation and Stability* (2000).

[138] A. Gleadall, J. Pan, and H. Atkinson. "A simplified theory of crystallisation induced by polymer chain scissions for biodegradable polyesters". *Polymer Degradation and Stability* 97.9 (2012), pp. 1616–1620.

[139] X. Han and J. Pan. "A model for simultaneous crystallisation and biodegradation of biodegradable polymers". *Biomaterials* 30.3 (2009), pp. 423–430.

[140] K. Wasanasuk, K. Tashiro, M. Hanesaka, T. Ohhara, K. Kurihara, R. Kuroki, T. Tamada, T. Ozeki, and T. Kanamoto. "Crystal Structure Analysis of Poly(L-lactic Acid) a Form On the basis of the 2-Dimensional Wide-Angle Synchrotron X-ray and Neutron Diffraction Measurements". *Macromolecules* 44 (2011), pp. 6441–6452.

[141] B. Eling, S. Gogolewski, and A. J. Pennings. "Biodegradable materials of poly(l-lactic acid): 1. Melt-spun and solution-spun fibres". *Polymer* (1982).

[142] J. Zhang, Y. Duan, H. Sato, H. Tsuji, I. Noda, S. Yan, and Y. Ozaki. "Crystal modifications and thermal behavior of poly(L-lactic acid) revealed by infrared spectroscopy". *Macromolecules* 38.19 (2005), pp. 8012–8021.

[143] J. Puiggali, Y. Ikada, H. Tsuji, L. Cartier, T. Okihara, and B. Lotz. "The frustrated structure of poly(L-lactide)". *Polymer* 41.25 (2000), pp. 8921–8930.

[144] L. Cartier, T. Okihara, Y. Ikada, H. Tsuji, J. Puiggali, and B. Lotz. "Epitaxial crystallization and crystalline polymorphism of polylactides". *Polymer* 41 (2000), pp. 8909–8919.

[145] Y. Ikada, K. Jamshidi, H. Tsuji, and S. H. Hyon. "Stereocomplex Formation between Enantiomeric Poly(lactides)". *Macromolecules* 20.4 (1987), pp. 904–906.

[146] P. De Santis and A. J. Kovacs. "Molecular conformation of poly(S-lactic acid)". *Biopolymers* 6.3 (1968), pp. 299–306.

[147] T. Okihara, M. Tsuji, A. Kawaguchi, K. I. Katayama, H. Tsuji, S. H. Hyon, and Y. Ikada. "Crystal Structure of Stereocomplex of Poly(L-lactide) and Poly(D-lactide)". *Journal of Macromolecular Science, Part B* 30.1-2 (1991), pp. 119–140.

[148] X. Zhang, M. Espiritu, A. Bilyk, and L. Kurniawan. "Morphological behaviour of poly(lactic acid) during hydrolytic degradation". *Polymer Degradation and Stability* 93 (2008), pp. 1964–1870.

[149] I. M. Hodge. "Enthalpy relaxation and recovery in amorphous materials". *Journal of Non-Crystalline Solids* 169 (1994), pp. 211–266.

[150] A. R. Berens and I. M. Hodge. "Effects of annealing and prior history on enthalpy relaxation in glassy polymers. 1. Experimental study on poly(vinyl chloride)". *Macromolecules* 15.3 (1982), pp. 756–761.

[151] I. M. Hodge and A. R. Berens. "Effects of Annealing and Prior History on Enthalpy Relaxation in Glassy Polymers. 2. Mathematical Modeling". *Macromolecules* 15 (1982), pp. 762–770.

[152] I. M. Hodge and G. S. Huvard. "Effects of Annealing and Prior History on Enthalpy Relaxation in Glassy Polymers. 3. Experimental and Modeling Studies of Polystyrene". *Macromolecules* 16 (1983), pp. 371–375.

[153] I. M. Hodge. "Effects of Annealing and Prior History on Enthalpy Relaxation in Glassy Polymers. 4. Comparison of Five Polymers". *Macromolecules* 16 (1983), pp. 898–902.

[154] A. C. Renouf-Glauser, J. Rose, D. F. Farrar, and R. E. Cameron. "The effect of crystallinity on the deformation mechanism and bulk mechanical properties of PLLA". *Biomaterials* 26.29 (2005), pp. 5771–5782.

[155] J. R. Jones. "Review of bioactive glass: From Hench to hybrids". *Acta Biomaterialia* 9.1 (2012), pp. 4457–4486.

[156] L. L. Hench, R. J. Splinter, W. C. Allen, and T. K. Greenlee. "Bonding mechanisms at the interface of ceramic prosthetic materials". *Journal of Biomedical Materials Research* 5.6 (1971), pp. 117–141.

[157] L. L. Hench. "The story of Bioglass®". *Journal of Materials Science: Materials in Medicine* 17.11 (2006), pp. 967–978.

[158] L. L. Hench. "Bioceramics". *Journal of the American Ceramic Society* 81.7 (1998), pp. 1705–1728.

[159] E. A. Abou Neel, D. M. Pickup, S. P. Valappil, R. J. Newport, and J. C. Knowles. "Bioactive functional materials: a perspective on phosphate-based glasses". *Journal of Materials Chemistry* 19.6 (2009), pp. 690–701.

[160] J. C. Knowles. "Phosphate based glasses for biomedical applications". *Journal of Materials Chemistry* 13.10 (2003), p. 2395.

[161] R. K. Brow. "Review: the structure of simple phosphate glasses". *Journal of Non-Crystalline Solids* 263 (2000), pp. 1–28.

[162] B.-S. Bae and M. C. Weinberg. "Oxidation-Reduction Equilibrium in Copper Phosphate Glass Melted in Air". *Journal of the American Ceramic Society* 74.12 (1991), pp. 3039–3045.

[163] F. Delahaye, L. Montagne, G. Palavit, J. Claude Touray, and P. Baillif. "Acid dissolution of sodium-calcium metaphosphate glasses". *Journal of Non-Crystalline Solids* 242.1 (1998), pp. 25–32.

[164] M. Uo, M. Mizuno, Y. Kuboki, A. Makishima, and F. Watari. "Properties and cytotoxicity of water soluble Na2O–CaO–P2O5 glasses". *Biomaterials* 19.24 (1998), pp. 2277–2284.

[165] K. Franks, I. Abrahams, and J. C. Knowles. "Development of soluble glasses for biomedical use Part I: In vitro solubility measurement". *Journal of Materials Science: Materials in Medicine* 11.10 (2000), pp. 609–614.

[166] E. A. Abou Neel, I. Ahmed, J. J. Blaker, A. Bismarck, A. R. Boccaccini, M. P. Lewis, S. N. Nazhat, and J. C. Knowles. "Effect of iron on the surface, degradation and ion release properties of phosphate-based glass fibres". *Acta Biomaterialia* 1.5 (2005), pp. 553–563.

[167] A. Parsons, L. Burling, C. Scotchford, G. Walker, and C. Rudd. "Properties of sodium-based ternary phosphate glasses produced from readily available phosphate salts". *Journal of Non-Crystalline Solids* 352.50 (2006), pp. 5309–5317.

[168] J. Knowles, K. Franks, and I. Abrahams. "Investigation of the solubility and ion release in the glass system K2O–Na2O–CaO–P2O5". *Biomaterials* 22.23 (2001), pp. 3091–3096.

[169] K. Franks, V. Salih, J. C. Knowles, and I. Olsen. "The effect of MgO on the solubility behavior and cell proliferation in a quaternary soluble phosphate based glass system". *Journal of Materials Science: Materials in Medicine* 13.6 (2002), pp. 549–556.

[170] I. Ahmed, A. Parsons, A. Jones, G. Walker, C. Scotchford, and C. Rudd. "Cytocompatibility and effect of increasing MgO content in a range of quaternary invert phosphate-based glasses." *Journal of biomaterials applications* 24.6 (2010), pp. 555–75.

[171] V. Salih, A. Patel, and J. C. Knowles. "Zinc-containing phosphate-based glasses for tissue engineering". *Biomedical Materials* 2.1 (2007), pp. 11–20.

[172] E. A. Abou Neel, L. A. O'Dell, W. Chrzanowski, M. E. Smith, and J. C. Knowles. "Control of surface free energy in titanium doped phosphate based glasses by co-doping with zinc". *Journal of Biomedical Materials Research Part B: Applied Biomaterials* 89B.2 (2009), pp. 392–407.

[173] N. J. Lakhkar, I. H. Lee, H. W. Kim, V. Salih, I. B. Wall, and J. C. Knowles. "Bone formation controlled by biologically relevant inorganic ions: Role and controlled delivery from phosphate-based glasses". *Advanced Drug Delivery Reviews* 65.4 (2013), pp. 405–420.

[174] E. A. Abou Neel, T. Mizoguchi, M. Ito, M. Bitar, V. Salih, and J. C. Knowles. "In vitro bioactivity and gene expression by cells cultured on titanium dioxide doped phosphate-based glasses". *Biomaterials* 28.19 (2007), pp. 2967–2977.

[175] E. A. Abou Neel and J. C. Knowles. "Physical and biocompatibility studies of novel titanium dioxide doped phosphate-based glasses for bone tissue engineering applications". *Journal of Materials Science: Materials in Medicine* 19.1 (2008), pp. 377–386.

[176] E. A. Abou Neel, W. Chrzanowski, and J. C. Knowles. "Effect of increasing titanium dioxide content on bulk and surface properties of phosphate-based glasses". *Acta Biomaterialia* 4.3 (2008), pp. 523–534.

[177] P. Haque, I. Ahmed, A. Parsons, R. Felfel, G. Walker, and C. Rudd. "Degradation properties and microstructural analysis of 40P2O5-24MgO-16CaO-16Na2O-4Fe2O3 phosphate glass fibres". *Journal of Non-Crystalline Solids* 375 (2013), pp. 99–109.

[178] M. Bitar, V. Salih, V. Mudera, J. C. Knowles, and M. P. Lewis. "Soluble phosphate glasses: in vitro studies using human cells of hard and soft tissue origin". *Biomaterials* 25.12 (2004), pp. 2283–2292.

[179] J. E. Gough, P. Christian, C. A. Scotchford, C. D. Rudd, and I. A. Jones. "Synthesis, degradation, and in vitro cell responses of sodium phosphate glasses for craniofacial bone repair". *Journal of Biomedical Materials Research* 59.3 (2002), pp. 481–489.

[180] J. E. Gough, P. Christian, C. A. Scotchford, and I. A. Jones. "Long-term craniofacial osteoblast culture on a sodium phosphate and a calcium/sodium phosphate glass". *Journal of Biomedical Materials Research* 66A.2 (2003), pp. 233–240.

[181] A. J. Parsons, M. Evans, C. D. Rudd, and C. A. Scotchford. "Synthesis and degradation of sodium iron phosphate glasses and their in vitro cell response". *Journal of Biomedical Materials Research - Part A* 71.2 (2004), pp. 283–291.

[182] A. M. Mackenzie, N. R. Kendall, D. V. Illingworth, D. W. Jackson, I. M. Gill, and S. B. Telfer. "The Effect of a Copper, Cobalt, and Selenium Bolus on Sheep from Three Upland Scottish Farms". In: *Trace Elements in Man and Animals 10*. Boston: Kluwer Academic Publishers, 2002, pp. 749–752.

[183] S. B. Telfer, D. V. Illingworth, P. J. B. Anderson, G. Zervas, and G. Carlos. "Effect of soluble-glass boluses on the copper, cobalt and selenium status of sheep". *Biochemical Society Transactions* 13.2 (1985).

[184] S. H. Cartmell, P. J. Doherty, J. A. Hunt, D. M. Healy, and T. Gilchrist. "Soft tissue response to glycerol-suspended controlled-release glass particulate". *Journal of Materials Science: Materials in Medicine* 9.12 (1998), pp. 773–777.

[185] A. M. Mulligan, M. Wilson, and J. C. Knowles. "Effect of increasing silver content in phosphate-based glasses on biofilms of Streptococcus sanguis". *Journal of Biomedical Materials Research - Part A* 67.2 (2003), pp. 401–412.

[186] A. M. Mulligan, M. Wilson, and J. C. Knowles. "The effect of increasing copper content in phosphate-based glasses on biofilms of Streptococcus sanguis". *Biomaterials* 67A.10 (2003), pp. 401–412.

[187] I. Ahmed, D. Ready, M. Wilson, and J. Knowles. "Antimicrobial effect of silver-doped phosphate-based glasses". *Journal of Biomedical Materials Research Part A* 79A.3 (2006), pp. 618–626.

[188] S. P. Valappil, J. C. Knowles, and M. Wilson. "Effect of silver-doped phosphate-based glasses on bacterial biofilm growth." *Applied and environmental microbiology* 74.16 (2008), pp. 5228–30.

[189] S. Valappil, D. Ready, E. Abou Neel, D. Pickup, L. O'Dell, W. Chrzanowski, J. Pratten, R. Newport, M. Smith, M. Wilson, and J. Knowles. "Controlled delivery of antimicrobial gallium ions from phosphate-based glasses". *Acta Biomaterialia* 5.4 (2009), pp. 1198–1210.

[190] E. A. Abou Neel, W. Chrzanowski, D. M. Pickup, L. A. O'Dell, N. J. Mordan, R. J. Newport, M. E. Smith, and J. C. Knowles. "Structure and properties of strontium-doped phosphate-based glasses". *Journal of the Royal Society Interface* 6 (2009), pp. 435–446.

[191] J. Vormann. "Magnesium: Nutrition and metabolism". *Molecular Aspects of Medicine* 24.1-3 (2003), pp. 27–37.

[192] J. Barralet, U. Gbureck, P. Habibovic, E. Vorndran, C. Gerard, and C. J. Doillon. "Angiogenesis in Calcium Phosphate Scaffolds by Inorganic Copper Ion Release". *Tissue Engineering Part A* 15.7 (2009), pp. 1601–1609.

[193] C. Gérard, L.-J. Bordeleau, J. Barralet, and C. J. Doillon. "The stimulation of angiogenesis and collagen deposition by copper". *Biomaterials* 31.5 (2010), pp. 824–831.

[194] E. D. Harris. "A Requirement for Copper in Angiogenesis". *Nutrition Reviews* 62.2 (2004), pp. 60–64.

[195] G.-f. Hu. "Copper stimulates proliferation of human endothelial cells under culture". *Journal of Cellular Biochemistry* 69.3 (1998), pp. 326–335.

[196] R. Villa-Bellosta, X. Wang, J. L. Millán, G. R. Dubyak, and W. C. O'Neill. "Extracellular pyrophosphate metabolism and calcification in vascular smooth muscle". *American Journal of Physiology - Heart and Circulatory Physiology* 301.1 (2011), pp. 61–68.

[197] R. Villa-Bellosta and J. Egido. "Phosphate, pyrophosphate, and vascular calcification: A question of balance". *European Heart Journal* 38.23 (2017), pp. 1801–1804.

[198] D. Azpiazu, S. Gonzalo, E. González-Parra, J. Egido, and R. Villa-Bellosta. "Role of pyrophosphate in vascular calcification in chronic kidney disease". *Nefrologia* 38.3 (2018), pp. 250–257.

[199] R. Villa-Bellosta and W. C. O'Neill. "Pyrophosphate deficiency in vascular calcification". *Kidney International* 93.6 (2018), pp. 1293–1297.

[200] L. Ma, R. K. Brow, and M. E. Schlesinger. "Dissolution behaviour of sodium calcium polyphosphate glasses". *Physics and Chemistry of Glasses: European Journal of Glass Science and Technology Part B* 59.5 (2018), pp. 205–212.

[201] B. Bunker, G. Arnold, and J. Wilder. "Phosphate glass dissolution in aqueous solutions". *Journal of Non-Crystalline Solids* 64.3 (1984), pp. 291–316.

[202] H. Gao, T. Tan, and D. Wang. "Dissolution mechanism and release kinetics of phosphate controlled release glasses in aqueous medium". *Journal of Controlled Release* 96.1 (2004), pp. 21–28.

[203] H. Gao, T. Tan, and D. Wang. "Dissolution mechanism and release kinetics of phosphate controlled release glasses in aqueous medium". *Journal of Controlled Release* 96 (2004), pp. 29–36.

[204] J. Massera, K. Bourhis, L. Petit, M. Couzi, L. Hupa, M. Hupa, J. Videau, and T. Cardinal. "Effect of the glass composition on the chemical durability of zinc-phosphate-based glasses in aqueous solutions". *Journal of Physics and Chemistry of Solids* 74.1 (2013), pp. 121–127.

[205] L. Ma, R. K. Brow, and M. E. Schlesinger. "Dissolution behavior of Na2O-FeO-Fe2O3-P2O5 glasses". *Journal of Non-Crystalline Solids* 463 (2017), pp. 90–101.

[206] I. Ahmed, M. Lewis, I. Olsen, and J. Knowles. "Phosphate glasses for tissue engineering: Part 2. Processing and characterisation of a ternary-based P2O5–CaO–Na2O glass fibre system". *Biomaterials* 25.3 (2004), pp. 491–499.

[207] W. Jander. "Reaktionen im festen Zustande bei höheren Temperaturen. Reaktionsgeschwindigkeiten endotherm verlaufender Umsetzungen". *Zeitschrift für anorganische und allgemeine Chemie* 163.1 (1927), pp. 1–30.

[208] M. N. Rahaman. *Ceramic processing and sintering*. 2nd ed. New York: Marcel Dekker Inc., 2003, p. 875.

[209] Y. Gu, W. Xiao, L. Lu, W. Huang, M. N. Rahaman, and D. Wang. "Kinetics and mechanisms of converting bioactive borate glasses to hydroxyapatite in aqueous phosphate solution". *Journal of Materials Science* 46.1 (2011), pp. 47–54.

[210] S. B. Jung and D. E. Day. "Conversion kinetics of silicate, borosilicate, and borate bioactive glasses to hydroxyapatite". *Physics and Chemistry of Glasses - European Journal of Glass Science and Technology Part B* 50.2 (2009), pp. 85–88.

[211] E. Diamanti and J. R. Sarasua. "Effects of Bioactive Glass Particles on the Mechanical and Thermal Behavior of Poly(ϵ- caprolactone)". *Macromolecular Symposia* 321-322.1 (2012), pp. 25–29.

[212] X. Li, J. Shi, X. Dong, L. Zhang, and H. Zeng. "A mesoporous bioactive glass/polycaprolactone composite scaffold and its bioactivity behavior". *Journal of Biomedical Materials Research Part A* 84A.1 (2008), pp. 84–91.

[213] E. Ural, K. Kesenci, L. Fambri, C. Migliaresi, and E. Piskin. "Poly(d,l-cactide/ϵ-caprolactone)/hydroxyapatite composites". *Biomaterials* 21.21 (2000), pp. 2147–2154.

[214] M. Shah Mohammadi, I. Ahmed, B. Marelli, C. Rudd, M. N. Bureau, and S. N. Nazhat. "Modulation of polycaprolactone composite properties through incorporation of mixed phosphate glass formulations". *Acta Biomaterialia* 6.8 (2010), pp. 3157–3168.

[215] M. Navarro, M. Ginebra, J. Planell, C. Barrias, and M. Barbosa. "In vitro degradation behavior of a novel bioresorbable composite material based on PLA and a soluble CaP glass". *Acta Biomaterialia* 1.4 (2005), pp. 411–419.

[216] Z. Yang, E. Thian, S. M. Best, and R. Cameron. "A Novel Way of Dispersing Fine Ceramic Particles in PLGA Matrix". *Key Engineering Materials* 330-332 (2007), pp. 511–514.

[217] Z. Yang, S. M. Best, and R. E. Cameron. "The influence of α-tricalcium phosphate nanoparticles and microparticles on the degradation of poly(D,L-lactide-co-glycolide)". *Advanced Materials* 21.38-39 (2009), pp. 3900–3904.

[218] S. I. J. Wilberforce, C. E. Finlayson, S. M. Best, and R. E. Cameron. "The influence of the compounding process and testing conditions on the compressive mechanical properties of poly(D,L-lactide-co-glycolide)/α-tricalcium phosphate nanocomposites". *Journal of the Mechanical Behavior of Biomedical Materials* 4.7 (2011), pp. 1081–1089.

[219] S.-S. Kim, M. S. Park, O. Jeon, C. Y. Choi, and B.-S. Kim. "Poly(lactide-co-glycolide)/hydroxyapatite composite scaffolds for bone tissue engineering". *Biomaterials* 27 (2006), pp. 1399–1409.

[220] A. R. Boccaccini, D. S. Brauer, and L. Hupa, eds. *Bioactive Glasses*. Smart Materials Series. Cambridge: Royal Society of Chemistry, 2016.

[221] S. I. J. Wilberforce, C. E. Finlayson, S. M. Best, and R. E. Cameron. "A comparative study of the thermal and dynamic mechanical behaviour of quenched and annealed bioresorbable poly-l-lactide/α-tricalcium phosphate nanocomposites". *Acta Biomaterialia* 7.5 (2011), pp. 2176–2184.

[222] E. Petinakis, X. Liu, L. Yu, C. Way, P. Sangwan, K. Dean, S. Bateman, and G. Edward. "Biodegradation and thermal decomposition of poly(lactic acid)-based materials reinforced by hydrophilic fillers". *Polymer Degradation and Stability* 95.9 (2010), pp. 1704–1707.

[223] A. K. Mohapatra, S. Mohanty, and S. Nayak. "Effect of PEG on PLA/PEG Blend and Its Nanocomposites: A Study of Thermo-Mechanical and Morphological Characterization". *Polymer Composites* 35.2 (2013), pp. 283–293.

[224] J. A. Odell and A. Keller. "Flow-induced chain fracture of isolated linear macromolecules in solution". *Journal of Polymer Science Part B: Polymer Physics* 24.9 (1986), pp. 1889–1916.

[225] J. J. Blaker, A. Bismarck, A. R. Boccaccini, A. M. Young, and S. N. Nazhat. "Premature degradation of poly(α-hydroxyesters) during thermal processing of Bioglass®-containing composites". *Acta Biomaterialia* 6.3 (2010), pp. 756–762.

[226] R. M. Felfel, K. M. Z. Hossain, A. J. Parsons, C. D. Rudd, and I. Ahmed. "Accelerated in vitro degradation properties of polylactic acid/phosphate glass fibre composites". *Journal of Materials Science* 50.11 (2015), pp. 3942–3955.

[227] N. Sharmin, M. S. Hasan, A. J. Parsons, C. D. Rudd, and I. Ahmed. "Cytocompatibility, mechanical and dissolution properties of high strength boron and iron oxide phosphate glass fibre reinforced bioresorbable composites". *Journal of the Mechanical Behavior of Biomedical Materials* 59 (2016), pp. 41–56.

[228] M. Shah Mohammadi, I. Ahmed, N. Muja, C. D. Rudd, M. N. Bureau, and S. N. Nazhat. "Effect of phosphate-based glass fibre surface properties on thermally produced poly(lactic acid) matrix composites". *Journal of Materials Science: Materials in Medicine* 22.12 (2011), pp. 2659–2672.

[229] R. Felfel, I. Ahmed, A. Parsons, G. Walker, and C. Rudd. "In vitro degradation, flexural, compressive and shear properties of fully bioresorbable composite rods". *Journal of the Mechanical Behavior of Biomedical Materials* 4.7 (2011), pp. 1462–1472.

[230] I. Ahmed, I. A. Jones, A. J. Parsons, J. Bernard, J. Farmer, C. A. Scotchford, G. S. Walker, and C. D. Rudd. "Composites for bone repair: phosphate glass fibre reinforced PLA with varying fibre architecture". *Journal of Materials Science: Materials in Medicine* 22.8 (2011), pp. 1825–1834.

[231] T. J. Corden, I. A. Jones, C. D. Rudd, P. Christian, and S. Downes. "Initial development into a novel technique for manufacturing a long fibre thermoplastic bioabsorbable composite: in-situ polymerisation of poly-e-caprolactone". *Composites Part A: Applied Science and Manufacturing* 30.6 (1999), pp. 737–746.

[232] T. J. Corden, I. A. Jones, C. D. Rudd, P. Christian, S. Downes, and K. E. Mcdougall. "Physical and biocompatibility properties of poly-ϵ-caprolactone produced using in situ polymerisation: a novel manufacturing technique for long-fibre composite materials". *Biomaterials* 21 (2000), pp. 713–724.

[233] G. Jiang, M. Evans, I. Jones, C. Rudd, C. Scotchford, and G. Walker. "Preparation of poly(ϵ-caprolactone)/continuous bioglass fibre composite using monomer transfer moulding for bone implant". *Biomaterials* 26.15 (2005), pp. 2281–2288.

[234] R. A. Khan, A. J. Parsons, I. A. Jones, G. S. Walker, and C. D. Rudd. "Surface treatment of phosphate glass fibers using 2-hydroxyethyl methacrylate: Fabrication of poly(caprolactone)-based composites". *Journal of Applied Polymer Science* 111.1 (2009), pp. 246–254.

[235] R. A. Khan, A. J. Parsons, I. A. Jones, G. S. Walker, and C. D. Rudd. "Preparation and Characterization of Phosphate Glass Fibers and Fabrication of Poly(caprolactone) Matrix Resorbable Composites". *Journal of Reinforced Plastics and Composites* 29.12 (2010), pp. 1838–1850.

[236] J.-H. Jo, E.-J. Lee, D.-S. Shin, H.-E. Kim, H.-W. Kim, Y.-H. Koh, and J.-H. Jang. "In vitro/in vivo biocompatibility and mechanical properties of bioactive glass nanofiber and poly(ϵ-caprolactone) composite materials". *Journal of Biomedical Materials Research Part B: Applied Biomaterials* 91B.1 (2009), pp. 213–220.

[237] M. Navarro, C. Aparicio, M. Charles-Harris, M. P. Ginebra, E. Engel, and J. A. Planell. "Development of a Biodegradable Composite Scaffold for Bone Tissue Engineering: Physicochemical, Topographical, Mechanical, Degradation, and Biological Properties". In: *Ordered Polymeric Nanostructures at Surfaces*. Springer Berlin Heidelberg, 2006, pp. 209–231.

[238] P. Haque, A. J. Parsons, I. A. Barker, I. Ahmed, D. J. Irvine, G. S. Walker, and C. D. Rudd. "Interfacial properties of phosphate glass fibres/PLA composites: Effect of the end functionalities of oligomeric PLA coupling agents". *Composites Science and Technology* 70.13 (2010), pp. 1854–1860.

[239] X. Liu, M. S. Hasan, D. M. Grant, L. T. Harper, A. J. Parsons, G. Palmer, C. D. Rudd, and I. Ahmed. "Mechanical, degradation and cytocompatibility properties of magnesium coated phosphate glass fibre reinforced polycaprolactone composites." *Journal of biomaterials applications* 29.5 (2014), pp. 675–87.

[240] M. S. Hasan, I. Ahmed, A. J. Parsons, C. D. Rudd, G. S. Walker, and C. A. Scotchford. "Investigating the use of coupling agents to improve the interfacial properties between a resorbable phosphate glass and polylactic acid matrix." *Journal of biomaterials applications* 28.3 (2013), pp. 354–66.

[241] M. Hasan, I. Ahmed, A. Parsons, G. Walker, and C. Scotchford. "Cytocompatibility and Mechanical Properties of Short Phosphate Glass Fibre Reinforced Polylactic Acid (PLA) Composites: Effect of Coupling Agent Mediated Interface". *Journal of Functional Biomaterials* 3.4 (2012), pp. 706–725.

[242] J. Rich, T. Jaakkola, T. Tirri, T. Närhi, A. Yli-Urpo, and J. Seppälä. "In vitro evaluation of poly(ϵ-caprolactone-co-DL-lactide)/bioactive glass composites". *Biomaterials* 23.10 (2002), pp. 2143–2150.

[243] I. Ahmed, A. Parsons, G. Palmer, J. Knowles, G. Walker, and C. Rudd. "Weight loss, ion release and initial mechanical properties of a binary calcium phosphate glass fibre/PCL composite". *Acta Biomaterialia* 4.5 (2008), pp. 1307–1314.

[244] G. Georgiou, L. Mathieu, D. P. Pioletti, P.-E. Bourban, J.-A. E. Månson, J. C. Knowles, and S. N. Nazhat. "Polylactic Acid–Phosphate Glass Composite Foams as Scaffolds for Bone Tissue Engineering". *J Biomed Mater Res Part B: Appl Biomater* 80 (2006), pp. 322–331.

[245] P. Uppstu, C. Paakki, and A. Rosling. "In vitro hydrolysis and magnesium release of poly(d, l -lactide-co-glycolide)-based composites containing bioresorbable glasses and magnesium hydroxide". *Journal of Applied Polymer Science* 132.41 (2015), pp. 1–11.

[246] A.-M. Haaparanta, P. Uppstu, M. Hannula, V. Ellä, A. Rosling, and M. Kellomäki. "Improved dimensional stability with bioactive glass fibre skeleton in poly(lactide-co-glycolide) porous scaffolds for tissue engineering." *Materials science & engineering. C, Materials for biological applications* 56 (2015), pp. 457–66.

[247] Z. Zhou, Q. Yi, X. Liu, L. Liu, and Q. Liu. "In vitro degradation behaviors of Poly-l-lactide/bioactive glass composite materials in phosphate-buffered solution". *Polymer Bulletin* 63.4 (2009), pp. 575–586.

[248] A. Stamboulis, L. L. Hench, and A. R. Boccaccini. "Mechanical properties of biodegradable polymer sutures coated with bioactive glass". *Journal of Materials Science: Materials in Medicine* 13.9 (2002), pp. 843–848.

[249] S. M. Bennett, M. Arumugam, S. Wilberforce, D. Enea, N. Rushton, X. C. Zhang, S. M. Best, R. E. Cameron, and R. A. Brooks. "The effect of particle size on the in vivo degradation of poly(d,l-lactide-co-glycolide)/α-tricalcium phosphate micro- and nanocomposites". *Acta Biomaterialia* 45 (2016), pp. 340–348.

[250] E. Pamula, J. Kokoszka, K. Cholewa-Kowalska, M. Laczka, L. Kantor, L. Niedzwiedzki, G. C. Reilly, J. Filipowska, W. Madej, M. Kolodziejczyk, G. Tylko, and A. M. Osyczka. "Degradation, Bioactivity, and Osteogenic Potential of Composites Made of PLGA and Two Different Sol–Gel Bioactive Glasses". *Annals of Biomedical Engineering* 39.8 (2011), pp. 2114–2129.

[251] F. Yang, W. Cui, Z. Xiong, L. Liu, J. Bei, and S. Wang. "Poly(l,l-lactide-co-glycolide)/tricalcium phosphate composite scaffold and its various changes during degradation in vitro". *Polymer Degradation and Stability* 91.12 (2006), pp. 3065–3073.

[252] A. R. Boccaccini and V. Maquet. "Bioresorbable and bioactive polymer/Bioglass® composites with tailored pore structure for tissue engineering applications". *Composites Science and Technology* 63.16 (2003), pp. 2417–2429.

[253] H.-W. Kim, E.-J. Lee, I.-K. Jun, H.-E. Kim, and J. C. Knowles. "Degradation and drug release of phosphate glass/polycaprolactone biological composites for hard-tissue regeneration". *Journal of Biomedical Materials Research Part B: Applied Biomaterials* 75B.1 (2005), pp. 34–41.

[254] R. L. Prabhakar, S. Brocchini, and J. C. Knowles. "Effect of glass composition on the degradation properties and ion release characteristics of phosphate glass—polycaprolactone composites". *Biomaterials* 26.15 (2005), pp. 2209–2218.

[255] M. Shah Mohammadi, I. Ahmed, N. Muja, S. Almeida, C. Rudd, M. Bureau, and S. Nazhat. "Effect of Si and Fe doping on calcium phosphate glass fibre reinforced polycaprolactone bone analogous composites". *Acta Biomaterialia* 8.4 (2012), pp. 1616–1626.

[256] S. Verrier, J. J. Blaker, V. Maquet, L. L. Hench, and A. R. Boccaccini. "PDLLA/Bioglass® composites for soft-tissue and hard-tissue engineering: an in vitro cell biology assessment". *Biomaterials* 25.15 (2004), pp. 3013–3021.

[257] O. Erdemli, O. Çaptug, H. Bilgili, D. Orhan, A. Tezcaner, and D. Keskin. "In vitro and in vivo evaluation of the effects of demineralized bone matrix or calcium sulfate addition to polycaprolactone–bioglass composites". *Journal of Materials Science: Materials in Medicine* 21.1 (2010), pp. 295–308.

[258] H.-W. Kim, H.-H. Lee, and G.-S. Chun. "Bioactivity and osteoblast responses of novel biomedical nanocomposites of bioactive glass nanofiber filled poly(lactic acid)". *Journal of Biomedical Materials Research Part A* 85A.3 (2008), pp. 651–663.

[259] H.-H. Lee, H.-S. Yu, J.-H. Jang, and H.-W. Kim. "Bioactivity improvement of poly(ϵ-caprolactone) membrane with the addition of nanofibrous bioactive glass". *Acta Biomaterialia* 4.3 (2008), pp. 622–629.

[260] X. B. Yang, D. Webb, J. Blaker, A. R. Boccaccini, V. Maquet, C. Cooper, and R. O. Oreffo. "Evaluation of human bone marrow stromal cell growth on biodegradable polymer/Bioglass® composites". *Biochemical and Biophysical Research Communications* 342.4 (2006), pp. 1098–1107.

[261] L. Elomaa, A. Kokkari, T. Närhi, and J. V. Seppälä. "Porous 3D modeled scaffolds of bioactive glass and photocrosslinkable poly(ϵ-caprolactone) by stereolithography". *Composites Science and Technology* 74 (2013), pp. 99–106.

[262] R. M. Day, A. R. Boccaccini, S. Shurey, J. A. Roether, A. Forbes, L. L. Hench, and S. M. Gabe. "Assessment of polyglycolic acid mesh and bioactive glass for soft-tissue engineering scaffolds". *Biomaterials* 25.27 (2004), pp. 5857–5866.

[263] M. Navarro, M. P. Ginebra, J. A. Planell, S. Zeppetelli, and L. Ambrosio. "Development and cell response of a new biodegradable composite scaffold for guided bone regeneration". *Journal of Materials Science: Materials in Medicine* 15.4 (2004), pp. 419–422.

[264] R. Felfel, I. Ahmed, A. Parsons, G. Palmer, V. Sottile, and C. Rudd. "Cytocompatibility, degradation, mechanical property retention and ion release profiles for phosphate glass fibre reinforced composite rods". *Materials Science and Engineering: C* 33.4 (2013), pp. 1914–1924.

[265] W. Chrzanowski, E. A. Abou Neel, K.-Y. Y. Lee, A. Bismarck, A. M. Young, A. D. Hart, M. J. Dalby, and J. C. Knowles. "Tailoring Cell Behavior on Polymers by the Incorporation of Titanium Doped Phosphate Glass Filler". *Advanced Engineering Materials* 12.7 (2010), B298–B308.

[266] K. J. Lowry, K. R. Hamson, L. Bear, Y. B. Peng, R. Calaluce, M. L. Evans, J. O. Anglen, and W. C. Allen. "Polycaprolactone/glass bioabsorbable implant in a rabbit humerus fracture model". *Journal of Biomedical Materials Research* 36.4 (1997), pp. 536–541.

[267] E. Y. Kang, E. Lih, I. H. Kim, Y. K. Joung, and D. K. Han. "Effects of poly(L-lactide-ϵ-caprolactone) and magnesium hydroxide additives on physicomechanical properties and degradation of poly(L-lactic acid)". *Biomaterials Research* 20.1 (2016), p. 7.

[268] M. C. Righetti, M. Gazzano, M. L. Di Lorenzo, and R. Androsch. "Enthalpy of melting of α- and α-crystals of poly(l-lactic acid)". 2015.

[269] M. Koenig and S. Huang. "Biodegradable blends and composites of polycaprolactone and starch derivatives". *Polymer* 36.9 (1995), pp. 1877–1882.

[270] V. Crescenzi, G. Manzini, G. Calzolari, and C. Borri. "Thermodynamics of fusion of poly-β-propiolactone and poly-ϵ-caprolactone. comparative analysis of the melting of aliphatic polylactone and polyester chains". *European Polymer Journal* 8.3 (1972), pp. 449–463.

[271] L. Wang, Z. Zhang, H. Chen, S. Zhang, and C. Xiong. "Preparation and characterization of biodegradable thermoplastic Elastomers (PLCA/PLGA blends)". *Journal of Polymer Research* 17.1 (2010), pp. 77–82.

[272] A. Agrawal, A. D. Saran, S. S. Rath, and A. Khanna. "Constrained nonlinear optimization for solubility parameters of poly(lactic acid) and poly(glycolic acid)—validation and comparison". *Polymer* 45.25 (2004), pp. 8603–8612.

[273] R. N. Oosterbeek, K. A. Kwon, P. Duffy, S. McMahon, X. C. Zhang, S. M. Best, and R. E. Cameron. "Tuning structural relaxations, mechanical properties, and degradation timescale of PLLA during hydrolytic degradation by blending with PLCL-PEG". *Polymer Degradation and Stability* 170 (2019), p. 109015.

[274] K. Van De Velde and P. Kiekens. "Biopolymers: overview of several properties and consequences on their applications". *Polymer Testing* 21 (2002), pp. 433–442.

[275] I. Martinez De Arenaza, E. Meaurio, B. Coto, and J.-R. Sarasua. "Molecular dynamics modelling for the analysis and prediction of miscibility in polylactide/polyvinilphenol blends". *Polymer* 51 (2010), pp. 4431–4438.

[276] D. K. Schneiderman, E. M. Hill, M. T. Martello, and M. A. Hillmyer. "Poly(lactide)-block-poly(ϵ-caprolactone-co-ϵ-decalactone)-block-poly(lactide) copolymer elastomers". *Polym. Chem.* 6.19 (2015), pp. 3641–3651.

[277] P.-G. de Gennes. *Scaling concepts in polymer physics*. Ithaca, NY: Cornell University Press, 1979.

[278] S. Y. Kim, T. Kanamori, Y. Noumi, P.-C. Wang, and T. Shinbo. "Preparation of porous poly(D,L-lactide) and poly(D,L-lactide-co-glycolide) membranes by a phase inversion process and investigation of their morphological changes as cell culture scaffolds". *Journal of Applied Polymer Science* 92.4 (2004), pp. 2082–2092.

[279] S. D'amico. "Influence of Humidity on Glass Transition of PLA Films". *Research and Reviews in Materials Science and Chemistry* 3.2 (2014), pp. 115–122.

[280] M. L. Dreher, S. Nagaraja, J. Bergstrom, and D. Hayman. "Development of a Flow Evolution Network Model for the Stress-Strain Behavior of Poly(L-lactide)". *Journal of Biomechanical Engineering* 139.9 (2017), p. 091002.

[281] P.-J. Wang, F. R. Nezami, M. B. Gorji, F. Berti, L. Petrini, T. Wierzbicki, F. Migliavacca, and E. R. Edelman. "Effect of working environment and procedural strategies on mechanical performance of bioresorbable vascular scaffolds". *Acta Biomaterialia* 82 (2018), pp. 34–43.

[282] A. S. Rao, M. S. Makaroun, L. K. Marone, J. S. Cho, R. Rhee, and R. A. Chaer. "Long-term outcomes of internal carotid artery dissection". *Journal of Vascular Surgery* 54.2 (2011), pp. 370–375.

[283] K. Nedeltchev, S. Bickel, M. Arnold, H. Sarikaya, D. Georgiadis, M. Sturzenegger, H. P. Mattle, and R. W. Baumgartner. "Recanalization of spontaneous carotid artery dissection." *Stroke* 40.2 (2009), pp. 499–504.

[284] P. W. Serruys, H. E. Luijten, K. J. Beaut, R. Geuskens, P. J. De Feyter, M. Van Den Brand, J. H. C. Reiber, H. J. Ten Katen, G. A. Van Es, and P. G. Hugenholtz. "Incidence of restenosis after successful coronary angioplasty: a time-related phenomenon". *Circulation* 77.2 (1988), pp. 361–371.

[285] S. Farah and D. G. Anderson. "Physical and mechanical properties of PLA, and their functions in widespread applications — A comprehensive review". *Advanced Drug Delivery Reviews* 107 (2016), pp. 367–392.

[286] J. Sarasua, A. L. Arraiza, P. Balerdi, and I. Maiza. "Crystallinity and mechanical properties of optically pure polylactides and their blends". *Polymer Engineering & Science* 45.5 (2005), pp. 745–753.

[287] L. T. Sin, A. R. Rahmat, and W. A. W. A. Rahman. *Polylactic acid : PLA biopolymer technology and applications*. Oxford: William Andrew, 2012.

[288] K. Tashiro, N. Kouno, H. Wang, and H. Tsuji. "Crystal Structure of Poly(lactic acid) Stereocomplex: Random Packing Model of PDLA and PLLA Chains As Studied by X-ray Diffraction Analysis". *Macromolecules* 50 (2017), pp. 8048–8065.

[289] R. Vasanthakumari and A. Pennings. "Crystallization kinetics of poly(l-lactic acid)". *Polymer* 24.2 (1983), pp. 175–178.

[290] L. Andreozzi, M. Faetti, M. Giordano, and F. Zulli. "Molecular-Weight Dependence of Enthalpy Relaxation of PMMA". *Macromolecules* 38.14 (2005), pp. 6056–6067.

[291] L. L. Hench and J. K. West. "The Sol-Gel Process". *Chemical Reviews* 90.1 (1990), pp. 33–72.

[292] D. Carta, D. M. Pickup, J. C. Knowles, M. E. Smith, and R. J. Newport. "Sol-gel synthesis of the P2O5-CaO-Na 2O-SiO2 system as a novel bioresorbable glass". *Journal of Materials Chemistry* 15.21 (2005), pp. 2134–2140.

[293] J. E. Shelby. *Introduction to glass science and technology*. Royal Society of Chemistry, 2005, p. 291.

[294] O. L. Anderson and D. A. Stuart. "Calculation of Activation Energy of Ionic Conductivity in Silica Glasses by Classical Methods". *Journal of the American Ceramic Society* 37.12 (1954), pp. 573–580.

[295] G. Venkateswara Rao and H. D. Shashikala. "Optical and mechanical properties of calcium phosphate glasses". *Glass Physics and Chemistry* 40.3 (2014), pp. 303–309.

[296] B. Udvardi, I. J. Kovacs, T. Fancsik, P. Konya, M. Batori, F. Stercel, G. Falus, and Z. Szalai. "Effects of Particle Size on the Attenuated Total Reflection Spectrum of Minerals". *Applied Spectroscopy* (2016).

[297] Y. Moustafa and K. El-Egili. "Infrared spectra of sodium phosphate glasses". *Journal of Non-Crystalline Solids* 240.1 (1998), pp. 144–153.

[298] P. Shih, S. Yung, and T. Chin. "FTIR and XPS studies of P2O5–Na2O–CuO glasses". *Journal of Non-Crystalline Solids* 244.2 (1999), pp. 211–222.

[299] E. A. Abou Neel, A. M. Young, S. N. Nazhat, and J. C. Knowles. "A Facile Synthesis Route to Prepare Microtubes from Phosphate Glass Fibres". *Advanced Materials* 19.19 (2007), pp. 2856–2862.

[300] J.-O. Byun, B.-H. Kim, K.-S. Hong, H.-J. Jung, S.-W. Lee, and A. Izyneev. "Properties and structure of RO-Na2O-Al2O3-P2O5 (R = Mg, Ca, Sr, Ba) glasses". *Journal of Non-Crystalline Solids* 190.3 (1995), pp. 288–295.

[301] D. Ilieva, B. Jivov, G. Bogachev, C. Petkov, I. Penkov, and Y. Dimitriev. "Infrared and Raman spectra of Ga2O3–P2O5 glasses". *Journal of Non-Crystalline Solids* 283.1 (2001), pp. 195–202.

[302] Coblentz Society Inc. "Evaluated Infrared Reference Spectra". In: *NIST Chemistry WebBook, NIST Standard Reference Database Number 69*. Ed. by P. Linstrom and W. Mallard. Gaithersburg MD, 20899: National Institute of Standards and Technology, 2017.

[303] N. F. Zobov, O. L. Polyansky, C. Le Sueur, and J. Tennyson. "Vibration-rotation levels of water beyond the Born-Oppenheimer approximation". *Chemical Physics Letters* 260.3-4 (1996), pp. 381–387.

[304] J. Arriagada, W. Burckhardt, and A. Feltz. "The influence of the water content on absorption and dispersion behaviour of calcium metaphosphate glasses". *Journal of Non-Crystalline Solids* 91.3 (1987), pp. 375–385.

[305] B. Karmakar, P. Kundu, A. K. Chaudhuri, K. Annapurna, A. Kumar, and R. N. Dwivedi. "Effect of hydroxyl content on the physical properties of calcium metaphosphate glasses". *Bulletin of Materials Science* 22.2 (1999), pp. 115–119.

[306] J. P. Fletcher, R. J. Kirkpatrick, D. Howell, and S. H. Risbud. "31P Magic-angle spinning nuclear magnetic resonance spectroscopy of calcium phosphate glasses". *Journal of the Chemical Society, Faraday Transactions* 89.17 (1993), p. 3297.

[307] P. Gras, A. Baker, C. Combes, C. Rey, S. Sarda, A. J. Wright, M. E. Smith, J. V. Hanna, C. Gervais, D. Laurencin, and C. Bonhomme. "From crystalline to amorphous calcium pyrophosphates: A solid state Nuclear Magnetic Resonance perspective". *Acta Biomaterialia* 31 (2016), pp. 348–357.

[308] A. Patel and J. C. Knowles. "Investigation of silica-iron-phosphate glasses for tissue engineering". *Journal of Materials Science: Materials in Medicine* 17 (2006), pp. 937–944.

[309] E. Abou Neel, I. Ahmed, J. Pratten, S. Nazhat, and J. Knowles. "Characterisation of antibacterial copper releasing degradable phosphate glass fibres". *Biomaterials* 26.15 (2005), pp. 2247–2254.

[310] I. Ahmed, M. Lewis, I. Olsen, and J. Knowles. "Phosphate glasses for tissue engineering: Part 2. Processing and characterisation of a ternary-based P2O5–CaO–Na2O glass fibre system". *Biomaterials* 25.3 (2004), pp. 491–499.

[311] I. Ahmed, C. Collins, M. Lewis, I. Olsen, and J. Knowles. "Processing, characterisation and biocompatibility of iron-phosphate glass fibres for tissue engineering". *Biomaterials* 25.16 (2004), pp. 3223–3232.

[312] J. R. Van Wazer and D. A. Campanella. “Structure and Properties of the Condensed Phosphates. IV. Complex Ion Formation in Polyphosphate Solutions”. *Journal of the American Chemical Society* 72.2 (1950), pp. 655–663.

[313] M. B. Tošić, R. Ž. Dimitrijević, M. M. Mitrović, and N. S. Blagojević. “Crystallization behavior of calcium phosphate glass powder”. *Journal of Materials Science* 37.20 (2002), pp. 4369–4377.

[314] P. James, Y. Iqbal, U. Jais, S. Jordery, and W. Lee. “Crystallisation of silicate and phosphate glasses”. *Journal of Non-Crystalline Solids* 219 (1997), pp. 17–29.

[315] S. Kargozar, F. Baino, S. Hamzehlou, R. G. Hill, and M. Mozafari. “Bioactive Glasses: Sprouting Angiogenesis in Tissue Engineering”. *Trends in Biotechnology* 36.4 (2018), pp. 430–444.

[316] R. Shah, A. Sinanan, J. Knowles, N. Hunt, and M. Lewis. “Craniofacial muscle engineering using a 3-dimensional phosphate glass fibre construct”. *Biomaterials* 26.13 (2005), pp. 1497–1505.

[317] N. Sharmin and C. D. Rudd. “Structure, thermal properties, dissolution behaviour and biomedical applications of phosphate glasses and fibres: a review”. *Journal of Materials Science* 52.15 (2017), pp. 8733–8760.

[318] D. Midgley. “The interpretation of non-ideal calibrations of ion-selective electrodes”. *Analytical Chemistry* 49.8 (1977), pp. 1211–1218.

[319] A. H. Truesdell and B. F. Jones. “WATEQ, a computer program for calculating chemical equilibria of natural waters”. *Journal of the U.S. Geological Survey* 2.2 (1974), pp. 233–248.

[320] R. M. Garrels and C. L. Christ. *Solutions, minerals, and equilibria*. New York: Harper & Row, 1965, p. 450.

[321] J. I. Drever. *The Geochemistry of Natural Waters*. Englewood Cliffs, N.J.: Prentic-Hall Inc., 1982, p. 388.

[322] F. Barrère, C. M. van der Valk, R. A. J. Dalmeijer, C. A. van Blitterswijk, K. de Groot, and P. Layrolle. “In vitro and in vivo degradation of biomimetic octacalcium phosphate and carbonate apatite coatings on titanium implants”. *Journal of Biomedical Materials Research Part A* 64A.2 (2003), pp. 378–387.

[323] W. Voigt. “Ueber die Beziehung zwischen den beiden Elasticitätsconstanten isotroper Körper”. *Annalen der Physik* 274.12 (1889), pp. 573–587.

[324] A. Reuss. “Berechnung der Fließgrenze von Mischkristallen auf Grund der Plastizitätsbedingung für Einkristalle”. *Journal of Applied Mathematics and Mechanics - Zeitschrift für Angewandte Mathematik und Mechanik* 9.1 (1929), pp. 49–58.

[325] U. J. Counto. “The effect of the elastic modulus of the aggregate on the elastic modulus, creep and creep recovery of concrete”. *Magazine of Concrete Research* 16.48 (1964), pp. 129–138.

[326] S. Y. Fu, X. Q. Feng, B. Lauke, and Y. W. Mai. "Effects of particle size, particle/matrix interface adhesion and particle loading on mechanical properties of particulate-polymer composites". *Composites Part B: Engineering* 39.6 (2008), pp. 933–961.

[327] S. Ahmed and F. R. Jones. *A review of particulate reinforcement theories for polymer composites*. 1990.

[328] L. Nicolais and M. Narkis. "Stress-strain behavior of styrene-acrylonitrile/glass bead composites in the glassy region". *Polymer Engineering and Science* 11.3 (1971), pp. 194–199.

[329] L. Nicolais and L. Nicodemo. "Strength of particulate composite". *Polymer Engineering and Science* 13.6 (1973), pp. 469–469.

[330] A. S. Kenyon and H. J. Duffey. "Properties of a particulate-filled polymer". *Polymer Engineering and Science* 7.3 (1967), pp. 189–193.

[331] Y. Nakamura, M. Yamaguchi, M. Okubo, and T. Matsumoto. "Effects of particle size on mechanical and impact properties of epoxy resin filled with spherical silica". *Journal of Applied Polymer Science* 45.7 (1992), pp. 1281–1289.

[332] B. Pukanszky and G. Vörös. "Mechanism of interfacial interactions in particulate filled composites". *Composite Interfaces* 1.5 (1993), pp. 411–427.

[333] C. Suryanarayana. "Mechanical alloying and milling". *Progress in Materials Science* 46.1-2 (2001), pp. 1–184.

[334] P. Baláž. "High-Energy Milling". In: *Mechanochemistry in Nanoscience and Minerals Engineering*. Berlin, Heidelberg: Springer Berlin Heidelberg, 2008, pp. 103–132.

[335] M. Quirós, S. Gražulis, S. Girdzijauskaitė, A. Merkys, and A. Vaitkus. "Using SMILES strings for the description of chemical connectivity in the Crystallography Open Database". *Journal of Cheminformatics* 10.1 (2018), p. 23.

[336] A. Merkys, A. Vaitkus, J. Butkus, M. Okulič-Kazarinas, V. Kairys, and S. Gražulis. "COD::CIF::Parser: An error-correcting CIF parser for the Perl language". *Journal of Applied Crystallography* 49 (2016), pp. 292–301.

[337] S. Gražulis, A. Merkys, A. Vaitkus, and M. Okulič-Kazarinas. "Computing stoichiometric molecular composition from crystal structures". *Journal of Applied Crystallography* 48.1 (2015), pp. 85–91.

[338] S. Gražulis, A. Daškevič, A. Merkys, D. Chateigner, L. Lutterotti, M. Quirós, N. R. Serebryanaya, P. Moeck, R. T. Downs, and A. Le Bail. "Crystallography Open Database (COD): An open-access collection of crystal structures and platform for world-wide collaboration". *Nucleic Acids Research* 40.D1 (2012).

[339] S. Gražulis, D. Chateigner, R. T. Downs, A. F. Yokochi, M. Quirós, L. Lutterotti, E. Manakova, J. Butkus, P. Moeck, and A. Le Bail. "Crystallography Open Database - An open-access collection of crystal structures". *Journal of Applied Crystallography* 42.4 (2009), pp. 726–729.

[340] R. T. Downs and M. Hall-Wallace. "The American Mineralogist crystal structure database". *American Mineralogist* 88.1 (2003), pp. 247–250.

[341] S. Ghosh, A. Sharma, and G. Talukder. "Zirconium An Abnormal Trace Element in Biology". *Biological Trace Element Research* 247.35 (1992).

[342] Z. H. Liu, K. W. Kwok, R. K. Li, and C. L. Choy. "Effects of coupling agent and morphology on the impact strength of high density polyethylene/CaCO3 composites". *Polymer* 43.8 (2002), pp. 2501–2506.

[343] V. M. Sglavo, D. Pugliese, F. Sartori, N. G. Boetti, E. Ceci-Ginistrelli, G. Franco, and D. Milanese. "Mechanical properties of resorbable calcium-phosphate glass optical fiber and capillaries". *Journal of Alloys and Compounds* 778 (2019), pp. 410–417.

[344] S.-H. Kang, I.-H. Chae, J.-J. Park, H. S. Lee, D.-Y. Kang, S.-S. Hwang, T.-J. Youn, and H.-S. Kim. "Stent Thrombosis With Drug-Eluting Stents and Bioresorbable Scaffolds". *JACC: Cardiovascular Interventions* 9.12 (2016), pp. 1203–1212.

[345] C. Indolfi, S. De Rosa, and A. Colombo. "Bioresorbable vascular scaffolds - basic concepts and clinical outcome". *Nature Reviews Cardiology* 13.12 (2016), pp. 719–729.

[346] M.-S. Scholz, J. Blanchfield, L. Bloom, B. Coburn, M. Elkington, J. Fuller, M. Gilbert, S. Muflahi, M. Pernice, S. Rae, J. Trevarthen, S. White, P. Weaver, and I. Bond. "The use of composite materials in modern orthopaedic medicine and prosthetic devices: A review". *Composites Science and Technology* 71.16 (2011), pp. 1791–1803.

[347] S. Ramakrishna, J. Mayer, E. Wintermantel, and K. W. Leong. "Biomedical applications of polymer-composite materials: a review". *Composites Science and Technology* 61.9 (2001), pp. 1189–1224.

[348] N. Boeree, J. Dove, J. Cooper, J. Knowles, and G. Hastings. "Development of a degradable composite for orthopaedic use: mechanical evaluation of an hydroxyapatite-polyhydroxybutyrate composite material". *Biomaterials* 14.10 (1993), pp. 793–796.

[349] W. Bonfield, M. Grynpas, A. Tully, J. Bowman, and J. Abram. "Hydroxyapatite reinforced polyethylene — a mechanically compatible implant material for bone replacement". *Biomaterials* 2.3 (1981), pp. 185–186.

[350] A. Naik, D. V. Shepherd, J. H. Shepherd, S. M. Best, and R. E. Cameron. "The effect of the type of HA on the degradation of PLGA/HA composites". *Materials Science and Engineering: C* 70 (2017), pp. 824–831.

[351] S. I. J. Wilberforce, C. E. Finlayson, S. M. Best, and R. E. Cameron. "The influence of hydroxyapatite (HA) microparticles (m) and nanoparticles (n) on the thermal and dynamic mechanical properties of poly-l-lactide". *Polymer* 52.13 (2011), pp. 2883–2890.

[352] A. R. Boccaccini, M. Erol, W. J. Stark, D. Mohn, Z. Hong, and J. F. Mano. "Polymer/bioactive glass nanocomposites for biomedical applications: A review". *Composites Science and Technology* 70.13 (2010), pp. 1764–1776.

[353] T. Ramanathan and H. Skinner. "Coronary blood flow". *Continuing Education in Anaesthesia Critical Care & Pain* 5.2 (2005), pp. 61–64.

[354] L. C. Struik. "The mechanical and physical ageing of semicrystalline polymers: 1". *Polymer* 28.9 (1987), pp. 1521–1533.

[355] L. C. Struik. "The mechanical behaviour and physical ageing of semicrystalline polymers: 2". *Polymer* 28.9 (1987), pp. 1534–1542.

[356] P. S. Theocaris, E. A. Kontou, and G. C. Papanicolaou. "The effect of moisture absorption on the thermomechanical properties of particulates". *Colloid and Polymer Science* 261 (1983), pp. 394–403.

[357] R. Kornowski, M. K. Hong, F. O. Tio, O. Bramwell, H. Wu, and M. B. Leon. "In-Stent Restenosis: Contributions of Inflammatory Responses and Arterial Injury to Neointimal Hyperplasia". *Journal of the American College of Cardiology* 31.1 (1998), pp. 224–230.

[358] T. M. Jeewandara, S. G. Wise, and M. K. C. Ng. "Biocompatibility of Coronary Stents". *Materials* 7 (2014), pp. 769–786.

[359] P. W. Serruys, N. Bullett, N. Foin, N. Ahmed, R. Al-Lamee, N. Bressloff, Y. Onuma, and K. Al-Lamee. *Bench-testing evaluation of a novel fully drug-eluting BRS*. 2016. URL: https://media.pcronline.com/diapos/EuroPCR2016/3635-20160519_1630_Room_351_Serruys_Patrick_W_0000_(18065)/Serruys_Patrick_W_20160519_1630_Room_351.pdf (visited on 06/17/2020).

[360] P. Haque, I. A. Barker, A. Parsons, K. J. Thurecht, I. Ahmed, G. S. Walker, C. D. Rudd, and D. J. Irvine. "Influence of compatibilizing agent molecular structure on the mechanical properties of phosphate glass fiber-reinforced PLA composites". *Journal of Polymer Science Part A: Polymer Chemistry* 48.14 (2010), pp. 3082–3094.

[361] D. A. Loy. "Hybrid Organic / Inorganic Materials". *MRS Bulletin* 26.5 (20001), pp. 364–367.

[362] K. Urman and J. U. Otaigbe. "New phosphate glass/polymer hybrids—Current status and future prospects". *Progress in Polymer Science* 32.12 (2007), pp. 1462–1498.